DOCTORAL THESIS

Active-Passive Two-Way Ranging Protocol for Positioning Systems

Taavi Laadung

Active-Passive Two-Way Ranging Protocol for Positioning Systems

TAAVI LAADUNG

TALLINN UNIVERSITY OF TECHNOLOGY
School of Information Technologies
Thomas Johann Seebeck Department of Electronics

The dissertation was accepted for the defence of the degree of Doctor of Philosophy (Information and Communication Technology) on 28 June 2023

Supervisor: Professor Muhammad Mahtab Alam
Thomas Johann Seebeck Department of Electronics, School of Information Technologies
Tallinn University of Technology
Tallinn, Estonia

Co-supervisor: Professor Yannick Le Moullec
Thomas Johann Seebeck Department of Electronics, School of Information Technologies
Tallinn University of Technology
Tallinn, Estonia

Co-supervisor: Dr. Sander Ulp, PhD,
Eliko Tehnoloogia Arenduskeskus OÜ
Tallinn, Estonia

Opponents: Professor Elena Simona Lohan
Tampere University
Tampere, Finland

Dr. Ahmed Zoha, PhD
University of Glasgow
Glasgow, Scotland, UK

Defence of the thesis: 21 August 2023, Tallinn

Declaration:
Hereby I declare that this doctoral thesis, my original investigation and achievement, submitted for the doctoral degree at Tallinn University of Technology, has not been submitted for any academic degree elsewhere.

Taavi Laadung

_____
signature

Aktiiv-passiivne kauguste mõõtmise protokoll positsioneerimissüsteemidele

TAAVI LAADUNG

**TAL
TECH**
KIRJASTUS

Contents

List of Publications

The present PhD thesis is based on the following publications that are referred to in the text by Roman numerals.

Publications

I   T. Laadung, S. Ulp, M. M. Alam, and Y. Le Moullec, "Active-Passive Two-Way Ranging Using UWB," in *14th International Conference on Signal Processing and Communication Systems (ICSPCS)*, pp. 1–5, IEEE, dec 2020

II T. Laadung, S. Ulp, M. M. Alam, and Y. Le Moullec, "Novel Active-Passive Two-Way Ranging Protocols for UWB Positioning Systems," *IEEE Sensors Journal*, vol. 22, no. 6, pp. 5223–5237, 2022

III T. Laadung, S. Ulp, M. M. Alam, and Y. Le Moullec, "Performance Evaluation of UWB Active-Passive Two-Way Ranging Distance Estimation Matrix Weighting Methods," in *12th International Conference on Indoor Positioning and Indoor Navigation (IPIN 2022)*, pp. 1–5, CEUR-WS, sep 2022

Under Review

IV T. Laadung, S. Ulp, A. Fjodorov, M. M. Alam, and Y. Le Moullec, "Adaptive Extended Kalman Filter Position Estimation Based on Ultra-Wideband Active-Passive Ranging Protocol," *Submitted to IEEE Access*, 2023

Other Publications

V   M. Tommingas, S. Ulp, M. M. Alam, I. Müürsepp, and T. Laadung, "Estimating UWB Positioning Integrity Based on Ranging Residuals," in *2023 24th International Conference on Applied Electromagnetics and Communications (ICECOM)*, pp. 1–6, Forthcoming, 2023

Author's Contributions to the Publications

I **Publication I:** In this paper, I was the first author. I provided an overview of the state-of-the-art Ultra-Wideband (UWB) protocols that utilize passive methods for indoor positioning, I proposed the Active-Passive Two-Way Ranging (AP-TWR) protocol, I provided the mathematical proof, I wrote the code for the simulation program, I carried out the simulations, I wrote the code for data acquisition of the experiments, I carried out experiments in Line of Sight (LoS) propagation conditions, I analysed the simulation and experimental results, alongside with the analysis on the protocol's impact to the air time, I prepared the figures and tables, I wrote the manuscript under the guidance of my supervisors, and I revised it based on the reviewers' comments.

II **Publication II:** In this paper, I was the first author. I provided the background on UWB passive ranging methods, I gave an overview on the most common practical active ranging methods utilizing Time of Flight (ToF) estimation: Single-Sided (SS) TWR, Symmetrical Double-Sided (SDS) TWR, and Alternative Double-Sided (AltDS) TWR. In addition to the AP-TWR method proposed in publication I, I proposed an additional method of passive ranging, totaling 6 distinct methods of AP-TWR, alongside the mathematical proofs. Furthermore, I wrote the code and conducted simulations and experiments for LoS propagation conditions, I analyzed the results from the standpoint of ranging Root-Mean-Squared-Error (RMSE) and air time efficiency, I prepared the figures and tables, I wrote the manuscript under the guidance of my supervisors, and I revised it according to the reviewers' comments.

III **Publication III:** In this paper, I was the first author. I presented the state-of-the-art UWB passive ranging methods, gave a background on the best performing AP-TWR method from Publication II, and proposed 7 methods for measurement matrix processing to increase the range estimation robustness, I wrote the code that implemented data acquisition and data processing, I prepared the experimental setup, I conducted the experiments in LoS and 2 separate Non-Line-of-Sight (NLoS) propagation conditions, I analyzed the results from the standpoint of ranging RMSE and Standard Deviation (SD), I prepared the figures, I wrote the manuscript under the guidance of my supervisors, and I revised it based on the reviewers' comments.

IV **Publication IV:** I was the first author. I gave an overview of the different methods of addressing errors originating from NLoS and formed a comprehensive analysis of the effects of various NLoS paths on the AP-TWR range estimates. Based on the resulting analysis and findings of other research papers, formulated a novel NLoS-robust positioning method, based on the AP-TWR protocol and the Extended Kalman Filter (EKF). I wrote the code for data acquisition and data processing and prepared the experimental setup. I then conducted experiments with a stationary and moving tag in an industrial environment, analyzed the results from the standpoint of position RMSE, prepared the figures and the tables, and wrote the manuscript under the guidance of my supervisors.

Abbreviations

2D	Two-Dimensional
3D	Three-Dimensional
ADS-TWR	Asymmetrical Double-Sided Two-Way Ranging
A-EKF	Adaptive Extended Kalman Filter
AltDS-TWR	Alternative Double-Sided Two-Way Ranging
AoA	Angle of Arrival
AP-TWR	Active-Passive Two-Way Ranging
A-TDoA	Asynchronous Time Difference of Arrival
CDF	Cumulative Distribution Function
CFO	Carrier Frequency Offset
CIR	Channel Impulse Response
CNN	Convolutional Neural Network
DR	Dead Reckoning
DWE	Distance Weighted Estimator
EKF	Extended Kalman Filter
GDoP	Geometric Dilution of Precision
GNSS	Global Navigation Satellite System
GPS	Global Positioning System
IC	Integrated Circuit
IDW	Inverse Distance Weighting
IMR	Iterative Minimum Residual
IPS	Indoor Positioning System
IR	Infrared
LCC-Rwgh	Lower Computational Complexity Residual Weighting Algorithm
LoB	Line of Bearing
LoS	Line-of-Sight
LS	Least Squares
LS-SVM	Least Squares Support Vector Machine
LSTM	Long Short-Term Memory
MAD	Mean Absolute Deviation
Med	Median
ML	Machine Learning
MLE	Maximum Likelihood Estimation
MLP	Multilayer Perceptron
MSR	Multiple Simultaneous Ranging
NFC	Near Field Communication
NLoS	Non-Line-of-Sight
OWR	One-Way Ranging
PE	Passive Extended
PnPLoc	Plug & Play Localization
PoE	Power over Ethernet
RF	Radio Frequency
RFID	Radio Frequency Identification
RMSE	Root-Mean-Square-Error
RSSI	Received Signal Strength Indicator
RTLS	Real-Time Location System
RToF	Return Time-of-Flight
Rwgh	Residual Weighting Algorithm

SD	Standard Deviation
SDS-TWR	Symmetrical Double-Sided Two-Way Ranging
SNR	Signal-to-Noise Ratio
SRAC	Simultaneous Ranging and Communication
SRwgh	Select Residual Weighting Algorithm
SS-TWR	Single-Sided Two-Way Ranging
TDoA	Time Difference of Arrival
ToA	Time of Arrival
ToF	Time of Flight
TWR	Two-Way Ranging
TW-ToA-C	Two-Way Time of Arrival with Correction
UWB	Ultra-Wideband
VL	Visible Light
WiFi	Wireless Fidelity
WLAN	Wireless Local Area Network
WLS	Weighted Least Squares
WM	Weighted Mean

1 Introduction

1.1 Background

Navigation and positioning has undergone substantial advancements since the introduction of the compass in the 11th century. Throughout history, diverse approaches have emerged for determining position and facilitating navigation, encompassing the utilization of landmarks, maps, celestial navigation, and more [6]. With the advent of electronic technology, a new era in positioning and navigation commenced through the development of different Radio Frequency (RF) signal-based positioning systems. Among others, notable examples include the German Telefunken Kompass Sender, which relied on radio direction finding, as well as ground-based hyperbolic multilateration systems like Gee in the UK and Loran in the USA. These advancements eventually led to the establishment of Global Navigation Satellite Systems (GNSS), providing global coverage [7].

The first GNSS, the Global Positioning System (GPS), was developed by the United States Department of Defense in the 1970s and launched in 1978. Initially developed for military purposes, GPS quickly became a civilian tool and has since become the most widely used GNSS in the world. Since then, other GNSS have been developed, including Russia's GLONASS (launched in 1982), China's BeiDou (launched in 2000), and the European Union's Galileo (launched in 2011) [8][1]. These GNSS utilize a network of satellites orbiting the Earth to provide precise positional information to users on the ground, anywhere in the world [9].

While GNSS' have been instrumental in improving navigation for outdoor environments, their use is limited in indoor environments due to the signal attenuation caused by not having a direct propagation path to GNSS satellites and multipath effects caused by complex propagation conditions imposed in indoor environments [10]. This has led to the development of Indoor Positioning Systems (IPS), which use alternative methods to determine the position of users or assets indoors.

The development of IPSs has opened up new possibilities for positioning and navigation, especially in environments where GNSS signals are unavailable or unreliable [11]. IPSs have been used in a variety of applications, including various location-based services [12], emergency response [13], asset tracking [14], etc. In recent years, there has been an increase in interest in IPS, driven by the growing demand for location-based services and the increasing use of mobile devices [15].

The subsequent subsection provides a short overview of the various signal types employed in the operation of IPSs, presenting a brief exploration of their characteristics.

1.2 Signal Classification in Indoor Positioning Systems

As GNSS' utilize RF signals in the localization process, there exist quite a few other signals that may be leveraged to provide position estimates. This section provides a brief overview of some of the most popular signals that are employed for IPSs, without going into the specific pros and cons of using each signal. Fig. 1 provides an overview of the signal classification for indoor positioning systems presented in the scope of this thesis, the details of which are discussed further in this section. It is noteworthy that the classification schemes employed in scientific publications for signal categorization in indoor positioning systems often exhibit variations. Different papers adopt distinct taxonomies, resulting in discrepancies in how signals are classified. For instance, certain publications

---

[1]The launch date of Galileo was added here by the thesis's author since the article by Hegarty and Chatre was published prior to the actual launch date.
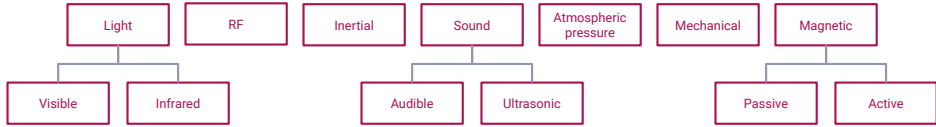
Figure 1: Classification of measured signals in indoor positioning systems.

list optical and vision systems separately [16], while others classify them under a broad "Light Based Localization" category [17].

Light: Although light is an electromagnetic signal just as the RF signals are, the underlying technologies for ranging are quite dissimilar. Light-based technologies fall into two broad domains: Infrared (IR), and Visible Light (VL). IR and VL applications are similar in principle: they both use emitted bursts of light which are detected with a photodiode to transfer information, the difference being in the portion of the electromagnetic spectrum used for transmission. VL uses the visible light portion of the electromagnetic spectrum and IR uses longer wavelengths than VL which are not perceived by the human eye. Optical and vision systems, which employ one or both of them, position the subject by employing an image or video stream from a camera [18].

Radiofrequency: RF signals in indoor positioning typically cover the electromagnetic spectrum from the kilohertz range of low-frequency Radio Frequency Identification (RFID) [19] up to 10.6 GHz used by UWB devices [20]. The position estimate is provided by assessing a certain parameter of the RF signal. Possible parameters include proximity detection based on demodulated signal used in RFID and Near Field Communication (NFC); Received Signal Strength Indicator (RSSI) value used in Zigbee, Wireless Local Area Network (WLAN), Cellular, and Bluetooth; and RF signal propagation time, typically used in UWB applications. In addition to range estimations, antenna arrays could be exploited to determine the direction of a transmitter.

Inertial: Modern inertial systems utilize digital accelerometers and gyroscopes to determine the direction and movement based on acceleration in certain directions. Typically, inertial technology is combined with information from other sensors [21]. This is the case for Dead Reckoning (DR), where the future position is predicted by combining well-known position information (provided by another sensor) and the movement information provided by inertial sensors [22].

Sound: Sound signals consist of pressure waves propagating in the air. The propagation time and the speed of sound are used to give a range estimate; additionally, an array of microphones could be used to detect the direction of the transmitter, similar to one of the previously mentioned RF methods. Sound-based technologies are arranged into two sub-categories: the more prevalent ultrasound and the lesser used audible sound technologies [23].

Atmospheric pressure: Although the atmospheric pressure measured by barometric sensors can only supply altitude difference information, not position estimates, it can still be used to augment other positioning methods to provide more robust and precise estimates [24, 25].

Mechanical: These sensors provide presence detection by means of physical interaction, i.e. pushing a button or a capacitive touch sensor located in specific locations [26] or by employing passive presence detection, i.e. smart floor applications using load cells measuring the ground reaction force [27, 28].

Magnetic: This technology exploits magnetic field detection to attain a position estimate. In addition to heading estimation via a compass, typically magnetic sensors are

used alongside the fingerprinting technique. Magnetic sensor technologies are divided into A) passive, which uses magnetic fields present naturally (earth's magnetic field or fields induced by ferromagnetic materials used in building constructions); and B) active, which generates artificial magnetic fields using special transmitters [23].

1.3 Localization Techniques

The usage of localization techniques discussed in what follows is typically dictated by the underlying technologies discussed above. Although various locating principles could be applied singularly, the combination of several principles and therefore technologies can be used to overcome the specific shortcomings of single techniques. This section states the main principles of operation for IPSs.

Triangulation: The triangulation technique uses the geometric properties of triangles to calculate a position estimate relative to at least two known reference points. The reference points (anchors) measure the direction from which a signal is received and calculate the position of the mobile device (tag) using the known positions of the anchors and the measured angles. The angles are typically acquired by sensor arrays: antenna arrays for RF and microphone arrays for sound-based signals [16].

Trilateration/multilateration: The trilateration technique utilizes the geometric properties of circles to give a position estimate. The position estimate for a two-dimensional space is calculated with distance measurements to three known reference points [23]. Scaling the system to estimate a Three-Dimensional (3D) position needs the availability of at least 4 reference anchors [7]. When measuring 4 or more distances, the trilateration technique is called multilateration. Although multilateration is typically used in RF-based systems, it could also be used in sound or light-based applications.

Fingerprinting: The position estimation in fingerprinting is performed independently of the previously discussed received signal angle or distance. The main principle of fingerprinting is to collect a unique location-dependent characteristic (or a set of characteristics) of a signal to estimate the position of the device. There are two stages for location fingerprinting: the offline (or training) phase where the mapping of characteristics to specific locations is made, and the online phase, where the real-time signal characteristics are compared to the offline data for location estimation [29]. Typical uses of this technique include RSSI mapping for WLAN and Bluetooth signals and magnetic field mapping for magnetic sensor-based applications.

Optical/Vision: This approach is where a position of a person or an object is determined by identifying a marker or an object (person) from an image or video stream [23]. Vision analysis can be performed in two different ways: fixed camera and mobile camera systems. Fixed camera systems utilize image sensors with a known location, the target of tracking is identified from the image stream and is positioned relative to the camera's location. Mobile camera systems make use of the mobile target with a camera: localization is performed by identifying several markers, and landmarks or by extracting environment-specific features [16].

Proximity: The proximity sensing technique positions the target object with respect to a known area. The object's presence in a particular area is sensed using a physical phenomenon with a limited range. The sensing could be carried out by physical interaction (touch sensors, pressure sensors, or capacitive sensors) [18], with more remote identification systems like NFC or RFID [21], detecting the presence via ranging data, or by visual detection, as explained above.

1.4 Performance Metrics

Several taxonomies have been proposed in the literature for benchmarking IPSs; the various proposed categories are summarized in table 1. This section provides a short overview of the most commonly utilized metrics from the literature for designing, comparing, and evaluating various indoor location systems and the underlying technologies. These metrics make it possible to compare and select a suitable solution based on the needs of a specific application and the available resources.

Accuracy: The accuracy metric is one of the most prevalent and important metrics for an IPS since in most cases accuracy defines the applicability of a system for a specific use case. Generally speaking, accuracy is defined as the average Euclidean distance between the estimated and the true position [15, 30].

Precision: While accuracy considers only the mean value of distance errors, the precision metric shows the repeatability, in other words, the closeness, of multiple measurements. The precision metric is often considered a part of the accuracy metric, naming it as the performance of an IPS. As some literature defines precision as the standard deviation of the location error or Geometric Dilution of Precision (GDoP), the cumulative distribution function (CDF) also serves as a clear way to assess the precision of a system [15].

Table 1: Taxonomies of indoor positioning system metrics.

	Liu [15]	Gu [30]	Sakpere [23]	Al Ammar [31]	Brena [18]	Al Nuaimi [32]	Mendoza-Silva [33]	Alarifi [22]	Zafari [34]	Sesyuk [35]	Savic [17]	Tariq [36]
Accuracy/precision	✓	✓	✓	✓	✓	✓	✓	✓	✓	✓	✓	✓
Complexity	✓	✓	✓				✓					✓
Scalability	✓		✓	✓					✓	✓		✓
Robustness	✓	✓					✓					✓
Cost	✓	✓	✓	✓	✓		✓	✓	✓	✓	✓	✓
Security/privacy		✓	✓	✓		✓	✓	✓				
User preference		✓										
Commercial availability		✓							✓	✓		
Limitations		✓									✓	✓
Availability				✓				✓				
Coverage				✓	✓	✓	✓	✓	✓	✓		
Power consumption							✓		✓	✓	✓	
Update rate/delay									✓		✓	
Central/local computing												✓

Complexity: Positioning systems have complexity in terms of software, hardware, and operation factors [23, 33]. Software complexity represents the computational complexity of the positioning algorithms, and hardware complexity is the number of deployable infrastructure elements. Operation factors describe the complexity of maintaining the daily operation of the IPS.

Scalability: This metric may be defined on the basis of two dimensions: density and geography. Density describing the maximum number of user terminals positioned per unit area and time: the positioning signal channel may become congested or further infras-

tructure will be needed to compute the location estimates. Geographic scalability refers to the availability to adjust the physical coverage area of the IPS by introducing additional devices [31].

Robustness: Robustness, or fault tolerance, is the measure that describes the system's resilience against various impairments, such that its performance is not degraded in a wide range of usage scenarios. Some publications also consider the LoS requirement as a part of the robustness metric, as opposed to stating it as a separate one [30].

Cost: Cost can take on several dimensions: financial, time, space, and energy. For example, the financial cost of the devices and their maintenance, deployment time, the dimensions of the devices (or the system in general), and the energy consumption of mobile devices. Typically the cost is closely related to the complexity metric [36].

Security/privacy: Privacy is an important metric concerning individuals using the system: in commercial applications, the users want to have full control over the usability of their location information. In a broad sense, the privacy metric can be divided into two: low and high. The former is the situation when location estimates are calculated in a centralized server and the latter is the opposite: location estimates are computed in the user's device [23].

User preference: The authors of [30] describe user preference as providing a comfortable user experience, contributing to intuitive usage and lightweight and easily usable wearable devices.

Commercial availability: This metric covers if a system is research-oriented with limited availability or readily obtainable as a commercially off-the-shelf product [35].

Limitations: Although the limitations of each system/technology can also be considered as part of other metrics, [30] and [36] stated them as a separate category. These limitations are related to the propagation medium, the need for special infrastructure, the maximum number of available devices, etc. For example, [17] states that the largest constraint for light and sound-based systems is the requirement of LoS.

Availability: Referred to as the percentage of time the IPS is functioning with the required accuracy. This is subject to change on the basis of factors such as downtime for maintenance, device battery charging, data traffic congestions, failures of devices, etc [31, 22].

Coverage: The physical area (surface area or room volume) the IPS is able to cover, providing the required accuracy. Coverage area could also be defined as one of 3 broad categories: local, scalable, or global with the latter having a worldwide coverage area, such as a GNSS [31].

Power consumption: The metric, commonly referred to as power consumption, energy consumption, energy efficiency, or battery life, is an important measure for the mobile user equipment, as these typically operate on battery power. Therefore, in order to increase the use time, high energy efficiency is desired [17].

Update rate/delay: Reference [17] defines the update rate as the frequency of the location estimates for a system, while [34] also adds the notion of latency, in order to describe the delays induced by utilizing multiple signal measurements, signal processing, etc.

Central/local computing: Finally, in [36] the authors stress the importance of whether the calculations are carried out in a centralized node or in the mobile devices themselves, referring to more consumed energy due to increased communications for a central computing node. On the other hand, local computing has the downside of needing additional information for position estimation. The available literature has also categorized this point under the Security/Privacy category, albeit for other reasons.

1.5 Ultra-Wideband Technology

Since many works in the literature extensively detail the strengths and weaknesses of each wireless positioning technology [23, 31, 18, 22, 16, 34, 35, 17] discussed in Section 1.3, the comparisons are not included in the scope of this thesis. **Rather, the reasoning behind shifting the focus on UWB technology is discussed.**

Research has shown that out of all of the wireless-based IPSs, UWB shows potential as it is the most accurate non-hybrid positioning technology offering an accuracy of <30 cm [15], with some implementations achieving as low as 2 cm accuracy [29], proving to be the most accurate RF-based positioning technology [33]. Additionally, UWB is seen as a promising technology, as it is highly scalable, employing a rather low cost of hardware and low energy consumption [37].

Similarly, a number of research papers in recent years show that UWB is the second most popular wireless-based positioning technology after WiFi [38]. Traditional narrowband systems could not distinguish multipath components, therefore they are susceptible to fading effects, as well as having inferior time-domain resolution. UWB technology with its nanosecond-range pulse duration provides resistance to multipath effects, as well as providing robustness against other communication devices and noise in the same frequency band [39, 22].

On top of the increased research interest in recent years, UWB transceiver integrated circuits (IC) have been included in numerous consumer products, such as smartphones Apple iPhone 11 models and up [40], Samsung Galaxy S21+ and up [41], to standards for smart car keys [42], which are implemented, for example, in BMW vehicles [43].

UWB can be used without licensing, as it operates in unlicensed parts of the RF spectrum [21]. As opposed to some of the other positioning technologies based on light or sound signals, the RF waves of UWB propagate through various obstacles and even solid walls [31]. In addition to the previously mentioned precise ranging capabilities, UWB can also be used for high-rate data transmission [23].

1.6 Problem Statement and Research Questions

From the perspective of a wireless positioning system, the key performance metrics that need to be improved are robustness, accuracy, precision, computational complexity, and power consumption. However, improving them is not a trivial task: often, boosting the performance of one metric decreases another metric – some trade-offs have to be made. The study of these areas of possible improvement led to the identification of certain sub-topics (STx) that are relevant to wireless positioning:

1. **ST1** Filtering of input and/or output data

2. **ST2** Position estimation algorithms

3. **ST3** Ranging protocols

4. **ST4** Non-Line-of-Sight (NLoS) conditions

The identification of the sub-topics led to the formulation of five research questions. The research questions with the corresponding sub-topics in parentheses are listed below:

1. **RQ1** How to improve location/ranging estimates in the case of noisy measurements? (ST1, ST2, ST3, ST4)

2. **RQ2** How to detect and possibly mitigate inaccuracies caused by NLoS? (ST4)

3. **RQ3** How to decrease the power consumption of the mobile node? (ST3)

4. **RQ4** How to decrease air-time occupancy? (ST3)

5. **RQ5** How to balance the inherent trade-offs in a real-time location system? (ST1, ST2, ST3, ST4)

These analytical questions focus on improvements by applying procedural, algorithmic, or signal-processing principles to data originating from the positioning system. This is different from focusing on gains attained by altering the hardware or the low-level algorithms implemented in the integrated circuits, which is not in the scope of this thesis.

1.7 Contribution of the Thesis

To respond to the research questions presented in the previous section, the following contributions are presented in this thesis, noting that RQ5 applies to all the points below:

- Firstly, contributing towards RQ1, RQ3, and RQ4 is proposing the first novel AP-TWR protocol for positioning systems. Although the AP-TWR protocol is designed with UWB in mind, its use is not explicitly limited to UWB technology. The proposed protocol allows for flexible configuration of anchor roles in a system, defining the number of active-passive and passive-only anchors. The first of which determines the total number of packets in a ranging sequence, while the latter provides extra range estimates without any additional cost to the air time. Reducing the air time by transmitting fewer packets also lowers the power consumption of the tag. This flexibility permits the positioning system to adapt to various requirements, whether it be prioritizing reduced air time (and power consumption), minimizing ranging errors, or achieving incremental improvements in both aspects (**Publication I**).

- In the quest to improve on the previous results, the research is continued by further developing the aforementioned protocol to provide an alternative way of calculating AP-TWR range estimates. Both AP-TWR methods are paired with 3 of the most common active ranging protocols to provide 6 distinct variations of AP-TWR protocols, which are compared to each other based on their theoretical accuracy, based on numerical simulations. The most promising of which is also tested experimentally to validate the results (**Publication II**).

- Finding an answer to RQ1 and RQ2 was followed by testing and advancing the robustness of the AP-TWR in LoS and NLoS propagation conditions. The previously used Least Squares (LS) method of finding the range estimates from the AP-TWR measurement matrix was compared to 6 other measurement matrix processing techniques. The findings indicated that a few of the tested methods further enhance the robustness of AP-TWR range estimates in NLoS scenarios when compared to the LS method (**Publication III**).

- Similar to the previous contribution, RQ1 and RQ2 were addressed in the position accuracy context by introducing a novel Adaptive Extended Kalman Filter (A-EKF) positioning method, based on AP-TWR. The formulation of which was in turn based on the comprehensive analysis of various possible NLoS cases given in the same publication. The proposed A-EKF positioning method showed a drastic reduction of positioning errors which are caused by NLoS effects in industrial environments (**Publication IV**).

1.8 Thesis Organization

The rest of the thesis is organized as follows:

Section 2 provides the background information on UWB positioning, detailing information on the most commonly used methods and protocols, and giving an overview of the state-of-the-art in this field. **Section 3** presents the formulation, numerical simulations, and experiments of the proposed UWB Active-Passive Two-Way Ranging (AP-TWR) protocols. **Section 4** introduces and experimentally analyzes the measurement matrix processing methods, which provide increased robustness to the AP-TWR range estimates. **Section 5** brings together the insights gained from previous research to propose a novel positioning method based on the AP-TWR protocol. Finally, in **Section 6**, the thesis is concluded, answering the posted research questions and offering future perspectives for research in this field.

2 UWB Technology-Based Positioning

UWB is a radio technology that permits robust transmission of data across a large bandwidth, which exceeds 500 MHz or 20% of the carrier center frequency; considering this, UWB technology is robust and suited for high-density, high data rate, low power, and low interference communications [44]. The IEEE 802.15.4a is an amendment to the IEEE 802.15.4-2006 Standard for Low-Rate Wireless Networks [45] describing additional physical layers to the original standard, which enables precise ranging for UWB devices [46]. While [21, 47] provide an in-depth overview of UWB, readers interested in an extensive overview of UWB-related standards and organizations are encouraged to read the comprehensive article by Coppens *et al.* in [48].

Despite the comparatively higher implementation costs associated with UWB, which necessitates the acquisition of additional devices unlike the widely adopted WiFi technology, it outshines other technologies in terms of its remarkable accuracy and lower power consumption [49]. Moreover, thanks to its high bandwidth and therefore high temporal resolution, UWB is more robust to multipath propagation effects than any other RF technology [33].

The possible methods for implementing positioning in a UWB system are A) the previously discussed fingerprinting based on the Channel Impulse Response (CIR) or power delay profile, B) distance estimation via path loss on RSSI or C) by Angle of Arrival (AoA) estimation. Although in their own right, these methods are sufficient for providing a position estimate, they propose some challenges: indicated by Mazhar *et al.* in [29], fingerprinting is a time-consuming method requiring building up a signal parameter database, which can change over time in the positioning area; the RSSI method is very susceptible to interference caused by multipath propagation; finally, AoA estimation requires nodes equipped with antenna arrays, which subsequently increases the size and cost of the devices.

The remaining prominent positioning techniques for UWB are referred to as follows: 1) Time of Flight (ToF), also known as Time of Arrival (ToA) or Return Time of Flight (RToF), and 2) Time Difference of Arrival (TDoA). The first of which will be addressed as ToF for the rest of the thesis. These methods leverage the exceptional temporal resolution achievable in UWB technology [50], which will be presented in subsequent sections.

As a short introduction, ToF makes use of the relationship between the distance traveled and the propagation time when knowing the propagation velocity of the signal, while TDoA employs the differences of arrival times of an emitted signal. Although TDoA enjoys a minimal impact on the traffic in the network, it, in turn, needs strict synchronization between anchors. Estimating the ToF via Two-Way Ranging (TWR) methods allows for removing stringent synchronization requirements between anchors while posing a drawback by increasing the air time, compared to TDoA [51]. This in turn lowers the achievable tag density and raises the energy consumption in typical ToF methods [52]. Although theoretical analysis and simulations show that ToF and TDoA are identical in their positioning performance, some practical cases show the superiority of ToF methods [53]. Moreover, it is noted that ToF methods are superior when it comes to positioning outside the convex hull defined by the anchors, as it is more agnostic to measurement errors than TDoA [54].

2.1 Methods for UWB Positioning

This section presents the most prevalent methods which are used in UWB-based positioning. There also exist other methods, such as positioning utilizing deep learning on the raw CIR [55], localization based on the analysis of RF signal fading [56], or hybrid systems containing multiple different methods [57], but these are not considered in the scope of

this section, as they are very specific positioning implementations, whereas the following introduces the most well-known methods.

2.1.1 Time of Flight-Based Circular Multilateration

The first time-based method is the previously mentioned ToF, which is based on the measure of one-way propagation time from a transmitter to a receiver. For practical use in a positioning system, the ToF of a signal, t, is converted to a physical distance, d, by multiplying the propagation time by the propagation velocity of the wave, c:

$$d = c \cdot t, \tag{1}$$

The approximate value of the speed of light is $c \approx 3 \cdot 10^8 \text{ms}^{-1}$ (for RF and light-based signals) and the speed of sound $c \approx 340 \text{ms}^{-1}$ (for sound-based signals), although using approximate values introduces systematic errors in the calculations [51]. The values are given as rough estimates to show the cardinality of the two mediums, in reality, the wave velocity depends on various environmental parameters [58].

In Fig. 2, each of the distance values d_i corresponds to a circle centered on the corresponding anchor A_i's location (x_i, y_i). This allows the construction of a system of circle equations that, in an ideal case, intersect at the position of the located object T with coordinates (x, y). In the figure, the concept of circular trilateration is illustrated since the positioning is done by utilizing three distance values [7]. Although similar, the term multilateration is used for disambiguation in cases where four or more distances are used.

It is important to note that the distance-based trilateration/multilateration is not exclusive to ToF methods, as it can also be employed for signal strength-based ranging as will be explained in Section 2.1.4.
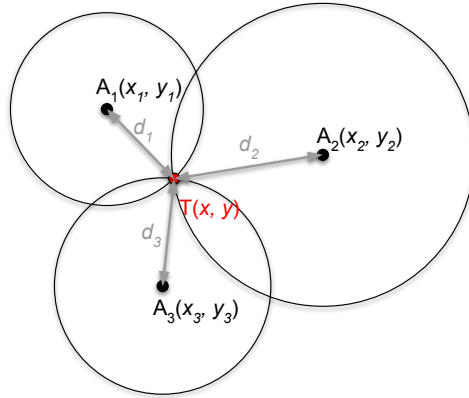
Figure 2: Geometrical representation of trilateration-based position estimation. Fixed anchor nodes A_i located at (x_i, y_i) measure the corresponding distances d_i to the tag T. The position estimate (x, y) of T is found as the intersection point of the circles constructed by (x_i, y_i) and their corresponding distances d_i.

Mathematically, the circular multilateration concept is described as a nonlinear system of equations, which is solved for coordinates x and y of the node T to be located:

$$\begin{bmatrix} d_1 \\ \vdots \\ d_i \end{bmatrix} = \begin{bmatrix} \sqrt{(x-x_1)^2 + (y-y_1)^2} \\ \vdots \\ \sqrt{(x-x_i)^2 + (y-y_i)^2} \end{bmatrix}, i = 1, \cdots, N, \tag{2}$$

20

where $N \geqslant 3$ is the total number of anchor nodes used for the Two-Dimensional (2D) position estimation [51].

Analytically, when dealing with underdetermined lateration cases, it can be seen from Fig. 2 that for the case $N = 2$ there can exist a maximum of 2 intersection points, from which the true location of T can be inferred by setting geometrical constraints on the possible location of the tag. A theoretical single intersection point exists in a degenerate case, where the tag is located on the line which passes through both of the anchors. Even in the case of $N = 1$, the location of the tag can still be found on a circle, allowing it to detect and measure proximity to an anchor.

Since there exist multiple different protocols for ToF estimation, each with their up- and downsides [50], they are separately discussed later in Section 2.2.

2.1.2 Time Difference of Arrival-Based Hyperbolic Multilateration

The second time-based method is TDoA. Although TDoA also utilizes the propagation time of signals, it examines the time differences at which the signal arrives at receivers rather than the absolute propagation time as in ToF. The time differences are then in turn calculated to distance differences $d_i - d_1$ via (1), where $i = 2, \cdots, N$, and N is the total number of anchor nodes taking part in the position estimation. An equation system of hyperbolas is then constructed, and the location estimate (x, y) lies at the intersection of said hyperbolic curves, the process which is called hyperbolic multilateration [7]. The geometric representation of hyperbolic multilateration is illustrated in Fig. 3.
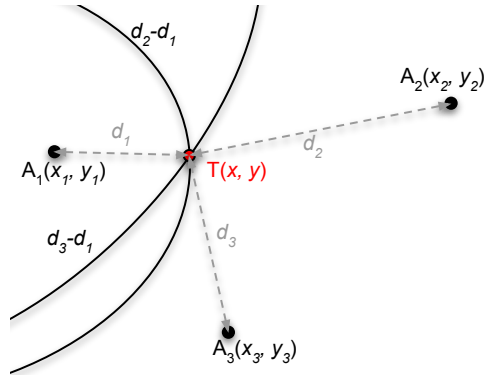
Figure 3: Hypebolic multilateration with TDoA measurements. Fixed anchor nodes A_i located at (x_i, y_i) measure the signal propagation time differences with respect to the reference anchor A_1. A_1 is chosen as the reference node since it is physically the closest to T. The time differences are converted to distance differences $d_3 - d_1$ and $d_2 - d_1$. Gray dotted lines indicate the theoretical distances d_i. The position estimate (x, y) of T is found at the intersection point of the hyperbolas constructed by the locations (x_i, y_i) of anchors A_i and the distance differences $d_3 - d_1$ and $d_2 - d_1$.

In mathematical terms, finding the TDoA position estimate of node T entails the process of solving the following system of equations for x and y:

$$\begin{bmatrix} d_2 - d_1 \\ \vdots \\ d_i - d_1 \end{bmatrix} = \begin{bmatrix} \sqrt{(x-x_2)^2 + (y-y_2)^2} - \sqrt{(x-x_1)^2 + (y-y_1)^2} \\ \vdots \\ \sqrt{(x-x_i)^2 + (y-y_i)^2} - \sqrt{(x-x_1)^2 + (y-y_1)^2} \end{bmatrix}, i = 2, \cdots, N, \quad (3)$$

where N is the total number of anchors taking part in the TDoA-based hyperbolic position estimation. Due to the time difference measurement concept, the underdetermined case

$N = 2$ provides only a parabolic line on which the tag is located, while no information on the position of T can be determined for $N = 1$ [51].

In order to measure TDoA values, the anchors need to be tightly synchronized to each other; for example, an offset of 1 ns translates to an error of 30 cm. On the other hand, since the tag only needs to transmit a single packet over the air for TDoA measurements, this amounts to substantial power saving on the tag hardware [59]. Additionally, transmitting only a single packet per positioning session provides the lowest possible utilization of the RF spectrum i.e. providing the lowest possible air time utilization.

2.1.3 Angle of Arrival-Based Triangulation

As opposed to time-based methods, AoA provides a measurement of the direction which a signal originates from. It is necessary for the nodes to use antenna arrays to estimate the AoA, which in turn requires separate RF front ends for the devices. This has a negative effect on the energy consumption, cost, and complexity of the devices. Another possibility would be to use directional antennas but this requires additional hardware as well. In contrast to ToF and TDoA estimation, AoA requires only two anchor nodes along with their AoA estimates to provide a 2D position estimate. For a 3D estimate, only 3 nodes with their AoA estimates are needed [51]. By providing both the azimuth and elevation angles, it becomes possible to obtain a 3D position estimate using only 2 anchors.

Acquiring 2 direction values from two known anchor nodes allows calculating a position estimate, which is found at the intersection of the 2 Lines of Bearing (LoB) originating from the known receivers. This concept is illustrated in the geometric representation in Fig. 4, where anchor nodes $A_i(x_i, y_i)$ measure their AoA values Θ_i to the position of the mobile node $T(x, y)$.
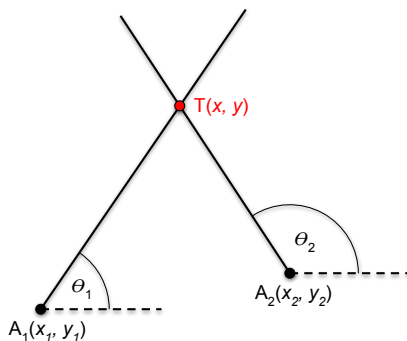
Figure 4: *Geometrical representation of triangulation-based position estimation with AoA measurements. Fixed anchor nodes A_i located at their corresponding coordinates (x_i, y_i) measure the directions Θ_i from which the signal from node T arrives. The position estimate (x, y) for T is found at the intersection point of the LOBs constructed by the anchor coordinates (x_i, y_i) and the measured directions Θ_i.*

The same principle expressed in mathematical terms equates to solving for x and y in the following system of linear equations:

$$
\begin{bmatrix} \tan(\Theta_1) \\ \vdots \\ \tan(\Theta_i) \end{bmatrix} = \begin{bmatrix} \dfrac{y - y_1}{x - x_1} \\ \vdots \\ \dfrac{y - y_i}{x - x_i} \end{bmatrix}, i = 1, \cdots, N, \tag{4}
$$

22

where $N \geqslant 2$ is the total number of anchor nodes taking part in the AoA position estimation.

Compared to other previously mentioned methods, AoA estimation is more complex and very sensitive to a multitude of factors, which cause errors in the position estimate. This is supported by practical comparisons of commercially available UWB-based positioning systems, where a TDoA and AoA hybrid system achieved inferior performance when compared to other TDoA and ToF systems [60]. Among other factors, the design of the antenna array geometry plays an important role in the estimation algorithm, whereas larger anchor-tag distances decrease the accuracy of the system [22].

Although AoA position estimation can be performed using as low as $N = 2$ anchor nodes, the cost reduction of removing one anchor (compared to ToF and TDoA) might not be productive, as the addition of antenna arrays and extra RF components needed for AoA drive up the cost and size of the receiving nodes. On the other hand, AoA estimation does not require strict synchronization between devices, in turn reducing the complexity of an AoA-based positioning system [61].

Analytically, leaning on the geometrical representation of AoA (Fig. 4), positioning with an underdetermined system where $N = 1$, the tag's location can be determined on the LoB defined by the direction and the anchor location; in other words, the tag can theoretically be located on an infinite amount of locations on that line.

2.1.4 Received Signal Strength Indicator-Based Position Estimation

Distinguishing itself from the measurement of propagation time and angle, the RSSI provides insight into the power level of a received signal. This signal property holds significant relevance in wireless positioning systems, as it can be effectively utilized in two key ways. Firstly, the RSSI measure serves as a direct input for fingerprinting techniques, allowing for the creation of signal strength maps and enabling location estimation based on signal characteristics. Secondly, the RSSI value can be employed as a distance estimator in trilateration (multilateration) algorithms, where the relative signal strengths from multiple sources are utilized to determine the position of the target device [62].

To achieve distance estimation based on RSSI, a model is established to establish the relationship between the RSSI value and the corresponding distance. Numerous theoretical and empirical models have been proposed and investigated in the literature for this specific purpose. These models provide a means to map RSSI measurements to distance estimates, facilitating positioning in indoor and outdoor environments [9].

2.2 ToF Estimation Protocols

The ranging protocols discussed in this section make use of additional tag synchronization constraints or increased air time in order to provide ToF estimates, as opposed to the TDoA method, where only the anchors needed to be synchronized.

The following notation for this section is adopted: τ_A is a timestamp value as measured by node A; $t_{A,B}$ and $t_{A,B'}$ are respectively the first and second time interval values measured by node A while communicating with node B; $t_{A \leftrightarrow B}$ is the true propagation time i.e. ToF between node A and B; $\hat{t}_{A \leftrightarrow B}$ is the estimate of the propagation time/ToF value.

2.2.1 One Way Ranging

In its simplest form, the ToF estimation can be carried out by a unidirectional message exchange, One Way Ranging (OWR) [63], which is depicted in Fig. 5, where the time axis is pictured as horizontal black lines. UWB transceiver devices such as the Qorvo DW1000 operate on the basis of accurately determining the timestamps of receiving/transmitting

time instances [64], which are universally noted as τ in this section.

The OWR protocol is as follows: tag node A initiates the ranging process by transmitting a packet at time instance τ_A, anchor node B receives the packet at time instance τ_B, from which, the ToF estimate $\hat{t}_{A \leftrightarrow B}$ (where the true ToF value is $t_{A \leftrightarrow B}$) can be calculated by

$$\hat{t}_{A \leftrightarrow B} = \tau_B - \tau_A. \tag{5}$$
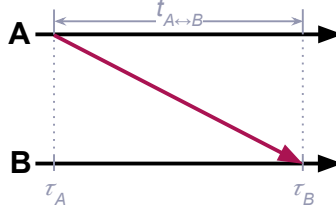
Figure 5: Timing of One-Way Ranging protocol.

Importantly, nodes A and B both have to be synchronized in order to calculate the value of $t_{A \leftrightarrow B}$ [65], setting it apart from TDoA, where only the anchors need to be synchronized. Practically, this turns out to be extremely difficult, as all of the nodes are physically spaced far apart, which makes wired synchronization extremely impractical [50]. In order to remove the need for synchronization, other methods are introduced, which are further discussed below.

2.2.2 Single-Sided Two-Way Ranging

The Single-Sided Two-Way Ranging (SS-TWR) is introduced to remove the need for node synchronization at the cost of an additional packet in the ranging sequence. SS-TWR relies on a bidirectional packet exchange, which is illustrated in Fig. 6. Although SS-TWR (and further methods) internally rely on the receive/transmit timestamps, rather than using the timestamp difference, the notation of time interval values (e.g. t_1, where $t_1 = \tau_2 - \tau_1$) is introduced and used further on in the thesis to keep the equations compact. The topic of relating the time intervals with timestamp differences is addressed in Appendix II of publication II.

Node A initiates the ranging sequence by transmitting a packet, which node B receives. After a processing delay $t_{B,A}$ (read as the time interval measured by B, while communicating with A), node B transmits its response. After receiving B's response, A records the time interval $t_{A,B}$. The ToF estimate $\hat{t}_{A \leftrightarrow B}$ is then calculated via

$$\hat{t}_{A \leftrightarrow B} = \frac{t_{A,B} - t_{B,A}}{2}. \tag{6}$$

Fig. 6 features a dotted line on the time axis, to emphasize the difference of time scales of the ToF $t_{A \leftrightarrow B}$ and the measured time intervals $t_{B,A}$ and $t_{A,B}$, as the former is in order of tens of nanoseconds, while the latter is in hundreds of microseconds [66].

In order to analyze the clock offset error for SS-TWR, eq. (5c) of [66] is adapted to the notation of this thesis, giving the following expression:

$$\hat{t}_{A \leftrightarrow B} - t_{A \leftrightarrow B} = e_A \cdot t_{A \leftrightarrow B} + \frac{t_{B,A}}{2}(e_A - e_B), \tag{7}$$
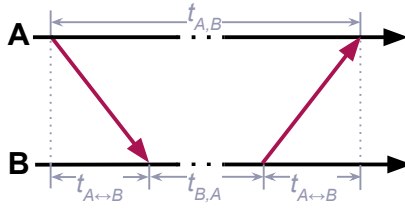
Figure 6: Timing of Single-Sided Two-Way Ranging protocol.

where the ToF estimation error $\hat{t}_{A\leftrightarrow B} - t_{A\leftrightarrow B}$ is computed using the frequency deviations (typically measured in parts per million, PPM) e_A and e_B of nodes A and B, respectively. Since $t_{B,A}$ is several orders of magnitude larger than $t_{A\leftrightarrow B}$, we see that it is the dominant factor in determining the size of the error, which could translate into ranging errors of several meters. The derivation and in-depth analysis of the error are given in [66].

However, Dotlic *et al.* proposed using the Carrier Frequency Offset (CFO) method to mitigate the frequency offset errors for SS-TWR. A device such as the DW1000 transceiver inherently measures the relative clock offset of two communicating devices, making it possible to correct the clock offset errors [67], therefore achieving a much smaller error:

$$\hat{t}_{A\leftrightarrow B} - t_{A\leftrightarrow B} = e_A \cdot t_{A\leftrightarrow B}. \tag{8}$$

2.2.3 Symmetrical Double-Sided Two-Way Ranging

The Symmetrical Double-Sided Two-Way Ranging (SDS-TWR) and the following protocols add an additional packet to the ranging sequence when compared to SS-TWR. The timing diagram of SDS-TWR is given in Fig. 7.

Similar to SS-TWR, SDS-TWR starts out with a packet transmitted by A, after which B sends its reply. Here, the SDS-TWR protocol adds a third, final packet transmitted by node A, which concludes the ranging sequence. Here, both nodes record two separate time interval values, which are used to calculate the ToF estimate $\hat{t}_{A\leftrightarrow B}$ with

$$\hat{t}_{A\leftrightarrow B} = \frac{t_{A,B} - t_{A,B'} + t_{B,A'} - t_{B,A}}{4}. \tag{9}$$
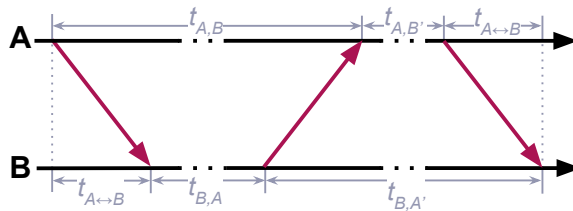
Figure 7: Timing of Symmetrical and Alternative Double-Sided Two-Way Ranging protocol.

The error expression for SDS-TWR is adopted from (18) of [68] to formulate

$$\hat{t}_{A\leftrightarrow B} - t_{A\leftrightarrow B} = \frac{1}{2}t_{A\leftrightarrow B}(e_A + e_B) + \frac{1}{4}(e_A - e_B)(t_{B,A} - t_{A,B'}), \tag{10}$$

25

from which we see that this expression will achieve a minimum when $t_{B,A}$ and $t_{A,B'}$ are equal, canceling out the final term of (10), resulting in

$$\hat{t}_{A \leftrightarrow B} - t_{A \leftrightarrow B} = \frac{1}{2} t_{A \leftrightarrow B} (e_A + e_B). \tag{11}$$

From the remaining term, we see that the clock offset errors of A and B are averaged. Although the clock drift error is brought down, ensuring the symmetry of $t_{B,A}$ and $t_{A,B'}$ in practice is rather challenging, while also making the whole packet exchange process longer than fundamentally required [69].

2.2.4 Alternative Double-Sided Two-Way Ranging

The need to eliminate the symmetry constraint of SDS-TWR motivated the development of the Alternative Double-Sided Two-Way Ranging (AltDS-TWR), proposed in [66].

The two-way packet exchange of AltDS-TWR is identical to the SDS-TWR as seen in Fig. 7, while the calculation of the ToF estimates $\hat{t}_{A \leftrightarrow B}$ is carried out alternatively:

$$\hat{t}_{A \leftrightarrow B} = \frac{t_{A,B} \cdot t_{B,A'} - t_{A,B'} \cdot t_{B,A}}{2(t_{B,A} + t_{B,A'})} \tag{12a}$$

$$\hat{t}_{A \leftrightarrow B} = \frac{t_{A,B} \cdot t_{B,A'} - t_{A,B'} \cdot t_{B,A}}{2(t_{A,B} + t_{A,B'})} \tag{12b}$$

$$\hat{t}_{A \leftrightarrow B} = \frac{t_{A,B} \cdot t_{B,A'} - t_{A,B'} \cdot t_{B,A}}{t_{B,A} + t_{B,A'} + t_{A,B} + t_{A,B'}}, \tag{12c}$$

resulting in three separate equations to estimate the ToF. Following the denominator of equation (12a), we see that it uses node B's time interval, while the denominator of equation (12b) includes the times of node A. Theoretically, it would be possible to use the times of both, A and B, as is done in equation (12c), but this is undesirable, as the error of both devices remain included in the calculation. This is illustrated in the respective error expressions

$$\hat{t}_{A \leftrightarrow B} - t_{A \leftrightarrow B} = k_B \cdot t_{A \leftrightarrow B} - t_{A \leftrightarrow B} = e_B \cdot t_{A \leftrightarrow B} \tag{13a}$$

$$\hat{t}_{A \leftrightarrow B} - t_{A \leftrightarrow B} = k_A \cdot t_{A \leftrightarrow B} - t_{A \leftrightarrow B} = e_A \cdot t_{A \leftrightarrow B} \tag{13b}$$

$$\hat{t}_{A \leftrightarrow B} - t_{A \leftrightarrow B} = \hat{t}_{A \leftrightarrow B} - \frac{k_A \cdot k_B (t_{A,B} \cdot t_{B,A'} - t_{A,B'} \cdot t_{B,A})}{k_A (t_{B,A} + t_{B,A'}) + k_B (t_{A,B} + t_{A,B'})}, \tag{13c}$$

where $k_A = 1 + e_A$ and $k_B = 1 + e_B$. The proofs of the error expressions can be found by following [66]. Calculating the ToF estimate via (12a) or (12b) yields errors (13a) (13b), respectively, which are in the same order of magnitude as the CFO corrected SS-TWR (8). Important to note that (13a) and (13b) suggest that the final ToF estimation error can be made dependent on either node, offering the choice to base the calculations on the information of the node with a more accurate clock source.

2.2.5 Asymmetrical Double-Sided Two-Way Ranging

Jiang and Leung proposed the Asymmetrical Double-Sided Two-Way Ranging (ADS-TWR) protocol in [69]. The main packet exchange concept is similar to SDS-TWR and AltDS-TWR, with the exception of setting the second reply time ($t_{A,B'}$ for SDS and AltDS-TWR) to zero, as pictured in Fig. 8. This yields the calculation of the ToF estimate $\hat{t}_{A \leftrightarrow B}$ by

$$\hat{t}_{A \leftrightarrow B} = \frac{t_{A,B} + t_{B,A'} - t_{B,A}}{4}, \tag{14}$$

for which the equivalent ToF error expression is written as

$$\hat{t}_{A\leftrightarrow B} - t_{A\leftrightarrow B} = \frac{1}{2}t_{A\leftrightarrow B}(e_A + e_B) + \frac{1}{4}t_{B,A}(e_A - e_B). \tag{15}$$

The second term of (15) is the dominant factor in the error, since $t_{A\leftrightarrow B} << t_{B,A}$, meaning that the ToF error is greatly dependent on $t_{B,A}$.
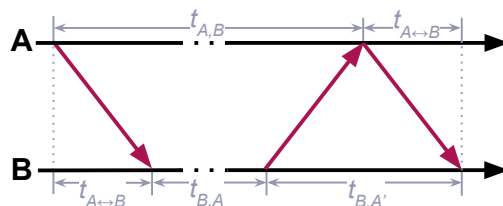
Figure 8: Timing of Asymmetrical Double-Sided Two-Way Ranging protocol.

Additionally, ADS-TWR poses some limitations due to setting the second reply time zero, as it is practically impossible to ensure an instant reply, meaning that a certain reply delay will always exist [65, 68].

2.2.6 Discussion

The used ranging protocol needs to accommodate the design needs of a ToF-based positioning system. In other words, the choice of a ranging protocol is dictated by the specific use case, depending on whether the positioning needs to take place in the mobile node itself (local positioning) or in a central server (central positioning), such that all of the needed information is present at that specific localizing node.

Furthermore, the choice of the initiator of a ranging session needs to be considered accordingly, to make sure that all the ranging data is present at the position estimator. If the data is not inherently present, the protocol needs to be adjusted to communicate the data back to the position estimator.

Additionally, the amount of data needed to send over the air affects the payload duration, which in turn influences the total time spent transmitting/receiving each of the packets. This length of time dictates the energy consumption of a tag [70] and the usage of the shared RF spectrum. Since the choice of ToF ranging protocol directly dictates the amount of data needed to transmit, it is a vital aspect to consider.

The choice of the ranging protocol also determines the power consumption of a UWB device in other ways. For example, the popular Qorvo DW1000 UWB transceiver [64] consumes more current in the receive mode when compared to the transmit mode (respectively, 150 mA vs 130 mA in [50]), while the consumption in sleep or deep sleep modes is multitudes lower (1 µA vs 50-100 nA, respectively) [70]. Consequently, in order to conserve energy in the tag, the protocol must be chosen such that the tag does not have to operate in transmit or receive modes for extended periods of time. The power consumption is reduced for tag-initiated protocols, as the tag can stay in a low power state until waking up by initiating the ranging sequence and returning to a low power state after the ranging sequence has been completed.

Although Publication II gives a short overview of some of the ToF ranging protocols, this section provides a more in-depth look at the protocols. Table 2 summarizes the most

important aspects of each of the discussed ToF ranging protocols, utilizing an aggregated transmission of packets where possible, as this conserves the air time and also consumed energy [71]. Meaning that if possible, the tag does not communicate with every single anchor, but rather sends a single broadcast packet to all of the anchors. Both, the central and local positioning schemes are considered, assuming that the central positioning schemes utilize a separate data transport backhaul from the anchors to the server to minimize the impact on the air time, while local schemes must utilize wireless data transport. The local/central schemes are in turn divided into categories for tag and anchor-initiated ranging sequences.

All of the resulting sub-classes of ToF protocols are then analyzed by the number of time interval values needed to send over the air (which dictate the length of the payload), most of which are dependent on the total number of anchors partaking in the ranging sequence, N. The values in parentheses note the total number of time interval values, which are sent in separate but naturally present packets in the protocol as the values without parenthesis denote the number of values sent in a single, final packet. Then the number of packets in a protocol is given as a function of the number of anchors N and the need for an additional (from a ranging standpoint redundant) packet to convey the needed information back to the positioning node, dictated by the positioning scheme. After which, the total number of packets in the protocol sub-classes is given. The robustness penalty of a system is a result in some of the sub-classes where the needed information is aggregated to, and transmitted from a single anchor (rather than sending the information from all of the anchors separately), resulting in a single point of failure where the loss of this packet renders the whole ranging sequence to be lost. Then, a rating (0 to 5 points) is given, 0 being the lowest score and 5 being the highest score for the applicability of the protocol in that specific sub-class. The derivation of the rating system is given in Appendix 5, alongside a figure used for the visualization of the protocols.

While OWR and ADS-TWR bolster rather high ratings, they are not considered in the scope of publications I - IV and in this thesis due to the constraint on the practicality of their use, as OWR requires strict synchronization between all nodes and ADS-TWR requires to have zero reply time in its transmission.

The following analysis of Table 2 in this section shifts the focus to the practically feasible protocols SS-TWR, SDS-TWR, and AltDS-TWR. It can be observed that the highest-rated ranging protocol for a local positioning system is tag-initiated SS-TWR, as it utilizes the shortest payload, while also providing the lowest total number of packets with no additional data transport packets and no robustness penalty.

The results for the central positioning schemes are closer, with tag-initiated SS-TWR, AltDS-TWR, and SDS-TWR scoring 3.61, 3.36, and 2.79, respectively. Although SS-TWR and AltDS-TWR both utilize the same total amount of packets in a ranging sequence ($N+2$), SS-TWR has a slight advantage on the number of data needed to transfer over the air(N for SS-TWR and $2N$ for AltDS-TWR). The SDS-TWR protocol sustains a lower rating, as the total number of packets in a ranging sequence is greatly increased to $2N+1$.

Table 2: Summary of the most popular ToF ranging protocols.

ToF method	Scheme	Initiator	Values	Packets	Added packet	Total packets	Robust. pen.	Rating	Comment
OWR	Central	T	1	1	No	1	No	5.00	Not practical (synchronization)
	Central	A	N	N	Yes	N+1	No	1.89	Not practical (synchronization), added packet: assuming aggregated response from T
	Local	T	N	1	Yes	2	Yes	3.96	Not practical (synchronization), added packet: aggregated response from only one of A's (robustness penalty)
	Local	A	(N)	N	No	N	No	2.18	Not practical (synchronization)
SS-TWR	Central	T	N	N+1	Yes	N+2	No	3.61	Added packet: assuming aggregated response from T
	Central	A	N	N+1	No	N+1	No	1.89	Added packet: assuming aggregated response from T
	Local	T	(N)	N+1	No	N+1	No	3.89	-
	Local	A	N	N+1	Yes	N+2	Yes	1.11	Added packet: aggregated response from only one of A's (robustness penalty)
SDS-TWR	Central	T	(2N)	2N+1	No	2N+1	No	2.79	-
	Central	A	2N	2N+1	Yes	2N+2	No	0.50	Added packet: assuming aggregated response from T
	Local	T	2N	2N+1	Yes	2N+2	Yes	2.00	Added packet: aggregated response from only one of A's (robustness penalty)
	Local	A	(2N)	2N+1	No	2N+1	No	0.79	-
AltDS-TWR	Central	T	2N	N+2	No	N+2	No	3.36	-
	Central	A	2N	2N+1	Yes	2N+2	No	0.50	Added packet: assuming aggregated response from T
	Local	T	2N	N+2	Yes	N+3	Yes	2.57	Added packet: aggregated response from only one of A's (robustness penalty)
	Local	A	(2N)	2N+1	No	2N+1	No	0.79	-
ADS-TWR	Central	T	(N)	2N+1	No	2N+1	No	3.04	Not practical (zero response time)
	Central	A	2N	2N+1	Yes	2N+2	No	0.50	Not practical (zero response time), added packet: assuming aggregated response from T
	Local	T	2N	2N+1	Yes	2N+2	Yes	2.00	Not practical (zero response time), added packet: aggregated response from only one of A's (robustness penalty)
	Local	A	(N)	2N+1	No	2N+1	No	1.04	Not practical (zero response time)

2.3 State-of-the-Art

According to Pascacio *et al.*, ToF and TDoA methods, when viewed separately, are less popular than the RSSI technique, as ToF and TDoA techniques both separately amass 23% of the papers as compared to the RSSI topic at 38% [38]. When viewing ToF and TDoA as consolidated time-based methods, we see that the combined research interest is higher (summing to 46%) than that of the RSSI method. This is due to the previously mentioned fact that utilizing the time-based methods in UWB is desired, providing higher accuracy and robustness against multipath.

Since ToF and TDoA have their own pros and cons, the notion of passive TWR is introduced to address the downsides of both. Passive ranging makes use of the fixed and known locations of anchors to provide ranging capabilities for passive anchors; those passive anchors do not actively take part in the packet exchange between anchors and a tag, therefore not affecting the air time. The active TWR coupled with passive ranging provides the positioning system with the same number of input data at a significantly reduced air time occupancy without the need for synchronization, providing a middle ground between the ToF and TDoA methods.

Conventionally, positioning systems assume that the tag is within the convex hull defined by the locations of the anchors [72] because it is the area of the highest precision [73]. As research has shown, the ToF-based positioning methods are more robust in positioning outside of the convex hull than TDoA methods [54]. An overview of the state-of-the-art for passive estimation and the recent advances in ToF-based NLoS-robust positioning is given in the next section.

2.3.1 Passive Estimation

In one of the seminal works presented by Fujiwara *et al.* in [72], where they developed and evaluated a hybrid UWB system, combining the usage of ToF and TDoA. This allowed for reducing the number of needed anchors compared to TDoA, while also reducing the impact of air time occupancy compared to ToF systems, but having a downside that the synchronization of nodes is still needed.

Next, Dotlic *et al.* proposed the CFO-correction and Asynchronous TDoA (A-TDoA) method, which permits the usage of a hybrid system, where the TDoA estimation functions without the use of synchronization between the anchors [67]. Similarly, Sidorenko *et al.* addressed the problems of hardware delay uncertainty, signal power level and clock drift in a ToF and TDoA fusion method [74].

The work of Fujiwara *et al.* was studied from a theoretical standpoint by Sahinoglu and Gezici in [75], deriving a Maximum Likelihood Estimator (MLE) for the hybrid method and assessing its theoretical limits on the accuracy by deriving the Cramer-Rao lower bound. Building upon this, Gholami *et al.* propose a more robust method by acquiring the solution from an intersection of convex sets from measurements, as the previously developed MLE might converge to local minima.

Gholami *et al.* further develop the usage of the ToF/TDoA hybrid system in [76, 77], to increase the number of tags as well as including them as TDoA estimators further contributing to the position estimation and improving on the accuracy.

Wang and Xiong proposed the Two-Way Time of Arrival with Correction (TW-ToA-C) [78], in which they employ passive anchors listening in on anchor-initiated active SS-TWR messaging, in the presence of clock errors. By transmitting a correction packet after a known correction time interval, the interval can be used to determine the relative clock offsets of each node. The addition of an extra packet in the SS-TWR scheme allows to greatly reduce the clock offset errors for both, the active and passive range estimates.

Noting that the SS-TWR protocol in this publication utilizes separate transmissions for data transport, increasing the overhead of air time.

Similarly, Hepp *et al.* present and experimentally validate a quadcopter-mounted system, which positions the tag located outside of the convex hull defined by the anchors [54]. The authors utilize an anchor-initiated SDS-TWR, consisting of 4 packets in the ranging sequence (the standard 3 packets of SDS-TWR plus a single wireless data transfer packet from the tag), while the passive anchors listen in on the transmissions, producing a protocol that achieves lower air time and reduced clock errors.

Horváth *et al.* developed Passive Extended (PE) ranging [79] by combining passive ranging with anchor-initiated SDS-TWR, achieving higher accuracy of positioning with the addition of the third packet in the SDS-TWR ranging sequence. With the addition of passive anchors in the PE ranging, a 2D or 3D position estimate can be calculated with only 3 exchanged packets in the ranging session, while active SDS-TWR needs respectively 9 and 12 packets. For reference, the number of packets for other ranging protocols can be calculated using column *Total packets* of table 2, by substituting $N = 3$ for 2D positioning and $N = 4$ for 3D positioning. In [80] the same authors improved on the PE ranging by introducing the alternative calculation of AltDS-TWR, making the protocol more robust against clock errors.

Shah and Demeechai proposed three Multiple Simultaneous Ranging methods (named MSR1 to MSR3) in [81] which make use of an active anchor communicating with the tag, and multiple passive anchors listening to the packet exchange. The MSR1 method employs a tag-initiated three-packet ranging sequence in which the tag sends the first and third packets while the active anchor transmits the second one, effectively overcoming the tag's increased power consumption of anchor-initiated protocols. The MSR2 method employs a similar packet exchange with four packets, with the exception that the initiator is the anchor: the first and third packet is transmitted by the active anchor, and the second and the fourth by the tag, as the extra packet is needed for wireless data transfer to the anchor. Additionally, a third method called MSR3 was proposed, which employs only a two-packet exchange initiated by the active anchor, further improving the air time efficiency of MSR1. Results show that the MSR methods offer a significant reduction of air time occupancy at the expense of slightly higher ranging RMSE (compared to an active-only ranging protocol) while offering similar performance to Horváth's AltDS-TWR-based PE ranging.

Mohammadmoradi *et al.* propose the Simultaneous Ranging and Communication (SRAC) protocol, where they utilize, in addition to the specific ranging packets, the existing communication packets to provide passive range estimates [82]. The proposed scheduling algorithm was experimentally validated to show that the measurement errors were well under 10 centimeters.

Chen *et al.* proposed the UWB-based PnPLoc (Plug & Play Localization), a scalable, synchronization-free TDoA-based positioning system in [83]. The resulting positioning system is a local scheme, i.e. the location estimation is performed on the tag, with the anchors ranging between each other using AltDS-TWR while the tag passively acquires the TDoA values by listening to the transmissions of the anchors. This allows the tag to locally provide a position estimate by remaining only in receive mode, while the AltDS-TWR provides inter-anchor distances for the anchor deployment algorithm.

Shah *et al.* further explored the benefits of passive ranging by employing a similar concept in UWB antenna delay calibration, reducing the number of packets while maintaining similar accuracy as the manufacturer suggested method [84]. The use of MSR methods allowed the development of a system that allows simultaneous ranging and antenna delay calibration [85] and an altogether antenna delay-independent ranging protocol [86].

2.3.2 Robust Estimators

Skipping ahead for a moment: since the AP-TWR protocols (proposed in Publications I and II and detailed in Section 3) simultaneously provide multiple ranging values for each anchor, some methods for processing the resulting ranging values needed to be explored. While the timestamp measurement noise is Gaussian [59], the NLoS propagation conditions could still translate into rather large ranging errors [87], and some applicable methods were investigated to lessen their impact of them.

Contrary to other ranging protocols, where the time series of the ranging value can be filtered across temporally spaced samples, the AP-TWR measurement matrix processing offers the possibility to additionally filter ranging values obtained in a single ranging sequence, as the values are estimated practically simultaneously. This concept makes it similar to ensemble averaging [88], where sets of observations are averaged to reduce the effect of errors originating from individual sets. As the AP-TWR measurement matrix concept is novel (in the sense that no previous research in this specific field was published before), and is now active and evolving, this section provides a non-comprehensive overview of applicable methods.

When estimating a constant from a vector of equally noisy measurements, one of the most trivial solutions is the LS estimation, as the solution simplifies to calculating the arithmetic average of all elements. In the case of a vector with measurements with variable noise, such as in the rows of an AP-TWR measurement matrix (18), the weighted least squares (WLS) method can be used, where the reciprocals of noise covariance are used as the weights, resulting in a weighted average [89]. Various methods of generating the weights for WLS are discussed in Section 4 and Publication III.

Compared to LS estimation, finding the median of a set is considered a more robust estimator, as it provides a fitting solution even in the presence of outliers [90]. This concept is further explored in [91], employing a parametric outlier removal based on a set's Mean Absolute Deviation (MAD), providing a flexible and robust method of outlier removal.

Commonly used as a method for interpolating a continuous surface from sparse data points, the Inverse Distance Weighting (IDW) method can also be used as a one-dimensional estimator by giving higher weights to values situated around the arithmetic mean of a set [92]. Similarly named, but an altogether different method of Distance Weighted Estimator (DWE) was proposed in [93] as an alternative to calculating a trimmed mean value. As opposed to IDW, the mean value of the set is not needed to calculate. Instead, the weights for WLS are formed on the basis of the average distance of an element to each member of the set.

2.3.3 NLoS Mitigation Based on Ranging and Residuals

Borras *et al.* proposed a binary decision framework consisting of 5 different test cases based on modeling the range measurements corrupted by NLoS-induced systematic error [94]. Since the information on the LoS and NLoS statistical parameters is needed, the running estimates of these parameters are calculated. The running estimates of statistical parameters in turn pose a problem for moving objects, as the parameters change over time.

Chen's Residual Weighting Algorithm (Rwgh) [95] offers an NLoS mitigation algorithm based on the residuals of positioning, omitting the need for *a priori* information. The algorithm is based on forming every possible subset of the available ranging values, calculating the position estimate of each subset, finding the normalized residual, and weighting each position estimate with it to provide a final position estimate. Although the results show a significant reduction in positioning errors, the computational complexity grows exponen-

tially as the number of input distances increases.

The issue of the computational complexity is addressed by the further developments of the Rwgh: Select Residual Weighting (SRwgh) [96], Lower-Computational-Cost Residual Weighting (LCC-Rwgh) [97], and Iterative Minimum Residual (IMR) [98] algorithms. Although the proposed methods significantly reduce the number of intermediate estimates of the final position estimate while also achieving comparable error performance to the Rwgh, the computational complexity is still rather high, needing at least tens of intermediate iterations, even for a small number of inputs [99]. Similarly, Yang and Wang reduced the mean error of a Bluetooth/UWB hybrid RSSI model-based positioning system with their iterative take on weighting the range estimates with residuals [100].

Chan *et al.* proposed identifying the set of LoS range estimates and performing the positioning with only those ranging values [101]. Firstly, a position estimate with all N distances is calculated, then a residual test is employed by comparing the residuals to a constant threshold. If only a small fraction of the residuals are over the threshold, the final position estimate has been found. If not, then subsets of $N-1$ anchors are formed and the process continues until the minimum amount of distance values is achieved (3 distances for 2D positioning, 4 for 3D positioning). This leads to additional latency and higher errors in cases where the number of final distances is low, as omitting range estimates rids of input distances, where discarded NLoS distances could even contain valuable information for position estimation.

Silva and Hancke studied detecting the presence of NLoS from statistical parameters calculated from residuals, such as mean, maximum, SD, and sum of squares [102]. The results suggest that the latter provides the best discrimination of NLoS presence using a Naive Bayes Classifier, offering very high accuracy, whereas the identification of individual NLoS range estimates provides low accuracy.

The authors of [103] proposed a through-the-wall ranging model, which uses the floor plans and the knowledge of the relative permittivity of walls to correct the NLoS range estimates and perform localization. Since the floor plans, wall thicknesses, and their relative permittivity are highly site-specific, setting up such a system needs a sizable amount of *a priori* information and/or time-consuming site surveying. Similarly, [104] used a known map layout to reduce the NLoS ranging error according to the position of the tag, anchors, and the obstacles in between.

2.3.4 NLoS Mitigation Based on Channel Impulse Response

A sizable amount of research has been conducted on the CIR of UWB devices. Using the CIR in UWB positioning has an upside as no historical time series data is not needed, as a CIR can be extracted per each tag-anchor pair separately during individual ranging sequences. Papers such as [105, 55] utilize Convolutional Neural Networks (CNN) for position estimation directly from the extracted CIR, which provide promising results even in high NLoS conditions, but need large amounts of training data and are dependent on the positioning environment.

Other works investigate the use of CIR statistics as an input to NLoS Detection and mitigation, such as [106] where smaller weights are assigned to NLoS-biased range estimates. Similarly, there exist several machine learning (ML) methods utilizing CIR statistics, such as Least-Squares Support-Vector Machines (LS-SVM) [107], Sparse Pseudo-Input Gaussian Process [108], Expectation-Maximization Gaussian Mixture Model [109], genetic algorithm-based feature subset selection SVM [110], CNN and Long Short-Term Memory (LSTM) [111], One-Dimensional Wavelet Packet Analysis with CNN [112], Multilayer Perceptron (MLP) [113], Capsule Networks [114], Morlet Wavelet Transform and CNN [115], CNN

and MLP [116], transformer deep learning model [117], etc.

Kim *et al.* proposed a method to overcome the limitations that site-specific data pose to the deployment of a system by performing LSTM training on raw CIR, to detect the magnitude of NLoS errors and the variance of measurements [118]. The corrected ranging data alongside the classified error variance are then used as inputs to an EKF-based position estimator.

In addition to ML, some other methods of using raw CIR exist: NLoS detection using fuzzy theory [119, 120], CIR-based fingerprinting [121], LoS/NLoS detection via probability density functions [122], optimal anchor selection by channel quality evaluation of the CIR [123], etc.

2.3.5 NLoS Mitigation Based on Received Signal Parameters

Wu *et al.* proposed an NLoS mitigation technique based on the path loss model of UWB signals [124]. The method showed promising results but is impaired by the fluctuating nature of the received signal power, as environmental factors such as obstacles, reflections, etc. cause signal interference and attenuation, as is also the case for RSSI-based positioning methods.

Schroeder *et al.* assumed that a sudden decrease of the Signal-to-Noise Ratio (SNR) indicates a move from an LoS to an NLoS environment, while an increase in SNR means a move from NLoS to LoS [125]. This infers the usage of historical time series data, introducing latency to the positioning.

Barral *et al.* introduced several ML methods for detecting and mitigating NLoS based on averaged ranging and RSSI data; even though the accuracy and performance of mitigation show promising results, the authors expressed doubts about the generality of such methods, as performance is rather dependent on the scenario and location on which the training data was captured [126].

Another well-researched area is the usage of UWB receive quality parameters reported by the DW1000 transceiver [64]. Parameters such as first path amplitude points 1-3, preamble accumulation count, CIR amplitude, accumulator data noise standard deviation, etc. are used as inputs to numerous machine learning methods in [127, 128], logistic regression [129], devised power-performance metric-based decision [130], fuzzy inference of parameters [131]. Even though such methods show promising accuracy, the models can be rather dependent on the specific conditions where the data was captured in, as typically the papers train and validate their models based on data from the same environment.

2.3.6 Discussion

The earliest works regarding passive anchors in UWB positioning systems include ToF/TDoA hybrid systems, which have higher implementation complexity, as the position estimation equations need to account for both positioning methods. Before the advent of the CFO correction, publications addressed correcting the clock offset errors by introducing additional packets in the ranging protocol, decreasing the overall air time efficiency. On the other hand, many papers utilize anchor-initiated ranging protocols, which focus on increasing the air time efficiency but at the same time increase the energy consumption of the tag, translating to shorter battery life. Additionally, since the packet exchange is conducted between only a single active anchor and a tag, a critical point of failure is created, i.e. if the single active ranging exchange malfunctions, all the accompanying passive range estimates are deemed to fail as well.

Chen *et al.* proposed a UWB positioning system utilizing clever reversal of roles: the

anchors range with each other while the tags listen to their packet exchange. This system is limited by providing only a local positioning scheme, meaning that the positioning takes place at the tag, providing a user the position information on only itself. In many cases, however, indoor positioning systems require a centralized approach, as a number of assets need to be tracked simultaneously in real-time. This includes use cases such as warehouse safety and management [132], industrial manufacturing [133], logistics management [21], sports tracking [134], navigation of multiple unmanned aerial vehicles [135], etc.

In contrast to the state-of-the-art papers, the Active-Passive Two-Way Ranging protocols proposed in this thesis (Chapter 3, and Publications I and II) offer a generalized approach to passive ToF ranging, which allows defining multiple active-passive and passive-only anchors. This has several benefits for use in a central scheme positioning system, as the generalized active-passive protocol allows a flexible choice between improved air time efficiency and improved robustness/accuracy (or improvements to both) while offering a lower power consumption for the tag, as the ranging sequence is initiated by the tag. Depending on the specific implementation of the system, the passive range estimates can be calculated in the anchor, in the central server, or partly in both. Moreover, the overall length of the protocol is optimized as well, so the least amount of data is transmitted over the air, keeping the air time as low as possible. An additional upside comes from the fact that the calculation of passive range estimates benefits from being agnostic to systematic errors originating from calibration, as stated by Shah *et al*.

Range-based methods rely on *a priori* distributions of errors or have latency due to running calculation of parameters. Along with raw CIR and signal parameter-based methods, the range-based methods provide NLoS detection prior to position estimation. This is not the case for residual-based methods, as they typically entail computationally complex iterative methods, calculating position estimates and comparing or weighting based on the resulting residuals.

Regardless of the fact that the methods utilizing raw CIR samples provide rather high performance for NLoS detection and mitigation, the scalability of said methods is poor when used in real-time applications. While small-scale and low update rate systems could greatly benefit from the raw CIR-based methods, increasing the number of tags or their position update rate degrades the real-time positioning performance, as extracting the CIR of a transceiver is a time-consuming process. Barral *et al*. [126] state that acquiring the CIR samples from an anchor could take about 300 ms, which limits the maximum position update rate to 3.33 Hz for one tag, meaning that each additional tag further reduces the achievable update rate. Since UWB positioning systems offer high update rates, such as the Pozyx system with up to 60 Hz per tag [136], the raw CIR methods drastically reduce the potential of an UWB-based Real-Time Location System (RTLS).

Machine learning models offer accurate NLoS detection and mitigation; however, these methods need large quantities of training data, which can also be site-specific. This means that the generated models are not applicable to a wide range of scenarios that the positioning system may be subjected to. Although some methods manage to circumvent the problem, they still need vast amounts of data to train a model, making the implementation of said models quite a tedious process. Although the computational load of training models is not often discussed, it is highlighted by Jiang *et al*. [111], stating that their research required a high-end computer, which took over an hour of real computing time to complete a single model. Assuming that models have to be refined and re-trained multiple times, this could amount to significant time consumption.

Compared to the state-of-the-art, the introduction of AP-TWR opens up new possibilities for position estimation. Firstly, the addition of each active-passive anchor simul-

taneously provides extra passive range estimates for all other anchors. This approach enables independent filtering of the data for each ranging sequence, eliminating additional filtering latency. In contrast, traditional methods filter temporally successive samples, which can introduce additional latency. The range estimate filtering methods made available by the usage of AP-TWR are addressed in more detail in Publication III. Secondly, the AP-TWR measurement matrix concept allows the calculation of statistical parameters for each ranging sequence separately, paving the way to the Adaptive Extended Kalman Filter (A-EKF) positioning in Publication IV. This method does not introduce additional latency to the positioning, is computationally efficient and scalable, and does not need any *a priori* information in order to reduce the effects of NLoS propagation.

The following three sections give an overview of the publications on which this thesis is based. Section 3 presents the proposed generalized AP-TWR methods, Section 4 gives an overview of the tested filtering methods for AP-TWR protocols, and Section 5 concludes the overview of the publications by including the results of the previous publications into formulating the proposed A-EKF positioning method.

3 Proposed Active-Passive Two-Way Ranging Protocols

In this section, two separate generalized AP-TWR protocols are developed, which address the shortcomings of both the ToF and TDoA estimation-based positioning systems. Unlike traditional passive ranging methods which prioritize air-time efficiency, the generalized AP-TWR protocols allow the flexibility to cater the protocol towards air-time efficiency, or increased robustness and accuracy. This section provides the theoretical basis for the proposed AP-TWR protocols, which are validated by numerical simulations and experiments, and analyzed based on the achieved results. While the AP-TWR protocol developed in this thesis has a primary focus on UWB technology, it is important to highlight that the protocol is not solely restricted to UWB and can be applied to other technologies utilizing TWR as well.

This section is based on Publications I and II:

- T. Laadung, S. Ulp, M. M. Alam, and Y. Le Moullec, "Active-Passive Two-Way Ranging Using UWB," in *14th International Conference on Signal Processing and Communication Systems (ICSPCS)*, pp. 1–5, IEEE, dec 2020

- T. Laadung, S. Ulp, M. M. Alam, and Y. Le Moullec, "Novel Active-Passive Two-Way Ranging Protocols for UWB Positioning Systems," *IEEE Sensors Journal*, vol. 22, no. 6, pp. 5223–5237, 2022

3.1 Proposed Protocols

The motivation for passive ranging comes from the need to overcome the limitations of ToF and TDoA methods. Namely, the increased air time of TWR-based ToF estimation methods and the synchronization problem of TDoA are discussed in Section 2.

Additionally, since the ToF-based positioning systems are more robust in positioning outside of the convex hull of the anchors and ToF positioning offers better performance in underdetermined positioning cases, the decision towards a ToF-based protocol was made. Coupled with the fact that many modern non-consumer use cases require a central scheme positioning and that it is desirable to keep the power consumption of the tags as low as possible, a tag-initiated ranging sequence was selected.

The resulting timing of the packet is illustrated in Fig. 9. The notation of the time intervals on the figure corresponds to the same as in Section 2.2. Tag T initiates the ranging sequence by transmitting a ranging request packet, to which the i-th active anchor Ai responds with a ranging response packet, and the sequence is concluded with a ranging report packet transmitted by T. While T and Ai actively partake in the packet exchange and record the corresponding time intervals, the currently passive anchor Aj listens to the communication and records its own time intervals.

Publication I firstly proposed an AP-TWR protocol, to which an alternative was proposed in Publication II. In order to avoid confusion between these two protocols, this section follows the nomenclature of Publication II, where these methods are referred to as Active-Passive Two-Way Ranging Methods 2 and 1 (AP2-TWR and AP1-TWR), respectively.

According to the timing of AP-TWR protocols in Fig. 9, the total set of AP1-TWR ToF estimates per ranging sequence is expressed by

$$t_{T \leftrightarrow Aj|Ai} = \begin{cases} t_{T \leftrightarrow Ai}, & \text{for } i = j \\ \\ t_{T \leftrightarrow Ai} + t_{Ai,T} + t_{Ai \leftrightarrow Aj} - t_{Aj,Ai}, & \text{for } i \neq j, \end{cases} \tag{16}$$
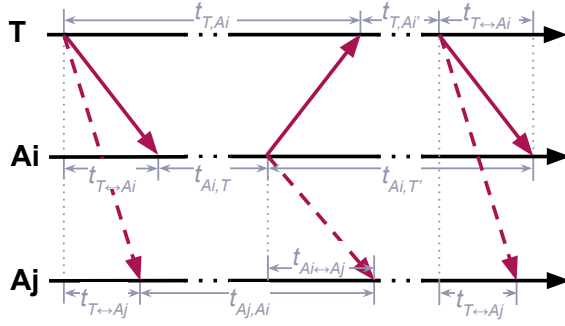
Figure 9: Timing of the Active-Passive Two-Way Ranging protocol.

whereas the total set of ToF estimates for AP2-TWR is written as

$$
t_{T \leftrightarrow Aj|Ai} = \begin{cases} t_{T \leftrightarrow Ai}, & \text{for } i = j \\[2mm] \dfrac{t_{Ai,T} + t_{T,Ai}}{2} + t_{Ai \leftrightarrow Aj} - t_{Aj,Ai}, & \text{for } i \neq j. \end{cases} \tag{17}
$$

It can be observed that the notation of ToF estimates in AP-TWR protocols is substituted by $t_{T \leftrightarrow Aj|Ai}$ to reflect that each passive anchor Aj provides a ToF estimate of the propagation time between itself and the tag during each and every Ai's active message exchange. This is made possible as the coordinates of each anchor are known; therefore, the inter-anchor ToF values $t_{Ai \leftrightarrow Aj}$ can be inferred from the relation in (1). The coordinates of the anchors can be obtained by a site survey process during the installation of the anchors, or by employing anchor coordinate self-calibration methods during which the inter-anchor distances are directly measured by the anchors themselves [47].

AP-TWR protocols function on the principle in which anchors that are currently not actively partaking in the packet exchange, listen to other transmissions, making them essentially active-passive anchors. Denoting the total number of active-passive anchors as m and the number of additional passive-only anchors as k, meaning the total number of anchors partaking in AP-TWR protocol is $n = m + k$, such that $i \in \{1, 2, \ldots, m\}$, $j \in \{1, 2, \ldots, n\}$ and $n \geqslant m$. Therefore the set of obtained ToF estimates per each ranging sequence can be written as the ToF measurement matrix T:

$$
T = \begin{bmatrix} t_{T \leftrightarrow A1|A1} & \cdots & t_{T \leftrightarrow A1|Am} \\ \vdots & \ddots & \vdots \\ t_{T \leftrightarrow An|A1} & \cdots & t_{T \leftrightarrow An|Am} \end{bmatrix}, \tag{18}
$$

from which the final filtered ToF estimates can be calculated as the mean values of the rows of T:

$$
\overline{T} = \begin{bmatrix} t_{T \leftrightarrow A1} \\ \vdots \\ t_{T \leftrightarrow An} \end{bmatrix}, \tag{19}
$$

38

where $t_{T\leftrightarrow A1}$ to $t_{T\leftrightarrow An}$ are the row vectors of (18):

$$t_{T\leftrightarrow A1} = \begin{bmatrix} t_{T\leftrightarrow A1|A1} & \cdots & t_{T\leftrightarrow A1|Am} \end{bmatrix}$$

$$\vdots$$

$$t_{T\leftrightarrow An} = \begin{bmatrix} t_{T\leftrightarrow An|A1} & \cdots & t_{T\leftrightarrow An|Am} \end{bmatrix}.$$

Considering that the term $t_{T\leftrightarrow Ai}$ of (16) and (17) can be calculated by utilizing SS-TWR (6), SDS-TWR (9), or AltDS-TWR (12), a grand total of six slightly differing AP-TWR protocols can be defined: AP1 and AP2 SS-TWR, AP1 and AP2 SDS-TWR, AP1 and AP2 AltDS-TWR.

3.2 Simulations

This section provides the prerequisites and additional information on the simulations for all of the preceding AP-TWR methods. As the numerical results for SS-TWR-based AP-TWR are also inherently included in Publication II, the results of Publication I are not explicitly discussed, but rather some general comments are given about the results of Publication I. The simulations of both publications were run under specific preconditions, which are discussed below.

The simulations of both publications are run such that only a single tag participates in the ranging process with a given amount of anchors, while the packet losses due to anchor response collisions are omitted. The clock offset errors are omitted, as they can be compensated by utilizing the CFO correction method. Systematic errors are omitted, as they can be removed by means of calibration. The propagation conditions are LoS, so the noise follows a zero-mean Gaussian distribution, while other environmental effects are omitted. The conversion between the ToF value and the distance is made with (1). The true distances of each tag-anchor pair are calculated by and known to the simulator software. Each protocol utilizes the ToF measurement matrix (18) row-wise averaging by (19). All protocols are simulated for a total of 1000 iterations, each time placing the tag in an arbitrary location in the simulated room; each iteration consists of 1000 separate ranging sequences. The final results are presented as the range estimate RMSE in centimeters, rather than the ToF value RMSE, as the inputs to a position estimator are typically given by distances in place of the signal propagation times.

Although most of the prerequisites are the same, the simulators of I and II differ to some extent. The simulator of Publication I is written as a dedicated software script in Python and forms the baseline active and passive anchor ranging performance based on the experimental values reported in [81]. The numerical tests were conducted in an arbitrarily sized (600 by 400 by 250 cm) room defined in the software.

The software for Publication II, on the other hand, was written in the programming language R and directly simulated the ToF time interval values for range estimation protocols. The baseline ToF estimation performance was acquired as the worst-case time measurement noise with a standard deviation of 150 ps of the DW1000 transceiver from [59], following a zero-mean Gaussian distribution, which was assumed for both the tag and the anchors. The numerical tests for this publication were also carried out in an arbitrarily sized virtual room (sized 500 by 700 by 250 cm).

Although the simulations of I and II were conducted on separate numerical testers and on different fundamental baseline performances, the results show similar performance.
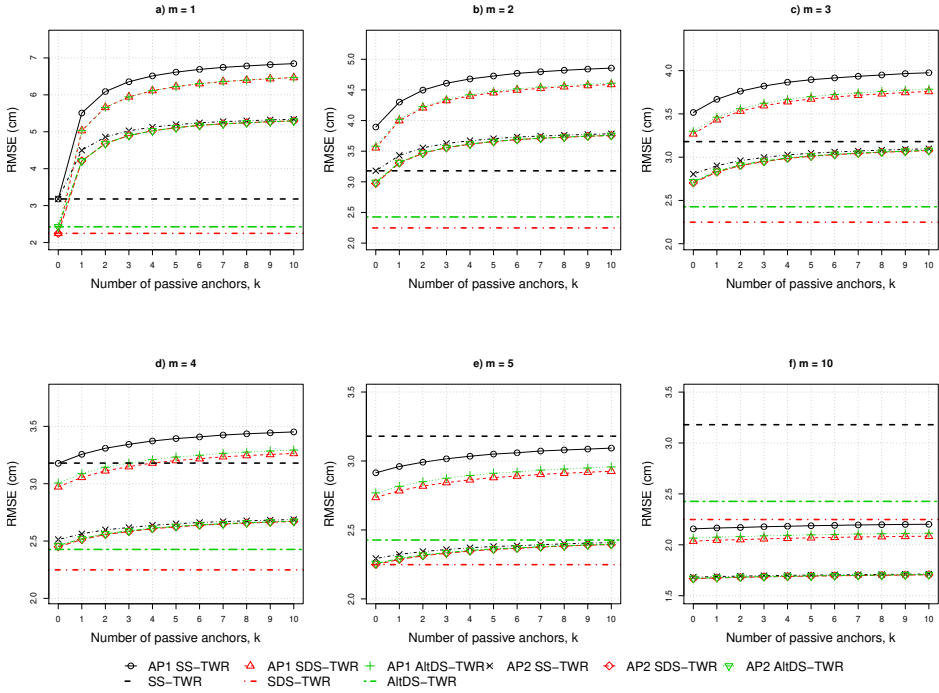
Figure 10: The numerical results for ranging RMSE of AP-TWR protocols proposed in Publication II. The figures show the dependence of RMSE depending on the number of additional passive-only anchors, k. Each sub-figure depicts a different number of active-passive anchors, m. The baseline performance of the active ranging methods is pictured as constant lines, as these do not employ passive ranging and therefore are not dependent on the number of passive-only anchors. Figure from Publication II.

This is evident when comparing Table 1 of Publication I[2] and Figures 6 and 10 of Publication II, where the trends of the performance are identical while the RMSE values differ by a maximum of 0.3 cm for lower m values. This slight discrepancy is easily explained by the fact that Publication II assumed the worst-case time measurement error, while the practical results of [81] achieved slightly better results as their devices did not operate on the worst-case time measurement noise. For an exact comparison, refer to Fig. 3 of [81] and Fig. 5 of Publication II.

The main numerical results of Publication II are shown in Fig. 10, which shows the ranging RMSE values depending on k, i.e. the number of additional passive-only anchors[3]. The values of m, the number of active-passive anchors, is varied according to the title of each sub-figure. The key takeaways from these results are discussed in the following paragraphs.

Although each additional active-passive anchor of every AP-TWR protocol adds a packet to the ranging sequence and therefore reduces air time efficiency, the ranging RMSE is also

---

[2]Note that in the body part of Publication I states that the value of passive-only anchors, k, is varied from 1 to 10. The correct values of k are in the range of 0 to 9, and Table 1 correctly displays this.

[3]Note that the caption of Fig. 6 in Publication II reads n as the number of additional passive-only anchors, the correct notation is k.

Table 3: AP2-based SS-TWR example. Number of anchors $n = m + k = 6$. Comparison with equivalent SS-TWR with 6 anchors (RMSE: 3.180 cm, number of packets: 8). Amount of available range estimates for both methods: 6. Table from Publication II.

m	k	RMSE (cm)	RMSE relative change (%)	Nº packets	Air time relative change (%)
6	0	2.120	-33.3	8	0
5	1	2.323	-26.9	7	-12.5
4	2	2.598	-18.3	6	-25.0
3	3	2.997	-5.8	5	-37.5
2	4	3.672	15.5	4	-50.0
1	5	5.192	63.3	3	-62.5

reduced at the same time. As the total number of anchors, n, directly defines the number of available range estimates, we observe that each added passive-only anchor provides an additional range estimate at no additional cost to the air time, while slightly increasing the RMSE. This is explained by the fact that passive range estimates typically offer slightly lower performance than their active ranging counterparts, as seen in Fig. 5 of Publication II. Hypothetically the number of available range estimates, which have no effect on the air time, is limited only by the number of passive-only devices.

The numerical results in Fig. 10 show that all AP2-TWR-based protocols outperform AP1-TWR protocols in every test scenario. This leads to the case $m = 3$, where the performance of every combination of AP2-TWR protocol surpasses SS-TWR and $m = 6$ (depicted on Fig. 10 of Publication II) where it exceeds the performance of all of the active ranging methods. The same critical points can be observed for AP1-TWR protocols in $m = 5$ and $m = 10$, respectively.

The effect of AP-TWR protocols can be illustrated with a specific example given in Table 3. The table[4] compares various AP2 SS-TWR m, k combinations (amounting to a total of $n = 6$ anchors) to an equivalent 6 anchor SS-TWR protocol. We discern that the extreme cases $m = 1, k = 5$ and $m = 6, k = 0$ are aimed towards improving the air time (reduction of air time by 63.5%) and RMSE (reduction of RMSE by 33.3%), respectively. Some intermediate cases such as $m = 4, k = 2$ show simultaneous improvements on both metrics, reducing the air time by 25% and the RMSE by 18.3%.

The above paragraphs described the simulations of Publication II and their main results, the subsequent section provides an overview of the corresponding practical experiments.

3.3 Practical Experiments

All of the experiments in the scope of this thesis were conducted using the Eliko UWB RTLS [137] system, built around the Qorvo DW1000 UWB transceiver [64]. The reference coordinates of the anchors and the tag were measured using the Leica DISTO S910 laser distance meter [138], mounted to the tripod adapter FTA 360S on the TRI120 tripod, as part of the P2P Package [139]. The DISTO S910 offers a worst-case distance measurement accuracy of $\pm$ 2 mm, which is well below the 1 cm ranging resolution of Eliko UWB RTLS devices (verified experimentally), making it suitable for providing the best ground truth reference points in the context of this thesis.

---

[4]Publication II lists the second column header of Table 1 as n, while the correct term is k.
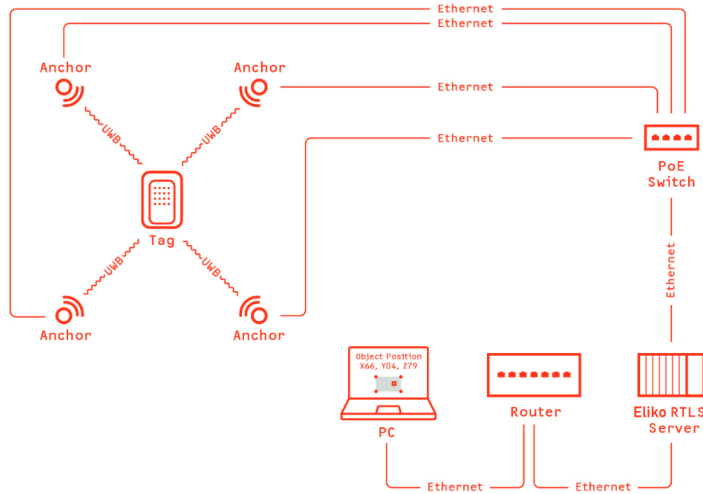
Figure 11: An example of a small-scale setup of Eliko UWB RTLS. Figure from [140], with permission from Eliko Tehnoloogia Arenduskeskus OÜ

Figure 11 depicts a typical Ethernet-based Eliko UWB RTLS setup, which is also representative of the setup used in the experiments conducted in this thesis, only at a smaller scale. The diagram illustrates a setup consisting of four UWB anchors and one tag. The anchors are powered via Power over Ethernet (PoE) connected to a PoE-supported Ethernet switch, which is in turn connected to the position estimator i.e. central RTLS server, while the Ethernet cabling also doubles as the means of transporting the ranging data. A user terminal connected to the server can be used to display the graphical user interface of the RTLS system, or stream the raw ranging data; the latter is used for the experiments in this thesis.

The actual Eliko UWB RTLS system setup used in the experiments of Publications I, II, and III is shown in Fig. 12. The six anchors are circled in red, the tag in dark blue, and the Leica DISTO S910 in light blue; the RTLS server is not visible in the photo because it is installed in a separate server room on the same floor. It is important to note that the top right anchor was not included in the experiments of Publication II, as it had Ethernet connectivity issues during the measurement campaign, while all of the six anchors were included in the experiments of Publication I. Yellow post-it notes are attached to the anchors and act as reflective surfaces for the Leica DISTO S910 at the approximate location of the anchor antenna, per the installation guide of Eliko UWB RTLS [140]. The concrete-walled room is sized about 7.2 by 6 by 2.6 m, fitted out with tables and computers.

Similar to the numerical simulations, the experiment test positions of the tag are chosen such that LOS propagation conditions between the tag and the anchors are ensured. The measurements for Publication I were collected in a single run of about 7200 ranging sequences with $m = 6, k = 0$, from which the 21 possible combinations of m, k were selected as subsets, for which the performance parameters were calculated.

The data for Publication II were collected separately for each of the 15 m, k combinations that were possible with a maximum of 5 anchors. The ranging data for each combination was collected at 5 randomly chosen locations in the room, each of which consisted of at least 600 separate ranging sequences. The choice of the participating anchors for cases where $m + k < 5$ was chosen at random by a dedicated data acquisition software

Figure 12: Test setup for experiments in Publications I, II, and III.

Table 4: Experimental results of AP2 SS-TWR from Publication I. Achieved RMSE (cm) for all m, k combinations possible with a maximum of 6 anchors. Table from Publication I.

k / m	0	1	2	3	4	5
1	3.286	4.608	5.334	5.337	5.466	5.533
2	3.259	3.764	3.838	3.958	4.076	
3	3.251	3.384	3.544	3.670		
4	2.946	3.144	3.268			
5	2.901	3.043				
6	2.892					

written in Python.

Additionally, the experiments of Publication II were run with only the AP2 SS-TWR protocol as the results could be directly comparable to results of Publication I; it requires the least amount of data to transmit over UWB; and the numerical results show that the performance is practically on the same level as the other AP2 protocols.

Due to a software bug impairing the performance of the devices at the time, Publication II's Table 2 listed the practical performance of AP2 SS-TWR as the standard deviation (SD) of ranging rather than the RMSE. This is due to the fact that the SD can be interpreted as the best-case RMSE value when the true distance is equal to the mean of the samples. Although the results showed somewhat similar trends to the numerical simulations, the experimental results of Publication I are more representative and give a better comparison with the numerical simulations, while also employing more anchors. Therefore, in the scope of this section, the experimental results of Publication I are given in Table 4.

Comparing the results given in Fig. 10 and Table 4 it can be observed that although the experiments show only about 0.4 cm higher RMSE on average, the overall trends discussed in the previous section are also clearly present in practice. Therefore, the results of the experiments support the simulations, validating the functionality of the proposed

AP2 SS-TWR method.

For a more detailed analysis of the results, the reader is encouraged to read the results sections of Publications I and II.

This section gave an overview of the UWB AP-TWR ranging protocols proposed in Publications I and II, providing the theory of the protocols and validating it by numerical simulations and practical experiments. The following section outlines the AP-TWR measurement matrix processing techniques, based on Publication III. In the remainder of the thesis, the SS-TWR-based AP2-TWR method is commonly referred to as the AP-TWR protocol for simplicity.

4 AP-TWR Measurement Matrix Processing

This section covers some of the possible ways of processing the ToF measurement matrix values given by (18) in order to provide more robust range estimates as the inputs for a positioning system. As the AP-TWR protocol along with the measurement matrix is a novel concept, some pre-existing methods put into a novel context were investigated. A portion of the explored methods is additionally mentioned in Section 2.3.2 of this thesis.

This section is based on Publication III:

- T. Laadung, S. Ulp, M. M. Alam, and Y. Le Moullec, "Performance Evaluation of UWB Active-Passive Two-Way Ranging Distance Estimation Matrix Weighting Methods," in *12th International Conference on Indoor Positioning and Indoor Navigation (IPIN 2022)*, pp. 1–5, CEUR-WS, sep 2022

4.1 Explored Methods for AP-TWR Measurement Matrix Processing

The first and most intuitive method for measurement matrix processing is the **LS** estimation of a constant, which was also used in Publications I and II. The LS estimation of a constant simplifies to calculating the arithmetic mean of samples. In the context of the AP-TWR ToF measurement matrix, we estimate ranging values row-wise; therefore, the LS estimation is performed via (19) by calculating the arithmetic mean of the rows.

A more robust estimator in the presence of a small number of outliers is the **median (Med)**, i.e. the middle value separating the top and bottom half of a data sample. To calculate the final range estimates and following the row vector notation of 20, the median of the vector is written with the tilde accent:

$$\hat{T}_{MED} = \begin{bmatrix} \tilde{t}_{T\leftrightarrow A1|A1:m} \\ \vdots \\ \tilde{t}_{T\leftrightarrow An|A1:m} \end{bmatrix}. \tag{20}$$

The Inverse Distance Weighting (IDW) method of [92] is an estimator of central tendency by providing higher weights to values closer to the arithmetic mean of the sample. It is calculated by

$$t_{T\leftrightarrow Aj} = \begin{cases} \dfrac{\sum\limits_{i=1}^{m} (t_{T\leftrightarrow Aj|Ai} \cdot d_{j,i}^{-1})}{\sum\limits_{i=1}^{m} d_{j,i}^{-1}}, & \text{if } d_{j,i} \neq 0 \text{ for all } i, \\[2em] \overline{t_{T\leftrightarrow Aj|A1:m}}, & \text{if } d_{j,i} = 0 \text{ for some } i, \end{cases} \tag{21}$$

where

$$d_{j,i} = |t_{T\leftrightarrow Aj|Ai} - \overline{t_{T\leftrightarrow Aj|A1:m}}|. \tag{22}$$

The following methods are based on the Weighted Least Squares (WLS) or colloquially named the Weighted Mean (WM), which utilizes non-negative weights $w_{j,i}$:

$$WM(\overline{t_{T\leftrightarrow Aj|A1:m}}) = \frac{\sum\limits_{i=1}^{m} (w_{j,i} \cdot t_{T\leftrightarrow Aj|Ai})}{\sum\limits_{i=1}^{m} w_{j,i}}. \tag{23}$$

The **Distance Weighted Estimator (DWE)**, in essence, provides a weight $w_{j,i}$, calculated as the inverse of the average distance of an observation to other data points in the sample:

$$w_{j,i} = \frac{m-1}{\sum_{l=1}^{m} |t_{T \leftrightarrow Aj|Ai} - t_{T \leftrightarrow Aj|Al}|}. \tag{24}$$

The **first WLS method (WLS1)** utilizes the active and passive anchor noise variances σ_a^2 and σ_p^2, which can be found from the results of previous publications, where $\sigma_a = 3.2$ cm and $\sigma_p = 5.5$ cm. Therefore the weights can be calculated by

$$w_{j,i} = \begin{cases} \dfrac{1}{\sigma_a^2}, & \text{for } i = j \\[2ex] \dfrac{1}{\sigma_p^2}, & \text{for } i \neq j. \end{cases} \tag{25}$$

The **formulation of the second WLS method (WLS2)** introduces a minute change in the notation compared to Publication III. Firstly, the centered measurement matrix values $c_{j,i}$ are found by subtracting the row mean from each row:[5]

$$c_{j,i} = t_{T \leftrightarrow Aj|Ai} - \overline{t_{T \leftrightarrow Aj|A1:m}}. \tag{26}$$

Then the column variances are found using the mean value of columns $\overline{c_{1:n,i}})^2$:

$$\sigma_i^2 = \frac{\sum_{j=1}^{n} (c_{j,i} - \overline{c_{1:n,i}})^2}{n}, \tag{27}$$

The variances are used for calculating the WLS2 weights $w_{j,i}$, which are the equal for each row:

$$w_{j,i} = \frac{1}{\sigma_i^2}, \text{ for all } j. \tag{28}$$

As the previous method was based on the column variances, the **third WLS method (WLS3)** makes use of the row variances σ_j^2 as well:

$$\sigma_j^2 = \frac{\sum_{i=1}^{m} c_{j,i}^2}{m}, \tag{29}$$

noting that the row mean term is omitted from the calculation, as it is already subtracted in (26). The resulting row and column variances are combined into $\sigma_{j,i}^2$ by

$$\sigma_{j,i}^2 = \frac{\sigma_j^2 + \sigma_i^2}{2}, \tag{30}$$

which permit the calculation of the WLS3 weights:

$$w_{j,i} = \frac{1}{\sigma_{j,i}^2}. \tag{31}$$

---

[5]Publication III Section 3.6 claims that the centering is done via (9) of that publication; theoretically, the correct way of centering is performed with (26) of this thesis. The results of this publication are not affected by this change.
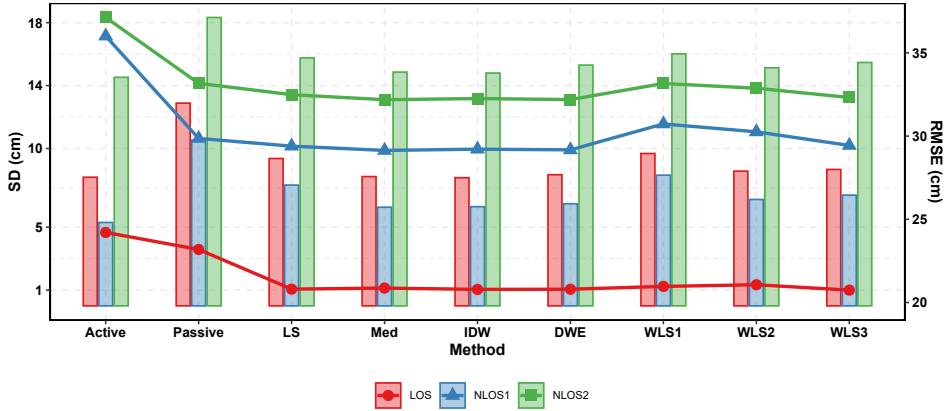
Figure 13: Results averaged across all test locations and propagation conditions: the RMSE (lines+markers) and SD values (bars) of the explored methods. Figure from Publication III.

4.2 Practical Experiments of Publication III

The experiments of this publication were conducted with the Eliko UWB RTLS system in the same conditions as outlined in Section 3.3, pictured in Fig. 12. As opposed to previous publications, the experiments of Publication III also include NLoS measurements in order to assess the performance of the different methods in more challenging circumstances.

The data acquisition was conducted by placing a tag in five randomly chosen locations in the room, making sure that, by default, LoS propagation conditions were met between each tag-anchor pair. At each location, an LoS and 2 separate NLoS tests were conducted, collecting a minimum of 1200 ranging sequences per test. The first NLoS test (NLOS1) was carried out where the propagation path between the tag and a certain set of anchors was disrupted with a 40-by-20 cm, 0.8 mm thick metal sheet, while the second NLoS test (NLOS2) utilized a live human body to block the same paths. During both of the NLoS tests, the element blocking the direct LoS path was placed approximately 5 cm away from the tag. The data of the $m = 6, k = 0$ AP-TWR protocol was captured from the Eliko RTLS server using a custom Python script, while the data processing and performance analysis was conducted via a dedicated script written in R.

Figure 13 presents the average RMSE (left-hand side vertical scale, data represented with lines and markers) and SD values (right-hand side vertical scale, data represented with bars) of the methods across all the LoS/NLoS tests and locations. To provide a base-line comparison, the performance of SS-TWR-based active ranging and AP-TWR passive range estimates are separately presented, in addition to the explored methods.

Firstly focusing on the SD values of the methods, it can be noted that active ranging provides the lowest SD values, and passive ranging provides the highest SD values, for example in LoS propagation conditions respectively about 7 cm, and 13 cm. Med, IDW, and DWE provide SD values in the same range as the SS-TWR active ranging, while the WLS methods offer slightly higher values. Across the LOS/NLOS1/NLOS2 propagation conditions, no significant differences in the trends can be observed.

The RMSE, on the other hand, offers some other insights: here it can be seen that the SS-TWR active ranging achieves significantly inferior results when compared to the AP-TWR passive range estimates, across all of the propagation conditions (for example

about 24 cm for SS-TWR active ranging, and the next least performing method WLS2 with a lower value of about 21 cm). Noting that in NLOS1/NLOS2 conditions, the performance gap of the active and passive ranging is larger than in LoS. In LoS propagation conditions, all of the explored methods performed equally well, besting the passive range estimates by about 2.2 cm RMSE. The performance in NLOS1 and NLOS2 conditions shows that the WLS methods offer up to about 1 cm higher RMSE when compared to LS, Med, IDW, and DWE methods.

The results show that Med, IDW, and DWE offer the lowest SD, being in the same range as the active SS-TWR ranging. The best RMSE was achieved by LS, Med, IDW, and DWE, offering up to almost 7 cm better RMSE performance when compared to the active ranging. Accounting for both metrics, the best-performing methods are Med, IDW, and DWE. Although the computational complexity of each method was not explicitly discussed in the Publication III, the equations for IDW (21) and DWE (24) analytically show that the number of calculations is higher, compared to finding the median of each row. For more information on the exact test setup, the location- and propagation condition-specific results, and additional analysis, the reader should refer to Publication III.

This section provided a summary of the AP-TWR ToF measurement matrix processing methods explored in Publication III. The methods were tested experimentally, in LoS and two different NLoS propagation conditions, finding that the Med, IDW, and DWE methods provide the lowest SD and RMSE out of all the tested methods. Next, based on Publication IV, the following section assembles the findings of the previous publications and ties them together to form a novel AP-TWR-based adaptive positioning method.

5 AP-TWR Positioning

The AP-TWR protocol and the proposed measurement matrix processing methods were validated via tests and experiments which evaluated the performance of ranging. As the UWB ranging is also utilized in positioning, the effect of AP-TWR on positioning had not been quantified in previous publications. This section covers the usage of the AP-TWR protocol to propose an Adaptive Extended Kalman Filter (A-EKF) position estimator for increased positioning accuracy.

This section is based on Publication IV:

- T. Laadung, S. Ulp, A. Fjodorov, M. M. Alam, and Y. Le Moullec, "Adaptive Extended Kalman Filter Position Estimation Based on Ultra-Wideband Active-Passive Ranging Protocol," *Submitted to IEEE Access*, 2023

5.1 Theoretical Background

The current section provides an overview of the theoretical background for utilizing the AP-TWR protocol in an RTLS. The position estimator based on the Extended Kalman Filter (EKF) and the mechanisms for penalizing longer distances and intermittent ranging values are given in separate subsections.

5.1.1 Active-Passive Two-Way Ranging

Taking the AP-TWR ToF measurement matrix (18), converting it to distances via (1) and giving it a designator for time steps (k) (noting the difference between the k used in previous sections) we get the n-by-m AP-TWR distance matrix $\mathbf{T}_{dk}$:

$$\mathbf{T}_{d,k} = c\mathbf{T}_k = \begin{bmatrix} d_{1|1,k} & \cdots & d_{1|m,k} \\ \vdots & \ddots & \vdots \\ d_{n|1,k} & \cdots & d_{n|m,k} \end{bmatrix} \tag{32}$$

Accounting for the results of previous publications, the range estimates for the position estimator are found by taking the median (denoted by the tilde) of each row of $\mathbf{T}_{d,k}$:

$$\mathbf{N}_k = \begin{bmatrix} \tilde{d}_{1|1:m,k} & \tilde{d}_{2|1:m,k} & \cdots & \tilde{d}_{n|1:m,k} \end{bmatrix}^T \tag{33}$$

To formulate the adaptive EKF positioning method for AP-TWR, the row variances of $\mathbf{T}_{dk}$ must be found at each time step, such that

$$\mathbf{S}_k = \begin{bmatrix} \sigma^2_{1|1:m,k} & \sigma^2_{2|1:m,k} & \cdots & \sigma^2_{n|1:m,k} \end{bmatrix}^T. \tag{34}$$

The complete analysis of the effect of the individual NLoS propagation paths on the AP-TWR distance (and ToF) matrix values, which gives the basis for the calculation of row variances, is given in Publication IV.

5.1.2 Distance Penalty

Earlier publications [141, 118] have shown that as the distance increases, the error magnitude is also larger. Therefore it is desired to utilize the shorter distances with a higher weight in the position estimation process.

As the EKF utilizes the weighting via observation/measurement noise variances (explained in more detail in Section 5.1.4), the higher weighted inputs get lower variance

values. This is conducted via a parametric exponential scaling vector $\mathbf{B}_k$:

$$\mathbf{B}_k = \left[e^{s_c \cdot \tilde{d}_{1|1:m,k}} \quad e^{s_c \cdot \tilde{d}_{2|1:m,k}} \quad \ldots \quad e^{s_c \cdot \tilde{d}_{n|1:m,k}} \right]^T, \tag{35}$$

where the parametric scaling constant is calculated by $s_c = \frac{\ln s_m}{s_d}$, and interpreted as having a scaling multiplier value of s_m at a distance of s_d, being a non-negative and a positive real number, accordingly.

5.1.3 Intermittency Penalty

The second way of augmenting the EKF observation noise parameters is based on the hypothesis that intermittent ranging values provide more inaccurate inputs to the position estimator. The intermittency penalty essentially gives lower weights to the sporadic ranging values, as the irregular resolving of distance values might indicate adverse propagation conditions in the positioning environment.

   Although this method insinuates the usage of historical time-series data, the time delay effects on position estimation are negated. This is explained by not using any historical ranging data, but rather augmenting the measurement noise based on the occurrences of missing data in the history.

   For the formulation of this method, we introduce two parameters: the look-back window size l_s and the intermittency multiplier l_m. The first of which defines the length of the history as a positive integer, while the latter defines the magnitude of the noise variance augmentation as a non-negative real number. In the case of $l_m = 0$, no intermittency penalty is applied. Noting the historical ranging values (spanning from the current sample at k to the end of the look-back window $k - l_s + 1$) of each anchor $A_1, A_2, \ldots, A_N$ as corresponding sets:

$$
\begin{aligned}
A_{1,k} &= \{d_{A_1,k}, \quad d_{A_1,k-1}, \quad \ldots, \quad d_{A_1,k-l_s+2}, \quad d_{A_1,k-l_s+1}\} \\
A_{2,k} &= \{d_{A_2,k}, \quad d_{A_2,k-1}, \quad \ldots, \quad d_{A_2,k-l_s+2}, \quad d_{A_2,k-l_s+1}\} \\
&\quad\quad\quad\quad\quad\quad\quad \vdots \\
A_{N,k} &= \{d_{A_N,k}, \quad d_{A_N,k-1}, \quad \ldots, \quad d_{A_N,k-l_s+2}, \quad d_{A_N,k-l_s+1}\},
\end{aligned}
$$

such that each element of a set gets a value of 0 when the corresponding anchor is not partaking in the ranging sequence at that specific time. Therefore, we get the number of missing ranging values within the window at time instance k for each anchor as

$$
\begin{aligned}
r_{A_1,k} &= |x_1 \in A_{1,k} : x_1 = 0| \\
r_{A_2,k} &= |x_2 \in A_{2,k} : x_2 = 0| \\
&\quad\quad \vdots \\
r_{A_N,k} &= |x_N \in A_{N,k} : x_N = 0|.
\end{aligned}
$$

The number of missing ranging values at k is then used to calculate the set of noise variance augmentation values at k:

$$L_k = \left\{ 1 + \tfrac{l_m}{l_s} \cdot r_{A_1,k}, \quad 1 + \tfrac{l_m}{l_s} \cdot r_{A_2,k}, \quad \ldots, \quad 1 + \tfrac{l_m}{l_s} \cdot r_{A_N,k} \right\}. \tag{36}$$

Then the final noise variance augmentation matrix at time instance k can be expressed in column form as

$$\mathbf{C}_k = \left[l_{i_1,k} \quad l_{i_2,k} \quad \ldots \quad l_{i_n,k} \right]^T, \tag{37}$$

where $l_{i_1,k}, l_{i_2,k}, \ldots, l_{i_n,k}$ represent the elements of the subset of set L_k, where $i_1, i_2, \ldots, i_n$ are the indices of the elements in the subset, which correspond to the anchors partaking in the ranging sequence at time instance k.

5.1.4 Extended Kalman Filter

In order to provide a 3D position based on AP-TWR ranging, a suitable EKF position estimator is formulated. Assuming a model of the position, velocity, and acceleration, the kinematics equations of each axis allow writing the state vector as:

$$\mathbf{X}_k = \begin{bmatrix} x_k \\ y_k \\ z_k \\ v_k^x \\ v_k^y \\ v_k^z \\ a_k^x \\ a_k^y \\ a_k^z \end{bmatrix} = \begin{bmatrix} x_{k-1} + T_s \cdot v_{k-1}^x + \frac{T_s^2}{2} a_{k-1}^x + \frac{T_s^3}{6} \omega_{k-1}^x \\ y_{k-1} + T_s \cdot v_{k-1}^y + \frac{T_s^2}{2} a_{k-1}^y + \frac{T_s^3}{6} \omega_{k-1}^y \\ z_{k-1} + T_s \cdot v_{k-1}^z + \frac{T_s^2}{2} a_{k-1}^z + \frac{T_s^3}{6} \omega_{k-1}^z \\ v_{k-1}^x + T_s \cdot a_{k-1}^x + \frac{T_s^2}{2} \omega_{k-1}^x \\ v_{k-1}^y + T_s \cdot a_{k-1}^y + \frac{T_s^2}{2} \omega_{k-1}^y \\ v_{k-1}^z + T_s \cdot a_{k-1}^z + \frac{T_s^2}{2} \omega_{k-1}^z \\ a_{k-1}^x + T_s \cdot \omega_{k-1}^x \\ a_{k-1}^y + T_s \cdot \omega_{k-1}^y \\ a_{k-1}^z + T_s \cdot \omega_{k-1}^z \end{bmatrix}, \tag{38}$$

where x_k, y_k, and z_k are the coordinates of the tag at time step k, while v_k^x, v_k^y, and v_k^z are the according velocities; a_k^x, a_k^y, and a_k^z are the acceleration values, and T_s is the sampling period between consecutive time steps $k-1$ and k. The final term of each component of the model denotes the process noise of position $((T_s^3/6)\omega_{k-1})$, velocity $((T_s^2/2)\omega_{k-1})$, and acceleration $(T_s \cdot \omega_{k-1})$. Reiterating that in the context of this section and Publication IV, k is the time step value, as opposed to the number of active-passive anchors used in the formulation of the AP-TWR protocol in Section 3.

Writing the process noise as a vector $\mathbf{w}_{k-1} = \begin{bmatrix} \omega_{k-1}^x & \omega_{k-1}^y & \omega_{k-1}^z \end{bmatrix}^T$ with a diagonal covariance matrix of $\mathbf{Q}_{k-1} = diag(\sigma_{ax}^2, \sigma_{ay}^2, \sigma_{az}^2)$, the formulation of the state vector can be written in matrix form:

$$\mathbf{X}_k = \mathbf{A}\mathbf{X}_{k-1} + \mathbf{G}\mathbf{w}_{k-1}, \tag{39}$$

where $\mathbf{A}$ and $\mathbf{G}$ are the state and noise transition matrices, respectively:

$$\mathbf{A} = \begin{bmatrix} 1 & 0 & 0 & T_s & 0 & 0 & \frac{T_s^2}{2} & 0 & 0 \\ 0 & 1 & 0 & 0 & T_s & 0 & 0 & \frac{T_s^2}{2} & 0 \\ 0 & 0 & 1 & 0 & 0 & T_s & 0 & 0 & \frac{T_s^2}{2} \\ 0 & 0 & 0 & 1 & 0 & 0 & T_s & 0 & 0 \\ 0 & 0 & 0 & 0 & 1 & 0 & 0 & T_s & 0 \\ 0 & 0 & 0 & 0 & 0 & 1 & 0 & 0 & T_s \\ 0 & 0 & 0 & 0 & 0 & 0 & 1 & 0 & 0 \\ 0 & 0 & 0 & 0 & 0 & 0 & 0 & 1 & 0 \\ 0 & 0 & 0 & 0 & 0 & 0 & 0 & 0 & 1 \end{bmatrix}, \tag{40}$$

$$\mathbf{G} = \begin{bmatrix} \frac{T_s^3}{6} & 0 & 0 \\ 0 & \frac{T_s^3}{6} & 0 \\ 0 & 0 & \frac{T_s^3}{6} \\ \frac{T_s^2}{2} & 0 & 0 \\ 0 & \frac{T_s^2}{2} & 0 \\ 0 & 0 & \frac{T_s^2}{2} \\ T_s & 0 & 0 \\ 0 & T_s & 0 \\ 0 & 0 & T_s \end{bmatrix}. \tag{41}$$

The observation vector is denoted as $\mathbf{Z}_k$, containing the AP-TWR ranging values and consisting of the true distances $d_{j,k}$ with their corresponding additive noise terms v_{ik} at time instant k:

$$\mathbf{Z}_k = \begin{bmatrix} z_{1,k} \\ z_{2,k} \\ \vdots \\ z_{n,k} \end{bmatrix} = \begin{bmatrix} d_{1,k} + v_{1,k} \\ d_{2,k} + v_{2,k} \\ \vdots \\ d_{n,k} + v_{n,k} \end{bmatrix} = \mathbf{D}_k + \mathbf{V}_k = \mathbf{H}_k \mathbf{X}_k + \mathbf{V}_k, \tag{42}$$

where $\mathbf{D}_k = \begin{bmatrix} d_{1,k} & d_{2,k} & \dots & d_{n,k} \end{bmatrix}^T$ is the vector containing the true distances, $\mathbf{V}_k = \begin{bmatrix} v_{1,k} & v_{2,k} & \dots & v_{n,k} \end{bmatrix}^T$ is the observation noise vector with a diagonal covariance matrix $\mathbf{R}_k = diag(\sigma_{d_1,k}^2, \sigma_{d_2,k}^2, \dots, \sigma_{d_n,k}^2)$, and $\mathbf{H}_k$ is the Jacobian matrix, which is expressed by (44). Similar to (2), the distance vector can also be written as equations relating to the locations of the corresponding anchors:

$$\mathbf{D}_k = \begin{bmatrix} \sqrt{(x_k - x_1)^2 + (y_k - y_1)^2 + (z_k - z_1)^2} \\ \sqrt{(x_k - x_2)^2 + (y_k - y_2)^2 + (z_k - z_2)^2} \\ \vdots \\ \sqrt{(x_k - x_n)^2 + (y_k - y_n)^2 + (z_k - z_n)^2} \end{bmatrix}. \tag{43}$$

As (43) is nonlinear, it is linearized by taking the first-order Taylor expansion given by the appropriately-sized Jacobian $\mathbf{H}_k$:

$$\mathbf{H}_k = \begin{bmatrix} \frac{\partial d_{1,k}}{\partial x_k} & \frac{\partial d_{1,k}}{\partial y_k} & \frac{\partial d_{1,k}}{\partial z_k} & 0 & 0 & 0 & 0 & 0 & 0 \\ \frac{\partial d_{2,k}}{\partial x_k} & \frac{\partial d_{2,k}}{\partial y_k} & \frac{\partial d_{2,k}}{\partial z_k} & 0 & 0 & 0 & 0 & 0 & 0 \\ & & & \vdots & & & & & \\ \frac{\partial d_{n,k}}{\partial x_k} & \frac{\partial d_{n,k}}{\partial y_k} & \frac{\partial d_{n,k}}{\partial z_k} & 0 & 0 & 0 & 0 & 0 & 0 \end{bmatrix}, \tag{44}$$

where the partial derivatives are

$$\frac{\partial d_{j,k}}{\partial x_k} = \frac{x_k - x_j}{\sqrt{(x_k - x_j)^2 + (y_k - y_j)^2 + (z_k - z_j)^2}} \tag{45a}$$

$$\frac{\partial d_{j,k}}{\partial y_k} = \frac{y_k - y_j}{\sqrt{(x_k - x_j)^2 + (y_k - y_j)^2 + (z_k - z_j)^2}} \tag{45b}$$

$$\frac{\partial d_{j,k}}{\partial z_k} = \frac{z_k - z_j}{\sqrt{(x_k - x_j)^2 + (y_k - y_j)^2 + (z_k - z_j)^2}}. \tag{45c}$$

Since, in the scope of this publication, the output position estimate is a 3D coordinate, there is a need for at least 4 range estimates in the input, such that the AP-TWR measurement matrix parameter $n \geq 4$, otherwise the position estimation for that ranging sequence is not performed.

Another special case is defined when the measurement matrix $m = 1$, which means that the measurement matrix consists of a single column, therefore it is directly used as an input to the EKF and the calculation of the row variances $\mathbf{S}_k$ from the measurement matrix is not possible. In this case, the row variance matrix $\mathbf{S}_k$ is given as a column vector, repeating n times the default observation noise variance σ_d^2.

Algorithm 1 EKF positioning for AP-TWR protocol

Input: $\mathbf{T}_{d,k} \in \mathbb{R}^{n \times m}$, $\{s_d, \sigma_d^2, \sigma_{ax}^2, \sigma_{ay}^2, \sigma_{az}^2\} \in \mathbb{R}_{>0}$, $\{s_m, l_m\} \in \mathbb{R}_{\geq 0}, l_s \in \mathbb{Z}_{>0}$

Output: $\hat{\mathbf{X}}_k$

Initialize: $\hat{\mathbf{X}}_0, \mathbf{P}_0$

1: **for** $k = 1, 2, \ldots, \infty$ **do**
    AP-TWR ranging
2:     **if** $n < 4$ **then**   ▷ Less than 4 distances in input
3:        *skip*
4:     **end if**
5:     **if** $m > 1$ **then**
6:        $\mathbf{Z}_k = \mathbf{N}_k$ ▷ Observation vector
7:        Calculate $\mathbf{S}_k$ ▷ Row variances
8:     **else**
9:        $\mathbf{Z}_k = \mathbf{T}_{d,k}$
10:       $\mathbf{S}_k = \left[\sigma_{d,k}^2 \quad \overset{\times n}{\ldots\ldots} \right]^T$ ▷ Assign default variance values
11:     **end if**
12:     Calculate $\mathbf{B}_k$ ▷ Distance penalty
13:     Calculate $\mathbf{C}_k$ ▷ Intermittency penalty
14:     $\mathbf{R}_k = \text{diag}(\mathbf{S}_k \odot \mathbf{B}_k \odot \mathbf{C}_k)$ ▷ Hadamard product
    EKF Prediction
15:     $\hat{\mathbf{X}}_k^- = \mathbf{A}\hat{\mathbf{X}}_{k-1}$ ▷ State prediction
16:     $\mathbf{P}_k^- = \mathbf{A}\mathbf{P}_{k-1}\mathbf{A}^T + \mathbf{G}\mathbf{Q}_{k-1}\mathbf{G}^T$ ▷ State covariation prediction
    EKF Correction
17:     $\mathbf{K}_k = \mathbf{P}_k^- \mathbf{H}_k^T (\mathbf{H}_k \mathbf{P}_k^- \mathbf{H}_k^T + \mathbf{R}_k)^{-1}$ ▷ Calculate Kalman gain
18:     $\hat{\mathbf{X}}_k = \hat{\mathbf{X}}_k^- + \mathbf{K}_k(\mathbf{Z}_k - \mathbf{D}_k^-)$ ▷ Correct the state estimate
19:     $\mathbf{P}_k = \mathbf{P}_k^- - \mathbf{K}_k\mathbf{H}_k\mathbf{P}_k^-$ ▷ Correct the state covariance
20:     **return** $\hat{\mathbf{X}}_k, \mathbf{P}_k$
21: **end for**

Algorithm 1 presents the complete procedure for the proposed EKF positioning for AP-TWR protocol. As the EKF procedure itself consists of two phases, the prediction, and the correction, the algorithm pseudo-code differentiates the products of the prediction phase with the minus $(-)$ superscript.

5.2 Practical Experiments of Publication IV

The proposed AP-TWR A-EKF positioning was validated by conducting experiments in an industrial environment at the manufacturing facilities of Krah Pipes OÜ [142], located near Tallinn, Estonia. The premises were chosen for the tests, as it provided adverse conditions for the positioning system, such as the presence of operating industrial machinery, metal, and concrete structures that interfere with LoS propagation, sub-optimal anchor placement due to the constraints on available installation locations, positioning the tag outside of the 3D convex hull defined by the anchors, etc.

Illustrated in Fig. 14, a part of the manufacturing facilities can be seen, with the Leica DISTO S910 circled in cyan and the Eliko UWB RTLS tripod-mounted tag in dark blue. In the background, some of the aforementioned industrial equipment can be seen. For more details on the exact placement of the anchors, test points, additional information and figures of the experimental setup, and parameter values, refer to Publication IV.
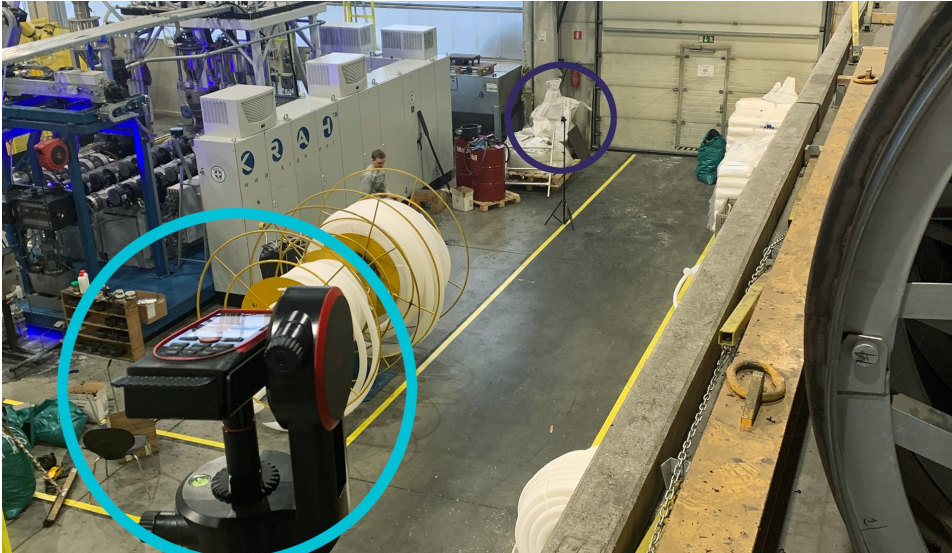
Figure 14: The test environment of the experiments of Publication IV. Leica DISTO S910 is circled in cyan, the tag is circled in dark blue.

In the first stage of experiments, ranging data was captured in 30 separate stationary points in the factory, with a tag mounted on a tripod. At each point, the true coordinate of the tag was surveyed with the Leica DISTO S910, and AP-TWR ranging data was captured for 30 seconds, resulting in data containing about 300 separate AP-TWR ranging sequences.

To validate the stationary experiment results, a second set of measurements were taken with a moving tag mounted on a tripod attached to a shelf trolley. The lines drawn on the factory floor were used as a reference for a true movement track and the trolley was used to follow this track as closely as possible, a photo of this experiment can be seen in Fig. 2 of Publication IV.

The experiments compared the proposed A-EKF method against the benchmarks of AP-TWR and SS-TWR in terms of 2D and 3D RMSE across 30 test points, as seen in Fig. 15. Overall, the A-EKF method demonstrated robustness in the industrial environment, performing at a similar or lower error level compared to the baseline methods. The proposed method significantly reduced errors at high-error test points of the benchmarks, providing a large reduction in absolute error values.

Comparing the A-EKF method to AP-TWR, it consistently achieved lower RMSE in both 2D and 3D positioning at most test points. The proposed method effectively mitigated the adverse effects of NLoS conditions encountered in the industrial environment. Similarly, when compared to SS-TWR, the A-EKF method showcased improved 2D positioning performance, greatly reducing errors at specific test points.

On average, the A-EKF method outperformed both AP-TWR and SS-TWR in terms of RMSE, achieving significantly better results in both, 2D and 3D. In 2D positioning, the proposed method achieved almost 1.6 times better performance than the next best method (SS-TWR), while in 3D positioning, it achieved over 3 times lower RMSE than the next best method (AP-TWR).

The experiments involving a moving tag aimed to validate the results obtained from the stationary tests and assess the impact of initialization on position estimates. Objec-
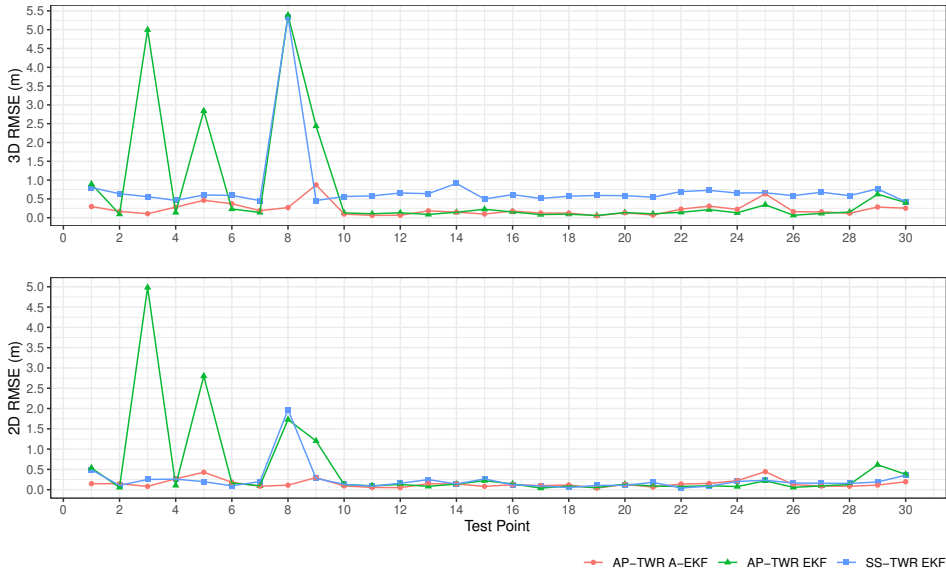
Figure 15: The 2D and 3D positioning RMSE results of the stationary tests of Publication IV. Figure from Publication IV.

tive error metrics were not calculated due to the requirement of knowing the true tag coordinates at each time step. The movement traces (seen in Fig. 5 of Publication IV) of the tested methods demonstrated that both the A-EKF and AP-TWR consistently provided more accurate results in the z-axis, as was also observed in the 3D RMSE graphs in Fig. 15. However, in certain segments, deviations from the true track were higher, particularly in the presence of obstacles such as the mezzanine floor and pipe manufacturing mandrels. Notably, the A-EKF method exhibited significantly lower deviations compared to SS-TWR and AP-TWR, reducing maximum errors by approximately 9 times.

Overall, these findings support the efficacy of the A-EKF method in maintaining accurate position estimates regardless of the tag staying stationary or moving in the environment, even in the presence of challenging propagation conditions. The proposed method showcases superior performance compared to the benchmark methods, particularly in mitigating large position deviations caused by obstructions and environmental factors. The A-EKF method shows promise for enhancing localization systems in industrial settings and offers the potential for more accurate and reliable positioning outcomes.

This section provided the theoretical background, experimental validation, and the results of the A-EKF positioning method based on the AP-TWR range estimates, proposed in Publication IV. The experiments, conducted in an industrial environment, showed the efficiency of the proposed method as it considerably reduced the positioning errors, compared to the baseline EKF methods. The following section provides the concluding remarks, answers the research questions raised in the first part of this thesis, and provides some future perspectives on the research direction.

6 Conclusion

The culmination of the research presented in this PhD thesis revolves around the formulation and investigation of the AP-TWR protocol in UWB positioning systems. This chapter serves as an abbreviated conclusion, drawing upon the key findings and contributions made through the four research papers presented within the scope of this thesis. By addressing the fundamental challenges and exploring novel methodologies, the aim was to advance the field of UWB positioning systems and pave the way for enhanced accuracy and reliability in real-world applications.

Firstly, this section offers an overview of the conducted research. Secondly, it addresses the research questions initially posed in the introduction, providing answers and insights gained through the investigations. Lastly, it outlines the future perspectives and potential avenues for further advancement in the field of AP-TWR in UWB systems, identifying areas for future research and development. Together, these components consolidate the contributions made in this thesis and shed light on the implications and possibilities that lie ahead in UWB positioning systems.[6]

6.1 Summary

This section provides an overview of this PhD thesis focused on the development and analysis of AP-TWR protocols in UWB positioning systems. The thesis explores the advantages and limitations of UWB technology, specifically the ToF and TDoA methods, and introduces the concept of passive ranging as a solution to address their drawbacks. The research consists of four papers that propose, test, and analyze novel AP-TWR protocols, leading to the development of a robust positioning method A-EKF.

The first research paper presents the generalized AP-TWR protocol for UWB and validates its performance through numerical simulations and experiments. The second paper introduces an alternative approach to calculating AP-TWR range estimates, combining multiple active ranging methods to create six distinct AP-TWR methods. These methods are compared through simulations, and the most promising approach is further tested experimentally. In the third paper, the robustness of AP-TWR range estimates is addressed by applying various measurement matrix processing techniques, which are evaluated with experimental testing. The findings from these papers are then consolidated in the fourth paper, which proposes an A-EKF-based positioning method using AP-TWR.

The significance of the AP-TWR protocol is highlighted by its distinct features. Unlike existing passive ranging methods that focus solely on improving air time efficiency, AP-TWR provides a generalized approach that allows UWB positioning systems to prioritize improvements in air time efficiency, ranging accuracy, or both. The results from the research papers demonstrate that AP-TWR yields more accurate range estimates compared to equivalent active-only ranging protocols, leading to more precise position estimates. Moreover, the proposed A-EKF positioning method based on AP-TWR offers robust and efficient positioning without requiring any additional information about the propagation channel or causing time delays.

---

[6]The English language of this chapter has been co-edited with ChatGPT [143].

6.2 Research Questions

The research questions proposed in Section 1.6 of this PhD thesis are answered below.

RQ1. How to improve location (ranging) estimates in the case of noisy measurements?

Section 1.6 of this thesis has highlighted several sub-topics that are pertinent to enhancing the accuracy of range or position estimates in wireless positioning systems. These sub-topics encompass filtering techniques, position estimation algorithms, different ranging protocols, and the detection and mitigation of NLoS conditions.

Traditionally, these sub-topics have been addressed individually through the application of advanced filtering methods, experimentation with various position estimation algorithms, exploration of different ranging protocols, error modeling, and employment of machine learning methods for NLoS detection and mitigation, among others. However, the proposed AP-TWR protocol offers a novel approach that enables simultaneous treatment of these sub-topics. Unlike conventional approaches that apply filtering to subsequent ranging values, the AP-TWR protocol performs filtering of ranging samples within each ranging sequence. Consequently, this protocol offers two-fold benefits: reduction of measurement noise impact and avoidance of filtering time delays that are typically encountered.

As the following research questions delve into the mentioned sub-topics in greater depth, the discussion pertaining to those aspects is elaborated upon in the answers to those specific research questions.

RQ2. How to detect (and mitigate) inaccuracies caused by NLoS?

Various techniques are employed for NLoS detection, such as statistical analysis, machine learning algorithms, and signal processing methods. Once NLoS is detected, mitigation strategies can be applied, including error modeling, geometric-based algorithms, and advanced filtering techniques. By effectively identifying and mitigating NLoS effects, UWB positioning systems can enhance their performance in challenging indoor environments, leading to more reliable and precise location estimates.

The research papers presented in this thesis have demonstrated that the inherent information provided by the measurement matrix of AP-TWR range estimates can be leveraged to detect and mitigate errors arising from NLoS propagation conditions. By integrating this capability into a position estimation algorithm, such as the proposed A-EKF, the accuracy of position estimates can be significantly enhanced, effectively incorporating all of the aforementioned sub-topics.

Therefore, the contributions and findings of this research provide a comprehensive framework that addresses the challenge of improving location (ranging) estimates in the presence of noisy measurements. The AP-TWR protocol, in conjunction with the A-EKF positioning method, not only reduces the impact of measurement noise and filtering time delays but also enables the detection and mitigation of errors caused by NLoS propagation conditions. This integrated approach represents a significant advancement in the field of wireless positioning systems and opens avenues for further research and development in this area.

RQ3. How to decrease the power consumption of the mobile node?

In the context of UWB technology, the reduction of power consumption in the mobile node, specifically the tag, is a critical consideration due to its reliance on battery operation. The preservation of energy is essential to extend the operating time of the tag. This

PhD thesis has addressed this concern by exploring design choices for a ranging protocol that minimizes the energy consumption of the tag. Section 2.2.6 of the thesis provided a comprehensive overview of these design choices, which were consistently implemented throughout the development of the AP-TWR protocol, resulting in enhanced energy efficiency for the overall system. Moreover, the inherent flexibility of the AP-TWR method allows the positioning system designer to optimize power consumption by selectively involving a limited number of anchors in the active ranging process, further contributing to the reduction of energy consumption by the tag.

RQ4. How to decrease air-time occupancy?

This research question is closely intertwined with the previous one, and some aspects of the answer have already been covered. However, let's briefly reiterate the key points here. The duration of air-time occupancy is directly influenced by the specific protocol used in the positioning system. Whether we consider TDoA or ToF estimation-based positioning methods, the choice of the ranging technique plays a vital role in determining the amount of time devices need to communicate wirelessly. As we discussed earlier in the context of energy consumption, the design choices embedded in the AP-TWR protocol are aimed at reducing energy usage, which naturally leads to a reduction in air-time occupancy. What makes the AP-TWR protocol particularly advantageous is its adaptability, enabling system designers to strike a balance between minimizing air-time occupancy and allocating additional air time to enhance the precision of ranging (position) estimates.

RQ5. How to balance the inherent trade-offs in a real-time location system?

Balancing the inherent trade-offs in a real-time location system poses a complex challenge for system designers. The optimization of competing objectives, including accuracy, latency, energy efficiency, and scalability, requires a comprehensive and multifaceted approach. The research question explores this fundamental dilemma and seeks to provide insights into achieving an optimal balance in real-time wireless location systems. While there is no single definitive answer to this question, as it largely depends on the specific needs and requirements dictated by system designers, the thesis delves into various considerations and factors that inform the decision-making process.

In answering this question there is a need for system designers to answer several key questions specific to their requirements. Factors such as the number of devices (anchors and tags), device density, coverage area, propagation conditions, position update rate, required accuracy, etc. play crucial roles in determining the trade-offs and making informed decisions.

In short, the question still remains open as there is no singular answer to how to balance the trade-offs in a real-time location system. Only through an in-depth analysis of the specific needs, positioning algorithms, ranging protocols, and filtering techniques, system designers can navigate the complexities and achieve high-performance wireless location systems operating in real-time scenarios.

6.3 Perspectives

The contributions and results achieved in this PhD thesis pave the way for further developments in the field of AP-TWR and the A-EKF positioning method based on it. These findings open up new possibilities and directions for future research and advancements in indoor positioning systems.

One potential avenue for exploration is the utilization of AP-TWR in calibrating the antenna delays of UWB devices. While passive ranging has already made strides in this area, the integration of AP-TWR for antenna delay calibration holds promise for achieving improved results.

Additionally, Publication IV focused on proposing the A-EKF position estimation method without delving into the optimal parameters for its implementation. Investigating and identifying the optimal parameters for the A-EKF method could be a small yet significant direction for future research, leading to enhanced performance and accuracy.

The NLoS error analysis of AP-TWR range estimation presented in Publication IV serves as a foundation for the A-EKF method. Exploring the specific error cases and developing techniques to detect and mitigate these errors can contribute to the development of a more robust and accurate positioning system. By addressing NLoS errors, the A-EKF method can further improve its performance in challenging environments.

Furthermore, integrating the A-EKF positioning method with a GNSS is another promising direction for future work. This integration would enable the creation of a seamless indoor-outdoor positioning system, providing accurate and reliable location information across different environments. By combining the strengths of A-EKF and GNSS, users can benefit from enhanced positioning capabilities for a wide range of applications.

In conclusion, the research conducted in this thesis sets the stage for future advancements in AP-TWR and the A-EKF positioning method. Exploring antenna delay calibration, optimizing parameters, addressing NLoS errors, and integrating with GNSS are just a few potential directions for future research that can further enhance the accuracy, robustness, and versatility of indoor positioning systems.

List of Figures

List of Tables

References

[1] T. Laadung, S. Ulp, M. M. Alam, and Y. Le Moullec, "Active-Passive Two-Way Ranging Using UWB," in *14th International Conference on Signal Processing and Communication Systems (ICSPCS)*, pp. 1–5, IEEE, dec 2020.

[2] T. Laadung, S. Ulp, M. M. Alam, and Y. Le Moullec, "Novel Active-Passive Two-Way Ranging Protocols for UWB Positioning Systems," *IEEE Sensors Journal*, vol. 22, no. 6, pp. 5223–5237, 2022.

[3] T. Laadung, S. Ulp, M. M. Alam, and Y. Le Moullec, "Performance Evaluation of UWB Active-Passive Two-Way Ranging Distance Estimation Matrix Weighting Methods," in *12th International Conference on Indoor Positioning and Indoor Navigation (IPIN 2022)*, pp. 1–5, CEUR-WS, sep 2022.

[4] T. Laadung, S. Ulp, A. Fjodorov, M. M. Alam, and Y. Le Moullec, "Adaptive Extended Kalman Filter Position Estimation Based on Ultra-Wideband Active-Passive Ranging Protocol," *Submitted to IEEE Access*, 2023.

[5] M. Tommingas, S. Ulp, M. M. Alam, I. Müürsepp, and T. Laadung, "Estimating UWB Positioning Integrity Based on Ranging Residuals," in *2023 24th International Conference on Applied Electromagnetics and Communications (ICECOM)*, pp. 1–6, Forthcoming, 2023.

[6] C. Hegarty and E. Kaplan, *Understanding GPS Principles and Applications*, *Second Edition*. Artech House, 2005.

[7] R. S. Campos and L. Lovisolo, *RF Positioning: Fundamentals, Applications, and Tools*. Artech House, 2015.

[8] C. J. Hegarty and E. Chatre, "Evolution of the Global Navigation SatelliteSystem (GNSS)," *Proceedings of the IEEE*, vol. 96, no. 12, pp. 1902–1917, 2008.

[9] Y. J. Morton, F. van Diggelen, J. J. Spilker Jr, B. W. Parkinson, S. Lo, and G. Gao, eds., *Position, Navigation, and Timing Technologies in the 21st Century: Integrated Satellite Navigation, Sensor Systems, and Civil Applications*, vol. 1-2. John Wiley & Sons, 1 ed., 2021.

[10] P. Puricer and P. Kovar, "Technical Limitations of GNSS Receivers in Indoor Positioning," in *2007 17th International Conference Radioelektronika*, pp. 1–5, 2007.

[11] F. Seco, A. R. Jiménez, C. Prieto, J. Roa, and K. Koutsou, "A survey of Mathematical Methods for Indoor Localization," in *2009 IEEE International Symposium on Intelligent Signal Processing*, pp. 9–14, IEEE, 2009.

[12] P. S. Farahsari, A. Farahzadi, J. Rezazadeh, and A. Bagheri, "A Survey on Indoor Positioning Systems for IoT-Based Applications," *IEEE Internet of Things Journal*, vol. 9, no. 10, pp. 7680–7699, 2022.

[13] X. Zhang, Y. Chen, L. Yu, W. Wang, and Q. Wu, "Three-Dimensional Modeling and Indoor Positioning for Urban Emergency Response," *ISPRS International Journal of Geo-Information*, vol. 6, no. 7, 2017.

[14] C. K. M. Lee, C. M. Ip, T. Park, and S. Chung, "A Bluetooth Location-based Indoor Positioning System for Asset Tracking in Warehouse," in *2019 IEEE International Conference on Industrial Engineering and Engineering Management (IEEM)*, pp. 1408–1412, 2019.

[15] H. Liu, H. Darabi, P. Banerjee, and J. Liu, "Survey of Wireless Indoor Positioning Techniques and Systems," *IEEE Transactions on Systems, Man, and Cybernetics, Part C (Applications and Reviews)*, vol. 37, no. 6, pp. 1067–1080, 2007.

[16] C. J. Syazwani, N. H. A. Wahab, N. Sunar, S. H. Ariffin, K. Y. Wong, and Y. Aun, "Indoor Positioning System: A Review," *International Journal of Advanced Computer Science and Applications*, vol. 13, no. 6, pp. 477–490, 2022.

[17] T. Savić, X. Vilajosana, and T. Watteyne, "Constrained Localization: A Survey," *IEEE Access*, vol. 10, pp. 49297–49321, 2022.

[18] R. F. Brena, J. P. García-Vázquez, C. E. Galván-Tejada, D. Muñoz-Rodriguez, C. Vargas-Rosales, and J. Fangmeyer, "Evolution of Indoor Positioning Technologies: A Survey," *Journal of Sensors*, vol. 2017, 2017.

[19] L. Mainetti, L. Patrono, and I. Sergi, "A Survey on Indoor Positioning Systems," in *2014 22nd International Conference on Software, Telecommunications and Computer Networks (SoftCOM)*, pp. 111–120, IEEE, 2014.

[20] Federal Communications Commission, "Revision of Part 15 of the Commission's Rules Regarding Ultra-Wideband Transmission Systems: First Report and Order," *FCC 02-48*, 2002.

[21] M. Elsanhoury, P. Mäkelä, J. Koljonen, P. Välisuo, A. Shamsuzzoha, T. Mantere, M. Elmusrati, and H. Kuusniemi, "Precision Positioning for Smart Logistics Using Ultra-Wideband Technology-Based Indoor Navigation: A Review," *IEEE Access*, vol. 10, pp. 44413–44445, 2022.

[22] A. Alarifi, A. Al-Salman, M. Alsaleh, A. Alnafessah, S. Al-Hadhrami, M. A. Al-Ammar, and H. S. Al-Khalifa, "Ultra Wideband Indoor Positioning Technologies: Analysis and Recent Advances," *Sensors*, vol. 16, no. 5, 2016.

[23] W. Sakpere, M. Adeyeye-Oshin, and N. B. Mlitwa, "A state-of-the-art survey of indoor positioning and navigation systems and technologies," *South African Computer Journal*, vol. 29, no. 3, pp. 145–197, 2017.

[24] G. Retscher, "Augmentation of Indoor Positioning Systems with a Barometric Pressure Sensor for Direct Altitude Determination in a Multi-storey Building," *Cartography and Geographic Information Science*, vol. 34, no. 4, pp. 305–310, 2007.

[25] Sewio Networks s.r.o., "Tag Leonardo Personal - Sewio Documentation." Available at `https://docs.sewio.net/docs/tag-leonardo-imu-personal-30146967.html` (22.02.2023).

[26] M. Valtonen, T. Vuorela, L. Kaila, and J. Vanhala, "Capacitive indoor positioning and contact sensing for activity recognition in smart homes," *Journal of Ambient Intelligence and Smart Environments*, vol. 4, no. 4, pp. 305–334, 2012.

[27] R. J. Orr and G. D. Abowd, "The Smart Floor: A Mechanism for Natural User Identification and Tracking," in *CHI '00 Extended Abstracts on Human Factors in Computing Systems*, CHI EA '00, (New York, NY, USA), p. 275–276, Association for Computing Machinery, 2000.

[28] C.-H. Pi, I.-F. Tsai, K.-S. Ou, and K.-S. Chen, "A one-dimensional touch panel based on strain sensing," *Mechatronics*, vol. 22, no. 6, pp. 802–810, 2012. Special Issue on Intelligent Mechatronics (LSMS2010 & ICSEE2010).

[29] F. Mazhar, M. G. Khan, and B. Sällberg, "Precise Indoor Positioning Using UWB: A Review of Methods, Algorithms and Implementations," *Wireless Personal Communications*, vol. 97, pp. 4467–4491, dec 2017.

[30] Y. Gu, A. Lo, and I. Niemegeers, "A Survey of Indoor Positioning Systems for Wireless Personal Networks," *IEEE Communications Surveys & Tutorials*, vol. 11, no. 1, pp. 13–32, 2009.

[31] M. A. Al-Ammar, S. Alhadhrami, A. Al-Salman, A. Alarifi, H. S. Al-Khalifa, A. Alnafessah, and M. Alsaleh, "Comparative Survey of Indoor Positioning Technologies, Techniques, and Algorithms," in *2014 International Conference on Cyberworlds*, pp. 245–252, 2014.

[32] K. Al Nuaimi and H. Kamel, "A Survey of Indoor Positioning Systems and Algorithms," in *2011 International Conference on Innovations in Information Technology*, pp. 185–190, 2011.

[33] G. M. Mendoza-Silva, J. Torres-Sospedra, and J. Huerta, "A Meta-Review of Indoor Positioning Systems," *Sensors*, vol. 19, no. 20, 2019.

[34] F. Zafari, A. Gkelias, and K. K. Leung, "A Survey of Indoor Localization Systems and Technologies," *IEEE Communications Surveys & Tutorials*, vol. 21, no. 3, pp. 2568–2599, 2019.

[35] A. Sesyuk, S. Ioannou, and M. Raspopoulos, "A Survey of 3D Indoor Localization Systems and Technologies," *Sensors*, vol. 22, no. 23, 2022.

[36] Z. B. Tariq, D. M. Cheema, M. Z. Kamran, and I. H. Naqvi, "Non-GPS Positioning Systems: A Survey," *ACM Comput. Surv.*, vol. 50, aug 2017.

[37] A. Yassin, Y. Nasser, M. Awad, A. Al-Dubai, R. Liu, C. Yuen, R. Raulefs, and E. Aboutanios, "Recent Advances in Indoor Localization: A Survey on Theoretical Approaches and Applications," *IEEE Communications Surveys and Tutorials*, vol. 19, no. 2, pp. 1327–1346, 2017.

[38] P. Pascacio, S. Casteleyn, J. Torres-Sospedra, E. S. Lohan, and J. Nurmi, "Collaborative Indoor Positioning Systems: A Systematic Review," *Sensors*, vol. 21, no. 3, 2021.

[39] M. Di Benedetto, *UWB Communication Systems: A Comprehensive Overview*. EURASIP book series on Signal Processing and Communications: European Association for Speech, Signal and Image Processing, Hindawi Publishing Corporation, 2006.

[40] Apple inc., "Ultra Wideband availability - Apple Support." Available at `https://support.apple.com/en-us/HT212274` (08.03.2023).

[41] Samsung Electronics Co., Ltd., "How does ultra-wideband work?." Available at `https://insights.samsung.com/2021/08/25/what-is-ultra-wideband-and-how-does-it-work-3/` (08.03.2023).

[42] Car Connectivity Consortium, "Digital Key Release 3," *Technical Specification*, *Version 1.1.0*, 2022.

[43] BMW AG, "All you need to know about Ultra Wideband tech." Available at `https://www.bmw.com/en/innovation/bmw-digital-key-plus-ultra-wideband.html` (08.03.2023).

[44] ITU, "ITU Recommendation ITU-R SM.1755-0: Characteristics of Ultra-Wideband technology," *ITU-R SM.1755-0*, pp. 1–20, May 2006.

[45] IEEE, "IEEE Standard for Information technology– Local and metropolitan area networks– Specific requirements– Part 15.4: Wireless Medium Access Control (MAC) and Physical Layer (PHY) Specifications for Low Rate Wireless Personal Area Networks (WPANs)," *IEEE Std 802.15.4-2006 (Revision of IEEE Std 802.15.4-2003)*, pp. 1–320, 2006.

[46] IEEE, "IEEE Standard for Information technology– Local and metropolitan area networks– Specific requirements– Part 15.4: Wireless Medium Access Control (MAC) and Physical Layer (PHY) Specifications for Low-Rate Wireless Personal Area Networks (WPANs): Amendment 1: Add Alternate PHYs," *IEEE Std 802.15.4a-2007 (Amendment to IEEE Std 802.15.4-2006)*, pp. 1–210, 2007.

[47] M. Ridolfi, A. Kaya, R. Berkvens, M. Weyn, W. Joseph, and E. D. Poorter, "Self-Calibration and Collaborative Localization for UWB Positioning Systems: A Survey and Future Research Directions," *ACM Computing Surveys*, vol. 54, may 2021.

[48] D. Coppens, A. Shahid, S. Lemey, B. Van Herbruggen, C. Marshall, and E. De Poorter, "An Overview of UWB Standards and Organizations (IEEE 802.15.4, FiRa, Apple): Interoperability Aspects and Future Research Directions," *IEEE Access*, vol. 10, pp. 70219–70241, 2022.

[49] J. Kunhoth, A. Karkar, S. Al-Maadeed, and A. Al-Ali, "Indoor positioning and wayfinding systems: a survey," *Human-centric Computing and Information Sciences*, vol. 10, pp. 1–41, 2020.

[50] R. Zandian, *Ultra-wideband Based Indoor Localization of Mobile Nodes in ToA and TDoA Configurations*. PhD thesis, Universität Bielefeld, 2019.

[51] S. A. R. Zekavat and R. M. Buehrer, eds., *Handbook of Position Location: Theory, Practice, and Advances*. Wiley, 2nd ed., 2019.

[52] M. Ridolfi, S. Van de Velde, H. Steendam, and E. De Poorter, "Analysis of the Scalability of UWB Indoor Localization Solutions for High User Densities," *Sensors*, vol. 18, no. 6, 2018.

[53] R. Kaune, "Accuracy Studies for TDOA and TOA Localization," in *2012 15th International Conference on Information Fusion*, pp. 408–415, 2012.

[54] B. Hepp, T. Nägeli, and O. Hilliges, "Omni-directional person tracking on a flying robot using occlusion-robust ultra-wideband signals," in *2016 IEEE/RSJ International Conference on Intelligent Robots and Systems (IROS)*, pp. 189–194, 2016.

[55] A. Niitsoo, T. Edelhäußer, E. Eberlein, N. Hadaschik, and C. Mutschler, "A Deep Learning Approach to Position Estimation from Channel Impulse Responses," *Sensors*, vol. 19, no. 5, 2019.

[56] C. Rizzo, T. Seco, J. Espelosín, F. Lera, and J. L. Villarroel, "An alternative approach for robot localization inside pipes using RF spatial fadings," *Robotics and Autonomous Systems*, vol. 136, p. 103702, 2021.

[57] E. Bogdani, D. Vouyioukas, N. Nomikos, D. N. Skoutas, and C. Skianis, "Angle-Based Time Fingerprint Positioning Technique for Indoor UWB Systems," in *2015 IEEE International Conference on Communications (ICC)*, pp. 6193–6198, 2015.

[58] G. S. K. Wong and T. F. W. Embleton, "Variation of the speed of sound in air with humidity and temperature," *The Journal of the Acoustical Society of America*, vol. 77, pp. 1710–1712, 05 1985.

[59] C. McElroy, D. Neirynck, and M. McLaughlin, "Comparison of wireless clock synchronization algorithms for indoor location systems," in *2014 IEEE International Conference on Communications Workshops (ICC)*, pp. 157–162, 2014.

[60] A. R. J. Ruiz and F. S. Granja, "Comparing Ubisense, BeSpoon, and DecaWave UWB Location Systems: Indoor Performance Analysis," *IEEE Transactions on Instrumentation and Measurement*, vol. 66, no. 8, pp. 2106–2117, 2017.

[61] G. Shi and Y. Ming, "Survey of Indoor Positioning Systems Based on Ultra-wideband (UWB) Technology," in *Wireless Communications*, *Networking and Applications* (Zeng, Qing-An, ed.), (New Delhi), pp. 1269–1278, Springer India, 2016.

[62] Y. Liu and Z. Yang, *Location, Localization, and Localizability*. Springer New York, 2011.

[63] G. Mao and B. Fidan, *Localization Algorithms and Strategies for Wireless Sensor Networks: Monitoring and Surveillance Techniques for Target Tracking: Monitoring and Surveillance Techniques for Target Tracking*. IGI Global, 2009.

[64] Qorvo, "DW1000 User Manual, Version 2.18." Available at `https://www.qorvo.com/products/d/da007967` (11.03.2023).

[65] M. Pelka, D. Amann, M. Cimdins, and H. Hellbrück, "Evaluation of time-based ranging methods: Does the choice matter?," in *2017 14th Workshop on Positioning, Navigation and Communications (WPNC)*, pp. 1–6, 2017.

[66] D. Neirynck, E. Luk, and M. McLaughlin, "An Alternative Double-Sided Two-Way Ranging Method," in *2016 13th Workshop on Positioning, Navigation and Communications (WPNC)*, pp. 1–4, 2016.

[67] I. Dotlic, A. Connell, and M. McLaughlin, "Ranging Methods Utilizing Carrier Frequency Offset Estimation," in *2018 15th Workshop on Positioning, Navigation and Communications (WPNC)*, pp. 1–6, 2018.

[68] C. Lian Sang, M. Adams, T. Hörmann, M. Hesse, M. Porrmann, and U. Rückert, "Numerical and Experimental Evaluation of Error Estimation for Two-Way Ranging Methods," *Sensors*, vol. 19, no. 3, 2019.

[69] Y. Jiang and V. C. Leung, "An Asymmetric Double Sided Two-Way Ranging for Crystal Offset," in *2007 International Symposium on Signals, Systems and Electronics*, pp. 525–528, 2007.

[70] Qorvo, "APS002 Application Note: Minimizing Power consumption in DW1000 Based Systems, Version 1.1." Available at `https://www.qorvo.com/products/d/da008437` (11.03.2023).

[71] H. Kim, "Double-Sided Two-Way Ranging Algorithm to Reduce Ranging Time," *IEEE Communications Letters*, vol. 13, no. 7, pp. 486–488, 2009.

[72] R. Fujiwara, K. Mizugaki, T. Nakagawa, D. Maeda, and M. Miyazaki, "TOA/TDOA Hybrid Relative Positioning System Using UWB-IR," in *2009 IEEE Radio and Wireless Symposium*, pp. 679–682, 2009.

[73] P. Grasso, M. S. Innocente, J. J. Tai, O. Haas, and A. M. Dizqah, "Analysis and Accuracy Improvement of UWB-TDoA-Based Indoor Positioning System," *Sensors*, vol. 22, no. 23, p. 9136, 2022.

[74] J. Sidorenko, V. Schatz, N. Scherer-Negenborn, M. Arens, and U. Hugentobler, "Fusion of time of arrival and time difference of arrival for ultra-wideband indoor localization," 2019.

[75] Z. Sahinoglu and S. Gezici, "Enhanced Position Estimation via Node Cooperation," in *2010 IEEE International Conference on Communications*, pp. 1–6, 2010.

[76] M. R. Gholami, S. Gezici, E. G. Ström, and M. Rydström, "Positioning algorithms for cooperative networks in the presence of an unknown turn-around time," in *2011 IEEE 12th International Workshop on Signal Processing Advances in Wireless Communications*, pp. 166–170, 2011.

[77] M. R. Gholami, S. Gezici, and E. G. Strom, "Improved Position Estimation Using Hybrid TW-TOA and TDOA in Cooperative Networks," *IEEE Transactions on Signal Processing*, vol. 60, no. 7, pp. 3770–3785, 2012.

[78] Y. Wang and W. Xiong, "Improving Ranging Accuracy of Active and Passive Anchors in the Presence of Clock Imperfection," in *2013 10th Workshop on Positioning, Navigation and Communication (WPNC)*, pp. 1–5, 2013.

[79] K. A. Horváth, G. Ill, and Á. Milánkovich, "Passive Extended Double-Sided Two-Way Ranging Algorithm for UWB Positioning," in *2017 Ninth International Conference on Ubiquitous and Future Networks (ICUFN)*, pp. 482–487, 2017.

[80] K. A. Horváth, G. Ill, and Á. Milánkovich, "Passive Extended Double-Sided Two-way Ranging with Alternative Calculation," in *2017 IEEE 17th International Conference on Ubiquitous Wireless Broadband (ICUWB)*, pp. 1–5, 2017.

[81] S. Shah and T. Demeechai, "Multiple Simultaneous Ranging in IR-UWB Networks," *Sensors*, vol. 19, no. 24, 2019.

[82] H. Mohammadmoradi, M. Heydariaan, and O. Gnawali, "SRAC: Simultaneous Ranging and Communication in UWB Networks," in *2019 15th International Conference on Distributed Computing in Sensor Systems (DCOSS)*, pp. 9–16, 2019.

[83] H. Chen and A. Dhekne, "PnPLoc: UWB Based Plug & Play Indoor Localization," in *2022 IEEE 12th International Conference on Indoor Positioning and Indoor Navigation (IPIN)*, pp. 1–8, 2022.

[84] S. Shah, K. Chaiwong, L.-O. Kovavisaruch, K. Kaemarungsi, and T. Demeechai, "Antenna Delay Calibration of UWB Nodes," *IEEE Access*, vol. 9, pp. 63294–63305, 2021.

[85] S. Shah, L.-O. Kovavisaruch, K. Kaemarungsi, and T. Demeechai, "Node Calibration in UWB-Based RTLSs Using Multiple Simultaneous Ranging," *Sensors*, vol. 22, no. 3, 2022.

[86] S. Shah, S. Chaudhary, R. Ullah, A. Parnianifard, M. Z. Siddiqi, P. Vanichchanunt, W. Santipach, and L. Wuttisittikulkij, "Antenna Delay-Independent Simultaneous Ranging for UWB-Based RTLSs," *Journal of Sensor and Actuator Networks*, vol. 12, no. 1, 2023.

[87] M. Dong, "A Low-Cost NLOS Identification and Mitigation Method for UWB Ranging in Static and Dynamic Environments," *IEEE Communications Letters*, vol. 25, no. 7, pp. 2420–2424, 2021.

[88] J. Rougier, "Ensemble Averaging and Mean Squared Error," *Journal of Climate*, vol. 29, no. 24, pp. 8865 – 8870, 2016.

[89] D. Simon, *Optimal State Estimation: Kalman, H Infinity, and Nonlinear Approaches*. USA: Wiley-Interscience, 2006.

[90] R. A. Maronna, R. D. Martin, V. J. Yohai, and M. Salibián-Barrera, *Robust Statistics: Theory and Methods (with R)*. John Wiley & Sons, 2019.

[91] C. Leys, C. Ley, O. Klein, P. Bernard, and L. Licata, "Detecting outliers: Do not use standard deviation around the mean, use absolute deviation around the median," *Journal of Experimental Social Psychology*, vol. 49, no. 4, pp. 764–766, 2013.

[92] D. Shepard, "A Two-Dimensional Interpolation Function for Irregularly-Spaced Data," in *Proceedings of the 1968 23rd ACM National Conference*, ACM '68, (New York, NY, USA), p. 517–524, Association for Computing Machinery, 1968.

[93] Y. S. Dodonov and Y. A. Dodonova, "Robust measures of central tendency: weighting as a possible alternative to trimming in response-time data analysis," *Psikhologicheskie Issledovaniya*, vol. 5, no. 19, pp. 1–11, 2011.

[94] J. Borras, P. Hatrack, and N. B. Mandayam, "Decision Theoretic Framework for NLOS Identification," in *VTC'98. 48th IEEE Vehicular Technology Conference. Pathway to Global Wireless Revolution (Cat. No. 98CH36151)*, vol. 2, pp. 1583–1587, IEEE, 1998.

[95] P.-C. Chen, "A Non-Line-of-Sight Error Mitigation Algorithm in Location Estimation," in *WCNC. 1999 IEEE Wireless Communications and Networking Conference (Cat. No.99TH8466)*, vol. 1, pp. 316–320 vol.1, 1999.

[96] J. Xing, J. Zhang, L. Jiao, X. Zhang, and C. Zhao, "A Robust Wireless Sensor Network Localization Algorithm in NLOS Environment," in *2007 IEEE International Conference on Control and Automation*, pp. 3244–3249, 2007.

[97] L. Jiao, J. Xing, X. Zhang, J. Zhang, and C. Zhao, "LCC-Rwgh: A NLOS Error Mitigation Algorithm for Localization in Wireless Sensor Network," in *2007 IEEE International Conference on Control and Automation*, pp. 1354–1359, 2007.

[98] X. Li, "An Iterative NLOS Mitigation Algorithm for Location Estimation in Sensor Networks," *Proceedings of the15 th IST Mobile and Wireless Communications Summit*, pp. 1–5, 2006.

[99] L. Jiao, J. Xing, and F. Y. Li, "Performance Comparison of Residual Related Algorithms for ToA Positioning in Wireless Terrestrial and Sensor Networks," in *2009 1st International Conference on Wireless Communication, Vehicular Technology, Information Theory and Aerospace & Electronic Systems Technology*, pp. 278–283, 2009.

[100] S. Yang and B. Wang, "Residual Based Weighted Least Square Algorithm for Bluetooth/UWB Indoor Localization System," in *2017 36th Chinese Control Conference (CCC)*, pp. 5959–5963, 2017.

[101] Y.-T. Chan, W.-Y. Tsui, H.-C. So, and P.-C. Ching, "Time-of-Arrival Based Localization Under NLOS Conditions," *IEEE Transactions on Vehicular Technology*, vol. 55, no. 1, pp. 17–24, 2006.

[102] B. J. Silva and G. P. Hancke, "Non-Line-of-Sight Identification Without Channel Statistics," in *IECON 2020 The 46th Annual Conference of the IEEE Industrial Electronics Society*, pp. 4489–4493, 2020.

[103] B. J. Silva and G. P. Hancke, "Ranging Error Mitigation for Through-the-Wall Non-Line-of-Sight Conditions," *IEEE Transactions on Industrial Informatics*, vol. 16, no. 11, pp. 6903–6911, 2020.

[104] Q.-T. Ngo, P. Roussel, B. Denby, and G. Dreyfus, "Correcting Non-Line-of-Sight Path Length Estimation for Ultra-Wideband Indoor Localization," in *2015 International Conference on Localization and GNSS (ICL-GNSS)*, pp. 1–6, 2015.

[105] A. Niitsoo, T. Edelhäußer, and C. Mutschler, "Convolutional Neural Networks for Position Estimation in TDoA-based Locating Systems," in *2018 International Conference on Indoor Positioning and Indoor Navigation (IPIN)*, pp. 1–8, IEEE, 2018.

[106] İ. Güvenç, C.-C. Chong, F. Watanabe, and H. Inamura, "NLOS Identification and Weighted Least-Squares Localization for UWB Systems Using Multipath Channel Statistics," *EURASIP Journal on Advances in Signal Processing*, vol. 2008, pp. 1–14, 2007.

[107] W. Li, T. Zhang, and Q. Zhang, "Experimental researches on an UWB NLOS identification method based on machine learning," in *2013 15th IEEE International Conference on Communication Technology*, pp. 473–477, 2013.

[108] X. Yang, "NLOS Mitigation for UWB Localization Based on Sparse Pseudo-Input Gaussian Process," *IEEE Sensors Journal*, vol. 18, no. 10, pp. 4311–4316, 2018.

[109] J. Fan and A. S. Awan, "Non-Line-of-Sight Identification Based on Unsupervised Machine Learning in Ultra Wideband Systems," *IEEE Access*, vol. 7, pp. 32464–32471, 2019.

[110] Z. Zeng, S. Liu, and L. Wang, "UWB NLOS identification with feature combination selection based on genetic algorithm," in *2019 IEEE International Conference on Consumer Electronics (ICCE)*, pp. 1–5, 2019.

[111] C. Jiang, J. Shen, S. Chen, Y. Chen, D. Liu, and Y. Bo, "UWB NLOS/LOS Classification Using Deep Learning Method," *IEEE Communications Letters*, vol. 24, no. 10, pp. 2226–2230, 2020.

[112] J. Wang, K. Yu, J. Bu, Y. Lin, and S. Han, "Multi-Classification of UWB Signal Propagation Channels Based on One-Dimensional Wavelet Packet Analysis and CNN," *IEEE Transactions on Vehicular Technology*, vol. 71, no. 8, pp. 8534–8547, 2022.

[113] C. Liu, Y. Cao, C. Sun, W. Shen, X. Li, and L. Gao, "An Outlier-Aware Method for UWB Indoor Positioning in NLoS Situations," in *2022 IEEE 25th International Conference on Computer Supported Cooperative Work in Design (CSCWD)*, pp. 1504–1509, 2022.

[114] Z. Cui, T. Liu, S. Tian, R. Xu, and J. Cheng, "Non-Line-of-Sight Identification for UWB Positioning Using Capsule Networks," *IEEE Communications Letters*, vol. 24, no. 10, pp. 2187–2190, 2020.

[115] Z. Cui, Y. Gao, J. Hu, S. Tian, and J. Cheng, "LOS/NLOS Identification for Indoor UWB Positioning Based on Morlet Wavelet Transform and Convolutional Neural Networks," *IEEE Communications Letters*, vol. 25, no. 3, pp. 879–882, 2020.

[116] M. Si, Y. Wang, H. Siljak, C. Seow, and H. Yang, "A Lightweight CIR-Based CNN With MLP for NLOS/LOS Identification in a UWB Positioning System," *IEEE Communications Letters*, pp. 1–1, 2023.

[117] S. Tomović, K. Bregar, T. Javornik, and I. Radusinović, "Transformer-based NLoS detection in UWB localization systems," in *2022 30th Telecommunications Forum (TELFOR)*, pp. 1–4, 2022.

[118] D.-H. Kim, A. Farhad, and J.-Y. Pyun, "UWB Positioning System Based on LSTM Classification With Mitigated NLOS Effects," *IEEE Internet of Things Journal*, vol. 10, no. 2, pp. 1822–1835, 2022.

[119] K. Wen, K. Yu, and Y. Li, "NLOS Identification and Compensation for UWB Ranging Based on Obstruction Classification," in *2017 25th European Signal Processing Conference (EUSIPCO)*, pp. 2704–2708, 2017.

[120] K. Yu, K. Wen, Y. Li, S. Zhang, and K. Zhang, "A Novel NLOS Mitigation Algorithm for UWB Localization in Harsh Indoor Environments," *IEEE Transactions on Vehicular Technology*, vol. 68, no. 1, pp. 686–699, 2019.

[121] M. H. Kabir and R. Kohno, "A Hybrid TOA-Fingerprinting Based Localization of Mobile Nodes Using UWB Signaling for Non Line-Of-Sight Conditions," *Sensors*, vol. 12, no. 8, pp. 11187–11204, 2012.

[122] Z. Zeng, R. Bai, L. Wang, and S. Liu, "NLOS identification and mitigation based on CIR with particle filter," in *2019 IEEE Wireless Communications and Networking Conference (WCNC)*, pp. 1–6, 2019.

[123] C. Chen, Z. Huang, J. Wang, L. Yuan, J. Bao, and Z. Chen, "Channel-Quality-Evaluation-Based Anchor Node Selection for UWB Indoor Positioning," *Electronics*, vol. 11, no. 3, 2022.

[124] S. Wu, Y. Ma, Q. Zhang, and N. Zhang, "NLOS Error Mitigation for UWB Ranging in Dense Multipath Environments," in *2007 IEEE Wireless Communications and Networking Conference*, pp. 1565–1570, 2007.

[125] J. Schroeder, S. Galler, K. Kyamakya, and K. Jobmann, "NLOS detection algorithms for Ultra-Wideband localization," in *2007 4th Workshop on Positioning*, *Navigation and Communication*, pp. 159–166, 2007.

[126] V. Barral, C. J. Escudero, J. A. García-Naya, and R. Maneiro-Catoira, "NLOS Identification and Mitigation Using Low-Cost UWB Devices," *Sensors*, vol. 19, no. 16, 2019.

[127] S. Krishnan, R. Xenia Mendoza Santos, E. Ranier Yap, and M. Thu Zin, "Improving UWB Based Indoor Positioning in Industrial Environments Through Machine Learning," in *2018 15th International Conference on Control*, *Automation, Robotics and Vision (ICARCV)*, pp. 1484–1488, 2018.

[128] F. Che, Q. Z. Ahmed, J. Fontaine, B. Van Herbruggen, A. Shahid, E. De Poorter, and P. I. Lazaridis, "Feature-Based Generalized Gaussian Distribution Method for NLoS Detection in Ultra-Wideband (UWB) Indoor Positioning System," *IEEE Sensors Journal*, vol. 22, no. 19, pp. 18726–18739, 2022.

[129] R. Zandian and U. Witkowski, "Differential NLOS Error Detection in UWB-based Localization Systems using Logistic Regression," in *2018 15th Workshop on Positioning*, *Navigation and Communications (WPNC)*, pp. 1–6, 2018.

[130] K. Gururaj, A. K. Rajendra, Y. Song, C. L. Law, and G. Cai, "Real-Time Identification of NLOS Range Measurements for Enhanced UWB Localization," in *2017 International Conference on Indoor Positioning and Indoor Navigation (IPIN)*, pp. 1–7, 2017.

[131] J. Wu, Z. Zhang, S. Zhang, Z. Kuang, and L. Zhang, "UWB Positioning Algorithm Based on Fuzzy Inference and Adaptive Anti-NLOS Kalman Filtering," *Applied Sciences*, vol. 12, no. 12, 2022.

[132] F. Halawa, H. Dauod, I. G. Lee, Y. Li, S. W. Yoon, and S. H. Chung, "Introduction of a real time location system to enhance the warehouse safety and operational efficiency," *International Journal of Production Economics*, vol. 224, p. 107541, 2020.

[133] A. Martinelli, S. Jayousi, S. Caputo, and L. Mucchi, "UWB Positioning for Industrial Applications: the Galvanic Plating Case Study," in *2019 International Conference on Indoor Positioning and Indoor Navigation (IPIN)*, pp. 1–7, 2019.

[134] K. Minne, N. Macoir, J. Rossey, Q. Van den Brande, S. Lemey, J. Hoebeke, and E. De Poorter, "Experimental Evaluation of UWB Indoor Positioning for Indoor Track Cycling," *Sensors*, vol. 19, no. 9, 2019.

[135] J. Tiemann and C. Wietfeld, "Scalable and Precise Multi-UAV Indoor Navigation Using TDOA-based UWB Localization," in *2017 International Conference on Indoor Positioning and Indoor Navigation (IPIN)*, pp. 1–7, 2017.

[136] Pozyx, "FAQ | Pozyx." Available at `https://www.pozyx.io/technology/faq` (30.03.2023).

[137] Eliko Tehnoloogia Arenduskeskus OÜ, "Eliko UWB RTLS." Available at `https://eliko.ee/uwb-rtls-ultra-wideband-real-time-location-system/` (11.04.2023).

[138] Leica Geosystems AG, "Leica DISTO S910 User Manual." Available at `https://shop.leica-geosystems.com/sites/default/files/2019-04/leica-disto-s910-user-manual-805080-808183-806677-en.pdf` (11.04.2023).

[139] Leica Geosystems AG, "Leica DISTO S910 P2P Package." Available at `https://www.leicadisto.co.uk/shop/leica-disto-s910-p2p-package/` (11.04.2023).

[140] Eliko Tehnoloogia Arenduskeskus OÜ, "Eliko UWB RTLS Installation Guide." Available at `https://eliko.tech/wp-content/uploads/2021/10/eliko_rtlss_installation_guide.pdf` (11.04.2023).

[141] I. Guvenc and C.-C. Chong, "A Survey on TOA Based Wireless Localization and NLOS Mitigation Techniques," *IEEE Communications Surveys & Tutorials*, vol. 11, no. 3, pp. 107–124, 2009.

[142] Krah Pipes OÜ. Available at `http://www.krah-pipes.ee/eng/` (11.04.2023).

[143] OpenAI, "ChatGPT." Available at `https://openai.com` (23.05.2023), 2021.

Acknowledgements

I would like to express my sincere gratitude to the Thomas Johann Seebeck Department of Electronics at Tallinn University of Technology and Eliko Tehnoloogia Arenduskeskus OÜ for providing me with the exceptional opportunity to pursue my PhD degree.

I extend my deepest appreciation to my esteemed supervisors, Sander Ulp from Eliko, Professor Muhammad Mahtab Alam, and Yannick le Moullec from Tallinn University of Technology. Their invaluable guidance, critical insights, and unwavering support have played a pivotal role in shaping this thesis, regardless of their vacation schedules or the time of day.

I would also like to thank my other colleagues at Eliko Tehnoloogia Arenduskeskus OÜ, especially Enar Reilent, Aleksei Fjodorov, and Mihkel Tommingas, for their expertise, assistance, and enjoyable camaraderie. Their contributions have greatly enriched my understanding and kept me on track throughout my journey towards the PhD degree.

Furthermore, I want to express my deepest appreciation to my beloved wife Gerda, my supportive family, my friends, and our two loyal dogs, Kirsi and Kali. Their unwavering faith, continuous encouragement, and unconditional love have been the pillars of strength that propelled me forward. The sacrifices they made and the patience they displayed have been a constant source of motivation.

I dedicate this thesis to everyone mentioned above, as their collective efforts have made it possible. I am eternally grateful for your invaluable contributions.

Thank you.

Abstract
Active-Passive Two-Way Ranging Protocol for Positioning Systems

Ultra-Wideband (UWB) indoor positioning has emerged as a significant area of interest for both consumers and researchers, with its use becoming increasingly prevalent. The integration of UWB chips into various devices has opened up new possibilities for precise and efficient indoor positioning, making it a popular choice for a wide range of applications. The high temporal resolution offered by UWB devices has led to the development of several positioning methods, each with its unique advantages and challenges.[7]

Among the various UWB-based positioning methods, Time of Flight (ToF) and Time Difference of Arrival (TDoA) are particularly noteworthy. These time-based methods fully exploit the high temporal resolution of UWB devices, enabling accurate and efficient positioning. However, both ToF and TDoA have their strengths and weaknesses, which are addressed by introducing the concept of passive ranging, which aims to mitigate the limitations of both of these methods.

The PhD thesis presents a pioneering first contribution in the form of the Active-Passive Two-Way Ranging (AP-TWR) protocol. In the scope of this thesis, the AP-TWR is developed with UWB in mind, although it should be noted that the AP-TWR protocol is not exclusively limited to UWB technology. This protocol stands out from existing passive ranging methods by offering a unique level of flexibility. It allows for the customization of anchor roles within a system, enabling the specification of the number of active-passive and passive-only anchors. The active-passive anchors determine the total count of packets in a ranging sequence, while the passive-only anchors provide additional range estimates without any increase in air time. What sets AP-TWR apart from the state-of-the-art passive ranging methods is its ability to adapt to a variety of requirements. While conventional methods strictly prioritize air time reduction, AP-TWR offers the flexibility to cater to different needs. It can focus on reducing air time and consequently, power consumption, minimizing ranging errors, or making incremental improvements in both aspects. As an example of improving both at the same time, the decrease of air time occupancy by 12.5% and the ranging Root-Mean-Square-Error (RMSE) by 7.4% was experimentally shown for one of the multiple possible AP-TWR configurations ($m = 5, k = 1$).

As a second contribution, the thesis further advances the field by refining the previously proposed AP-TWR protocol and introducing an alternative method for calculating AP-TWR range estimates. This development expands the application of the protocol, pairing both methods with three of the most commonly used active ranging protocols. This pairing results in six unique variations of the AP-TWR protocol.

These variations are then compared based on their theoretical accuracy through numerical simulations, providing a comprehensive performance analysis of the air time occupancy and the ranging RMSE. The most well-rounded method, as determined by these comparisons, undergoes further experimental testing to validate the simulation results. The relative decrease of RMSE and air time by 18.3% and 25%, respectively was shown with the AP-TWR ($m = 4, k = 2$).

The third key contribution of this thesis lies in the rigorous testing and enhancement of the AP-TWR protocol's robustness under both Line-of-Sight (LoS) and Non-Line-of-Sight (NLoS) propagation conditions. The study involved a comparative analysis of the previously used Least Squares (LS) method for deriving range estimates from the AP-TWR measurement matrix against six other measurement matrix processing techniques. The

---

[7]The English language of this abstract has been co-edited with ChatGPT [143].

results of this comparison revealed that in LoS most of the methods performed similarly. While several of the tested methods demonstrated improved robustness of AP-TWR range estimates in NLoS scenarios compared to the baseline Single-Sided Two-Way Ranging (SS-TWR), achieving upwards of 19% reduction of ranging RMSE.

The fourth and final contribution of this thesis pivots from the previous focus on range estimates to address position accuracy. This is achieved through the introduction of a novel Adaptive Extended Kalman Filter (A-EKF) positioning method, which is based on the AP-TWR protocol.

The formulation of the A-EKF positioning method is rooted in a comprehensive analysis of various potential Non-Line-of-Sight (NLoS) scenarios. The implementation of this innovative A-EKF positioning method has demonstrated a significant reduction in positioning errors caused by NLoS effects, particularly in challenging industrial environments. A number of 3D positioning experiments showed an average reduction of positioning RMSE by 3 times, achieving 0.224 m, when compared with the next-best method, while the absolute maximum error was reduced by 9 times (from 4.5 m to a maximum of 0.5 m).

This thesis makes strides in the field of UWB positioning systems through the development of the Active-Passive Two-Way Ranging (AP-TWR) protocol and the Adaptive Extended Kalman Filter (A-EKF) positioning method. These advancements contribute to more accurate indoor positioning, opening up new avenues for further research and development in this field. The potential for future enhancements to these methods promises to further refine the accuracy and efficiency of UWB positioning systems.

Kokkuvõte
Aktiiv-passiivne kauguste mõõtmise protokoll positsioneerimis-süsteemidele

Ülilairiba tehnoloogial (*Ultra-Wideband*, *UWB*) põhinev siseruumides positsioneerimine on viimastel aastatel kujunenud muuhulgas üheks perspektiivikamaks uurimussuunaks nii teaduses kui ka äratanud huvi kommertstarbijate seas. UWB kiipide laiem levik on avanud tee uudsete täppis-sisepositsioneerimise süsteemide ning nendel põhinevate asukohapõhiste teenuste arengule. UWB tehnoloogia kasuks räägib kõrge ajaliste pulsside eristusvõime, mille tõttu on võimalik suure täpsusega määrata objektide asukohti.

UWB tehnoloogiat on mitmeti võimalik rakendada positsioneerimise protsessis, pikemalt peatumata teistel meetoditel, on eelmainitud ajaliste pulsside eraldusvõime tõttu kõige mõistlikum rakendada leviaja põhist (*Time of Flight*, *ToF*) või leviaegade erinevuse põhist (*Time Difference of Arrival*, *TDoA*) positsioneerimist. Mõlema meetodi puhul eksisteerivad ka omad positiivsed ja negatiivsed küljed, millest viimaste leevendamiseks on kasvutusele võetud passiivsed kauguste mõõtmise protokollid.

Esmalt kirjeldab käesolev doktoritöö uudse Aktiiv-Passiiv Kauguse Mõõtmise Protokolli (*Active-Passive Two-Way Ranging*, *AP-TWR*) välja arendamist. Kuigi antud doktoritöö raames on AP-TWR välja arendatud silmas pidades UWB tehnoloogiat, on oluline mainida, et antud protokolli kasutus ei ole siiski piiratud ainult UWB'ga. Välja arendatud protokoll pakub paindlikkust mõõteseadmete rollide ning nende arvu määramisel, mistõttu defineeritakse kahte tüüpi ankurseadmed: aktiiv-passiiv seadmed ning passiivseadmed. Esimesed neist osalevad aktiivselt mõõtmisprotsessis ning kuulavad teiste seadmete suhtlust kui nad ise pole saaterežiimis, teised neist aga pakuvad positsioneerimiseks lisainformatsiooni ilma, et aktiivselt osaleksid paketivahetuses. Kui muud teaduskirjanduses levinud protokollid on suunitletud kauguse mõõtmise protokollis eetriaja (seekaudu ka tarbitud energia) kokkuhoidmisele, siis AP-TWR puhul on tegemist protokolliga, mida saab mugandada vastavalt süsteemi täpsuse või eetriaja kokkuhoidmise vajadustele. Esimeses teadusartiklis toodud üks mitmest võimalikust AP-TWR protokolli konfiguratsioonidest (kus aktiiv-passiivankruid on 5 ning passiivankruid 1), näidati katseliselt, et AP-TWR'i kasutus vähendas kauguse mõõtmise ruutkeskmist viga 7.4%, samal ajal vähendades eetris saatel oldud aega 12.5%.

Teise panusena uuriti antud teemat edasi, pakkudes välja alternatiivse aktiiv-passiiv kauguse mõõtmise arvutusmeetodi. Kõrvutades kahte välja pakutud aktiiv-passiiv protokolli koos enamlevinud aktiivsete leviaja mõõtmise meetoditega, pakuti teadustöös välja kuus erinevat varianti aktiiv-passiiv kauguse mõõtmise protokollist, mis kõrvutati üksteisega arvutikatsetes saavutatava ruutkeskmise mõõtmisvea ning eetrikasutuse seisukohalt. Saavutatud ruutkeskmise mõõtevea tulemuste ning eetrikasutuse seisukohalt valiti parim meetod ning veenduti selle toimimises ka katseliselt: 4 aktiiv-passivankru ning 2 passivankruga positsioneerimissüsteemiga suudeti saavutada ruutkeskmise vea vähenemine 18.3% ning eetriaja vähenemine 25%.

Kolmandaks uurimuse suuremaks suunaks oli AP-TWR kaugusemõõtmiste maatriksi erinevate töötlemismeetodite jõudluse uurimine, eesmärgiga muuta antud meetod veelgi vastupidavamaks erinevatest allikatest tulenevatele mõõtemüradele. Teadusartikli raames uuriti lisaks eelnevalt kasutusel olevale vähimruutude meetodile kuute erinevat töötlemismeetodit. Meetodite kõrvutamiseks kauguse mõõtmise ruutkeskmise vea alusel sooritati UWB seadmetega katsed kolmes levikeskkonnas: takistuseta otselevi, levitingimused kus kahe seadme vahel oli takistuseks metallplaat ning tingimused kus takistavaks teguriks oli inimkeha. Võrreldes ekvivalentse aktiiv-kaugusmõõtmise protokolliga *Single-*

Sided Two-Way Ranging (SS-TWR), leiti, et taktistusteta levi puhul suudavad kõik meeto-did pakkuda sarnast täpsust. Erinevused tulid aga sisse takistatud leviteekondadel, mille puhul suudeti ruutkesmist viga vähendada kuni 19%.

Neljanda ning viimase panuse andis teadusartikkel, mis esmalt koondas enesesse eel-nevate panuste teadmised, sellel põhjal formuleeris põhjaliku ülevaate erinevate veail-mingute kooslustest mida tekitavad leviteekonna takistused ning omakorda selle põhjal pakkus välja uudse Adaptiivse Laiendatud Kalmani Filtri (*Adaptive Extended Kalman Filter, A-EKF*) põhise positsioneerimise meetodi. A-EKF meetodi valideerimiseks sooritati katsed tööstuslikus keskkonnas milles asus mitmeid leviteekonda segavaid tegureid nagu suured metallist toruvormid, lakke paigaldatud liikuv kraana, tehase inventar jne. Kolmemõõt-melise positsioneerimise katsete tulemused näitasid, et välja pakutud A-EKF positsionee-rimismeetod saavutas positsioneerimise ruutkeskmise vea 0.224 m, mis oli üle 3 korra parem kui sellest järgmine meetod, seejuures vähendades osades asukohapunktides ilm-nenud maksimaalset 4.5 m suurust viga lausa 9 korda, saavutades maksimaalseks kõrva-lekaldeks rasketes levitingimustes maksimaalselt umbes 0.5 m.

Käesolevas doktoritöös pakuti välja ning arendati edasi uudne kauguste mõõtmise pro-tokoll ning integreeriti see uudsesse A-EKF positsioneerimismeetodisse, mis võimaldas saavutada täpsemaid kauguste mõõtmise ning siseositsioneerimise tulemusi, sealjuu-res võimaldades ka kokku hoida eetriaja ning energiatarbe arvelt. Antud töö avab uued võimalused tulevasteks teadustöödeks, täiendamaks eelmainitud AP-TWR protokolli ning samaaegselt panustades, loomaks täpsemaid ning efektiivsemaid UWB siseositsioneeri-mise lahendusi.

Appendix 1

Publication I

Active-Passive Two-Way Ranging Using UWB

Taavi Laadung† ‡, Sander Ulp‡, Muhammad Mahtab Alam†, Yannick Le Moullec†

Thomas Johann Seebeck Department of Electronics
† Tallinn University of Technology
‡ Eliko Tehnoloogia Arenduskeskus OÜ
Tallinn, Estonia
{taavi.laadung, muhammad.alam, yannick.lemoullec}@taltech.ee, sander.ulp@eliko.ee

Abstract—This paper proposes a generalized approach combining two-way ranging (TWR) and passive ranging methods, called active-passive two-way ranging (AP-TWR). The proposed approach offers a generalized solution for a wide range of anchor configurations in positioning systems. The possibility to define active-passive and passive-only anchor roles allows scaling the system to improve the root-mean-square-error (RMSE) of the ranging estimations and the air time occupancy. Practical experiments show that with the proposed method consisting of 5 active-passive anchors and a single passive anchor, the RMSE is improved by 7.4% and the air time occupancy by 12.5% as compared to the single-sided TWR method with a 6 anchor configuration. Moreover, simulation results show that a maximum theoretical RMSE improvement of 31.7% can be achieved with the proposed setup.

Index Terms—UWB, two-way ranging, passive ranging

I. INTRODUCTION

The market for a wide range of location-based services (asset tracking, object locating, navigation, etc.) has been growing over the last years. The demand for ubiquitous access to these services has pushed for the development of indoor positioning systems, as opposed to classical Global Navigation Satellite Systems (GNSS) which typically operates outdoors. Indoor propagation conditions have raised new challenges for positioning systems: requirement for high accuracy, low interference towards other systems, robustness to multi-path effects, etc [1].

Ultra-Wideband (UWB) technology-based indoor positioning systems are becoming more popular over the last years. This is primarily due to their achievable accuracy of positioning as well as their robustness to multipath effects and presence of obstructions [2]. The most widely used range-based methods for UWB positioning are ToA (Time of Arrival) and TDoA (Time Difference of Arrival). The former is used to calculate distance by measuring the round-trip time of a ranging packet, and the latter employs synchronized anchors to calculate the distance differences of a tag to several anchors. Since ToA does not need clock synchronization between anchors, the complexity of these systems is generally lower [3].

Since employing ToA requires more air-time occupancy due to a larger amount of packets transmitted per ranging session

and also depending on the ranging rate, the number of tags operating in a positioning system becomes limited [4]. To push the limitation, state of the art passive ranging schemes should be implemented, where the system consists of a single active anchor which is transmitting, and a number of passive anchors which are in dedicated receive mode. These passive methods allow decreasing the number of transmitted packets, effectively decreasing the air time and allowing more tags to operate in a system.

This paper proposes a generalized method which combines active and passive ranging to provide a flexible positioning system configuration. Depending on the requirements, the final configuration could be oriented towards better ranging precision, shorter protocol, or a balanced configuration offering slight improvements to both. The main principle is providing the active anchors with the functionality of passive ranging, making them so-called active-passive anchors. This ranging scheme allows each active-passive anchor to provide several range estimates during a single ranging sequence, compared to a single range estimate provided by conventional active ranging. Furthermore, the addition of passive-only anchors provides even more range estimates without increasing the number of transmitted packets, theoretically removing the limit to the maximum number of anchors participating in ranging. Depending on the number of active-passive anchors, the passive-only anchors also provide multiple measurements per ranging sequence, making them more precise.

The structure of this paper is as follows. Section II provides the state-of-the-art works on passive ranging; Section III describes the main idea of passive two-way ranging (TWR) and proposes the active-passive TWR (AP-TWR) method; Sections IV and V provide the numerical and experimental results of the proposed method, respectively. Finally, the conclusions are drawn in Section VI.

II. RELATED WORKS

This section gives an overview of the state of the art related to the usage of passive ranging schemes in UWB based systems.

Fujiwara, Mizugaki, Nakagawa, Maeda and Miyazaki [5] developed a seminal UWB ToA/TDoA hybrid positioning system, which reduces the needed number of anchors and packet exchanges in a positioning sequence. Sahinoglu and Gezici [6] give a theoretical analysis of the ToA/TDoA hybrid

method provided in the previous paper. Although the usage of a hybrid system gives more accurate position estimations, the proposed system consisted of only 2 anchors. This would mean that only a 2-dimensional position estimation could be derived by setting geometric constraints for the tag location.

Gholami, Gezici, Rydström and Ström [7] develop a maximum likelihood estimator (MLE) in conjunction with the hybrid ToA/TDoA for position estimation. Due to the simultaneous usage of ToF and TDoA, the proposed system needs complicated post-processing, combining range and time difference based positioning methods. In [8], [9] the previous idea is expanded, so not only the anchors, but also the tags provide the TDoA values by acting as passive listeners. Although, this method provides improved performance in terms of position estimation root-mean-square-error (RMSE), the implementation raises some practical limitations. Firstly, in order for the tags to provide the TDoA values, they should be in receive mode at all times, which drains the batteries quicker than being in sleep mode in between data transmissions. Furthermore, the tags would need *a priori* knowledge of the location of anchors, or in the case of a centralized positioning system, the TDoA values need to be communicated to a positioning server, requiring more time spent transmitting.

A mixture of symmetric double-sided two-way ranging (SDS-TWR) and passive ranging, called Passive Extended (PE) ranging, is presented by Horvath, Ill and Milankovich [10]. The PE ranging increases the accuracy of ranging at the cost of adding a single packet to a positioning sequence, when compared to standard passive ranging. The same authors further improved on PE ranging by introducing an alternative calculation to the method in [11], providing more robustness against time measurement errors in nodes. In addition to the added packet, the practical implementation of said method is again bounded by the battery life of tags, as the ranging is initiated by the anchor, meaning the tag has to be in constant receive mode, rather than sleeping in between rangings.

The three Multiple Simultaneous Ranging (MSR) methods presented by Shah and Demeechai [12] employ a single active and multiple passive anchors to estimate the distances to a tag during a single positioning sequence. The main idea is to provide the estimated anchor-to-tag distances with the lowest possible airtime occupancy. While reducing the number of needed packets in a positioning sequence, MSR method 1 also tackles the previously mentioned practical limitations by setting the tag as the ranging session initiator. Results show that the airtime occupancy is reduced at the cost of range estimation RMSE. Although, the protocol length is reduced by using this method, the authors only focus on the case of a single active anchor and k number of passive anchors,

This paper proposes a ranging scheme which combines active and passive ranging to provide a system configuration with m active-passive anchors and k passive anchors. Depending on the requirements of the system, a network could be constructed to optimize the range estimate RMSE, the length of protocol or providing a balancing point in between.

III. RANGING METHODS

This section describes the main idea of passive ranging and the proposed AP-TWR method.

A. Passive Two-Way Ranging

Passive ranging is based on the assumption of having anchors at a fixed, known location, so the distances between each anchor can be calculated beforehand. In the scope of this paper, a tag-initiated single-sided two-way-ranging (SS-TWR) method is used for the active transmission, the clock offsets are not considered as they can be compensated for SS-TWR [13]. This method allows the tag to remain in sleep mode to conserve its battery charge when not ranging.

Figure 1 describes the TWR method using passive anchors that do not participate in active packet exchange, the notation is as follows:

- $t_\triangleleft^\diamond$ is $\diamond$-th time interval measured by node $\triangleleft$
- $t_{\bullet\leftrightarrow\circ}$ is time of flight (ToF) from node $\bullet$ to node $\circ$

Tag T initiates the ranging sequence with a ranging request. Upon receiving it, anchor A responds with a ranging reply after processing time t_A^I. The tag in turn sends out a ranging report after its own processing time t_T^{II}, while the passive listening anchor L receives all the packets and records the corresponding timestamps.

Note that the value of $t_{A\leftrightarrow L}$ can be calculated with (1) via speed of light c since the physical distance $d_{A\leftrightarrow L}$ between A and L is known.

$$t_\star = \frac{d_\star}{c} \Leftrightarrow d_\star = ct_\star \tag{1}$$
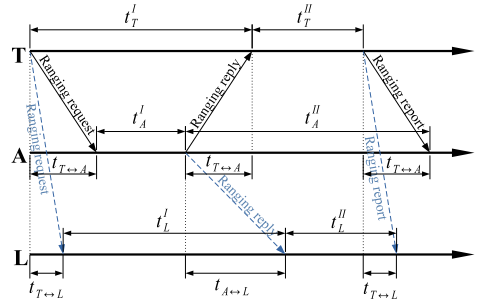
Fig. 1. Passive ranging packet exchange

The ToF value from T to L, $t_{T\leftrightarrow L}$ can be calculated in two ways: by using the 1st and 2nd, or 2nd and 3rd packet exchange, respectively, as can be seen from Fig. 1:

$$t_{T\leftrightarrow L} = t_{T\leftrightarrow A} + t_A^I + t_{A\leftrightarrow L} - t_L^I \tag{2a}$$

$$t_{T\leftrightarrow L} = t_L^{II} + t_{A\leftrightarrow L} - t_{T\leftrightarrow A} - t_T^{II} \tag{2b}$$

Then the sum of (2a) and (2b) becomes

$$2t_{T\leftrightarrow L} = 2t_{A\leftrightarrow L} + t_A^I - t_L^I + t_L^{II} - t_T^{II} \tag{3}$$

Since $t_T^I + t_T^{II} = t_L^I + t_L^{II}$, rearranging it so that $t_T^{II} = t_L^I + t_L^{II} - t_T^I$ and substituting it into (3), then by simplifying it becomes

$$t_{T\leftrightarrow L} = \frac{t_A^I + t_T^I}{2} + t_{A\leftrightarrow L} - t_L^I \tag{4}$$

Equation (4) serves the basis for passive ToF measurement, employing dedicated active and passive anchors. It is also a simplified form of Multiple Simultaneous Ranging (MSR) Equation (16) published in [12].

B. Proposed Method

The proposed method takes the concept described in Section III-A and generalizes it, so a total of m active anchors and n passive anchors take part in the ranging process, noting that the active anchors simultaneously take part in passive ranging as well. In order to develop the generalized equation for the proposed method, some changes to the notation of equations presented in Section III-A had to be made:

- t_{Ti} - i^{th} time interval measured by tag T
- t_{Ai} - processing time of active anchor i
- t_{Li} - passive anchor time interval of ith active anchor
- $t_{Ai\leftrightarrow Aj}$ - ToF from anchor i to anchor j
- $t_{i,j}$ - ToF from tag to passive anchor j while listening on anchor i's transmission

This also is illustrated in Figure 2. Note that the report packet which contains the information from ranging is omitted from the figure.

Similar to previous Section, the tag T starts the ranging sequence by transmitting a ranging request packet to active anchor A_i, which responds after its reply processing time t_{Ai}. The tag records the round-trip time corresponding to anchor i as t_{Ti}, while the passive anchor A_j measures the time intervals corresponding to anchor i as t_{Li}. $t_{Ai\leftrightarrow Aj}$ denotes the ToF value from anchor i to anchor j. Finally, the estimated ToF from tag T to listener anchor A_j while listening to anchor A_i's transmissions is denoted as $t_{i,j}$.

The first part of (5) corresponds to active ranging employing the SS-TWR method [13]. The second part illustrates passive ranging, which is the product of generalizing (4). The resulting equation covers active-passive ranging for a total of n anchors from which m are active-passive anchors, making the number of passive-only anchors as $k = n - m$.

$$t_{i,j} = \begin{cases} \dfrac{t_{Ti} - t_{Ai}}{2}, & \text{for } i = j \\[2mm] \dfrac{t_{Ti} + t_{Ai}}{2} + t_{Ai\leftrightarrow Aj} - t_{Li}, & \text{for } i \neq j \end{cases} \tag{5}$$

where $i \in \{1, 2, \ldots, m\}$, $j \in \{1, 2, \ldots, n\}$ and $n \geqslant m$. The constraint of $n \geqslant m$ is introduced to eliminate sub-optimal cases. Assuming the anchors are not power constrained, there is no added cost for anchors to listen to other transmissions. So it is sensible to receive every active ranging packet.

Equation (5) allows to construct a m by n matrix each ranging sequence, where the ToF estimates from active ranging lay on the main diagonal, and passive rangings off the main diagonal:
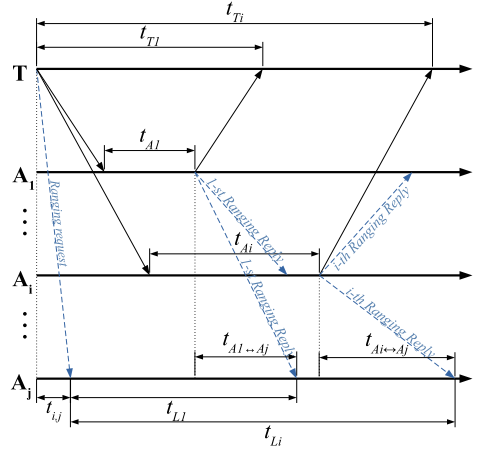
Fig. 2. Proposed generalized active-passive ranging. T initiates sequence, A_1 and A_i respond, A_j listens.

$$M = \begin{bmatrix} t_{1,1} & \cdots & t_{1,m} \\ \vdots & \ddots & \\ t_{n,1} & & t_{n,m} \end{bmatrix} \tag{6}$$

Equation (6) enables row-wise averaging to reduce the effect of range estimation noise. The resulting values correspond to averaged anchor-to-tag ToF values, which can be used as inputs for position estimation.

IV. NUMERICAL SIMULATION RESULTS

This section provides an overview of the numerical simulation results for the proposed active-passive ranging scheme. The performance of the range estimation, as well as the impact on air-time occupancy are considered.

A. Ranging Performance

The ranging performance was assessed by conducting Monte Carlo simulations over 1000 iterations, each consisting of 1000 separate ranging sequences. During each iteration, the anchors and tag were placed at random positions in a simulated 600 by 400 by 250 cm room. Each ranging sequence, the measurement matrix was constructed with (6) and the active and passive range estimations were averaged row-wise to reduce the effect of measurement noise. Finally, the RMSE values were calculated.

In order to evaluate the performance of AP-TWR, the following assumptions were made to the numerical simulations: propagation condition is line-of-sight (LoS), range estimation noise follows a Gaussian distribution, clock errors are omitted, calibration errors are omitted, distances between anchors are known and exact, ToF values in (6) are converted to distances via (1), baseline active and passive anchor performance values taken from [12].

k / m	0	1	2	3	4	5	6	7	8	9
1	3.159	4.236	4.539	4.682	4.768	4.822	4.860	4.891	4.913	4.931
2	2.997	3.211	3.313	3.370	3.410	3.437	3.459	3.474	3.487	3.496
3	2.620	2.704	2.752	2.783	2.807	2.825	2.836	2.846	2.856	2.861
4	2.342	2.384	2.411	2.431	2.446	2.456	2.466	2.473	2.479	2.483
5	2.132	2.157	2.174	2.187	2.196	2.206	2.212	2.218	2.223	2.226
6	1.968	1.984	1.996	2.006	2.013	2.019	2.023	2.028	2.032	2.035
7	1.838	1.848	1.857	1.864	1.869	1.874	1.878	1.881	1.884	1.886
8	1.728	1.737	1.744	1.748	1.753	1.757	1.759	1.762	1.764	1.766
9	1.638	1.643	1.649	1.652	1.656	1.659	1.662	1.664	1.666	1.667
10	1.559	1.564	1.568	1.571	1.574	1.576	1.578	1.581	1.582	1.583

k / m	0	1	2	3	4	5
1	3.286	4.608	5.334	5.337	5.466	5.533
2	3.259	3.764	3.838	3.958	4.076	
3	3.251	3.384	3.544	3.670		
4	2.946	3.144	3.268			
5	2.901	3.043				
6	2.892					

Table I presents the results of numerical simulations. The results show the final RMSE values (cm) depending on the number of active-passive anchors m and the number of additional passive-only anchors k. The case of $m = 1$ and $k = 0$ represents the performance of an active anchor utilizing only SS-TWR.

Each additional active-passive anchor decreases the resulting RMSE. This can be seen in case $k = 0$ where increasing the number of active-passive anchors m in the range of 1...10 the RMSE decreases from 3.159 cm to 1.559 cm as well as each case up to the maximum of $k = 10$ where the RMSE values decrease from 4.931 cm to 1.583 cm, respectively. Furthermore, additional passive-only anchors increase the RMSE, which can be seen for each case where $m = $ const, increasing the number of passive-only anchors k from 1 to 10. Although passive anchors have less precision than active anchors with TWR, employing 3 active-passive anchors provides a situation where all added passive anchors perform better than an active anchor with TWR.

B. Air Time Occupancy

The air time occupancy, or protocol length, is measured as the total number of packets transmitted per single ranging sequence in the scope of this paper.

The AP-TWR method proposed in this paper entails the tag initiating a ranging sequence with a ranging request packet and concluding it with a ranging report. From the standpoint of air time efficiency, it is not reasonable to transmit a separate ranging report packet to each of the active anchors, so the range estimation results are aggregated and broadcast as a single report packet. Thereby, SS-TWR systems consisting of N active anchors transmit a total of $N + 2$ packets in each ranging sequence: a ranging request, a ranging reply and N packets corresponding to each actively transmitting anchor.

The minimum number of range estimates needed for a 3-dimensional position estimation is 4. Therefore, a standard TWR application (with 4 active-only anchors) requires the transmission of at least 6 packets per ranging sequence. However, compared to AP-TWR case $m = 3$ and $k = 1$, the number of packets transmitted is 5, since there are 3 active-passive anchors. In this example, compared to standard TWR, the protocol length and measurement RMSE both decrease by 16.7% (number of transmitted packets decrease from 6 to 5) and 14.4%, respectively.

V. EXPERIMENTAL RESULTS

This section presents the outcome and analysis of experimental tests, which were conducted to validate the simulation results. The experiments were conducted with Decawave DW1000 UWB IC [14] based devices: 6 anchors and 1 tag, ensuring that LoS propagation conditions were met between all devices.

Table II presents the resulting RMSE values dependent on the number of active-passive anchors m and the number of additional passive anchors k. With the available 6 anchors it is possible to compose all combinations from 6 active-passive anchors to 1 active-passive + 5 passive anchors. Although the experimental system shows slightly inferior performance than in the simulations, it can be seen that starting from case $m = 4$, the RMSE starts to overtake the standard SS-TWR case ($m = 1, k = 0$).

The simulation results showed that using 3 active-passive anchors, along with data averaging, the precision of ranging is improved for each additional passive anchor, when compared

to regular TWR. The preliminary experimental results provide lower performance compared to simulations, showing that 5 active-passive anchors and 1 passive-only anchor provide a 7.4% decrease in RMSE and 12.5% decrease of air time compared to SS-TWR with 6 anchors (number of transmitted packets decreased from 6 to 5). Despite this, it is fair to say that experimental results support the results of the simulations.

VI. Conclusion and Future Works

This article proposed a method for combining active and passive ranging in an UWB network, providing a generalized equation for active-passive and passive-only anchors. The proposed AP-TWR concept allows each active anchor to simultaneously act as a passively ranging node, in addition to extra passive-only anchors. Furthermore, all anchors gain additional measurements based on the number of active-passive anchors. This information can be averaged to increase the precision of ranging, which is demonstrated in the simulation and experimental results. Moreover, the proposed method allows to reduce the air time by making use of passive-only anchors, with no impact on the number of range estimations per ranging sequence.

The numerical results show that for an example case of 4 anchors, compared to SS-TWR, the AP-TWR method (with 3 active-passive anchors and 1 passive-only anchor) provides a decrease of RMSE by 14.4% and the air time by 16.7% by decreasing the number of transmitted packets from 4 to 3. The RMSE or air time efficiency could be further improved by respectively increasing or decreasing the number of active-passive anchors in a system. The addition of passive-only anchors provides more range estimates while the air time efficiency is not hindered. The results also show that a configuration of 3 active-passive anchors along with any number of passive anchors provides more precise ranging estimates than an active SS-TWR method.

The simulation results were validated by experimental tests. The tests indicated that the active-passive ranging method performed as it should, with only a slight decrease in performance compared to simulations. Results showed that, for example utilizing 5 active-passive anchors and 1 passive-only anchor the RMSE and air time decreased 7.4% and 12.5% respectively, when compared to 6 anchor SS-TWR.

The experimental results show that for future works there is still room for improvement in the practical system. Alongside striving for better performance, the table presented in Section V could be expanded to match the 10-by-10 table of numerical results. The performance of active-passive ranging could be further improved by employing weighted averaging on range estimations. The proposed method should also be implemented into a positioning system to assess the impact on position estimates.

References

[1] P. Davidson and R. Piché, "A Survey of Selected Indoor Positioning Methods for Smartphones," *IEEE Communications Surveys and Tutorials*, vol. 19, no. 2, pp. 1347–1370, 2017.

[2] G. M. Mendoza-Silva, J. Torres-Sospedra, and J. Huerta, "A meta-review of indoor positioning systems," *Sensors (Switzerland)*, vol. 19, no. 20, 2019.

[3] A. Alarifi, A. Al-Salman, M. Alsaleh, A. Alnafessah, S. Al-Hadhrami, M. A. Al-Ammar, and H. S. Al-Khalifa, "Ultra wideband indoor positioning technologies: Analysis and recent advances," *Sensors (Switzerland)*, vol. 16, no. 5, pp. 1–36, 2016.

[4] M. Ridolfi, S. van de Velde, H. Steendam, and E. De Poorter, "Analysis of the scalability of UWB indoor localization solutions for high user densities," *Sensors (Switzerland)*, vol. 18, no. 6, pp. 1–19, 2018.

[5] R. Fujiwara, K. Mizugaki, T. Nakagawa, D. Maeda, and M. Miyazaki, "TOA/TDOA hybrid relative positioning system using UWB-IR," *RWS 2009 IEEE Radio and Wireless Symposium, Proceedings*, pp. 679–682, 2009.

[6] Z. Sahinoglu and S. Gezici, "Enhanced position estimation via node cooperation," *IEEE International Conference on Communications*, 2010.

[7] M. R. Gholami, S. Gezici, M. Rydström, and E. G. Ström, "A distributed positioning algorithm for cooperative active and passive sensors," *IEEE International Symposium on Personal, Indoor and Mobile Radio Communications, PIMRC*, pp. 1713–1718, 2010.

[8] M. R. Gholami, S. Gezici, E. G. Ström, and M. Rydström, "Positioning algorithms for cooperative networks in the presence of an unknown turn-around time," in *IEEE Workshop on Signal Processing Advances in Wireless Communications, SPAWC*, 2011, pp. 166–170.

[9] M. R. Gholami, S. Gezici, and E. G. Ström, "Improved position estimation using hybrid TW-TOA and TDOA in cooperative networks," *IEEE Transactions on Signal Processing*, vol. 60, no. 7, pp. 3770–3785, 2012.

[10] K. A. Horvath, G. Ill, and A. Milankovich, "Passive extended double-sided two-way ranging algorithm for UWB positioning," in *International Conference on Ubiquitous and Future Networks, ICUFN*, 2017, pp. 482–487.

[11] ——, "Passive extended double-sided two-way ranging with alternative calculation," in *2017 IEEE 17th International Conference on Ubiquitous Wireless Broadband, ICUWB 2017 - Proceedings*, 2017, pp. 1–5.

[12] S. Shah and T. Demeechai, "Multiple simultaneous ranging in IR-UWB networks," *Sensors (Switzerland)*, vol. 19, no. 24, pp. 1–14, 2019.

[13] I. Dotlic, A. Connell, and M. McLaughlin, "Ranging methods utilizing carrier frequency offset estimation," in *2018 15th Workshop on Positioning, Navigation and Communications, WPNC 2018*, no. 2. IEEE, 2018, pp. 1–6.

[14] DW1000 Datasheet V2.22. Decawave. Accessed Oct. 19, 2020. [Online]. Available: https://www.decawave.com/wp-content/uploads/2020/04/DW1000_Datasheet.pdf

Appendix 2

Publication II

Novel Active-Passive Two-Way Ranging Protocols for UWB Positioning Systems

Taavi Laadung, *Student Member, IEEE*, Sander Ulp,
Muhammad Mahtab Alam, *Senior Member, IEEE*, and Yannick Le Moullec, *Senior Member, IEEE*

Abstract—This paper proposes two general active-passive two-way ranging (TWR) methods: AP1-TWR and AP2-TWR. The proposed methods rely on 2 types of anchors: active-passive and passive-only. The first type actively takes part in packet exchange and listens to transmissions of other active-passive anchors, and the second type only listens. Pairing these concepts with active single-sided (SS), symmetrical double-sided (SDS), and alternative double-sided (AltDS) TWR methods provides a total of six different active-passive

methods. As a result of assigning different numbers of the two anchor types, the range estimation root-mean-square-error (RMSE), or the air time efficiency, or both, can be improved. Simulation results show that AP1-TWR surpasses the performance of the best active two-way ranging method by employing 10 active-passive anchors, while AP2-TWR surpasses the same mark with only 6 active-passive anchors. Further results validate and show that, compared to AP1-TWR, the AP2-TWR gives a relative improvement of range estimation RMSE about 10 to 20% in every configuration, making AP2-TWR the overall better performing method. Without a loss in the number of available range estimates, both methods could also increase the air time efficiency by keeping the number of active-passive anchors to a minimum while increasing the amount of passive anchors.

Index Terms—Ultra-wideband technology, UWB ranging, ranging protocol, two-way ranging, active-passive ranging, passive ranging.
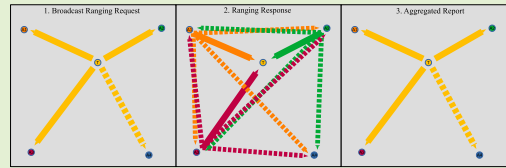
I. INTRODUCTION

COMPARING previous [1] and more recent [2] survey articles covering various indoor positioning systems shows that in recent years the research interest in Ultra-Wideband (UWB) based indoor positioning has grown. UWB is an attractive technology having low power consumption, high immunity to interference from other devices, ability to penetrate various obstacles, short pulse duration for increasing robustness to multipath, and providing localization accuracy

up to decimeter level in indoor scenarios [3]. The level of interest in UWB positioning is also demonstrated by its various applications for industrial [4], emergency [5], soldiers and first responders [6], unmanned aerial vehicle (UAV) [7], sports [8], and sensor fusion [9] positioning and navigation, to name a few.

The possible methods for positioning in an UWB system include fingerprinting based on the channel impulse response or power delay profile, distance estimation via path loss on received signal strength indicator (RSSI) or by angle of arrival (AOA) estimation. Although in their own right these methods are sufficient for providing a position estimate, they have some downsides. As indicated in [10], fingerprinting is a time consuming method requiring building up a signal parameter database, which can change over time with the positioning area; the RSSI method is very susceptible to interference caused by multipath propagation; finally, AOA estimation requires nodes equipped with antenna arrays, which subsequently increases the size and cost of the devices.

The remaining and more attractive positioning methods for UWB are called 1) time of flight (TOF), which is also called time of arrival (TOA), and 2) time difference of arrival (TDOA). TOF makes use of the relationship between the distance travelled and the propagation time when knowing the propagation speed, while TDOA employs the differences of arrival times of an emitted signal [11]. Although TDOA enjoys a minimal impact to the traffic in the network, it in turn

needs strict synchronization between anchors. Estimating the TOF via two-way ranging (TWR) methods allows removing stringent synchronization requirements between anchors while posing a drawback by increasing the air time, compared to TDOA [12]. This in turn lowers the achievable tag density and raises the energy consumption in TOA/TOF methods [13]. Although, theoretical analysis and simulations show that TOA/TOF and TDOA are identical in their positioning performance, some practical cases show the superiority of TOA/TOF methods [14]. Pascacio *et al.* found that among researchers of indoor positioning, the topic of TOA/TOF is quite more popular than TDOA, although the reasons of the popularity were not investigated [15]. In order to take advantage of the relaxed synchronization requirements of TWR methods, while reducing the air time and power consumption, the notion of passive ranging with TWR is introduced. These methods incorporating passive ranging essentially provide a middle ground between TOF and TDOA position estimation by utilizing the positive sides of TDOA and reducing the negative effects of TWR methods.

Fujiwara *et al.* proposed a TOF/TDOA hybrid positioning system based on UWB transceivers developed in [16]. The system utilized a combination of single-sided two-way ranging (SS-TWR) TOF measurement by an active anchor, and a TDOA measurement employing a passive anchor, calculating the second TOF value using the TDOA measurement. By setting a geometric constraint to the possible location of a tag, the positioning system was able to provide a position estimate with only 2 anchors, with which it enabled to also reduce the number of communication times compared to TOF systems. Sahinoglu and Gezici expanded on the system in [17], and introduced a combination of multiple active and passive nodes with a maximum likelihood estimator (MLE), providing improved accuracy at reduced number of transmissions compared to conventional TOF systems.

Horváth *et al.* proposed Passive Extended Asymmetric Double-Sided Two-Way Ranging (PE-ranging) in which they combine passive ranging proposed by [18] with symmetrical double-sided two-way ranging (SDS-TWR) [19]. This combination allowed to increase the ranging accuracy compared to previous SS-TWR-based passive ranging at the expense of adding a packet to the active ranging sequence. In [20] the same authors replaced SDS-TWR with Alternative Double-Sided Two-Way Ranging (AltDS-TWR), to eliminate the response delay time constraint that exists in SDS-TWR.

Shah *et al.* present in [21] three methods of passive ranging coupled with active ranging. The three methods achieve similar ranging performance to previous methods with the same or lower air time occupancy depending on the initiator of the ranging. This and the previous methods mainly aimed to reduce the air time of ranging methods by introducing passive ranging, only occasionally improving ranging accuracy by presenting new active ranging schemes. Additionally, the concept of a single active anchor proposes a single failure point where the disruption in the communication between the active anchor and tag also renders the passive range estimates incorrect, or even worse – losing the range estimates of that sequence altogether.

The authors of [22] expanded and generalized on Shah *et al.*'s concept to include multiple active-passive anchors alongside the passive anchors, calling it Active-Passive Two-Way Ranging (AP-TWR). Introducing hybrid role active-passive anchors, which also listen in on other transmissions when they themselves are not transmitting. Simulations and experimental results showed that the proposed method allowed to flexibly increase ranging accuracy even higher than the active ranging method could, while still offer reduced air time occupancy. Additionally, the problem of the single failure point was remedied by introducing multiple active-passive anchors ranging with the tag. However the paper only focused on using SS-TWR as the active ranging method, without considering other methods to improve ranging accuracy.

This paper extends on the active-passive two-way ranging (AP-TWR) method proposed by us in [22] to include previously overlooked active methods SDS-TWR and AltDS-TWR to further improve the method's ranging performance. In addition to this AP-TWR method, we also propose a new calculation method for passive range estimates in conjunction with active methods SS-TWR, SDS-TWR and AltDS-TWR, providing a second active-passive TWR method. Both of the investigated AP-TWR methods allow to choose a combination of active-passive and passive-only anchors to improve ranging accuracy and air-time efficiency compared to an equivalent active ranging method.

The remainder of the article is organized as follows. Section II provides the theoretical part of the active ranging methods. The formulation of the proposed active-passive methods is given in Section III; in Section IV we explain the concept of the measurement matrix which assembles the results of active-passive ranging and is the basis of the ranging accuracy improvement. Sections V and VI present the basis and the results of numerical and experimental results, respectively. Finally, a conclusion is drawn in Section VII.

II. ACTIVE RANGING METHODS

This section presents the time-based active ranging methods which are used in practical UWB based positioning systems. These methods calculate an estimate of the time of flight (TOF) between two nodes by utilizing two-way packet exchanges. The resulting time of flight estimates can be converted to physical distance estimates by using

$$\hat{s} = c \cdot \hat{t}, \tag{1}$$

where $\hat{s}$ is the distance estimate, $\hat{t}$ the TOF estimate and c is the speed of light.

A single range estimate is acquired by utilizing a specific ranging method between an anchor and a tag. This implies that the number of range estimates per tag is directly dependent on the number of anchors with which the tag communicates. This is critical for positioning, as at least three range estimates are needed for a position estimate [23]. Moreover, having a larger number of range estimates also allows to lower the location estimation noise [24].

Sang *et al.* analyzed the errors of single-sided (SS), symmetrical double-sided (SDS), asymmetrical double-sided (ADS) and alternative double-sided (AltDS) two-way ranging (TWR)

Fig. 1. Single-sided two-way ranging packet exchange.
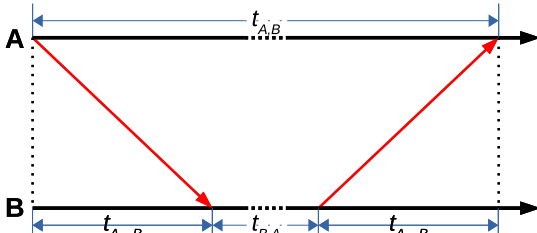
Fig. 2. Symmetrical- and alternative double-sided two-way ranging packet exchange.

methods in [25]. All stated active methods, excluding ADS-TWR, are considered in this paper. ADS-TWR was omitted since it requires the last response delay time to be zero, which is unattainable in practical systems [21].

A. Single-Sided Two-Way Ranging

The IEEE 802.15.4a is an amendment to the IEEE 802.15.4 standard which introduced additional physical layers, which enabled precise wireless ranging [26]. In the standard, one of the specified ranging methods was Single-Sided Two-Way Ranging (SS-TWR), on which Sahinoglu and Gezici gave an overview and analysis in [27].

The SS-TWR method provides a TOF estimate by exchanging two packets between nodes. The method is illustrated in Fig. 1, where node A begins the sequence by simultaneously activating a timer and transmitting a packet to node B, which propagates through the air for its time of flight of $t_{A\leftrightarrow B}$. Upon arrival, node B responds after its response delay time $t_{B,A}$, which can be interpreted as the time interval measured by B, communicating with A. After propagating again for $t_{A\leftrightarrow B}$, node A receives the response and stops its timer, providing the round-trip time $t_{A,B}$, interpreted as the time interval measured by A in communication with B.

Generally the response delay time of nodes (in this specific case $t_{B,A}$) is several orders of magnitude larger than the TOF $t_{A\leftrightarrow B}$ [28]. The dotted lines of the time axis in Fig. 1 are used to denote the differences of scale.

The TOF between nodes A and B, $t_{A\leftrightarrow B}$, can then be calculated by

$$t_{A\leftrightarrow B} = \frac{t_{A,B} - t_{B,A}}{2}. \quad (2)$$

B. Symmetrical Double-Sided Two-Way Ranging

IEEE 802.15.4a standard also specified, in addition to SS-TWR, a second ranging method called Symmetrical Double-Sided Two-Way Ranging (SDS-TWR). Compared to SS-TWR, SDS-TWR adds an additional packet to the ranging sequence. The introduction of the third packet to the ranging sequence allows to improve ranging accuracy [27], [28].

The packet exchange procedure for SDS-TWR is demonstrated in Fig. 2. As can be seen, the exchange of the first two packets is the same as in SS-TWR, discussed in Section II-A. After successfully receiving node B's response, node A transmits the third packet after its processing delay $t_{A,B'}$ (also interpreted as the second time interval measured by A when communicating with B). After propagating for $t_{A\leftrightarrow B}$, the final
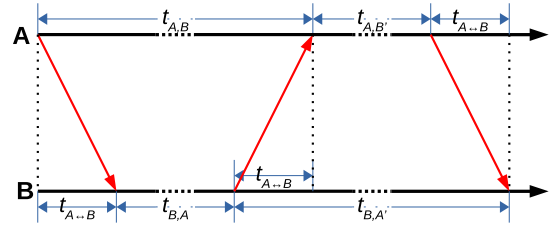
packet arrives at B, where the round-trip time of the last 2 packets, $t_{B,A'}$, is recorded.

Similarly to Fig. 1, the larger time scale of response delay times $t_{B,A}$ and $t_{A,B'}$ in Fig. 2 are illustrated by the dotted lines.

The four time intervals measured by nodes A and B can be used to estimate the TOF between them:

$$t_{A\leftrightarrow B} = \frac{t_{A,B} - t_{A,B'} + t_{B,A'} - t_{B,A}}{4}. \quad (3)$$

The error analysis of SDS-TWR presented in [25], [28] found that in order to minimize the TOF estimation error, A and B's response delays ($t_{B,A}$ and $t_{A,B'}$) have to be equal, hence the name symmetrical double-sided TWR. In a practical positioning system with multiple nodes it means that the final response packets to each node cannot be aggregated into a single response, raising the total number of packets in a ranging sequence. The effect on the air-time efficiency is further discussed in Section V-C.

C. Alternative Double-Sided Two-Way Ranging

The AltDS-TWR method utilizes the same exact packet exchange protocol as SDS-TWR, pictured in Fig. 2. The specifics of this protocol are discussed in the previous subsections.

The difference between SDS-TWR and AltDS-TWR becomes evident with the alternative derivation of the calculation of TOF proposed by Neirynck *et al.* in [28]:

$$t_{A\leftrightarrow B} = \frac{t_{A,B} \cdot t_{B,A'} - t_{A,B'} \cdot t_{B,A}}{2(t_{B,A} + t_{B,A'})} \quad (4a)$$

$$= \frac{t_{A,B} \cdot t_{B,A'} - t_{A,B'} \cdot t_{B,A}}{2(t_{A,B} + t_{A,B'})} \quad (4b)$$

$$= \frac{t_{A,B} \cdot t_{B,A'} - t_{A,B'} \cdot t_{B,A}}{t_{B,A} + t_{B,A'} + t_{A,B} + t_{A,B'}}. \quad (4c)$$

As a result, the four measured time intervals can be used to provide a TOF estimate in three distinct ways. The estimate can be calculated either by having node B's (4a), node A's (4b) or both nodes' (4c) measured time intervals in the denominator.

The error analysis of [25], [28] found that the alternative calculation of AltDS-TWR removes the symmetry constraint of response delays which hindered the SDS-TWR method. In a multiple-node system the dismissal of the symmetry constraint in turn allows to aggregate the final packets of node A to a single packet, reducing the total number of packets transmitted in a ranging sequence [29]. Additionally, using (4a) or (4b)
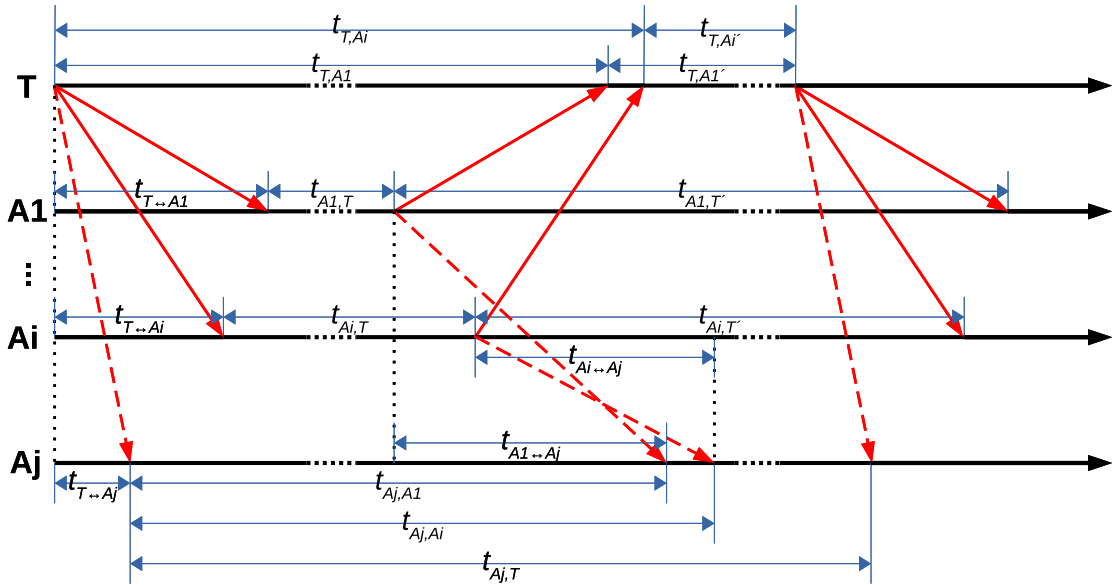
Fig. 3. A single ranging sequence for active-passive methods utilizing SS-TWR and AltDS-TWR with aggregated tag response. Tag T initiates the ranging sequence with a ranging request packet; anchors A1 to Ai receive it and answer with a ranging response. After receiving all responses, T ends the ranging sequence with a ranging report packet. Anchor Aj listens to all packet exchanges and records corresponding time intervals.

permits to improve the TOF estimation performance if node B or node A has a better timing reference, respectively. If the nodes have clock sources with the same timing performance, the TOF estimate can also be obtained by (4c).

On account of offering the previously discussed improvement to SDS-TWR, AltDS-TWR has replaced it in the latest amendment to the IEEE 802.15.4 standard. The IEEE 802.15.4z amendment now specifies SS-TWR and AltDS-TWR as the main TOF-based ranging methods [30].

III. Proposed Active-Passive Ranging Methods

In this section we introduce two methods to provide ranging capabilities for passive anchors, which are also called listeners. Since the location of each anchor is fixed and known, the *a priori* information, in conjunction with information obtained during the ranging sequence, is used to passively provide estimates of distance between a listener and tag. The two proposed methods are collectively called the Active-Passive Two-Way Ranging (AP-TWR) due to the fact that the developed passive ranging capabilities are used in conjunction with existing active methods.

The proposed methods utilize a tag-initiated ranging sequence to provide the longest possible sleep time for the tag between consecutive ranging sequences. Employing an anchor-initiated ranging sequence was not considered, since the tag would have to be in a constant receive mode, which would reduce the tags battery life. For example, the widely used [31] Qorvo/Decawave DW1000 transceiver IC consumes more power during receiving than transmitting, let alone being asleep [32]. This constraint is introduced since tags are typically battery-operated and need to conserve power where possible.

This in turn means that an assumption is made i.e. anchors are not power-constrained, allowing them to remain in transmit or receive mode without sleeping between ranging sequences. The notion is justified by the fact that generally anchors are a part of fixed infrastructure, having dedicated data and supply power lines, not running on batteries.

Since the anchors are not limited by supply power, it is practical to listen to every packet exchange that it receives, to provide additional information for ranging. This applies not only to the passive anchors, but to active anchors as well: when active anchors are not transmitting they can listen to transmissions between the tag and other active anchors. This allows for the distinction between active-passive and passive-only anchors.

In the scope of this paper the following abbreviations for system node names is adopted to help describe the principles of AP-TWR methods. Anchors numbered $1, 2, i$, which are actively participating in ranging, are abbreviated as A1, A2 and Ai, accordingly. The passive anchor is noted as Aj, and the tag as T.

A. Active-Passive Two-Way Ranging Method 1

This section proposes active-passive TWR method 1 (AP1-TWR), which exploits an active ranging method's packet exchange protocol alongside with knowledge about the anchor locations to provide passive range estimates alongside with active ranging results.

Fig. 3 represents a ranging sequence of AP-TWR methods utilizing SS-TWR and AltDS-TWR with aggregated tag report packet. Tag T starts the sequence with a ranging request, to which all active anchors A1 to Ai answer with a response. When T has received all responses, it ends the sequence with

Fig. 4. A single ranging sequence for active-passive methods SDS-TWR without aggregated tag response. Tag T initiates the ranging sequence with a ranging request packet; anchors A1 to Ai receive it and answer with a ranging response. After receiving responses from the anchors, T transmits an anchor-specific report packet after delaying its response time equal to the anchor's processing time. Anchor Aj listens to all packet exchanges and records corresponding time intervals.

a broadcast ranging report packet which is received by each anchor. Passive anchor Aj listens in on the packet exchanges in the air and registers the corresponding time intervals of packet arrivals. Note that the final packet broadcast by T is an aggregated packet containing a response to all anchors; in this way T does not have to respond to each anchor individually so the effect on air time is reduced. This is discussed in more detail in Section V-C.

Fig. 4 gives the ranging sequence for AP-TWR methods utilizing the SDS-TWR. Although the packet exchange is similar to that of Fig. 3 for the first part of the sequence, the final responses sent by the tag are sent to individual anchors separately, to adhere to the response time symmetry constraint discussed in Section II-B. This means that the final response packets cannot be aggregated to a single one to reduce the air time.

The following notation of time intervals is used to describe the AP-TWR methods. The TOF between node A and B is represented by $t_{A\leftrightarrow B}$. Note that in Fig. 3 and 4 the TOFs are only labelled on the first packet but the same notation applies for TOFs in responses and in the report packet; this choice makes the figure less cluttered. The notation of $t_{A,B}$ is used to describe the time interval measured by node A, corresponding to packet exchange with node B. Since each active anchor measures two different time intervals associated with the same node, the distinction of the second time interval is made by adopting the notation $t_{A,B'}$.

The only differences between SS-TWR/AltDS-TWR and SDS-TWR based AP-TWR approaches is the notation of the listening anchor Aj's time intervals. In case of Fig. 3 depicting SS-TWR and AltDS-TWR based method, Aj records the time intervals corresponding to each active anchor ($t_{Aj,Ai}$), and the tag's final aggregated response $t_{Aj,T}$. For the SDS-TWR based

approach, the final response packets are sent to each anchor separately, so Aj records the time intervals corresponding to each active anchor ($t_{Aj,Ai}$) plus the tag's response to each of the anchors ($t_{Aj,T,Ai}$).

Similar to active method, depicted in figures 1 and 2 and discussed in Section II, the time axis on Fig. 3 and 4 include the dotted lines to note time scale differences of tag and active anchor response delay times and the TOFs between nodes.

In order to have a generalized approach for AP1-TWR, we shall focus on the interaction between tag T, active anchor Ai and passive anchor Aj. It can be observed from both, Fig. 3 and Fig. 4 that the following time intervals are equal:

$$t_{T\leftrightarrow Ai} + t_{Ai,T} + t_{Ai\leftrightarrow Aj} = t_{T\leftrightarrow Aj} + t_{Aj,Ai}. \qquad (5)$$

Rearranging (5) for $t_{T\leftrightarrow Aj}$ and adopting the notation of $t_{T\leftrightarrow Aj|Ai}$, we get

$$t_{T\leftrightarrow Aj|Ai} = t_{T\leftrightarrow Ai} + t_{Ai,T} + t_{Ai\leftrightarrow Aj} - t_{Aj,Ai} \qquad (6a)$$

$$t_{T\leftrightarrow Aj|Ai} = t_{T\leftrightarrow Ai} + t_{Ai,1} - \tau_{Ai,0} + t_{Ai\leftrightarrow Aj} \\ - \tau_{Aj,Ai} - \tau_{Aj,0}, \qquad (6b)$$

where $t_{T\leftrightarrow Ai}$ is the TOF between T and Ai, estimated by an active ranging method, and $t_{Ai\leftrightarrow Aj}$ is the *a priori* known TOF from Ai to Aj. The rest of the terms in Eq. (6a) represent the calculation using the specific time intervals on Fig. 3, and Eq. (6b) presents the same calculation using timestamp notation as per Appendix II. The time interval notation of eq. (6a) can be used instead of the timestamp notation in eq. (6b), since the time base of each transmitting device can be converted to the time base of the receiver via Carrier Frequency Offset estimation method proposed by Dotlic *et al.* in [33]. This is further explained in Appendix II.

The notation of $t_{T \leftrightarrow Aj|Ai}$ is adopted instead of $t_{T \leftrightarrow Aj}$, to clarify that the TOF from tag T to listener Aj is calculated by using the data from active anchor Ai. This adaptation allows the calculation of TOF between tag T and listener Aj during each Ai's ranging session.

Since (6a) covers only the passive ranging results, the total set of ranging data acquired in a single ranging sequence can be expressed as:

$$t_{T \leftrightarrow Aj|Ai} = \begin{cases} t_{T \leftrightarrow Ai}, & \text{for } i = j \\ t_{T \leftrightarrow Ai} + t_{Ai,T} + t_{Ai \leftrightarrow Aj} - t_{Aj,Ai}, & \text{for } i \neq j, \end{cases} \quad (7)$$

where the first part corresponds to active ranging (since an anchor cannot listen to its own ranging session) and the second part to passive ranging using time interval notation. Note that the term $t_{T \leftrightarrow Ai}$ exists in both parts, meaning that the passive ranging is directly dependent on the active method with which the TOF is acquired.

Since active ranging can be utilized either by SS-TWR, SDS-TWR, or AltDS-TWR, the term $t_{T \leftrightarrow Ai}$ can be substituted by (2), (3) or (4), respectively. The substitution provides three distinctive active-passive methods called AP1 SS-TWR, AP1 SDS-TWR and AP1 AltDS-TWR.

B. Active-Passive Two-Way Ranging Method 2

The second active-passive two-way ranging method (AP2-TWR) utilizes the same packet exchange sequence as AP1-TWR, but makes use of different measured time intervals to provide passive range estimates.

Fig. 3 illustrates the packet exchange protocol for AP2-TWR, and was already explained in detail in Section III-A. The figure allows us to observe that both of the following equalities hold:

$$t_{T \leftrightarrow Aj} + t_{Aj,Ai} = t_{T \leftrightarrow Ai} + t_{Ai,T} + t_{Ai \leftrightarrow Aj} \quad (8a)$$
$$t_{T \leftrightarrow Aj} + t_{T,Ai'} + t_{T \leftrightarrow Ai} = t_{Ai \leftrightarrow Aj} + t_{Aj,T} - t_{Aj,i}. \quad (8b)$$

Adding 8a to 8b, and solving for $t_{T \leftrightarrow Aj}$, we get the following expression:

$$t_{T \leftrightarrow Aj} = \frac{t_{Ai,T} + t_{Aj,T} - t_{T,Ai'}}{2} + t_{Ai \leftrightarrow Aj} - t_{Aj,Ai}. \quad (9)$$

According to Fig. 3 we know that $t_{Aj,T} = t_{T,Ai} + t_{T,Ai'}$. Substituting it into (9) and adopting the notation of $t_{T \leftrightarrow Aj|Ai}$ yields the final form for the passive part of AP2-TWR:

$$t_{T \leftrightarrow Aj|Ai} = \frac{t_{Ai,T} + t_{T,Ai}}{2} + t_{Ai \leftrightarrow Aj} - t_{Aj,Ai} \quad (10a)$$

$$t_{T \leftrightarrow Aj|Ai} = \frac{\tau_{Ai,1} - \tau_{Ai,0} + \tau_{T,Ai} - \tau_{T,0}}{2} + t_{Ai \leftrightarrow Aj} - \tau_{Aj,Ai} + \tau_{Aj,0}, \quad (10b)$$

where Eq. (10a) presents the AP2-TWR passive TOF estimate calculation via time interval notation, and Eq. (10b) with timestamp notation from Appendix II. The term $t_{Ai \leftrightarrow Aj}$ referring to the known TOF between Ai and Aj for both equations.

Similarly to Section III-A, this notation is introduced to emphasize that the TOF from passive anchor Aj to tag T can be calculated using every active anchor's ranging data. In addition, both time interval and timestamp notations are valid for the calculations, due to the possibility to translate the clock time bases between devices, explained in Appendix II.

The above proof applies to SS-TWR or AltDS-TWR based AP2-TWR methods, however we arrive to the same exact result using SDS-TWR as well. The proof for this is presented in Appendix I, where we show that utilizing the former and the latter methods for AP2-TWR, accordingly produce the same exact results in (10a) and (18).

Equations (10a) and (18) cover only the passive part of the ranging sequence. To define all the active and passive ranging data of a single ranging sequence, we express it as:

$$t_{T \leftrightarrow Aj|Ai} = \begin{cases} t_{T \leftrightarrow Ai}, & \text{for } i = j \\ \frac{t_{Ai,T} + t_{T,Ai}}{2} + t_{Ai \leftrightarrow Aj} - t_{Aj,Ai}, & \text{for } i \neq j, \end{cases} \quad (11)$$

where, again, the first part corresponds to an active ranging method and the second part corresponds to passive ranging with time interval notation. Similarly to III-A, the active ranging can be utilized either by SS-TWR, SDS-TWR, or AltDS-TWR, meaning that $t_{T \leftrightarrow Ai}$ can be substituted by (2), (3) or (4), respectively. This produces the active-passive methods AP2 SS-TWR, AP2 SDS-TWR and AP2 AltDS-TWR.

Although the main concept of AP2-TWR was already published in [22], that paper did not consider employing the SDS-TWR and AltDS-TWR methods. Only the effects of AP2 SS-TWR was simulated and shown to work in practical experiments.

IV. MEASUREMENT MATRIX

After a ranging sequence has occurred, all the estimated TOF values of the AP-TWR methods can be expressed as an n by m measurement matrix T, where m is the number of active-passive anchors and n the total number of anchors, making the number of passive-only anchors as $k = n - m$:

$$T = \begin{bmatrix} t_{T \leftrightarrow A1|A1} & \cdots & t_{T \leftrightarrow A1|Am} \\ \vdots & \ddots & \vdots \\ t_{T \leftrightarrow An|A1} & \cdots & t_{T \leftrightarrow An|Am} \end{bmatrix}, \quad (12)$$

where, per (7) and (11), the active distance measurements lay on the main diagonal, and the passive measurements off the diagonal. T is an n by m matrix, meaning that we acquire a total of $n \cdot m$ raw range estimates for each ranging sequence, whereas an active-only method could only deliver m range estimates.

Each row of T contains the set of TOFs between an anchor and tag acquired during a ranging sequence. To express the coherence of these sets, we denote the rows of (12) as n vectors:

$$t_{T \leftrightarrow A1} = \begin{bmatrix} t_{T \leftrightarrow A1|A1} & \cdots & t_{T \leftrightarrow A1|Am} \end{bmatrix}$$
$$\vdots$$
$$t_{T \leftrightarrow An} = \begin{bmatrix} t_{T \leftrightarrow An|A1} & \cdots & t_{T \leftrightarrow An|Am} \end{bmatrix}.$$

Considering that each vector contains m estimates of the same TOF value, we can filter the noise by finding the mean

value of each row vector, such that

$$\overline{T} = \begin{bmatrix} t_{T \leftrightarrow A1} \\ \vdots \\ t_{T \leftrightarrow An} \end{bmatrix}, \qquad (13)$$

where $\overline{T}$ is a column vector containing n elements of filtered TOFs from tag to every anchor, effectively providing a set of range estimates as inputs for a positioning engine. This filtering takes place during each ranging sequence.

It is important to understand that for AP-TWR methods, as can be seen by the number of elements of (13), the total quantity of anchors n, directly defines the number of range estimates. At the same time, m only defines the cardinality of the row vectors of $\overline{T}$, affecting only the calculation of mean values in (13). On the other hand, active-only ranging methods with m range estimates do not offer the filtering of a single ranging sequence's TOF values, the filtering can only be done with values of temporally consecutive ranging sequences.

V. SIMULATIONS AND RESULTS

In the following subsections we give the background of the simulation tool, present the preconditions, and compare the simulated methods from the standpoint of range estimation root-mean-square-error (RMSE) and air-time efficiency.

A. Background and Conditions

In order to run the simulations for the proposed methods, a dedicated software tool was developed in R programming language. The software simulates all the required time intervals to calculate the various combinations of active and passive TOF estimates using (7) and (11).

Although the software does not simulate a full physical layer, the response times of each anchor are delayed separately to avoid collisions at the tag. Moreover, since only a single tag is simulated, a multiple access scheme for the tags is not implemented in the scope of this paper. Accounting these points, the events of packet loss are omitted from the simulations.

The simulations were carried out in a virtual room sized 500 cm × 700 cm × 250 cm. The combinations of AP-TWR methods were simulated for 1000 separate iterations. During each iteration, the tag and anchors were placed at randomly generated positions in the virtual room. Each iteration in turn consisted of 1000 separate ranging sequences.

In order to assess and compare the ranging performance of the methods, the range estimate RMSE is calculated using the following equation:

$$RMSE_d = \sqrt{\frac{\sum_{i=1}^{N}(d_i - d_t)^2}{N}}, \qquad (14)$$

where d_i denotes the i-th range estimate, d_t the true range, and N the total number of range estimates.

The propagation conditions are set as line-of-sight, so the time measurement noise follows Gaussian distribution with a time measurement noise standard deviation of 150ps. The

standard deviation is taken as the worst case scenario reported by McElroy *et al.* in [34] for Qorvo/Decawave DW1000.

Clock offset errors are omitted, since they can be compensated for, as Dotlic *et al.* proposed in [33]. All simulated nodes are assumed to have the same timing reference performance, meaning the 150ps standard deviation applies to both, the tag and anchors. Tag and anchor distance calibration errors are omitted, assuming that they are calibrated correctly.

The inter-anchor distances needed to calculate the passive range estimates are known and exact since anchors are assumed to be as a part of a fixed infrastructure with known locations (see Section III). Therefore, the inter-anchor TOFs can be found via the relation expressed by (1).

Each AP-TWR method utilized measurement matrix row-wise averaging by (13) to provide final TOF estimates. The TOF estimates were converted to distances using (1), to provide the final RMSE results in centimeters.

Section III stated that both of the described AP-TWR methods can be used in conjunction with each of the active methods. Since in the scope of this paper, tag and anchors are assumed to have the same timing reference performance, we calculate AltDS-TWR method with (4c). As a total we simulate a combination of six active-passive methods: combining (7) and (11) with (2), (3), and (4c), we accordingly get AP1 and AP2 SS-TWR, AP1 and AP2 SDS-TWR, AP1 and AP2 AltDS-TWR.

B. Ranging Performance

In this section, the ranging performance of AP1 SS-TWR, AP1 SDS-TWR, AP1 AltDS-TWR, AP2 SS-TWR, AP2 SDS-TWR and AP2 AltDS-TWR is presented and discussed. The performance of these methods is compared in terms of range estimation RMSE in centimeters instead of TOF value, since distance is the final product of the ranging process in a practical sense.

Firstly, the individual performance of each active and passive method is observed separately. This is illustrated in Fig. 5, where the RMSEs of active methods SS-TWR, SDS-TWR, ADS-TWR, and passive parts of AP1 SS-TWR, AP1 SDS-TWR, AP1 AltDS-TWR and AP2-TWR methods are presented. Compared to AP1 methods, only a single combination of AP2-TWR is displayed, since this method is independent of the active ranging TOF estimation, as discussed in Section III.

The results show that at 2.25 cm RMSE, SDS-TWR has the best performance of all of the active methods, closely followed by 2.43 cm RMSE for AltDS-TWR; a bit further behind we find SS-TWR with 3.18 cm RMSE. Out of the passive methods we see that AP2-TWR performs the best with 5.51 cm RMSE, outperforming the next best, AP1 SDS-TWR, by a margin of 1.23 cm. Closely following it, we find AP1 ADS-TWR with 6.81 cm and last we find AP1 SS-TWR with an RMSE of 7.11 cm.

The individual results show that the best performance can be obtained using SDS-TWR for active ranging and AP2-TWR for passive ranging, while the least performing methods are SS-TWR and AP1 SS-TWR, respectively.
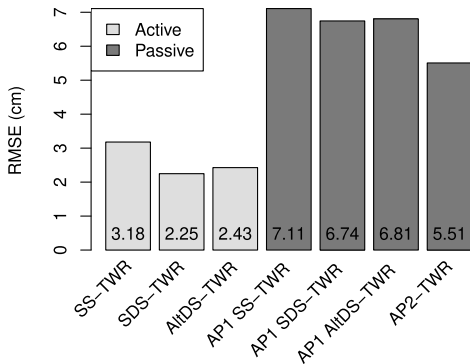
Fig. 5. Ranging performance of active and passive ranging methods.

m	n	RMSE (cm)	RMSE relative change (%)	№ packets	Air time relative change (%)
6	0	2.120	-33.3	8	0
5	1	2.323	-26.9	7	-12.5
4	2	2.598	-18.3	6	-25.0
3	3	2.997	-5.8	5	-37.5
2	4	3.672	15.5	4	-50.0
1	5	5.192	63.3	3	-62.5

Fig. 6 presents the graphs of total system RMSE depending on the number of additional passive anchors, k, for each proposed active-passive method coupled with a measurement matrix averaging by (13). The individual graphs correspond to different values of m – the number of active-passive anchors. The methods are benchmarked against active-only SS-TWR, SDS-TWR and ADS-TWR methods, which are rendered as constant lines. They are depicted as constant lines since these methods do not provide passive ranging, they are therefore agnostic to the number of passive anchors.

The following trend for each method can be observed: system RMSE increases with each increment of the k value. This means that every additional passive range estimate value, which is supplied at no cost to the number of packets in a ranging sequence, contributes to an increase of the system RMSE. However, increasing m in turn decreases the system RMSE at the cost of an added packet in the ranging sequence. The impact of the method type and used anchor types on the air time is further discussed in Section V-C.

All AP2-TWR based methods outperform AP1-TWR based methods in every case of m, k value. For example from case $m = 3$ (Fig. 6 c) and upwards, AP2-TWR methods provide about 10 to 20 % decrease in RMSE when compared to AP1-TWR, depending on the specific case and method chosen. Cases below $m = 3$ still offer a decrease in RMSE, but the gain is less uniform across the graphs.

In both AP methods, it can be seen that employing AltDS-TWR and SDS-TWR active ranging methods yield almost identical RMSE, while also performing better than SS-TWR. It is important to note that the AP2 SS-TWR is inferior to AP2 SDS-TWR and AP2 AltDS-TWR by a slight margin of about 0.01 to 0.30 cm, which means all three AP2 methods provide almost the same performance. For AP1-TWR methods it can be seen that SS-TWR based method lags behind AltDS-TWR and SDS-TWR by a larger margin of about 0.10 to 0.50 cm. Aligning with the results of individual active and passive anchor performance, AP2 SDS-TWR and AP2 AltDS-TWR yield the lowest RMSE values while AP1 SS-TWR yield the highest ones, at every m, k value.

Fig. 6 c, $m = 3$ shows a breaking point where all the AP2-based active-passive methods have surpassed the ranging performance of active-only SS-TWR. Further increasing

the number of active-passive anchors, we can see that all AP1-based active-passive methods achieve performance superior to active-only SS-TWR at $m = 5$. Accordingly for the same case, AP2-based methods have passed the performance of active AltDS-TWR. Case $m = 10$ illustrates that all the active-passive methods have surpassed every active-only method. Appendix III presents Fig. 10, where we can see that $m = 6$ is the critical value where all AP2-TWR methods catch up with the best performing active method SDS-TWR.

Table I presents an example case of AP2 SS-TWR compared to active-only SS-TWR. The example is constructed such that for both methods the total number of anchors is $n = m + k = 6$, where AP2 SS-TWR allows a total of six different active-passive and passive-only anchor m, k combinations. The results are compared to active-only SS-TWR which operates at 3.180 cm RMSE with 6 anchors. This specific case was selected since: 1) the amount of data to transmit is lower (refer to Section V-C); 2) according to Fig. 6, the RMSE cost of using AP2 SS-TWR instead of AP2 SDS or AP2 AltDS-TWR is only in the range of about 0.01 to 0.1 cm; 3) the results are directly comparable to what was published in [22].

It is important to reiterate that the number of available range estimates for active-only methods is defined by the number of active anchors, but for AP methods it is dependent on the total number of anchors, as was discussed in Section IV. Additionally, all anchor combinations resulting $n < 3$ are unusable from the standpoint of positioning, since it was determined in Section I that providing a position estimate requires at least three range estimates. For the specific example drawn in Table I the number of available range estimates is 6 for all combinations.

The results show that depending on the m, k combinations, the RMSE of AP2 SS-TWR can increase up to 63.3% ($m = 1$, $k = 5$) or decrease down to -33.3% ($m = 6$, $k = 0$), compared to SS-TWR. Accordingly, while the air time is decreased by down to -62.5% or left unchanged at 0%. The table shows the critical point where moving from 2 to 3 active-passive anchors in AP2 SS-TWR starts to provide constantly better RMSE results than active-only SS-TWR. The choice of m, k provides a flexibility to steer the system towards increased accuracy or decreased air time while providing the same number of range estimates. The intermediate cases and the interplay with air time efficiency is further discussed in Section V-C.

C. Air Time

The air time efficiency of an UWB system can be assessed by two main categories: the amount of data to be transmitted
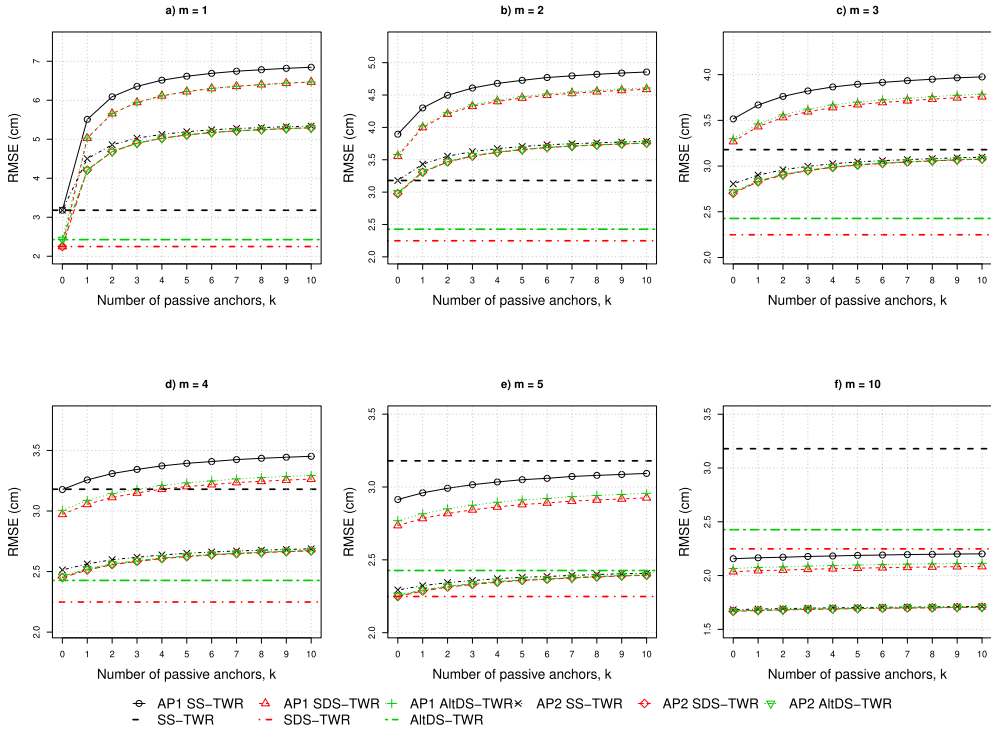
Fig. 6. Ranging performance of active-passive methods with measurement matrix averaging. The graphs are plotted to show each method's dependence of RMSE on n - the number of additional passive-only anchors. Each individual graph represents a different value for m - the number of active-passive anchors. The performance of active methods is pictured as constant lines, since they do not depend on number of passive anchors.

over the air and the number of packets needed to transmit per each ranging sequence. The quantity of transmitted data directly impacts the effective length of the packet in bits, while a higher number of transmitted packets increases the total time spent transmitting in each ranging sequence.

Demanding applications where a large quantity of tags needs to be located simultaneously, the air-time occupancy and ranging rate may become a limiting factor to the maximum number of tags. Desirably both of the defining air time efficiency parameters should be kept to a minimum, since they dictate the maximum number of tags that can operate in a given area [13].

According to equations (3) and (4) in Sections II-B and II-C we see that in the case of ADS-TWR and AltDS-TWR the TOF from tag to anchor is calculated using four different variables. Two of these values are measured by the tag and need to be communicated back to the corresponding anchor. Since equation (2) for SS-TWR only needs a single time interval value from the tag to calculate the TOF, this effectively means that half as much information needs to be communicated back to corresponding anchors. This concept comes to play when the amount of transmitted data is limited or the shortest possible packet is desired. Since the spectrum is a shared resource, a shorter packet allows to increase the device density due

to less time spent transmitting and resulting in a shorter protocol.

Since the packets also contain varying length overhead in the form of preambles and headers etc., it is difficult to quantify the effect of transmitted data on the total length of a packet and therefore on the whole ranging sequence. Due to this, Fig. 7 only illustrates the total number of data fragments needed to communicate to anchors over the air, depending on the number of active anchors in a system. It can be seen that SS-TWR provides the lowest amount of data to be transmitted by the tag.

Furthermore, the second important part of air time efficiency is the number of packets in a ranging sequence. When considering a tag-initiated sequence with aggregated response as discussed in III and depicted in Fig. 3, the total number of packets in a sequence can be calculated as $N_a = m + 2$. Where N consists of a ranging request packet sent by the tag, m number of replies from each active anchor and an aggregated ranging report packet sent by the tag. The number of packets for a non-aggregated response would be calculated as $N_{na} = 2m + 1$, where the sequence consists of a ranging request sent by the tag, m responses from each active anchor and m ranging reports sent by the tag. In conclusion, the aggregated response packet saves us from transmitting $N_{na} - N_a = 2m + 1 - (m + 2) = m - 1$ packets. The described
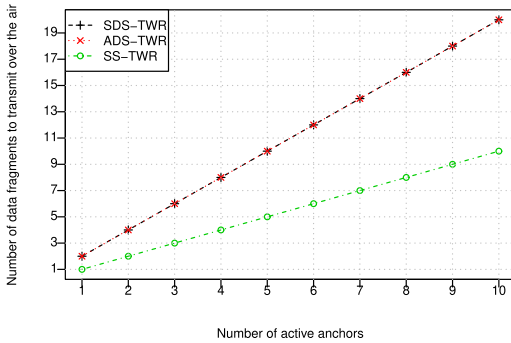
Fig. 7.   Number of time interval values transmitted over the air by the tag, depending on the number of active anchors.

calculations of the number of packets in a sequence applies to both active-only and active-passive methods, depending only on the number of anchors actively taking part of the ranging.

It is important to reiterate the fact discussed in Section II-B that due to the response delay symmetry constraint the final packet of a SDS-TWR ranging session cannot be aggregated to a single one. This means that all methods (including AP-TWR methods) incorporating SDS-TWR transmit $N_{na} = 2m + 1$ packets in a single ranging sequence. Meaning SDS-TWR has a disadvantage of transmitting more packets in cases where $m > 1$.

The strengths of active-passive methods come to play with the addition of passive-only anchors. Passive-only anchors provide extra range estimates between themselves and the tag, while the number of packets in a ranging sequence is defined only by the number of active-passive anchors. This combats the main shortcoming of increased air time of TWR methods compared to TDOA methods, as discussed in Section I. Theoretically it would be possible to provide an unlimited amount of range estimates with only 3 packets in a ranging sequence when $m = 1$ and $k \longrightarrow \infty$, only limited by the number of physical anchor devices.

The example in Table I showed that depending on the m, k values in this case, the air time of AP2 SS-TWR can be decreased down to -62.5% compared to SS-TWR. The presented air time results are not only specific to AP2 SS-TWR: they also expand to other AP methods with aggregated packets with the same m, k values. This leaves out the methods which are based on SDS-TWR, since the relative air time change is calculated differently on the account of using unaggregated response packets.

Case $m = 6$, $k = 0$ the RMSE of ranging values is at its lowest with a -33.3% reduction compared to SS-TWR. The number of active-passive anchors is the same as the benchmark SS-TWR, at $m = 6$ with the number of transmitted packets at 8, giving no advantage of air time reduction. The other extreme case where $m = 1$, $k = 5$, the RMSE is at its highest of 5.192 cm with an increase of 63.3% compared to SS-TWR. This time the air time is at its lowest with 3 packets transmitted, giving an air time reduction of -62.5% compared to 8 packets transmitted in SS-TWR. The intermediate cases show that a middle ground where improvements for both

parameters can be found. For example $m = 4$, $k = 2$ where both, the RMSE and air time, are decreased by -18.3% and -25%, respectively. Once again, the trends become obvious: each additional passive-only anchor increases the RMSE while the air time is decreased, and each additional active-passive anchor decreases the RMSE while adding a packet to the ranging sequence.

These results also align with the previous study placing our results between the simulation and experimental performance given in [22].

VI. EXPERIMENTAL RESULTS

The following section gives an overview of the practical experiments conducted. For the practical experiments the AP2 SS-TWR solution was selected as it requires the least amount of information and packets sent over the air and is comparable to the performance of the AP2 SDS-TWR and AP2 AltDS-TWR. The background information, experimental set up description and the results and analysis of the practical experiments utilizing AP2 SS-TWR are given in the following paragraphs. The results are analyzed from the standpoint of ranging performance.

A. Test Setup

The experiments took place at Tallinn University of Technology (TalTech), Thomas Johann Seebeck Department of Electronics. The tests were conducted using Eliko UWB RTLS [35], based on the Decawave/Qorvo DW1000 UWB transceiver. The test system composed of 5 anchors and a single tag.

The anchors and tag were placed in arbitrarily chosen locations in the U02-406 classroom at TalTech, making sure that a visual line of sight between all devices exists. This is illustrated on Fig. 8, where the anchors are marked with blue color and the tag marked with red.

The Leica DISTO S910 laser distance meter [36] was used to survey the true coordinates of the anchors and the tag relative to the front left corner of the classroom when entering it. The position of the laser distance meter is marked with yellow color in Fig. 8.

With 5 anchor network configuration the total number of possible m, k combinations is 15. For each combination 5 separate tests were performed to avoid outliers, and from each test 600 rangings were collected.

The captured ranging data packets in the form of text files were processed and analyzed using a dedicated software written in the programming language R.

The practical performance of the AP2 SS-TWR was evaluated using σ, the standard deviation, as opposed to RMSE. This choice was made to eliminate the impact of device calibration errors and other static errors during measurements. The calculation of RMSE and standard deviation is similar: for RMSE the term d_t in (14) refers to the true distance, but in the calculation of standard deviation in (15) the term $\overline{d}$ is the mean value of all samples. This way the standard deviation reflects the best case RMSE value, assuming that the sample
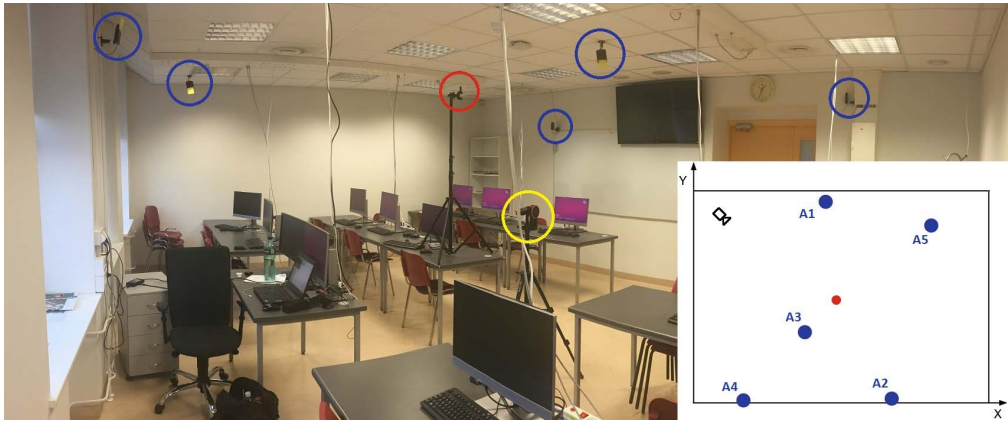
Fig. 8. The physical layout of the experimental setup. In the photograph, the five anchors are circled with blue, the single tag with red, and the Leica DISTO S910 laser distance meter with yellow. The approximate location from which the photograph was taken is marked with a camera symbol in the diagram.

TABLE II
EXPERIMENTAL RESULTS: AP2 SS-TWR RANGING STANDARD DEVIATION (cm) FOR A MAXIMUM NUMBER OF $n = 5$ ANCHORS

m \ k	0	1	2	3	4
1	2.475	3.742	4.408	5.068	5.287
2	2.929	3.005	3.058	3.132	
3	3.248	3.315	3.525		
4	3.583	3.708			
5	3.888				

TABLE III
SIMULATION RESULTS: AP2 SS-TWR RANGING RMSE (cm) FOR A MAXIMUM NUMBER OF $n = 5$ ANCHORS

m \ k	0	1	2	3	4
1	3.180	4.500	4.858	5.027	5.192
2	3.180	3.432	3.555	3.626	
3	2.805	2.901	2.960		
4	2.513	2.563			
5	2.293				

mean value is equal to the true distance:

$$\sigma_d = \sqrt{\frac{\sum_{i=1}^{N}(d_i - \overline{d})^2}{N}}. \tag{15}$$

It is also important to note that care was taken to monitor the sample mean values and the true distances to each anchor during all measurement sessions. This was done to verify that the practical measurement results conformed to real world anchor-tag distances, confirming that the method under test produces practically viable ranging results.

B. Experimental Results

This section presents the experimental results of AP2 SS-TWR, compares it with the performance attained in simulations and gives the analysis of said differences.

As also stated in the previous section, the practical results are presented as σ, the standard deviation of the measurements, which can be interpreted as the best-case RMSE value.

Table II presents the achieved AP2 SS-TWR method measurement standard deviation in centimeters for all allowed m, k combinations for a total number of $n = 5$ anchors. For the practical experiments, the baseline SS-TWR performance of case $m = 1$, $k = 0$ is taken as the average standard deviation of active ranging across the whole measurement campaign. In order to compare the experimental results, Table III presents the theoretical results for the same m, k combinations.

The results and the main trends of the theoretical results were discussed in Section V-B. The following analysis focuses on the experimental results in Table II.

An overall trend can be observed, where the experimental results are comparable to the simulation results. Increasing the number of passive-only anchors k, the standard deviation of ranging results also increase.

The cases of $m = 1$ and $m = 2$ show that the practical AP2 SS-TWR functions better or similar compared to the simulation results, validating the method. The increased performance can be attained to the simulations assuming the worst case scenario for time measurement standard deviation discussed in Section V-A, while the practical system surpasses this performance.

For cases where $m > 2$ the experimental results show higher standard deviation than the simulation results. The differences between the experimental and theoretical results are further discussed in the following paragraphs.

In order to analyze performance differences of the practical and simulated AP2 SS-TWR, two of the most notable cases were selected to illustrate the reasons. Based on Table II, the positive case of $m = 2$, $k = 3$ selected since the performance increased compared to previous $m = 1$ case, and the worst case of $m = 5$, $k = 0$ selected to reflect the worst overall performance.

Table IV represents the standard deviations in centimeters of the individual elements of the measurement matrix across all samples collected for case $m = 5$, $k = 0$. The column headers denote the transmitting anchor in the order of participating in the ranging sequence, while the row headers note the listening anchor. The standard deviation of each anchor's active measurement lays on the main diagonal.

Similarly to Table IV, the standard deviations of the individual elements of the measurement matrix for case $m = 2$,

TABLE IV

EXPERIMENTAL RESULTS. MEASUREMENT MATRIX STANDARD DEVIATIONS (cm) ACROSS ALL MEASUREMENTS FOR $m = 5$, $k = 0$. TRANSMITTING ANCHORS HEXADECIMAL IDS DEPICTED COLUMN WISE, LISTENING ANCHORS IDS ROW WISE, ACTIVE MEASUREMENTS ON MAIN DIAGONAL

	A1	A2	A3	A4	A5
A1	2.412	6.288	6.888	6.787	8.011
A2	6.092	2.485	6.001	5.745	7.116
A3	6.482	6.032	3.165	6.472	7.472
A4	6.274	5.122	6.184	3.148	5.767
A5	5.896	6.136	5.785	4.715	4.071

TABLE V

EXPERIMENTAL RESULTS. MEASUREMENT MATRIX STANDARD DEVIATIONS (cm) ACROSS ALL MEASUREMENTS FOR $m = 2$, $k = 3$. TRANSMITTING ANCHOR DEPICTED COLUMN WISE, LISTENING ANCHORS ROW WISE, ACTIVE MEASUREMENTS ON MAIN DIAGONAL

	A1	A2
A1	2.144	4.916
A2	5.012	2.490
A3	6.143	6.322
A4	5.690	5.943
A5	5.830	4.378

$k = 3$ are presented in Table V, where again transmitting and listening anchors are displayed column and row wise, respectively.

Inspecting the active measurement standard deviations on the main diagonal of both of the tables, it can be seen that the values typically increase for each next active measurement in the ranging sequence. This is also confirmed by viewing the average standard deviation for active measurements of both cases: $m = 5$, $k = 0$ has 5 active measurements with an average standard deviation of 3.056 cm, while $m = 2$, $k = 3$ has a an average standard deviation of 2.317 across the 2 active measurements per ranging sequence. Comparing with the SS-TWR RMSE of 3.18 cm from Fig. 5, we observe that the Eliko UWB RTLS offers better active ranging performance than simulations suggest.

Although the passive measurement standard deviations positioned off the main diagonal show slightly higher standard deviation compared to the simulated passive measurement RMSE of 5.51 cm stated on Fig. 5, there are some passive measurements that achieve better results. Among others achieving as low as 4.378 cm passive measurement standard deviation for anchor A5 listening on A2 in Table V.

On average, the standard deviation of passive measurements for $m = 5$, $k = 0$ is 6.263 cm and 5.530 cm for $m = 2$, $k = 3$. The former providing a higher standard deviation due to the higher errors in the final column of Table IV.

Overall, the standard deviations for measurements between practical and simulation results are comparable. The differences could be attributed to additional error sources from protocol timing errors, surrounding environment effects or device orientation propagation effects. For future work, the sources of errors could be researched and investigated.

VII. CONCLUSION

This article proposed an alternative calculation method for active-passive ranging and additionally expanded on the previous work done in [22] by including SDS-TWR and AltDS-TWR active methods with the proposed active-passive

method, which was previously assessed only using SS-TWR. The proposed active-passive TWR methods called AP1 and AP2, respectively, were both paired with active ranging methods SS-TWR, SDS-TWR and AltDS-TWR. All of the six combinations of methods were validated by running simulations and comparing their range estimation RMSE and air time.

The results showed that all three AP2-TWR methods consistently outperform AP1-TWR methods by about 10 to 20%, depending on the chosen m, k. The SDS-TWR and AltDS-TWR variants perform almost identically, while exceeding SS-TWR's RMSE performance in both of the corresponding AP-TWR methods. Interestingly, depending on m, k values in AP2-TWR, the other active TWR variants outperform SS-TWR by only a maximum of 0.30 cm RMSE. Briefly, from the standpoint of range estimate RMSE, the best performing active-passive method is a tie between AP2 SDS-TWR and AP2 AltDS-TWR, with AP2 SS-TWR following very closely behind.

In addition to the range estimate RMSE, the amount of data needed to transmit and air time efficiency were also discussed as important performance indicators. It was found that in order to provide the shortest packet, i.e. the least amount of data needed to transmit from the tag, the SS-TWR is found to be most desirable requiring half as much data to be transmitted, compared to other active methods.

The air time efficiency was assessed as the number of packets exchanged in a ranging sequence. It was also found that in order to optimize the air-time efficiency for active TWR methods, an aggregated packet exchange protocol needs to be employed. Out of all the methods, unfortunately, SDS-TWR is the only one that does not support packet aggregation due to its symmetrical response delay time requirement.

The air time efficiency can be further improved with the introduction of AP-TWR methods. The AP-TWR methods can provide the same amount of range estimates with less packets exchanged when compared to an equivalent active TWR method. As stated before, depending on the choice of m, k, the RMSE could be simultaneously lowered as well.

The AP2 SS-TWR method was chosen as a well-rounded example, offering a good balance between RMSE performance, number of transmitted data, and air time efficiency compared to other AP-TWR variants. Comparing it with an equivalent 6 anchor SS-TWR active method, the example $m = 4$, $k = 2$ showed a relative decrease of RMSE and air time by -18.3% and -25%, respectively. Sacrificing air time, the RMSE could be further reduced down to -33.3% ($m = 6$, $k = 0$); or vice-versa yield in RMSE, so the air time could be reduced down to -62.5% ($m = 1$, $k = 5$).

The practical experiments with AP2 SS-TWR verified the validity of the method and the results were comparable to the simulation results.

For future works, the practical performance of the other proposed active-passive methods could be evaluated. Additionally, the current practical experiments could be expanded and their performance assessed in non-line-of-sight conditions. Finally, the AP methods could be enhanced by additional measurement matrix analysis and processing to provide better performance and robustness of ranging.
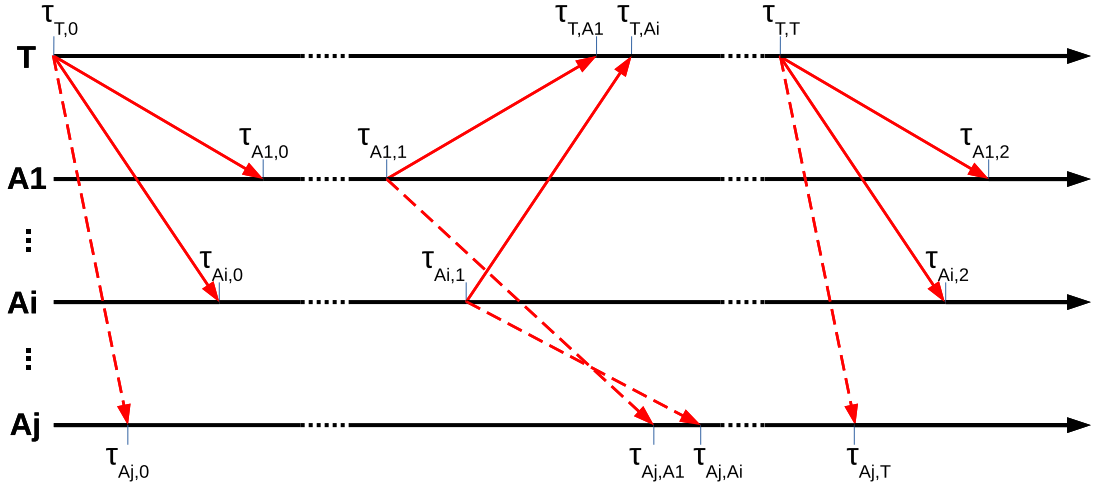
Fig. 9. Timestamps in SS-TWR and AltDS-TWR based active-passive methods. Each device records timestamps at packet transmission or reception times, relative to their local counter. These timestamp values can in turn be used to find the specific time intervals utilized in the proofs of AP-TWR methods proposed in this article.

TABLE VI

CORRESPONDENCE OF TIME INTERVAL NOTATION ON FIG. 3 TO THE TIMESTAMP NOTATION ON FIG. 9, DEPENDING ON THE SOURCE DEVICE

Device	Correspondence			
T	$t_{T,A1} = \tau_{T,A1} - \tau_{T,0}$	$t_{T,A1'} = \tau_{T,T} - \tau_{T,A1}$	$t_{T,Ai} = \tau_{T,Ai} - \tau_{T,0}$	$t_{T,Ai'} = \tau_{T,T} - \tau_{T,Ai}$
Aj	$t_{Aj,A1} = \tau_{Aj,A1} - \tau_{Aj,0}$	$t_{Aj,Ai} = \tau_{Aj,Ai} - \tau_{Aj,0}$	$t_{Aj,T} = \tau_{Aj,T} - \tau_{Aj,0}$	
A1	$t_{A1,T} = \tau_{A1,1} - \tau_{A1,0}$	$t_{A1,T'} = \tau_{A1,2} - \tau_{A1,1}$		
Ai	$t_{Ai,T} = \tau_{Ai,1} - \tau_{Ai,0}$	$t_{Ai,T'} = \tau_{Ai,2} - \tau_{Ai,1}$		

APPENDIX I
PROOF FOR SDS-TWR BASED AP2-TWR

The SDS-TWR based AP2-TWR method on Fig. 4 allows us to observe that both of the following equalities hold:

$$t_{T \leftrightarrow Aj} + t_{Aj,Ai} = t_{T \leftrightarrow Ai} + t_{Ai,T} + t_{Ai \leftrightarrow Aj} \quad (16a)$$

$$t_{T \leftrightarrow Aj} + t_{T,Ai'} + t_{T \leftrightarrow Ai} = t_{Ai \leftrightarrow Aj} + t_{Aj,T,Ai} - t_{Aj,i}. \quad (16b)$$

Adding 16a to 16b, and solving for $t_{T \leftrightarrow Aj}$, we get the following expression:

$$t_{T \leftrightarrow Aj} = \frac{t_{Ai,T} + t_{Aj,T,Ai} - t_{T,Ai'}}{2} + t_{Ai \leftrightarrow Aj} - t_{Aj,Ai}. \quad (17)$$

According to Fig. 4 we know that $t_{Aj,T,Ai} = t_{T,Ai} + t_{T,Ai'}$. Substituting it into (17) and adopting the notation of $t_{T \leftrightarrow Aj|Ai}$ yields the final form for the SDS-TWR based AP2-TWR passive TOF estimate:

$$t_{T \leftrightarrow Aj|Ai} = \frac{t_{Ai,T} + t_{T,Ai}}{2} + t_{Ai \leftrightarrow Aj} - t_{Aj,Ai}. \quad (18)$$

Again, similarly to Section III-A, the notation of $t_{T \leftrightarrow Aj|Ai}$ is introduced to emphasize that the TOF from passive anchor Aj to tag T can be calculated using every active anchor's ranging data. It can also be seen that the final form of (18) is the same as (10a).

APPENDIX II
TIMESTAMPS IN AP-TWR

In the scope of this paper, the proof of AP-TWR methods is presented by using the notation of time intervals, as can be seen in Fig. 3. This notation is introduced to keep the intermediate equations concise. However, in practical transceivers such as the Qorvo/Decawave DW1000, on transmission or reception of an UWB frame each device returns a specific timestamp relative to its own internal counter instead of a time interval, marking that the devices have their own time base due to the clock offsets between them.

The Carrier Frequency Offset (CFO) estimation proposed by Dotlic *et al.* in [33] allows the clock offset values of a transmitter-receiver pair to be estimated, therefore the time base of the transmitter can be translated to the time base of the receiving device.

This concept is illustrated on Fig. 9, in which the ranging sequence is identical to the one pictured on Fig. 3, differing only by the notation used in the time axes of the devices. The former utilizing the timestamp, and the latter resorting to time interval notation for the time axes of each device.

On Fig. 9, the timestamps are universally marked by τ, the disambiguation is made by the components presented in its subscript. The first component of the subscript marks the device which returns its current timestamps. For T and Aj, the second component marks the device the transmission originates from, and for A1 and Ai, the second component marks the number of the timestamp corresponding to packet exchange with T, since active anchors have two-way communication with the tag.

Comparing the notation of Fig. 3 and Fig. 9, it can be seen that a bijection between the two exists. This is further illustrated in Table VI, where in each row, a device's recorded time interval lengths on Fig. 3 is put into correspondence with the specific timestamps of Fig. 9. The bijection is valid if and
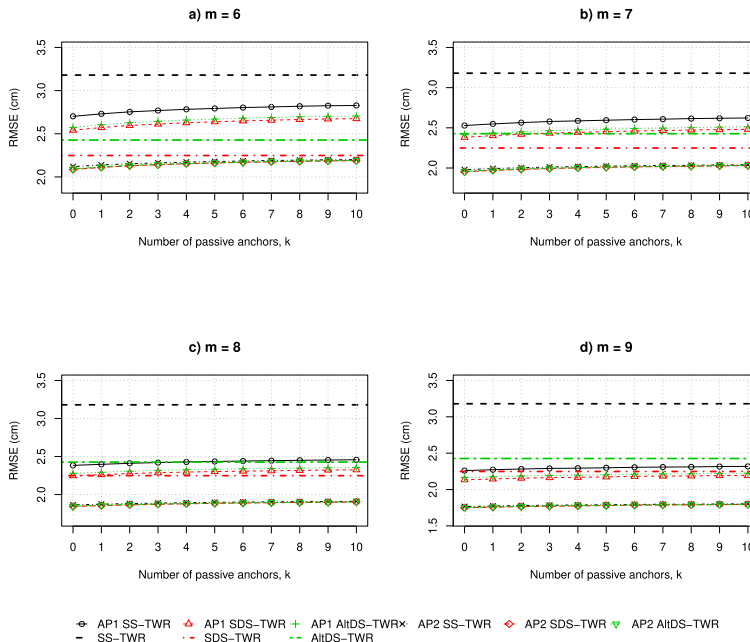
Fig. 10. Ranging performance of active-passive methods with measurement matrix averaging. Number of active-passive anchors $m = 6 \ldots 9$.

only if the timestamps are in the same time base, which can be achieved using the aforementioned CFO estimation method.

Practical transceivers such as the DW1000 internally measure time in the form of timestamps [32]. In order to calculate range estimates they need to forward the measured time values as timestamp differences i.e. time intervals, so the conversions stated in Table VI need to be done in the devices. This is also the reason why the time interval notation is mainly used in the equations presented in this paper.

APPENDIX III
ADDITIONAL SIMULATION RESULTS

See Fig. 10.

REFERENCES

[1] G. Deak, K. Curran, and J. Condell, "A survey of active and passive indoor localisation systems," *Comput. Commun.*, vol. 35, no. 16, pp. 1939–1954, Sep. 2012.

[2] G. M. Mendoza-Silva, J. Torres-Sospedra, and J. Huerta, "A meta-review of indoor positioning systems," *Sensors*, vol. 19, no. 20, p. 4507, Oct. 2019.

[3] F. Zafari, A. Gkelias, and K. K. Leung, "A survey of indoor localization systems and technologies," *IEEE Commun. Surveys Tuts.*, vol. 21, no. 3, pp. 2568–2599, 3rd Quart. 2017.

[4] B. Silva, Z. Pang, J. Akerberg, J. Neander, and G. Hancke, "Experimental study of UWB-based high precision localization for industrial applications," in *Proc. IEEE Int. Conf. Ultra-WideBand (ICUWB)*, Sep. 2014, pp. 280–285.

[5] S. J. Ingram, D. Harmer, and M. Quinlan, "UltraWideBand indoor positioning systems and their use in emergencies," in *Proc. Position Location Navigat. Symp. (PLANS)*, 2004, pp. 706–715.

[6] J. Rantakokko *et al.*, "Accurate and reliable soldier and first responder indoor positioning: Multisensor systems and cooperative localization," *IEEE Wireless Commun.*, vol. 18, no. 2, pp. 10–18, Apr. 2011.

[7] J. Tiemann, F. Schweikowski, and C. Wietfeld, "Design of an UWB indoor-positioning system for UAV navigation in GNSS-denied environments," in *Proc. Int. Conf. Indoor Positioning Indoor Navigat. (IPIN)*, Oct. 2015, pp. 1–7.

[8] M. Ridolfi *et al.*, "Experimental evaluation of UWB indoor positioning for sport postures," *Sensors*, vol. 18, no. 1, p. 168, 2018.

[9] D. Feng, C. Wang, C. He, Y. Zhuang, and X.-G. Xia, "Kalman-filter-based integration of IMU and UWB for high-accuracy indoor positioning and navigation," *IEEE Internet Things J.*, vol. 7, no. 4, pp. 3133–3146, Apr. 2020.

[10] F. Mazhar, M. G. Khan, and B. Sällberg, "Precise indoor positioning using UWB: A review of methods, algorithms and implementations," *Wireless Pers. Commun.*, vol. 97, no. 3, pp. 4467–4491, Dec. 2017.

[11] R. Zekavat and R. M. Buehrer, *Handbook of Position Location: Theory, Practice and Advances.* Hoboken, NJ, USA: Wiley, 2011, vol. 27.

[12] R. Zandian, "Ultra-wideband based indoor localization of mobile nodes in ToA and TDoA configurations," Ph.D. dissertation, Dept. Technol., Center Excellence–Cogn. Interact. Technol., Univ. Bielefeld, Bielefeld, Germany, 2019.

[13] M. Ridolfi, S. van de Velde, H. Steendam, and E. De Poorter, "Analysis of the scalability of UWB indoor localization solutions for high user densities," *Sensors*, vol. 18, no. 6, pp. 1–19, 2018.

[14] R. Kaune, "Accuracy studies for TDOA and TOA localization," in *Proc. 15th Int. Conf. Inf. Fusion*, 2012, pp. 408–415.

[15] P. Pascacio, S. Casteleyn, J. Torres-Sospedra, E. S. Lohan, and J. Nurmi, "Collaborative indoor positioning systems: A systematic review," *Sensors*, vol. 21, no. 3, p. 1002, Feb. 2021.

[16] R. Fujiwara, K. Mizugaki, T. Nakagawa, D. Maeda, and M. Miyazaki, "TOA/TDOA hybrid relative positioning system using UWB-IR," in *Proc. IEEE Radio Wireless Symp.*, Jan. 2009, pp. 679–682.

[17] Z. Sahinoglu and S. Gezici, "Enhanced position estimation via node cooperation," in *Proc. IEEE Int. Conf. Commun.*, May 2010, pp. 1–6.

[18] M. R. Gholami, S. Gezici, M. Rydstrom, and E. G. Strom, "A distributed positioning algorithm for cooperative active and passive sensors," in *Proc. 21st Annu. IEEE Int. Symp. Pers., Indoor Mobile Radio Commun.*, Sep. 2010, pp. 1713–1718.

[19] K. A. Horvath, G. Ill, and A. Milankovich, "Passive extended double-sided two-way ranging algorithm for UWB positioning," in *Proc. 9th Int. Conf. Ubiquitous Future Netw. (ICUFN)*, Jul. 2017, pp. 482–487.

[20] K. A. Horvath, G. Ill, and A. Milankovich, "Passive extended double-sided two-way ranging with alternative calculation," in *Proc. IEEE 17th Int. Conf. Ubiquitous Wireless Broadband (ICUWB)*, Sep. 2017, pp. 1–5.

[21] S. Shah and T. Demeechai, "Multiple simultaneous ranging in IR-UWB networks," *Sensors*, vol. 19, no. 24, pp. 1–14, 2019.

[22] T. Laadung, S. Ulp, M. M. Alam, and Y. Le Moullec, "Active-passive two-way ranging using UWB," in *Proc. 14th Int. Conf. Signal Process. Commun. Syst. (ICSPCS)*, Dec. 2020, pp. 1–5.

[23] N. Lasla, A. Bachir, and M. Younis, "Area-based vs. multilateration localization: A comparative study of estimated position error," in *Proc. 13rd Int. Wireless Commun. Mobile Comput. Conf. (IWCMC)*, Jun. 2017, pp. 1138–1143.

[24] G. Shen, R. Zetik, and R. S. Thoma, "Performance comparison of TOA and TDOA based location estimation algorithms in LOS environment," in *Proc. 5th Workshop Positioning, Navigat. Commun. (WPNC)*, Mar. 2008, pp. 71–78.

[25] C. L. Sang, M. Adams, T. Hörmann, M. Hesse, M. Porrmann, and U. Rückert, "Numerical and experimental evaluation of error estimation for two-way ranging methods," *Sensors*, vol. 19, no. 3, p. 616, Feb. 2019.

[26] *Part 15.4: Wireless Medium Access Control (MAC) and Physical Layer (PHY) Specifications for Low-Rate Wireless Personal Area Networks (WPANs)*, Standards 802.15.4, 2007.

[27] Z. Sahinoglu and S. Gezici, "Ranging in the IEEE 802.15.4a standard," in *Proc. IEEE Annu. Wireless Microw. Technol. Conf.*, Dec. 2006, pp. 1–5.

[28] D. Neirynck, E. Luk, and M. McLaughlin, "An alternative double-sided two-way ranging method," in *Proc. 13rd Workshop Positioning, Navigat. Commun. (WPNC)*, Oct. 2016, pp. 16–19.

[29] H. Kim, "Double-sided two-way ranging algorithm to reduce ranging time," *IEEE Commun. Lett.*, vol. 13, no. 7, pp. 486–488, Jul. 2009.

[30] *IEEE Standard for Low-Rate Wireless Networks—Amendment 1: Enhanced Ultra Wideband (UWB) Physical Layers (PHYs) and Associated Ranging Techniques*, Standards 802.15.4z, 2020.

[31] L. Flueratoru, S. Wehrli, M. Magno, and D. Niculescu, "On the energy consumption and ranging accuracy of ultra-wideband physical interfaces," in *Proc. IEEE Global Commun. Conf. (GLOBECOM)*, Dec. 2020, pp. 1–7.

[32] *DW1000 User Manual V2.18. Decawave*. Accessed: Mar. 28, 2021. [Online]. Available: https://www.decawave.com/dw1000/usermanual/

[33] I. Dotlic, A. Connell, and M. McLaughlin, "Ranging methods utilizing carrier frequency offset estimation," in *Proc. 15th Workshop Positioning, Navigat. Commun. (WPNC)*, Oct. 2018, pp. 1–6.

[34] C. McElroy, D. Neirynck, and M. McLaughlin, "Comparison of wireless clock synchronization algorithms for indoor location systems," in *Proc. IEEE Int. Conf. Commun. Workshops (ICC)*, Jun. 2014, pp. 157–162.

[35] Eliko Tehnoloogia Arenduskeskus OÜ. (Jul. 15, 2021). *Eliko UWB RTLS*. [Online]. Available: https://eliko.ee/uwb-rtls-ultra-wideband-real-time-location-system/

[36] Leica Geosystems AG. *Leica DISTO S910 User Manual*. Accessed: Jul. 16, 2021. [Online]. Available: https://shop.leica-geosystems.com/sites/default/files/2019-04/leicadisto-s910-user-manual-805080-808183-806677-en.pdf

Taavi Laadung (Student Member, IEEE) was born in Tallinn, Estonia, in 1990. He received the B.Sc. and M.Sc. degrees in telecommunication from the Tallinn University of Technology, Tallinn, in 2013 and 2016, respectively, where he is currently pursuing the Ph.D. degree in information and communication technology. From 2015 to 2016, he was a course Practical Work Supervisor at the Tallinn University of Technology. From 2017 to 2019, he worked with the Estonian Defence Forces as a Communication Systems Research and Development Specialist. Since 2019, he has been working as a Researcher at Eliko Tehnoloogia Arenduskeskus OÜ, Tallinn. His research interests include the improving of algorithms and methods utilized in wireless indoor tracking, positioning, and object locating systems.

Sander Ulp received the M.Sc. degree in telecommunication and the Ph.D. degree in information and communication technology from the Tallinn University of Technology (TTÜ), in 2013 and 2019, respectively. Since 2018, he has been working as a Researcher at Eliko Tehnoloogia Arenduskeskus OÜ. Since 2019, he has been the CTO of the Competence Center, which develops novel indoor positioning research and technologies. His research interests are in distributed estimation, learning and adaptation over networks, digital signal processing, localization technologies, and indoor positioning.

Muhammad Mahtab Alam (Senior Member, IEEE) received the M.Sc. degree in electrical engineering from Aalborg University, Denmark, in 2007, and the Ph.D. degree in signal processing and telecommunication from the INRIA Research Center, University of Rennes 1, France, in 2013. He joined the Swedish College of Engineering and Technology, Pakistan, in 2013, as an Assistant Professor. He did his postdoctoral research at the Qatar Mobility Innovation Center, Qatar, from 2014 to 2016. In 2016, he joined as the European Research Area Chair holder and an Associate Professor with the Thomas Johann Seebeck Department of Electronics, Tallinn University of Technology, where he was elected as a Professor, in 2018. In 2019, he becomes the Head of the Communication Systems Research Group and leading number of national and international projects. His research interests include the fields of wireless communications and connectivity, NB-IoT 5G/B5G smart networks and services, and low-power wearable networks for SmartHealth.

Yannick Le Moullec (Senior Member, IEEE) received the M.Sc. degree from the Université de Rennes I, France, in 1999, and the Ph.D. and H.D.R. (accreditation to supervise research) degrees from the Université de Bretagne Sud, France, in 2003 and 2016, respectively. From 2003 to 2013, he successively held a Postdoctoral Researcher, an Assistant Professor, and an Associate Professor positions with the Department of Electronic Systems, Aalborg University, Denmark. He then joined the Thomas Johann Seebeck Department of Electronics, Tallinn University of Technology, Estonia: a Senior Researcher (from 2013 to 2016) and professorship (since 2017). He has supervised or co-supervised more than 50 M.Sc. students and 11 Ph.D. students. He has been involved in more than 20 projects, including five as PI, co-PI, or co-main applicant; one such notable project was the H2020 COEL ERA-Chair project from 2015 to 2019. His research interests include embedded systems, reconfigurable systems, the IoT, and the application thereof. He is a member of the IEEE Sustainable ICT Technical Community and the IEEE Circuits and Systems Society.

Appendix 3

Publication III

T. Laadung, S. Ulp, M. M. Alam, and Y. Le Moullec, "Performance Evaluation of UWB Active-Passive Two-Way Ranging Distance Estimation Matrix Weighting Methods," in *12th International Conference on Indoor Positioning and Indoor Navigation (IPIN 2022)*, pp. 1–5, CEUR-WS, sep 2022

Performance Evaluation of UWB Active-Passive Two-Way Ranging Distance Estimation Matrix Weighting Methods

Taavi **Laadung**[1,2,*], Sander **Ulp**[2], Muhammad Mahtab **Alam**[1] and Yannick **Le Moullec**[1]

[1]*Tallinn University of Technology, Ehitajate tee 5, Tallinn, 19086, Estonia*
[2]*Eliko Tehnoloogia Arenduskeskus OÜ, Aiandi 13/1, Tallinn, 12918, Estonia*

Abstract

This paper explores least squares (LS), median (MED), inverse distance weighting (IDW), distance weighted estimator (DWE) and three different weighted least squares (WLS) methods for Ultra-Wideband (UWB) active-passive two-way ranging (AP-TWR) measurement matrix estimation. The proposed methods were tested with practical experiments in line-of-sight (LOS) and two different non-line-of-sight (NLOS) conditions, and were benchmarked against an active-only single-sided two-way ranging (SS-TWR) method.

  The results show that the proposed methods MED, IDW and DWE achieve comparable standard deviation values, while outperforming the root-mean-squared-error (RMSE) of SS-TWR ranging by up to 14.3% in LOS and 19.08% in NLOS conditions. The experiments validate that the MED, IDW and DWE methods for AP-TWR are NLOS-robust and achieve better RMSE performance than active-only SS-TWR ranging.

Keywords

Active-Passive Two-Way Ranging, Ultra Wideband, Line-of-Sight, Non-Line-of-Sight

1. Introduction

During recent years, Ultra-Wideband (UWB) technology based positioning has been considered as an attractive and one of the most promising method to provide various location-based services. The increased interest for UWB can be explained by various traits that it offers: in addition to positioning, it can be also be used for data transfer, it provides high robustness to multipath, it does not strictly require line-of-sight (LOS) conditions, and it provides high accuracy in the order of centimeters [1].

  Typically, UWB positioning is based on exploiting the propagation time of radio frequency signals due to the usage of temporally very short pulses. The main time-based methods are Time of Flight (ToF), which estimates the propagation time between two nodes, and time difference

of arrival (TDoA), which estimates the differences of arrival time of a signal between multiple nodes [2].

TDoA offers an air time advantage, where only a single packet per position estimate is needed, which decreases the overall energy consumption of the system and could theoretically support a high device density in the service area. The main disadvantage of TDoA is that the anchors of a system need to be synchronized very accurately, adding to the complexity of the system. Time of flight (ToF) estimates are typically achieved via two-way ranging (TWR) methods, which remove the need for tightly synchronized anchors at the expense of additional air time. This in turn increases the energy consumption and lowers the tag density in the service area [3].

In order to overcome the shortcomings of both methods, a compromise is found by using passive anchor nodes to assist in the positioning process. The estimates supplied by passive nodes allow to reduce the number of packets a system has to transmit in a TWR sequence, effectively allowing to reduce the energy consumption and increase the air time efficiency, while still benefiting from the relaxed anchor synchronization requirement.

For example, Hepp *et al.* in [4] provide an anchor-initiated active-passive ranging protocol, mounted on a quadcopter. Horváth *et al.* proposed another passive ranging method used in conjunction with double-sided (DS) TWR with an alternative calculation method for increased robustness [5]. These methods have been more focused on increasing the air time efficiency.

Although the seminal concept of tag-initiated Active-Passive Two-Way Ranging (AP-TWR) was published in [6], the concept of generalized tag-initiated AP-TWR was introduced in [7]. This method was further expanded in [8] to include an additional passive ranging method and assess the performance of AP-TWR in conjunction with different active ranging methods.

The main idea of AP-TWR is to employ *a priori* information about anchor locations to calculate extra passive range estimates in addition to standard TWR estimates, without any additional impact on the air time. When maximum air time efficiency is not critical, the system can be scaled such that multiple active anchors are used, so the ranging performance can be increased. The achieved range estimates can then be arranged in a measurement matrix, which holds all the ranging data for a single ranging sequence. The previous papers have only utilized averaging of the measurement matrix rows to provide final range estimates, without looking into other methods. Additionally, the experiments were exclusively in line-of-sight (LOS) propagation conditions [7, 8].

In this paper we investigate methods to further improve AP-TWR range estimation via the manipulation of the resulting measurement matrix. These methods are then compared in various locations, in LOS and two separate non-line-of-sight (NLOS) propagation conditions. The rest of this paper is structured as follows: in Section 2 we give the theoretical background for AP-TWR, Section 3 lists the estimation methods to process the measurement matrix, Section 4 provides information on the experimental test setup, Section 5 presents the experimental results and the analysis; finally, the conclusions are drawn.

2. AP-TWR

AP-TWR defines two types of anchors, active-passive and passive-only, the former taking part of the ranging via standard TWR methods and listening to other transmissions while

not transmitting. The second type of anchors only listen to ongoing transmissions in the air, providing range estimates without actively partaking in them.

The work in [8] defined separate AP1-TWR and AP2-TWR methods, where the results showed that AP2-TWR is the better performing method. Therefore, in the scope of this paper we will be focusing on this method, while calling it just AP-TWR in order to avoid confusion.

The UWB ranging protocol is pictured in Fig. 1, where tag T initiates a ranging sequence by starting its internal timer and transmitting an UWB frame to active anchor Ai, which starts its timer and responds after its processing time $t_{Ai,T}$. Upon receiving Ai's reply, T sends out a final UWB frame after its processing time $t_{T,Ai'}$. Passive anchor Aj listens in on all the transmissions during the ranging sequence and records the corresponding times.

All the relevant time intervals for AP-TWR are described in more detail after the introduction of (1). As per Fig. 1 and [8], the AP-TWR employing Single-Sided Two-Way Ranging (SS-TWR) active method is described as

$$
t_{T\leftrightarrow Aj|Ai} = \begin{cases} \dfrac{t_{T,Ai} - t_{Ai,T}}{2}, & \text{for } i = j \\[2ex] \dfrac{t_{Ai,T} + t_{T,Ai}}{2} + t_{Ai\leftrightarrow Aj} - t_{Aj,Ai}, & \text{for } i \neq j, \end{cases} \tag{1}
$$

where $t_{T\leftrightarrow Aj|Ai}$ is the calculated time of flight (ToF) between the tag T and the j-th passive anchor Aj, while the i-th active anchor Ai is partaking in the ranging sequence. This distinction is made because a single passive anchor can produce an estimate of the ToF between T and Aj following each Ai's response. In the special case where $i = j$, only the active range estimate can be calculated; in this case it is calculated using SS-TWR. This is done by time intervals $t_{Ai,T}$ - the time interval measured by Ai corresponding to reception of T, and $t_{T,Ai}$ - time interval measured by T corresponding to the reception of Ai. In other cases, the passive estimate is calculated using the above mentioned $t_{Ai,T}$, $t_{T,Ai}$, the known ToF between Ai and Aj - $t_{Ai\leftrightarrow Aj}$, and $t_{Aj,Ai}$ - the time interval measured by Aj corresponding to the reception of Ai.

Calculating all possible $t_{T\leftrightarrow Aj|Ai}$ values via (1) results in the following n-by-m ToF measurement matrix $\mathbf{T}$:

$$
T = \begin{bmatrix} t_{T\leftrightarrow A1|A1} & \cdots & t_{T\leftrightarrow A1|Am} \\ \vdots & \ddots & \vdots \\ t_{T\leftrightarrow An|A1} & \cdots & t_{T\leftrightarrow An|Am} \end{bmatrix}, \tag{2}
$$

where $\{i \in \mathbb{Z} : 1 \leq i \leq m\}, \{j \in \mathbb{Z} : 1 \leq j \leq n\}$ and the total number of anchors n consists of the number of active-passive anchors m and passive-only anchors k, such that $n = m + k$.

It can be observed that the ToF estimates achieved via active TWR methods are located on the main diagonal of $\mathbf{T}$, and the passive estimates of AP-TWR are situated off the main diagonal, so rows $\{j \in \mathbb{Z} : m < j \leq n\}$ contain only passive ToF estimates.

The active SS-TWR method, as a result of its shorter measurement period, provides a lower relative motion induced error than the effectively longer Asymmetric Double-Sided Two-Way Ranging (ADS-TWR). The larger error is on account of including the final frame of the tag in the calculation of the range estimate [9].

It can be observed from Fig. 1 that the duration of the frame exchange regarding the calculation of the passive range estimates is in the same range as SS-TWR, since the time intervals incorporating the third UWB frame of the tag are not used in (1). Therefore we can assume that the relative motion error for AP-TWR passive range estimates is lower than ADS-TWR, for example.
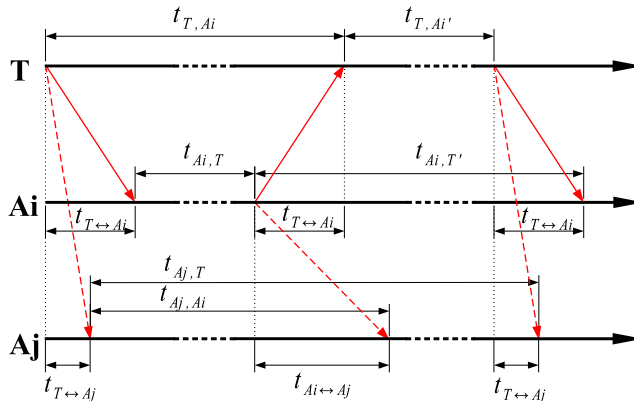
Figure 1: AP-TWR: Message exchange of tag T and active anchor Ai, while passive anchor Aj listens to the transmissions.

Moreover, assuming that the total length of the ranging protocol is in the order of milliseconds, we can infer that the error originating from the tag's relative movement to the anchors can altogether be omitted [10, 11].

AP-TWR cases $m > 1$ produce a ToF estimate matrix (2) consisting of more than one column and row, where the elements of each row are individual estimates of the true ToF between T and Aj, $t_{T \leftrightarrow Aj}$. Considering all the above, we can assume that elements of each row are independent estimates of $t_{T \leftrightarrow Aj}$, the values of which can be considered as constants for the duration of a single ranging sequence.

The number of rows show the number of unique distance measurements between the tag and anchors, and the values in each row are separate estimates of a single anchor-to-tag distance value. That is, the number of columns represents the number of measurements that can be processed to provide a final range estimate for that specific anchor. The row values need to be processed in order to provide a more accurate, precise and robust final distance estimate.

The following section focuses on the methods of estimating the values of $t_{T \leftrightarrow Aj}$ from the measurement matrix presented by (2).

3. Estimation methods

This section describes the methods of processing the raw measurement matrix values to achieve the final distance values as inputs for a positioning system. Many of the described methods

employ estimation of $t_{T\leftrightarrow Aj}$ via calculating a weighted arithmetic mean, differing by only how the weights are generated.

The weighted mean (WM) of the j-th row of the measurement matrix can be expressed as:

$$WM(\overline{t_{T\leftrightarrow Aj|A1:m}}) = \frac{\sum_{i=1}^{m}(w_{j,i} \cdot t_{T\leftrightarrow Aj|Ai})}{\sum_{i=1}^{m} w_{j,i}}, \tag{3}$$

where $w_{j,i}$ are the non-negative weights corresponding to each of the measurement matrix element $t_{T\leftrightarrow Aj|Ai}$. The special case where all the weights are equal, the solution simplifies to a standard arithmetic mean:

$$AM(\overline{t_{T\leftrightarrow Aj|A1:m}}) = \frac{\sum_{i=1}^{m} t_{T\leftrightarrow Aj|Ai}}{m}, \tag{4}$$

which will be discussed in the following Section.

3.1. Least Squares

In order to better describe the concept, we deconstruct the measurement matrix (2) to a set of n row vectors:

$$
\begin{aligned}
\boldsymbol{t_{T\leftrightarrow A1}} &= \begin{bmatrix} t_{T\leftrightarrow A1|A1} & \cdots & t_{T\leftrightarrow A1|Am} \end{bmatrix} \\
&\vdots \\
\boldsymbol{t_{T\leftrightarrow An}} &= \begin{bmatrix} t_{T\leftrightarrow An|A1} & \cdots & t_{T\leftrightarrow An|Am} \end{bmatrix}
\end{aligned} \tag{5}
$$

The problem of estimating the value of a constant using Least Squares (LS) is reduced to finding the mean value of the individual elements of the input vector [12]. The method is desirable because no additional information of the ToF estimates is needed and thus calculating weights is not needed.

As stated above, the LS solution for estimating a constant simplifies to calculating the arithmetic mean by applying (4) to (5):

$$\hat{T}_{LS} = \begin{bmatrix} \overline{t_{T\leftrightarrow A1|A1:m}} \\ \vdots \\ \overline{t_{T\leftrightarrow An|A1:m}} \end{bmatrix}, \tag{6}$$

where $\hat{T}_{LS}$ is a vector containing n final LS estimates of the ToF between the tag and the anchors.

3.2. Median

Like in the previous section, we adopt the vector notation of (5) to provide the solution of the next method.

Then the vector of final ToF estimates can be found as the median values of each vector of (5) as follows:

$$\hat{T}_{MED} = \begin{bmatrix} \tilde{t}_{T \leftrightarrow A1|A1:m} \\ \vdots \\ \tilde{t}_{T \leftrightarrow An|A1:m} \end{bmatrix}, \tag{7}$$

where the tilde accent notes the mathematical operation of median, which does not require extra information on measurements, while being a more robust estimator in presence of outliers than LS.

3.3. Inverse Distance Weighting

The Inverse Distance Weighting (IDW) method was introduced by Shepard in [13], which was devised as an interpolation function to produce a continuous surface from discrete data points.

Following the idea of Shepard, we take the liberty to rewrite the concept of IDW into the context of the current paper:

$$t_{T \leftrightarrow Aj} = \begin{cases} \dfrac{\sum\limits_{i=1}^{m}(t_{T \leftrightarrow Aj|Ai} \cdot d_{j,i}^{-1})}{\sum\limits_{i=1}^{m} d_{j,i}^{-1}}, & \text{if } d_{j,i} \neq 0 \text{ for all } i, \\[4mm] \overline{t_{T \leftrightarrow Aj|A1:m}}, & \text{if } d_{j,i} = 0 \text{ for some } i, \end{cases} \tag{8}$$

where

$$d_{j,i} = |t_{T \leftrightarrow Aj|Ai} - \overline{t_{T \leftrightarrow Aj|A1:m}}|. \tag{9}$$

Equation (9) is the first-order distance function of $t_{T \leftrightarrow Aj|Ai}$. Since we are working in one dimension, the value of the distance function $d_{j,i}$ is calculated as the absolute value of the difference of $t_{T \leftrightarrow Aj|Ai}$ and the arithmetic mean of row j.

The value of $d_{j,i}$ is in turn used in the calculation of the first-order IDW estimate by (8), where the order is specified by the magnitude of the negative exponent of $d_{j,i}$. Larger exponent values effectively give larger weight to ToF estimates which are closer to the arithmetic mean.

3.4. Distance Weighted Estimator

Dodonov and Dodonova introduced the Distance Weighted Estimator (DWE) in [14], which provides a robust estimate of central tendency without the need of separately calculating a mean value.

Adopting our notation to (9) of [14], we get the expression to calculate the DWE weights as follows:

$$w_{j,i} = \frac{m-1}{\sum\limits_{l=1}^{m} |t_{T \leftrightarrow Aj|Ai} - t_{T \leftrightarrow Aj|Al}|} \tag{10}$$

where each of the weights are calculated as the inverse mean distance of $t_{T\leftrightarrow Aj|Ai}$ and other elements of row j. These weights are in turn used in (3), to provide the set of final ToF estimates $t_{T\leftrightarrow Aj}$.

3.5. Weighted Least Squares 1

The solution to Weighted Least Squares (WLS) estimation reduces to weighting the measured values with their corresponding noise variance, keeping in mind that the noise for each measurement is considered zero-mean and independent [12].

Firstly, we consider the theoretical noise variance values as the basis for the weights to calculate an estimate for the WLS1 method.

Considering the results of [6, 8], we can assume that active ranging (SS-TWR and AltDS-TWR, respectively) performs at about 3.2 cm root-mean-square error (RMSE) and passive ranging of AP-TWR in the range of 5.2 to 5.5 cm RMSE.

The RMSE values are presented in centimeters to reflect the final product of ranging, as opposed to providing the RMSE in picoseconds for the ToF measurements. Both representations can be used interchangeably, since the ToF time t_{ToF} and the distance value d are related to each other via the propagation speed c (in this case, the speed of light) through the expression $d = c \cdot t_{ToF}$.

As the WLS solution employs weighting based on the noise variance, the WLS1 weights for the measurement matrix can be written as

$$w_{j,i} = \begin{cases} \dfrac{1}{\sigma_a^2}, & \text{for } i = j, \\[2mm] \dfrac{1}{\sigma_p^2}, & \text{for } i \neq j, \end{cases} \tag{11}$$

where σ_a^2 is the variance of the active measurements, and σ_p^2 is the variance of the AP-TWR passive measurements. The calculated weights $w_{j,i}$ are in turn used in (3) for the calculation of the final estimate.

The calculation of RMSE and standard deviation is somewhat similar, where the former is calculated using the known true value and the latter employing the sample mean value [8]. Therefore when the true value is equal to the sample mean, the RMSE and standard deviation values are also equal. Assuming the same data, but where the true value is not equal to the sample mean, the RMSE value is higher than the standard deviation of the data set.

Therefore in the scope of this paper we assume the value of standard deviation for the passive range estimates at $\sigma_p = 5.5$ cm, and for active estimates $\sigma_a = 3.2$ cm, inferred from the RMSE results of previous papers.

3.6. Weighted Least Squares 2

Following the approach of weights calculated using the theoretical variances, we propose the second method of weighted least squares (WLS2).

Firstly, we find each elements' distance from their corresponding row mean of the ToF measurement matrix T by adopting (9). By doing so, we formulate a mean-shifted measurement matrix T_S:

$$T_S = \begin{bmatrix} d_{1,1} & \cdots & d_{1,m} \\ \vdots & \ddots & \vdots \\ d_{n,1} & \cdots & d_{n,m} \end{bmatrix}. \tag{12}$$

Since the newly formed T_S is centered around its mean values, we can calculate column-wise variances:

$$\sigma_i^2 = \frac{\sum_{j=1}^{n}(d_{j,i} - \overline{d_{1:n,i}})^2}{n}, \tag{13}$$

where $\overline{d_{1:n,i}}$ is the mean value of column i of (12) and σ_i^2 are the calculated column-wise variances. Then the according weights can be calculated as

$$w_{j,i} = \frac{1}{\sigma_i^2}, \text{ for all } j. \tag{14}$$

The weights calculated by this method are the same for each row of the measurement matrix, changing only with each successive ranging sequence. Similarly to the previous section, the resulting weights are then used in (3) for the final ranging estimates.

3.7. Weighted Least Squares 3

In this section, we propose a third method for Weighted Least Squares (WLS3), for which the noise variance-based weights are also calculated for each row separately.

In order to calculate the final weights, the measurement matrix needs to be centered via (12) and the column-wise variances calculated, similarly to the previous section. Then the row-wise variances of T_S need to be calculated as well:

$$\sigma_j^2 = \frac{\sum_{i=1}^{m}(d_{j,i} - \overline{d_{j,1:m}})^2}{m}, \tag{15}$$

where $\overline{d_{j,1:m}}$ is the mean value of row j, and σ_j^2 is the row-wise variance of the measurement matrix. Following the calculation of σ_i^2 and σ_j^2, we then combine them into $\sigma_{j,i}^2$ by the following expression:

$$\sigma_{j,i}^2 = \frac{\sigma_j^2 + \sigma_i^2}{2}. \tag{16}$$

Based on (16), we can then calculate the weights by

$$w_{j,i} = \frac{1}{\sigma_{j,i}^2}, \tag{17}$$

which are in turn used as weights in (3) for the final AP-TWR ranging estimates.
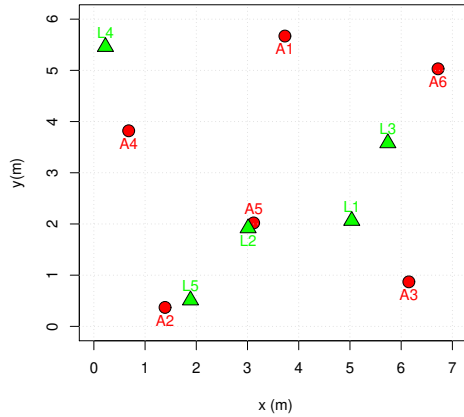
Figure 2: Representation of the test room setup in XY-plane. Anchors are marked with red circles and the test locations of the tag with green triangles.

4. Test Setup

In order to assess the performance of each of the previously specified methods, practical experiments were conducted. In this section we describe the preliminaries for the experiments.

The tests were ran in a 7.2 m by 6 m university laboratory room with concrete-walls, furnished with desks and computers. The UWB system used for experiments was the Eliko UWB RTLS [15] consisting of 6 active-passive anchors and a single tag. The active and passive range estimates were gathered via a laptop connected to the ranging engine of the Eliko UWB RTLS.

The active range estimates were attained using SS-TWR, and the passive estimates via the AP-TWR passive method described in Section 2. The gathered estimates were post-processed using a custom script written in R, implementing all the methods described in Section 3. Additionally, the script also calculates various statistical parameters, including RMSE and standard deviation, which are the basis for the results presented in Section 5. Apart from the proposed estimation methods, no additional filtering or trimming was applied to the measurement matrix.

The true coordinates of the anchors and of the tag at various positions were measured with a Leica Disto S910 laser distance meter [16]. In addition, the anchor-tag true distances were also verified with the Leica Disto S910, in order to calculate some of the needed performance parameters.

The data was gathered with a tag installed on a tripod at 5 arbitrarily chosen points in the room, which are marked on Fig. 2 alongside the locations of the anchors; the anchors are

Table 1
Test setup: anchors (Ax) subjected to NLOS in the 5 test locations (Loc x).

Loc 1	Loc 2	Loc 3	Loc 4	Loc 5
A1, A2, A4, A5	A2, A4	A1, A2, A4, A5	ALL	A3, A6

marked with red circles and the locations of the tag with green triangles.

In each location 3 separate tests were conducted: one line-of-sight (LOS) test and two separate non-line-of-sight (NLOS) tests. The NLOS tests were conducted by disrupting the LOS between anchors and a tag by either a 40 cm by 20 cm, 0.8 mm thick sheet of metal (NLOS1) or a human body chest area (NLOS2), placed at a distance of about 5 cm from the tag. Note that for both NLOS tests, the propagation paths to the same exact anchors were disrupted to have a fair comparison of the different NLOS conditions. Table 1 gives the details of NLOS tests, i.e. which anchors have NLOS propagation conditions at each of the test locations.

During each separate test, data from a minimum of 1200 separate ranging sequences were collected. Considering that the setup consisted of AP-TWR $m = 6, k = 0$, this amounts to at a minimum of 43200 raw range values across all the captured measurement matrices.

5. Experimental Results

The results of the experiments are given in Fig. 3, where the RMSE and standard deviation (SD) values for each of the test locations is given, depending on the propagation conditions. Fig. 3 a, b and c give the RMSE values for LOS, NLOS1 and NLOS2, respectively. Fig. 3 d, e, f give the respective SD values for the same propagation conditions. Additionally, a zoomed-in region of each of the sub-figures is given four location 4 since the traces can be placed quite densely.

Alongside the seven proposed methods (LS, Med, IDW, DWE, WLS1, WLS2, WLS3), the performance of active-only (SS-TWR) and AP-TWR passive-only ranging estimates from the same exact measurements is also given. They are separately pictured in order to give a baseline comparison of the performance of the proposed methods.

It can be observed from Fig. 3 a - c that the RMSE of passive measurements is almost always lower than the active-only method, with the exception of locations 1 and 2 in Fig. 3 a. On the other hand, the results for SD show the opposite: active-only estimates outperform the passive-only methods in every single test and location by a very slight margin. This is also in line with the results attained in previous publications regarding AP-TWR [6, 7, 8].

Although in regards of SD, the proposed methods' performance always places between the active and passive-only methods, the RMSE values show that many of the proposed methods provide better results than even the baseline better-performing passive-only estimates.

The average SD across all locations, depending on the method used, is shown as the bars on Fig. 4. From these results we can again see that the active estimates provide the lowest SD, while the passive estimates perform the least. The results from all three propagation condition tests show that utilizing the MED, IDW or DWE methods provide comparable performance to the most precise active-only estimates.

Across all locations the average RMSE values of LOS, NLOS1 and NLOS2 conditions depending on the method are given in Fig. 4, pictured by the lines+markers. The following analysis focuses on the RMSE improvements compared to a active-only SS-TWR method (Active method RMSE of Fig. 4), which achieved an RMSE of 24.209 cm in LOS, 36.006 cm in NLOS1 and 37.123 cm in NLOS2.

The WLS3 method provides the lowest RMSE of all the methods in LOS conditions at 20.742 cm (decrease of 14.3%), followed closely by IDW (20.785 cm, decrease of 14.14%) and DWE
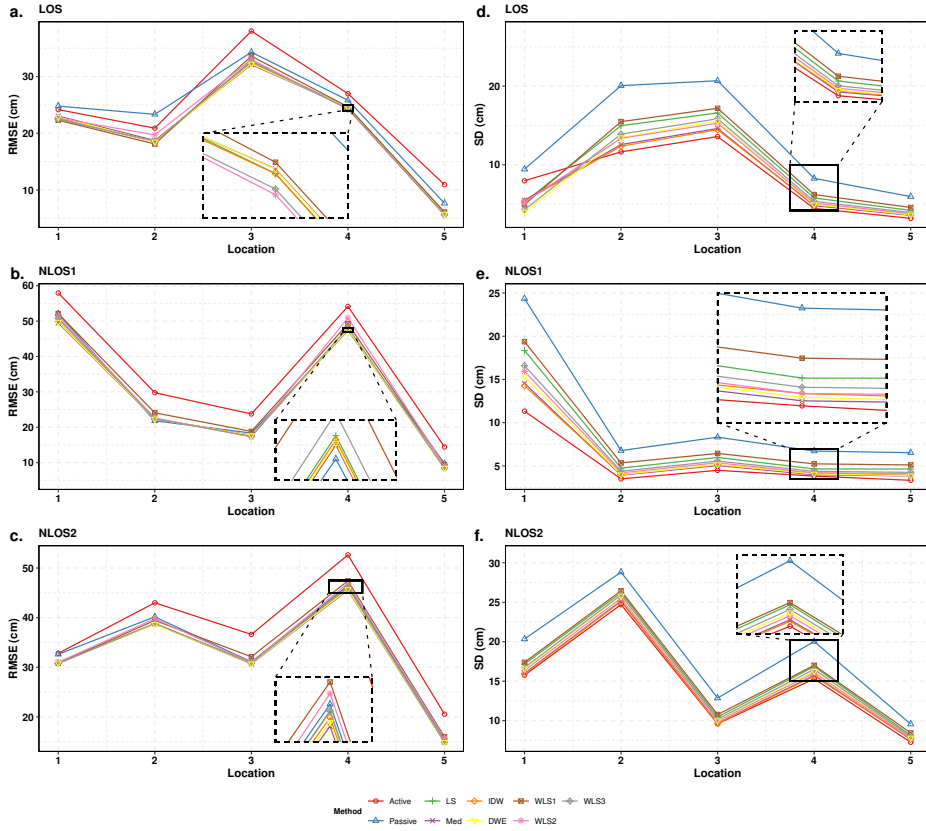
Figure 3: Results of experiments at each individual location. Parts a, b, c present the RMSE of the proposed methods in LOS, NLOS1 and NLOS2 propagation conditions; parts d, e, f present the respective standard deviation (SD) values. Lower is better for all of the figures, note the different scales on each figure.

(20.795 cm, decrease of 14.10%), up to the least performing method of WLS2 (21.064 cm, decrease of 13.00%). The results show that in LOS conditions all of the proposed methods perform similarly, with a difference of 0.322 cm between the best and worst performing method.

NLOS1 conditions showed the best performing method to be MED at 29.135 cm RMSE (decrease of 19.08%), followed by DWE at 29.169 cm (18.99% decrease) and IDW at 29.210 cm (18.87% decrease), with the lowest performing method WLS1 at 30.727 cm (14.66% decrease). It can be observed that in NLOS1 the absolute difference of the best and least performing methods, at 1.592 cm, is larger than in LOS.

NLOS2 conditions produced similar results where MED achieved the best results at 32.183 cm (13.31% decrease), followed by DWE at 32.190 cm (13.29%) and IDW at 32.251 cm (13.12%)
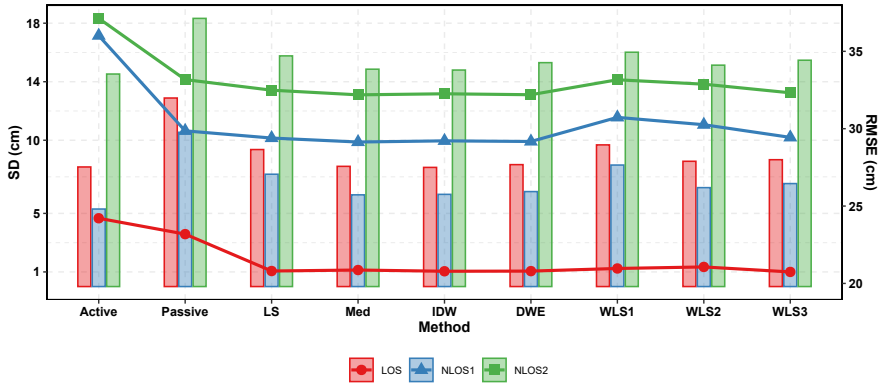
Figure 4: The average RMSE (lines+markers) and SD values (bars) for the proposed methods across all locations, depending on the tested propagation conditions. Lower is better.

with WLS1 landing at the last place with 33.157 cm RMSE (decrease of 10.68%). Similar to the previous result, the absolute difference of the methods is lower than NLOS1 but is still about 3 times as large as in LOS with 0.974 cm.

In terms of RMSE, the LS, MED, IDW and DWE methods show millimeter level differences between each other in LOS and NLOS, providing essentially the same performance. Coupled with the fact that MED, IDW and DWE offer comparable SD performance to active estimates, it can be claimed that the MED, IDW and DWE methods are the best-suited measurement matrix estimation methods.

Compared to results shown in previous papers reporting on AP-TWR [6, 7, 8], the attained RMSE values were slightly higher than expected. This is partly due to the fact that earlier papers ran only LOS tests, so naturally the added NLOS would provide degraded performance due to the impairment of propagation conditions, but the reported LOS results showed slightly lower performance as well.

This could be explained by some systematic errors introduced in the system. These errors could be attributed to imperfect calibration of antenna delays, range bias (effect of signal strength to the reported ranging value) [17], multipath propagation [18] or even errors originating from the physical orientation of the devices in regards to each other [19].

6. Conclusion

The experiments validated that all of the methods decrease the ranging RMSE in LOS propagation conditions, while also showing that NLOS propagation conditions do not break down the methods but rather increase the performance in demanding propagation conditions.

Results also showed that the selection of the specific method is not so critical in LOS conditions, as all the methods perform equivalently. The two tested NLOS conditions showed that in both, absolute values and relative decrease of RMSE, are further increased by selecting the appropriate

method, meaning that the choice of methods becomes more crucial for real-life applications experiencing mixed LOS/NLOS conditions.

In LOS, all the methods perform almost identically - achieving up to 14.3% lower RMSE when using WLS3 method compared to SS-TWR. NLOS conditions showed that up to 19.08% decrease of RMSE can be achieved compared to SS-TWR by employing MED to the measurement matrix, whereas the LS, IDW and DWE methods' performance lies within a few millimeters of it.

Comparing with the standard deviation of the best-performing SS-TWR active ranging, it was observed that the MED, IDW and DWE achieve comparable results, implicating that the precision of these methods is approximately on the same level. Meaning that these methods offer no significant degradation of the precision when compared to the active-only ranging.

In conclusion, across the tested LOS, NLOS1 and NLOS2 propagation conditions the methods MED, IDW and DWE showed similar SD, while providing considerably higher RMSE performance compared to SS-TWR. Taking into account these results it can be claimed that either one of the MED, IDW or DWE methods are sufficient for the AP-TWR measurement matrix estimation, while showing that these methods are also robust in NLOS conditions.

For future work, new experiments could be conducted in larger and more complex environments with harsher multipath effects present. Moreover, additional locations and tag orientations should be investigated to average out the device orientation errors and tests with varying number of active-passive anchors (m) should be conducted to see how it affects the performance of the proposed methods.

Acknowledgments

References

[1] A. Alarifi, A. Al-Salman, M. Alsaleh, A. Alnafessah, S. Al-Hadhrami, M. A. Al-Ammar, H. S. Al-Khalifa, Ultra wideband indoor positioning technologies: Analysis and recent advances, Sensors (Switzerland) 16 (2016) 1–36. doi:10.3390/s16050707.

[2] H. Liu, H. Darabi, P. Banerjee, J. Liu, Survey of wireless indoor positioning techniques and systems, IEEE Transactions on Systems, Man and Cybernetics Part C: Applications and Reviews 37 (2007) 1067–1080. doi:10.1109/TSMCC.2007.905750.

[3] M. Ridolfi, S. van de Velde, H. Steendam, E. De Poorter, Analysis of the scalability of UWB indoor localization solutions for high user densities, Sensors (Switzerland) 18 (2018) 1–19. doi:10.3390/s18061875.

[4] B. Hepp, T. Nägeli, O. Hilliges, Omni-directional person tracking on a flying robot using occlusion-robust ultra-wideband signals, in: IEEE International Conference on Intelligent Robots and Systems, volume 2016-Novem, 2016, pp. 189–194. doi:10.1109/IROS.2016.7759054.

[5] K. A. Horvath, G. Ill, A. Milankovich, Passive extended double-sided two-way ranging with alternative calculation, in: 2017 IEEE 17th International Conference on Ubiquitous Wireless Broadband, ICUWB 2017 - Proceedings, 2017, pp. 1–5. doi:10.1109/ICUWB.2017.8250972.

[6] S. Shah, T. Demeechai, Multiple simultaneous ranging in IR-UWB networks, Sensors (Switzerland) 19 (2019) 1–14. doi:10.3390/s19245415.

[7] T. Laadung, S. Ulp, M. M. Alam, Y. Le Moullec, Active-Passive Two-Way Ranging Using UWB, in: 2020 14th International Conference on Signal Processing and Communication Systems (ICSPCS), IEEE, 2020, pp. 1–5. doi:10.1109/ICSPCS50536.2020.9309999.

[8] T. Laadung, S. Ulp, M. M. Alam, Y. L. Moullec, Novel Active-Passive Two-Way Ranging Protocols for UWB Positioning Systems, IEEE Sensors Journal 22 (2022) 5223–5237. doi:10.1109/JSEN.2021.3125570.

[9] C. Lin, X. Jin, S. Mo, C. Hou, W. Zhang, Z. Xu, Z. Jin, Performance analysis and validation of precision multisatellite RF measurement scheme for microsatellite formations, Measurement Science and Technology 33 (2022). doi:10.1088/1361-6501/ac37ea.

[10] Y. Jiang, V. C. Leung, An asymmetric double sided two-way ranging for crystal offset, in: Conference Proceedings of the International Symposium on Signals, Systems and Electronics, Crdpj 320552, 2007, pp. 525–528. doi:10.1109/ISSSE.2007.4294528.

[11] J. Cano, G. Pages, E. Chaumette, J. LeNy, Clock and Power-Induced Bias Correction for UWB Time-of-Flight Measurements, IEEE Robotics and Automation Letters 7 (2022) 2431–2438. doi:10.1109/LRA.2022.3143202.

[12] D. Simon, Optimal State Estimation: Kalman, H Infinity, and Nonlinear Approaches, Wiley-Interscience, USA, 2006.

[13] D. Shepard, A two- dimensional interpolation function for irregularly- spaced data, in: Proceedings of the 1968 23rd ACM national conference, 1968, pp. 517–524.

[14] Y. S. Dodonov, Y. A. Dodonova, Robust measures of central tendency: Weighting as a possible alternative to trimming in response-time data analysis, Psikhologicheskie Issledovaniya 5 (2011) 1–11.

[15] Eliko Tehnoloogia Arenduskeskus OÜ, Eliko UWB RTLS, 2022. URL: https://eliko.ee/uwb-rtls-ultra-wideband-real-time-location-system/, accessed May 5, 2022.

[16] Leica Geosystems AG, Leica DISTO S910 User Manual, 2019. URL: https://shop.leica-geosystems.com/sites/default/files/2019-04/leica-disto-s910-user-manual-805080-808183-806677-en.pdf, accessed May 5, 2022.

[17] Decawave/Qorvo, APS011 Application Note: Sources Of Error In DW1000 Based Two-Way Ranging (TWR) Schemes, 2018. URL: https://www.qorvo.com/products/d/da008446, accessed July 13, 2022.

[18] A. D. Preter, G. Goysens, J. Anthonis, J. Swevers, G. Pipeleers, Range bias modeling and autocalibration of an UWB positioning system, in: 2019 International Conference on Indoor Positioning and Indoor Navigation, IPIN 2019, IEEE, 2019, pp. 1–8. doi:10.1109/IPIN.2019.8911815.

[19] P. Krapež, M. Vidmar, M. Munih, Distance measurements in uwb-radio localization systems corrected with a feedforward neural network model, Sensors 21 (2021) 1–18. doi:10.3390/s21072294.

Appendix 4

Publication IV

T. Laadung, S. Ulp, A. Fjodorov, M. M. Alam, and Y. Le Moullec, "Adaptive Extended Kalman Filter Position Estimation Based on Ultra-Wideband Active-Passive Ranging Protocol," *Submitted to IEEE Access*, 2023

Adaptive Extended Kalman Filter Position Estimation Based on Ultra-Wideband Active-Passive Ranging Protocol

TAAVI LAADUNG[1,2]**, SANDER ULP**[2]**, ALEKSEI FJODOROV**[1,2]**, MUHAMMAD MAHTAB ALAM**[1]**, (Senior Member, IEEE), YANNICK LE MOULLEC**[1]**, (Senior Member, IEEE)**

[1]Thomas Johann Seebeck Department of Electronics, Tallinn University of Technology, 12616, Tallinn, Estonia (e-mail: {taavi.laadung, aleksei.fjodorov1, muhammad.alam, yannick.lemoullec}@taltech.ee)

[2]OÜ Eliko Tehnoloogia Arenduskeskus, 12918, Tallinn, Estonia (e-mail: {taavi.laadung, sander.ulp, aleksei.fjodorov}@taltech.ee)

Corresponding author: Taavi Laadung (e-mail: taavi.laadung@taltech.ee).

ABSTRACT This paper first presents a comprehensive analysis of Non-Line-of-Sight (NLoS) error cases in the Ultra-Wideband (UWB) Active-Passive Two-Way Ranging (AP-TWR) protocol. Based on this analysis, we then propose the Adaptive Extended Kalman Filter (A-EKF) positioning method, utilizing variances calculated from AP-TWR range estimates, which are adapted based on the distance and intermittency of the range estimates. The proposed method needs no training data, nor any additional information about the environment the system is deployed in and does not yield any additional time delays. Based on experiments conducted in an industrial environment, the results show that the proposed method outperforms standard non-adaptive AP-TWR and active-only Single-Sided Two-Way Ranging (SS-TWR) methods in both stationary and movement tests. The stationary tests show that on average the proposed A-EKF method provides more than three times lower Root-Mean-Square-Error (RMSE) than the next best method (AP-TWR) in 3D positioning, while SS-TWR consistently performs worse by about 0.4 m in the z-axis. Additionally, the movement tests confirm the findings of the stationary tests and show that the challenging propagation conditions of the testing environment cause maximum errors at about 4.5 m for AP-TWR and SS-TWR, whereas the proposed A-EKF managed to mitigate these effects and reduce the error by 9 times, resulting in a maximum error of 0.5 m.

INDEX TERMS A-EKF, AP-TWR, EKF, Position Estimation, SS-TWR, UWB

I. INTRODUCTION

ULTRA-WIDEBAND (UWB) is a term used for radio communication that covers a bandwidth of over 500 MHz or 20% of the carrier center frequency. With the IEEE 802.15.4a-2007 amendment to the original IEEE 802.15.4-2006 standard, additional physical layers were introduced, which enabled precise ranging for UWB devices [1].

Utilizing UWB technology provides several benefits. The first one is the reduced interference with other narrowband wireless technologies thanks to the low transmission power of the wideband signal [2]. Another benefit of UWB is the nanosecond-range duration of the signal pulses, which reduces the effect of multipath as the signals from multiple propagation paths can be determined and filtered out accordingly [3]. Additionally, the high temporal resolution allows for centimeter-level ranging by utilizing Time of Flight (ToF) estimation by various Two-Way Ranging methods or using the Time Difference of Arrival (TDoA) method [4].

Like Bluetooth or WiFi, UWB also relies on the propagation of Radio Frequency (RF) waves, allowing it to function effectively even in Non-Line-of-Sight (NLoS) situations, although with diminished performance [2], [5]. In contrast, indoor positioning systems based on light, vision, or infrared technologies are unable to operate in these conditions [6].

To reduce the accuracy/precision penalties induced by NLoS propagation conditions, numerous NLoS detection

IEEE *Access*

Laadung *et al.*: Adaptive Extended Kalman Filter Position Estimation Based on Ultra-Wideband Active-Passive Ranging Protocol

and/or mitigation methods have been proposed [7]. In the literature, these strategies typically fall into three distinct but not mutually exclusive categories which are briefly discussed in the following paragraphs.

Firstly, channel statistics-based methods exploit the additional information about the propagation channel itself. These methods may use the various channel state parameters directly supplied by UWB transceiver chips (i.e. Qorvo DW1000 [8]) or the raw Channel Impulse Response (CIR) values. The former provides quickly accessible values, while the latter entails more time-consuming processes to extract the CIR [9].

Krishnan *et al.* employed machine learning (ML) methods (Multi-Layer Perceptron and Boosted Decision Trees) with the DW1000 supplied parameters of first path power and total received power to achieve a classification accuracy of up to 87% [10]. Similarly, [11] utilized readily available signal parameters reported by the DW1000 transceiver chip and proposed classifiers based on Gaussian Distribution and Generalized Gaussian Distribution models, outperforming multiple state-of-the-art ML techniques. The authors of [12] put forward a Neural Network model, which was trained on distance measurements, the running standard deviation of these measurements, and several received signal parameters. The purpose was to derive weights for a weighted least squares position estimator, aiming to minimize the impact of NLoS. In addition to ML, various other methods have been researched, such as fuzzy inference of NLoS parameters combined with adaptive Kalman filtering [13], utilizing logistic regression for NLoS detection [14], and devising a power-performance metric based on the estimated first path power and the total received power [15].

A sizable amount of research has been conducted by using the raw CIR: NLoS detection via Capsule Networks [16], proposing an NLoS-induced outlier-aware positioning method based on multilayer perception [17], signal decomposition by One-Dimensional Wavelet Packet Analysis in conjunction with Convolutional Neural Networks (CNN) [18], Transformer deep learning model [19], combining the Multilayer Perceptron with CNN to reduce calculation complexity [20], overcoming the problem of site-specific models by conducting Long Short-Term Memory training to predict NLoS error magnitude and variance of measurements [21], to name a few of the latest. In addition to ML and deep learning, other methods utilizing the raw CIR are explored: NLoS detection using fuzzy comprehensive evaluation [22], a weighted particle filter based on probability density functions of Line-of-Sight (LoS)/NLoS correlation coefficients [23], and adaptively selecting the optimal anchors based on the channel quality indicators [24].

Although the methods based on raw CIR typically offer higher accuracy than methods based on the readily available channel parameters, they propose a drawback on the scalability of a positioning system as the extraction of the raw CIR values from the transceiver is a time-consuming process [9].

Moreover, employing ML models requires large amounts of high-quality training data, which makes the data-gathering process tedious, while the training and implementation of models could turn out computationally expensive [20], [25].

Secondly, the position estimate-based category is with the broadest reach, covering methods that use position estimation residuals, redundancy of ranging estimates, environment (geometrical and propagation) data, or time series of position estimates.

In [26], Chen proposed the seminal Residual Weighting (Rwgh) algorithm, in which the position estimates and their residuals are calculated with every possible range estimate combination. The final position estimate is found as a residual-weighted linear combination of the intermediate position estimates. Jiao *et al.* improved on the work of Chen, lowering the computational cost by introducing an iterative approach to residual weighting [27]. Given N range estimates, this method calculates position estimates and residuals with $N-1$ combinations, choosing the one with the lowest average residual. It then selects the subsets until possible and calculates the final weighted position estimate based. Even though the computational complexity is reduced compared to Chen's algorithm, the method still requires in the order of tens of intermediate position estimate calculations to provide a final estimate.

Similar to the previous methods, [28] utilized the ranging residuals to propose an iterative residual test to identify and use only the detected LoS distances for positioning. Excluding NLoS distances, particularly in situations where multiple anchors are affected by the NLoS conditions, may lead to the inadvertent dismissal of crucial data for accurate positioning. In [29], the authors detected the presence of NLoS from statistical parameters calculated from the ranging residuals. While the general detection of Non-Line-of-Sight (NLoS) presence in positioning demonstrated high accuracy, discerning individual NLoS range estimates became more challenging as the accuracy decreased.

In [30] the authors addressed NLoS-corrupted measurements by detecting points of intersection with known obstacles present in a room. Subsequently, they computed correction terms based on these intersections to rectify the inaccuracies caused by NLoS effects. Similarly, Silva *et al.* utilized the geometric floor plan of the positioning environment, alongside information about the surrounding walls' composition, to propose a through-the-wall ranging model for positioning [31]. As this information is highly specific to the positioning environment, the setup of such a positioning system needs extra steps, such as acquiring floor plans or site surveying and matching them to the specific refractive indices of the walls of the positioning environment.

Thirdly, range-based methods utilize the time series of ranging values to detect and mitigate NLoS-induced position errors, for example by using the running variance of range estimates or a known probability density function for Line

IEEE *Access*

Laadung *et al.*: Adaptive Extended Kalman Filter Position Estimation Based on Ultra-Wideband Active-Passive Ranging Protocol

of Sight (LoS)/NLoS detection [32]. Applying such methods requires *a priori* error distributions or introduces time latency to the detection [22]. Furthermore, without additional constraints, the running variance method could lead to false classification if the tag is moving during the estimation process [33]. Momtaz *et al.* proposed a statistical method of detecting and eliminating the NLOS errors with lower computational complexity and increased accuracy [34], allowing for a more scalable solution than the previously mentioned Rwgh algorithm. As a downside, this method requires a specific online training phase, in which the noise term has to be measured. In order to circumvent some of the restrictions caused by extracting the CIR samples from the transceiver chip, Barral *et al.* opted to use the received signal value in conjunction with ranging data as features for multiple ML techniques for LoS/NLoS classification [9].

A. CONTRIBUTIONS

The advent of the UWB Active-Passive Two-Way Ranging (AP-TWR) protocol researched in [35], [36] opens up a new way of providing robust positioning in the presence of NLoS conditions. The following paragraphs outline the contributions of this paper.

While previous studies have focused on the performance of AP-TWR ranging, this paper goes further to examine how AP-TWR range estimates affect positioning accuracy. The proposed AP-TWR-based positioning method is validated and benchmarked in a real industrial environment to assess its performance.

The formulation of the proposed positioning method involves a thorough analysis of different NLoS error cases of AP-TWR, a novel contribution that has not been explored in the existing literature. Utilizing the redundant range estimates of AP-TWR allows for the calculation of range estimate noise variances, which is based on the previous analysis representative of NLoS propagation conditions. The noise variance is coupled with the proposed distance and intermittency penalties and used as input parameters to an Extended Kalman Filter (EKF) to provide a novel NLoS-robust and accurate positioning method.

The uniqueness of the proposed method lies in its avoidance of computationally expensive iterative NLoS detection techniques, lack of reliance on channel statistics or CIR information, independence from acquiring large datasets and labeling for model training, retention of all ranging data by not discarding any information, absence of latency issues typically found in methods computing running parameters, and the ability to operate without any knowledge about the environment, such as the composition and placement of walls or obstructions in a room. The proposed method stands out as a scalable, relatively easy-to-implement, and accurate NLoS-robust positioning solution, capable of efficiently adapting to various environments and ensuring reliable performance even in challenging propagation conditions.
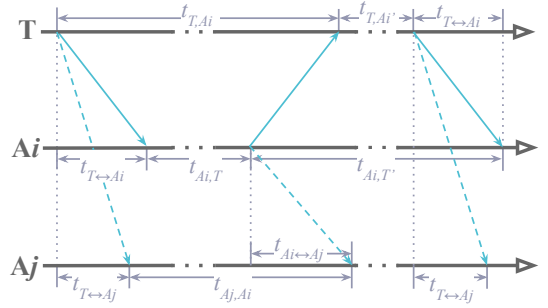
FIGURE 1. The Active-Passive Two-Way Ranging protocol. Tag T starts the ranging process by transmitting a packet, to which the active anchor Ai responds, after which T finishes the ranging sequence with a final transmitted packet. The passive anchor Aj listens to the active transmission in the air and calculates its passive range estimate.

The rest of the paper is organized as follows: Section II gives the theoretical background of the AP-TWR protocol, Section III presents the effects of NLoS on the AP-TWR range estimates and formulates the proposed method based on it, Section IV describes the environment and the parameter values used in the experiments, Section V provides the analysis of the results, and Section VI concludes this paper.

II. ACTIVE-PASSIVE TWO-WAY RANGING

The AP-TWR protocol packet exchange diagram is pictured in Fig. 1, where the mobile device (tag T) starts the ranging sequence by transmitting a ranging request packet. Upon receiving that packet, the current active anchor Ai responds after its processing time $t_{Ai,T}$, which T promptly receives and records the round trip time interval $t_{T,Ai}$. The final ranging report packet sent by T is irrelevant from the standpoint of producing time interval values; rather it is used to communicate the $t_{T,Ai}$ values back to the anchors for final range calculation. Meanwhile, the passive anchor Aj listens to the packet exchange of T and Ai and records the time interval between receiving T's first packet and Ai's response, $t_{Aj,Ai}$.

The resulting values are used in calculating the AP-TWR Time of Flight (ToF) estimates via:

$$t_{T\leftrightarrow Aj|Ai} = \begin{cases} \dfrac{t_{T,Ai} - t_{Ai,T}}{2}, & \text{for } i = j \\[2ex] \dfrac{t_{T,Ai} + t_{Ai,T}}{2} + t_{Ai\leftrightarrow Aj} - t_{Aj,Ai}, & \text{for } i \neq j, \end{cases}$$
$$(1)$$

where the first part corresponds to the active ranging by Single-Sided Two-Way Ranging (SS-TWR), and the second part is used to calculate the passive range estimates, hence the name AP-TWR. The resulting term $t_{T\leftrightarrow Aj|Ai}$ is the estimated ToF between T and Aj, calculated with the information acquired from listening to Ai's active ranging. The ToF between

IEEE *Access*

Laadung *et al.*: Adaptive Extended Kalman Filter Position Estimation Based on Ultra-Wideband Active-Passive Ranging Protocol

Ai and Aj, $t_{Ai \leftrightarrow Aj}$, is considered known as the anchors are part of a fixed infrastructure, with known coordinates. Therefore $t_{Ai \leftrightarrow Aj}$ can be measured by ranging between the anchors or calculated theoretically.

The values of the active anchor index are in the range of $1 \leq i \leq m$ and the index for passive anchors is $1 \leq j \leq n$, where the total number of additional passive-only anchors is $l = n - m$, such that $n \geq m$, meaning that the active anchors act as passive anchors while they are not actively transmitting.

The resulting ToF estimates are converted to range estimates via the expression $d_{j|i} = c \cdot t_{T \leftrightarrow Aj|Ai}$, where c is the wave velocity in the propagation medium. In this case, we assume the velocity to be the speed of light in vacuum $c \approx 3 \cdot 10^8$ m/s, as UWB is based on radio-frequency electromagnetic waves. Designating k as the temporal measure i.e. the ranging sequence number, we get the AP-TWR range estimate measurement matrix at time step k as $\mathbf{T}_{d,k}$:

$$\mathbf{T}_{d,k} = \begin{bmatrix} d_{1|1,k} & \cdots & d_{1|m,k} \\ \vdots & \ddots & \vdots \\ d_{n|1,k} & \cdots & d_{n|m,k} \end{bmatrix}. \qquad (2)$$

Previous studies [35], [36] have solely focused on evaluating the performance of the AP-TWR, based on the ranging Root-Mean-Square Error (RMSE). However, in this paper, we extend the evaluation to include the precision of position estimates as the primary consideration. Additionally, a novel position estimation algorithm based on the EKF is proposed, aiming to further enhance the performance. The specific contributions of this paper were explained in more detail in Section I.

III. PROPOSED METHOD

This section provides the theoretical background and formulation of the proposed AP-TWR-based Adaptive Extended Kalman Filter (A-EKF) positioning system. The following subsections present the essential information about the effects of NLoS on AP-TWR range estimates, the mechanisms for penalizing the inputs based on the distance and the intermittency of the range estimates, and finally the theory and the algorithm formulation of the proposed method.

A. EFFECT OF NLOS TO AP-TWR ESTIMATES

In order to quantify the effect of NLoS on AP-TWR estimates, (1) is analytically observed when arbitrary NLoS one-way bias factors β are introduced into the equations, depending on the severity of the NLoS case. Noting that for the formulation of this specific AP-TWR NLoS analysis, all other sources of errors are omitted. Table 1 presents the seven cases of errors possible for the trio of T, Ai, and Aj. The different NLoS propagation paths are viewed as separate cases between the tag and active anchor (T ↔ Ai), the tag and the passive anchor (T ↔ Aj), the active and passive anchors (Ai ↔ Aj), and all possible combinations thereof. Each case introduces a specific set of bias factors β to the propagation times $t_{T \leftrightarrow Ai}$, $t_{T \leftrightarrow Aj}$, and $t_{Ai \leftrightarrow Aj}$.

In the context of Table 1, the variables with the hat $(\hat{\cdot})$ are affected by the NLoS bias, whereas the equivalent variables without the hat $(\cdot)$ are the true values, unaffected by the bias. The fourth column presents the NLoS-affected term(s) of Eq. (1), referenced to Fig. 1. The final two columns present the net effect of NLoS on the active and passive range estimates of AP-TWR, respectively.

The results of Table 1 show that in Cases 1, 4, 6, and 7, the active range estimate is additively impaired by a factor $\beta_{T \leftrightarrow Ai}$ due to the existing NLoS path between T and Ai. Interestingly, the passive range estimates are unaffected by the NLoS between T and Ai, as its bias term cancels out in the calculation of the passive range estimates.

On the other hand, the passive range estimates are similarly affected by NLoS in pairwise Cases 2 & 4, 3 & 6, and 5 & 7. Noting that an obstruction between Ai and Aj (Cases 3, 5, 6, 7) causes a negative $\beta_{Ai \leftrightarrow Aj}$ NLoS term to emerge, which could translate to an altogether negative NLoS bias in the passive range estimates, as opposed to a strictly positive NLoS bias for standard active ranging protocols [37], [38].

The effects of NLoS presented in Table 1 align with the observed error cases for TDoA defined by Zandian and Witkowski in [39], while also expanding on it by adding the NLoS link between the active and passive anchor.

The presence of variable NLoS biases in the AP-TWR estimates can be used to one's advantage, as the rows of (2) may contain estimates from many anchors with various propagation conditions between them and the tag. This translates into fluctuating range estimates in the rows of the measurement matrix, the measure of which can be expressed by the row variances $\sigma_{j|1:m,k}^2$ corresponding to each time step k, expressed in matrix form:

$$\mathbf{S}_k = \begin{bmatrix} \sigma_{1|1:m,k}^2 & \sigma_{2|1:m,k}^2 & \cdots & \sigma_{n|1:m,k}^2 \end{bmatrix}^T. \qquad (3)$$

Previous research [36] has shown that taking the medians of the AP-TWR measurement matrix rows provides robust range estimates for positioning, therefore we denote the final range estimates of each time step k in matrix form as:

$$\mathbf{N}_k = \begin{bmatrix} \tilde{d}_{1|1:m,k} & \tilde{d}_{2|1:m,k} & \cdots & \tilde{d}_{n|1:m,k} \end{bmatrix}^T, \qquad (4)$$

where the tilde markers denote the mathematical operation of median across each row $d_{1|1:m,k} \ldots d_{n|1:m,k}$ of (2). The values of (4) act as the input to the EKF position estimation.

B. DISTANCE PENALTY

Research has shown that the accuracy of position estimation may be impaired because the ranging error magnitude has a distance-dependent component [7], [21]. However, some results show that this relationship is not exactly linear [5].

As a way to give higher weights to shorter distances, we propose a parametric exponential scaling coefficient $e^{s_c \cdot \tilde{d}_{j|1:m,k}}$, where the scaling constant is defined as $s_c = \frac{\ln s_m}{s_d}$. It is calculated via user-set parameters s_m and s_d such that the exponential scaler provides a multiplier of s_m at distance s_d.

TABLE 1. The AP-TWR errors in various NLoS cases between the devices.

Case	NLoS path	Bias factor(s)	Affected term in equations	Calculation of $\hat{t}_{T\leftrightarrow Ai \mid Ai}$	Calculation of $\hat{t}_{T\leftrightarrow Aj \mid Ai}$
1	T↔Ai	$\beta_{T\leftrightarrow Ai}$	$\hat{t}_{T,Ai} = t_{T,Ai} + 2\beta_{T\leftrightarrow Ai},$ $\hat{t}_{Aj,Ai} = t_{Aj,Ai} + \beta_{T\leftrightarrow Ai}$	$t_{T\leftrightarrow Ai \mid Ai} + \beta_{T\leftrightarrow Ai}$	-
2	T↔Aj	$\beta_{T\leftrightarrow Aj}$	$\hat{t}_{Aj,Ai} = t_{Aj,Ai} - \beta_{T\leftrightarrow Aj}$	-	$t_{T\leftrightarrow Aj \mid Ai} + \beta_{T\leftrightarrow Aj}$
3	Ai↔Aj	$\beta_{Ai\leftrightarrow Aj}$	$\hat{t}_{Aj,Ai} = t_{Aj,Ai} + \beta_{Ai\leftrightarrow Aj}$	-	$t_{T\leftrightarrow Aj \mid Ai} - \beta_{Ai\leftrightarrow Aj}$
4	T↔Ai, T↔Aj	$\beta_{T\leftrightarrow Ai},$ $\beta_{T\leftrightarrow Aj}$	$\hat{t}_{T,Ai} = t_{T,Ai} + 2\beta_{T\leftrightarrow Ai},$ $\hat{t}_{Aj,Ai} = t_{Aj,Ai} - \beta_{T\leftrightarrow Aj} + \beta_{T\leftrightarrow Ai}$	$t_{T\leftrightarrow Ai \mid Ai} + \beta_{T\leftrightarrow Ai}$	$t_{T\leftrightarrow Aj \mid Ai} + \beta_{T\leftrightarrow Aj}$
5	T↔Aj, Ai↔Aj	$\beta_{T\leftrightarrow Aj},$ $\beta_{Ai\leftrightarrow Aj}$	$\hat{t}_{Aj,Ai} = t_{Aj,Ai} - \beta_{T\leftrightarrow Aj} + \beta_{Ai\leftrightarrow Aj}$	-	$t_{T\leftrightarrow Aj \mid Ai} - \beta_{Ai\leftrightarrow Aj} + \beta_{T\leftrightarrow Aj}$
6	T↔Ai, Ai↔Aj	$\beta_{T\leftrightarrow Ai},$ $\beta_{Ai\leftrightarrow Aj}$	$\hat{t}_{T,Ai} = t_{T,Ai} + 2\beta_{T\leftrightarrow Ai},$ $\hat{t}_{Aj,Ai} = t_{Aj,Ai} + \beta_{Ai\leftrightarrow Aj} + \beta_{T\leftrightarrow Ai}$	$t_{T\leftrightarrow Ai \mid Ai} + \beta_{T\leftrightarrow Ai}$	$t_{T\leftrightarrow Aj \mid Ai} - \beta_{Ai\leftrightarrow Aj}$
7	T↔Ai, T↔Aj, Ai↔Aj	$\beta_{T\leftrightarrow Ai},$ $\beta_{T\leftrightarrow Aj},$ $\beta_{Ai\leftrightarrow Aj}$	$\hat{t}_{T,Ai} = t_{T,Ai} + 2\beta_{T\leftrightarrow Ai},$ $\hat{t}_{Aj,Ai} = t_{Aj,Ai} + \beta_{Ai\leftrightarrow Aj} + \beta_{T\leftrightarrow Ai} - \beta_{T\leftrightarrow Aj}$	$t_{T\leftrightarrow Ai \mid Ai} + \beta_{T\leftrightarrow Ai}$	$t_{T\leftrightarrow Aj \mid Ai} - \beta_{Ai\leftrightarrow Aj} + \beta_{T\leftrightarrow Aj}$

The resulting values corresponding to each distance are then expressed as the exponential scaling vector:

$$\mathbf{B}_k = \begin{bmatrix} e^{s_c \cdot \tilde{d}_{1 \mid 1:m,k}} & e^{s_c \cdot \tilde{d}_{2 \mid 1:m,k}} & \dots & e^{s_c \cdot \tilde{d}_{n \mid 1:m,k}} \end{bmatrix}^T, \quad (5)$$

which is used to modify the measurement noise vector in the AP-TWR A-EKF positioning scheme. The usage of the scaling vector is further explained in Section III-D.

C. INTERMITTENCY PENALTY

The UWB range estimates can be impaired by intermittent noise, multipath, and obstacles in the environment the system is operating in [40]. As a result of some or many of the aforementioned effects, the range estimates supplied by the UWB system might arrive intermittently.

To establish the intermittency penalty method, we hypothesize that the intermittent values are inherently less accurate, as the intermittent values show that the system works on the edge of its detection limit in the ranging process. We set forward two parameters, a positive integer l_s and a non-negative real number l_m, i.e., the time history length, and the intermittency multiplier, respectively.

Representing all the historical ranging values as sets on numbers with a cardinality of l_s, corresponding to all anchors in the system $A_1, A_2, \dots, A_N$ at time step k, we get:

$$
\begin{aligned}
A_{1,k} &= \{d_{A_1,k}, d_{A_1,k-1}, \dots, d_{A_1,k-l_s+2}, d_{A_1,k-l_s+1}\} \\
A_{2,k} &= \{d_{A_2,k}, d_{A_2,k-1}, \dots, d_{A_2,k-l_s+2}, d_{A_2,k-l_s+1}\} \\
&\vdots \\
A_{N,k} &= \{d_{A_N,k}, d_{A_N,k-1}, \dots, d_{A_N,k-l_s+2}, d_{A_N,k-l_s+1}\}.
\end{aligned}
$$

The elements of the sets of time history values assume the value of 0 in the case where a specific anchor does not produce a range estimate at that time instance. So, at each time instance, we get the number of missing range estimates in the history window for each anchor:

$$
\begin{aligned}
r_{A_1,k} &= |x_1 \in A_{1,k} : x_1 = 0| \\
r_{A_2,k} &= |x_2 \in A_{2,k} : x_2 = 0| \\
&\vdots \\
r_{A_N,k} &= |x_N \in A_{N,k} : x_N = 0|.
\end{aligned}
$$

The resulting numbers of missing values are in turn used to calculate the total set of intermittency penalty multipliers for each anchor in the system, for each time step value k:

$$L_k = \left\{ 1 + \frac{l_m}{l_s} \cdot r_{A_1,k}, \quad \dots, \quad 1 + \frac{l_m}{l_s} \cdot r_{A_N,k} \right\}. \quad (6)$$

Similar to (5), the intermittency penalty multiplier vector at time instance k is then formulated as:

$$\mathbf{C}_k = \begin{bmatrix} l_{i_1,k} & l_{i_2,k} & \dots & l_{i_n,k} \end{bmatrix}^T, \quad (7)$$

such that the values $l_{i_1,k}, l_{i_2,k}, \dots, l_{i_n,k}$ are elements of the subset of L_k and $i_1, i_2, \dots, i_n$ are the indices of the subset elements, marking the specific anchors providing their corresponding range estimates at time instance k.

Since only the intermittency penalty magnitude and not the input positioning data is dependent on time series history, no extra time-domain latency is introduced to the positioning process.

D. EXTENDED KALMAN FILTER

The literature encompasses a wide range of position estimation algorithms, spanning various Linear Least Squares (LLS), Nonlinear Least Squares (NLS), and multiple Bayesian Filter approaches, to name a few [41]. Among these methods, the EKF has demonstrated excellent performance in LoS scenarios while outperforming other methods in NLoS conditions, on par with the performance of the Unscented Kalman Filter (UKF) [42]. Furthermore, the EKF exhibits lower complexity, resulting in calculation times that are more than three times shorter than those of the UKF [39]. Considering these factors, the EKF was selected as the foundation for the method proposed in this paper.

Furthermore, in the scope of this paper, a single-model approach is utilized due to the absence of information regarding whether the tag is moving or stationary. However, incorporating sensors that provide additional information on the tag's movement/stationary state could enable adopting a multi-model approach. For instance, the switch to a zero-velocity model could be considered for cases where the tag is detected to be stationary [43].

Following previous works [21], [44], we expand the position, velocity, and acceleration model of EKF to three dimensions (3D). We do so by expressing the corresponding values

IEEE *Access*

Laadung *et al.*: Adaptive Extended Kalman Filter Position Estimation Based on Ultra-Wideband Active-Passive Ranging Protocol

at each time step as $\mathbf{X}_k$, and tying them with information from the previous time step $k-1$ using the appropriate kinematics equations:

$$\mathbf{X}_k = \begin{bmatrix} x_k \\ y_k \\ z_k \\ v_k^x \\ v_k^y \\ v_k^z \\ a_k^x \\ a_k^y \\ a_k^z \end{bmatrix} = \begin{bmatrix} x_{k-1} + T_s \cdot v_{k-1}^x + \frac{T_s^2}{2}a_{k-1}^x + \frac{T_s^3}{6}w_{k-1}^x \\ y_{k-1} + T_s \cdot v_{k-1}^y + \frac{T_s^2}{2}a_{k-1}^y + \frac{T_s^3}{6}w_{k-1}^y \\ z_{k-1} + T_s \cdot v_{k-1}^z + \frac{T_s^2}{2}a_{k-1}^z + \frac{T_s^3}{6}w_{k-1}^z \\ v_{k-1}^x + T_s \cdot a_{k-1}^x + \frac{T_s^2}{2}w_{k-1}^x \\ v_{k-1}^y + T_s \cdot a_{k-1}^y + \frac{T_s^2}{2}w_{k-1}^y \\ v_{k-1}^z + T_s \cdot a_{k-1}^z + \frac{T_s^2}{2}w_{k-1}^z \\ a_{k-1}^x + T_s \cdot w_{k-1}^x \\ a_{k-1}^y + T_s \cdot w_{k-1}^y \\ a_{k-1}^z + T_s \cdot w_{k-1}^z \end{bmatrix}, \tag{8}$$

where at time step k the coordinates, velocities, and acceleration values for each of the three axes are defined as $\{x_k \quad y_k \quad z_k\}$, $\{v_k^x \quad v_k^y \quad v_k^z\}$, and $\{a_k^x \quad a_k^y \quad a_k^z\}$, respectively. The kinematics equations and sampling time T_s are used to express the dependency of values at time step k from values at $k-1$. The last terms of each row represent the position $(T_s^3/6)w_{k-1}$, velocity $(T_s^2/2)w_{k-1}$, and acceleration $(T_s \cdot w_{k-1})$ noise of the model, respectively.

The process noise can be rewritten as a vector $\mathbf{w}_{k-1} = \begin{bmatrix} w_{k-1}^x & w_{k-1}^y & w_{k-1}^z \end{bmatrix}^T$ with a covariance matrix $\mathbf{Q}_{k-1} = diag(\sigma_{jx}^2, \sigma_{jy}^2, \sigma_{jz}^2)$. Therefore, the state vector (8) can be expressed as a series of matrix calculations, such that:

$$\mathbf{X}_k = \mathbf{A}\mathbf{X}_{k-1} + \mathbf{G}\mathbf{w}_{k-1}, \tag{9}$$

where matrix $\mathbf{A}$ is the state transition matrix and is written as:

$$\mathbf{A} = \begin{bmatrix} 1 & 0 & 0 & T_s & 0 & 0 & \frac{T_s^2}{2} & 0 & 0 \\ 0 & 1 & 0 & 0 & T_s & 0 & 0 & \frac{T_s^2}{2} & 0 \\ 0 & 0 & 1 & 0 & 0 & T_s & 0 & 0 & \frac{T_s^2}{2} \\ 0 & 0 & 0 & 1 & 0 & 0 & T_s & 0 & 0 \\ 0 & 0 & 0 & 0 & 1 & 0 & 0 & T_s & 0 \\ 0 & 0 & 0 & 0 & 0 & 1 & 0 & 0 & T_s \\ 0 & 0 & 0 & 0 & 0 & 0 & 1 & 0 & 0 \\ 0 & 0 & 0 & 0 & 0 & 0 & 0 & 1 & 0 \\ 0 & 0 & 0 & 0 & 0 & 0 & 0 & 0 & 1 \end{bmatrix}, \tag{10}$$

and $\mathbf{G}$ represents the noise transition matrix as:

$$\mathbf{G} = \begin{bmatrix} \frac{T_s^3}{6} & 0 & 0 \\ 0 & \frac{T_s^3}{6} & 0 \\ 0 & 0 & \frac{T_s^3}{6} \\ \frac{T_s^2}{2} & 0 & 0 \\ 0 & \frac{T_s^2}{2} & 0 \\ 0 & 0 & \frac{T_s^2}{2} \\ T_s & 0 & 0 \\ 0 & T_s & 0 \\ 0 & 0 & T_s \end{bmatrix}. \tag{11}$$

The AP-TWR range estimates $z_{j,k}$ are placed in the observation/measurement vector $\mathbf{Z}_k$, which consists of the sum of the true distance vector $\mathbf{D}_k = $

$\begin{bmatrix} d_{1,k} & d_{2,k} & \ldots & d_{n,k} \end{bmatrix}^T$ and the observation noise vector $\mathbf{V}_k = \begin{bmatrix} v_{1,k} & v_{2,k} & \ldots & v_{n,k} \end{bmatrix}^T$. The latter of which has a covariance matrix of $\mathbf{R}_k = diag(\sigma_{d_1,k}^2, \sigma_{d_2,k}^2, \ldots, \sigma_{d_n,k}^2)$:

$$\mathbf{Z}_k = \begin{bmatrix} z_{1,k} \\ z_{2,k} \\ \vdots \\ z_{n,k} \end{bmatrix} = \begin{bmatrix} d_{1,k} + v_{1,k} \\ d_{2,k} + v_{2,k} \\ \vdots \\ d_{n,k} + v_{n,k} \end{bmatrix} = \mathbf{D}_k + \mathbf{V}_k = \mathbf{H}_k\mathbf{X}_k + \mathbf{V}_k. \tag{12}$$

The vector $\mathbf{D}_k$ can be rewritten in the form of circle equations, where the centers are defined by the anchor coordinates $\{x_j \quad y_j \quad z_j\}$:

$$\mathbf{D}_k = \begin{bmatrix} \sqrt{(x_k - x_1)^2 + (y_k - y_1)^2 + (z_k - z_1)^2} \\ \sqrt{(x_k - x_2)^2 + (y_k - y_2)^2 + (z_k - z_2)^2} \\ \vdots \\ \sqrt{(x_k - x_n)^2 + (y_k - y_n)^2 + (z_k - z_n)^2} \end{bmatrix}. \tag{13}$$

Because the resulting equations are nonlinear, the first-order Taylor expansion is utilized for linearization, to produce the Jacobian matrix $\mathbf{H}_k$:

$$\mathbf{H}_k = \begin{bmatrix} \frac{\partial d_{1,k}}{\partial x_k} & \frac{\partial d_{1,k}}{\partial y_k} & \frac{\partial d_{1,k}}{\partial z_k} & 0 & 0 & 0 & 0 & 0 & 0 \\ \frac{\partial d_{2,k}}{\partial x_k} & \frac{\partial d_{2,k}}{\partial y_k} & \frac{\partial d_{2,k}}{\partial z_k} & 0 & 0 & 0 & 0 & 0 & 0 \\ & & & & \vdots & & & & \\ \frac{\partial d_{n,k}}{\partial x_k} & \frac{\partial d_{n,k}}{\partial y_k} & \frac{\partial d_{n,k}}{\partial z_k} & 0 & 0 & 0 & 0 & 0 & 0 \end{bmatrix}, \tag{14}$$

such that the partial derivatives are calculated at each time step k as:

$$\frac{\partial d_{j,k}}{\partial x_k} = \frac{x_k - x_j}{\sqrt{(x_k - x_j)^2 + (y_k - y_j)^2 + (z_k - z_j)^2}} \tag{15a}$$

$$\frac{\partial d_{j,k}}{\partial y_k} = \frac{y_k - y_j}{\sqrt{(x_k - x_j)^2 + (y_k - y_j)^2 + (z_k - z_j)^2}} \tag{15b}$$

$$\frac{\partial d_{j,k}}{\partial z_k} = \frac{z_k - z_j}{\sqrt{(x_k - x_j)^2 + (y_k - y_j)^2 + (z_k - z_j)^2}}. \tag{15c}$$

E. PROPOSED ADAPTIVE EKF METHOD

The proposed positioning method is described in the algorithm's pseudocode in Alg. 1, which consists of three distinct phases: AP-TWR ranging, EKF prediction, and EKF correction. The algorithm is also visualized as a flowchart in Fig. 2.

As a first step, the EKF initial state and state covariance matrices need to be initialized; this part is described in more detail in Section IV. After initialization, the first phase is launched, where the AP-TWR measurement matrix is acquired. Since the coordinate is calculated for three axes, a minimum of four input range estimates is needed. Otherwise, the position estimation process is skipped for this time step.

When the number of columns of the measurement matrix is larger than one i.e., $m > 1$, the row medians (4) and variances (3) are calculated. In the other case, the measurement matrix is directly taken as the observation vector and an

---

Algorithm 1 EKF positioning for AP-TWR protocol

Input: $\mathbf{T}_{d,k} \in \mathbb{R}^{n \times m}$, $\{s_d, \sigma_d^2, \sigma_{jx}^2, \sigma_{jy}^2, \sigma_{jz}^2\} \in \mathbb{R}_{>0}$, $\{s_m, l_m\} \in \mathbb{R}_{\geq 0}, l_s \in \mathbb{Z}_{>0}$
Output: $\hat{\mathbf{X}}_k$
Initialize: $\hat{\mathbf{X}}_0, \mathbf{P}_0$

1: **for** $k = 1, 2, \dots, \infty$ **do**
   AP-TWR ranging
2:   **if** $n < 4$ **then**   ▷ Less than 4 distances in input
3:       *skip*
4:   **end if**
5:   **if** $m > 1$ **then**
6:       $\mathbf{Z}_k = \mathbf{N}_k$ ▷ Observation vector
7:       Calculate $\mathbf{S}_k$ ▷ Row variances
8:   **else**
9:       $\mathbf{Z}_k = \mathbf{T}_{d,k}$
10:      $\mathbf{S}_k = \begin{bmatrix} \sigma_d^2 & \overset{\times n}{\dots\dots} \end{bmatrix}^T$ ▷ Assign default variance
11:   **end if**
12:   Calculate $\mathbf{B}_k$ ▷ Distance penalty
13:   Calculate $\mathbf{C}_k$ ▷ Intermittency penalty
14:   $\mathbf{R}_k = \text{diag}(\mathbf{S}_k \odot \mathbf{B}_k \odot \mathbf{C}_k)$ ▷ Hadamard product
   EKF Prediction
15:   $\hat{\mathbf{X}}_k^- = \mathbf{A}\hat{\mathbf{X}}_{k-1}$ ▷ Predict state
16:   $\mathbf{P}_k^- = \mathbf{A}\mathbf{P}_{k-1}\mathbf{A}^T + \mathbf{G}\mathbf{Q}_{k-1}\mathbf{G}^T$ ▷ Predict state cov.
   EKF Correction
17:   $\mathbf{K}_k = \mathbf{P}_k^- \mathbf{H}_k^T (\mathbf{H}_k \mathbf{P}_k^- \mathbf{H}_k^T + \mathbf{R}_k)^{-1}$ ▷ Kalman gain
18:   $\hat{\mathbf{X}}_k = \hat{\mathbf{X}}_k^- + \mathbf{K}_k(\mathbf{Z}_k - \mathbf{D}_k^-)$ ▷ Correct state estimate
19:   $\mathbf{P}_k = \mathbf{P}_k^- - \mathbf{K}_k \mathbf{H}_k \mathbf{P}_k^-$ ▷ Correct state cov.
20:   **return** $\hat{\mathbf{X}}_k, \mathbf{P}_k$
21: **end for**

FIGURE 2. The flowchart of the proposed AP-TWR A-EKF method.

appropriately-sized row variance vector $\mathbf{S}_k$ is constructed by repeating a default observation noise variance, σ_d^2. Then the distance and intermittency penalty vectors are calculated, and the observation covariance matrix $\mathbf{R}_k$ is formed as a diagonal matrix composed of the Hadamard product of vectors $\mathbf{S}_k$, $\mathbf{B}_k$, and $\mathbf{C}_k$.

In the following phase, the state and its covariance matrices are predicted, noting that the predicted values are marked with a "minus" superscript. Finally, the Kalman gain is computed and used to correct the state estimate and covariance providing a position estimate for that time step.

We adopt the naming convention used in previous studies [45], [46] that refer to the Kalman Filter as adaptive when the covariance matrices $\mathbf{Q}$ and $\mathbf{R}$ are dynamically modified. Accordingly, we introduce our approach as the Active-Passive Two-Way Ranging Adaptive Extended Kalman Filter (AP-TWR A-EKF) positioning method.

IV. EXPERIMENTAL SETUP

This section provides an overview of the experiments to validate the proposed AP-TWR A-EKF positioning method.

The experiments were conducted using the AP-TWR protocol implemented in the Eliko UWB RTLS system [47], which is based on the Qorvo DW1000 UWB transceiver chip

[8]. The true coordinates of the anchors' and tag's locations were surveyed using the Leica DISTO S910 laser distance meter, which provides three-dimensional coordinates [48].

The Eliko UWB RTLS was deployed in an industrial environment, at the premises of Krah Pipes OÜ [49] which specializes in producing large thermoplastic pipes. The factory premises were selected for conducting the experiments as they provide challenging conditions for the positioning system and the proposed method. These conditions include 1) restrictions on the placement of the anchors: most of the anchors have to be mounted near the ceiling, thus the tag is almost always positioned outside the 3D convex hull of the anchors; and 2) the presence of large metal and concrete objects obstructing the propagation path, etc.

The factory environment of the experiments can be seen in Fig. 3 where the Leica Disto S910 is marked in cyan, the two visible anchors in red, and the tag in dark blue color. Additionally, an industrial crane is mounted on rails on the ceiling, but it cannot be seen clearly: only the hook block of the crane is visible in the upper center part of the photo. The Leica DISTO S910 was installed on a concrete mezzanine floor, with a height of about 4.5 meters from the ground floor, such that it could provide the tag and anchor's true location across the whole area. The locations of the anchors, measured with the Leica DISTO S910, are given in Table 2.

The first set of tests was conducted with a stationary tag, mounted on a tripod, at 30 separate test points across the factory. The locations of the test points (TP), anchors (A), and the Leica DISTO S910 can be seen in Fig. 4. At each of the 30 test points the AP-TWR range estimates were captured for 30 seconds, using a tag with an update rate of 10 Hz, providing data from approximately 300 ranging sequences.

IEEE *Access*

Laadung *et al.*: Adaptive Extended Kalman Filter Position Estimation Based on Ultra-Wideband Active-Passive Ranging Protocol

FIGURE 3. Setup for the movement tests in the industrial environment. Visible anchors A_1 and A_6 are circled in red, the Leica DISTO S910 in cyan, and the tripod-mounted tag on the shelf trolley in dark blue. The tag is moved in reference to the lines on the factory floor.

TABLE 2. The coordinates of the anchors used in the experiments.

Anchor	x (m)	y (m)	z (m)
A_1	0.17	-0.05	4.50
A_2	47.52	-6.67	10.5
A_3	29.63	0.10	4.50
A_4	23.62	10.37	10.05
A_5	41.59	4.28	9.98
A_6	17.65	0.51	7.50
A_7	47.52	14.66	10.68
A_8	11.32	4.46	9.99

The second set of experiments was conducted to validate the results of the stationary tests. The experiment was performed with a moving tag which was mounted on a tripod, attached to a shelf trolley. The tag was moved throughout the factory with reference to the printed lines on the floor, where the critical points, i.e. turning points, are previously surveyed to provide a reference true track. The shelf trolley and the reference lines are also visible in Fig. 3. The data was captured throughout the movement process for 99 seconds, resulting in data of 990 separate ranging sequences.

The parameter values of the AP-TWR A-EKF used in the experiments are given in Table 3. The Eliko UWB RTLS was configured such that the maximum number of active anchors $m_{\max}$ of AP-TWR protocol is 6. Although the intermittency and distance penalty parameters were chosen heuristically, it is likely that the chosen values are sub-optimal, not providing the best achievable positioning performance for the proposed

method. Finding the optimal parameter values could be considered in future work.

TABLE 3. The parameters for the proposed AP-TWR A-EKF positioning method used in the experiments.

Parameter	Value
$m_{\max}$	6
s_d	100 m
l_s	6
l_m	100
σ_d^2	0.01 m^2
$\sigma_{jx}^2, \sigma_{jy}^2, \sigma_{jz}^2$	0.01 m^2/s^6
T_s	from tag clock
x_0, y_0, z_0	from true position
v_0^x, v_0^y, v_0^z	0 m/s
a_0^x, a_0^y, a_0^z	0 m/s^2
$\mathbf{P}_0$	I_9

The default observation noise variance σ_d^2 and the process noise covariance values of $\mathbf{Q}_{k-1}$ are inferred from [21]. The sampling interval T_s was extracted from the tag's internal clock during each ranging sequence.

The very first step of the EKF process requires initializing the values of the initial state vector $\mathbf{X}_0$ and the state covariance matrix $\mathbf{P}_0$. The initial coordinates $\{x_0 \quad y_0 \quad z_0\}$ of the state vector are given as the true coordinate by the DISTO S910 for all of the tested EKF variants, which are discussed in the following paragraphs. This is done to give all the methods the same initial conditions and to eliminate the additional errors from converging to the correct location
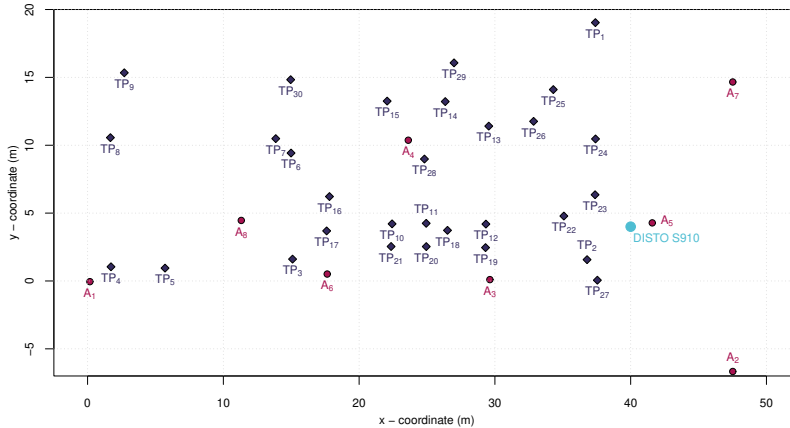
FIGURE 4. The test setup plan. Test point locations are marked with numbered "TP" markers in dark blue, anchor locations with numbered "A" markers in red, and the location of the Leica DISTO S910 laser distance meter is marked with a cyan circle.

when the initial position is set to the coordinate origin, for example. The initial speed and acceleration values for each axis are set to zero. The initial state covariance matrix $\mathbf{P}_0$ is set as a 9-by-9 identity matrix, corresponding to the size of the state vector.

The proposed A-EKF positioning method is compared to the baseline EKF methods, accordingly using standard AP-TWR range estimates (4) and SS-TWR active-only range estimates as input. The exact same dataset is utilized for all of the comapred methods, as both the SS-TWR and AP-TWR range estimates are inherently present in it, making the results of different methods directly comparable. The initial state, initial covariance, and $\mathbf{Q}_{k-1}$ matrix values are the same as stated in Table 3, whereas the diagonal of the appropriately-sized $\mathbf{R}_k$ matrix is filled with the default variance σ_d^2 values.

The data acquisition was performed via a custom Python script that interfaces with the Eliko UWB RTLS server, extracts the required UWB range estimate packets, and saves them to a text file. Then a custom script written in R was used to parse and process the data, as well as to calculate the range estimates and the metrics for all three methods. Although this specific implementation provides the results by post-processing the range estimates, the proposed system is able to work in real-time applications.

The comprehensive dataset with supplemental materials and detailed explanations is uploaded to the IEEE Dataport repository and can be found in [50].

V. RESULTS
This section provides the results of the stationary and moving experiments and the analysis thereof.

A. STATIONARY TESTS
The results of the stationary experiments are given in Fig. 5, where the 2D and 3D Root-Mean-Square-Error (RMSE) of the SS-TWR, standard AP-TWR EKF, and the proposed A-

EKF positioning method are given across all of the 30 test points.

Firstly, focusing on the 2D results, it can be seen that for most cases all of the tested methods provide comparable performance at approximately 0.15 m RMSE. The SS-TWR EKF shows a more uniform performance across the test points, with an exception at TP_1 and TP_8, where the 2D RMSE is significantly higher than usual, obtaining values of 0.49 m and 1.97 m, respectively. The higher RMSE of TP_8 is a result of the blocking of the LoS of the tag and A_1, A_6 due to large pipe mandrels made of metal, visible in the upper-left side of Fig. 3, while in TP_1, the direct propagation path to anchor A_7 is obstructed by the mezzanine floor.

The differences for the standard AP-TWR EKF are more diverse, as in test points 1, 3, 5, 8, 9, and 29 the 2D RMSE obtains significantly higher values than normal, ranging from 0.53 m (TP_1) up to 4.98 m (TP_3). Although the reasons are not as evident as for SS-TWR EKF, the analysis presented in Table 1 suggests that AP-TWR range estimates are impaired because of the compound NLoS effects of different propagation paths encountered during each ranging sequence. The effects could be a result of a combination of the aforementioned pipe mandrels, the overhead crane blocking propagation paths between anchors, all of the assets in the factory, etc.

As both, the standard AP-TWR and SS-TWR, methods do not provide the EKF with any additional information on the measurement noise that may be present, the input distances are treated as equal and the distances with larger error contribute to an increase in the positioning error.

The proposed AP-TWR A-EKF positioning method, on the other hand, is robust against the adverse propagation conditions present in the industrial environment. The proposed method typically performs at a similar or lower error level than the baseline methods, whereas the largest differences come into play at the previously mentioned high error
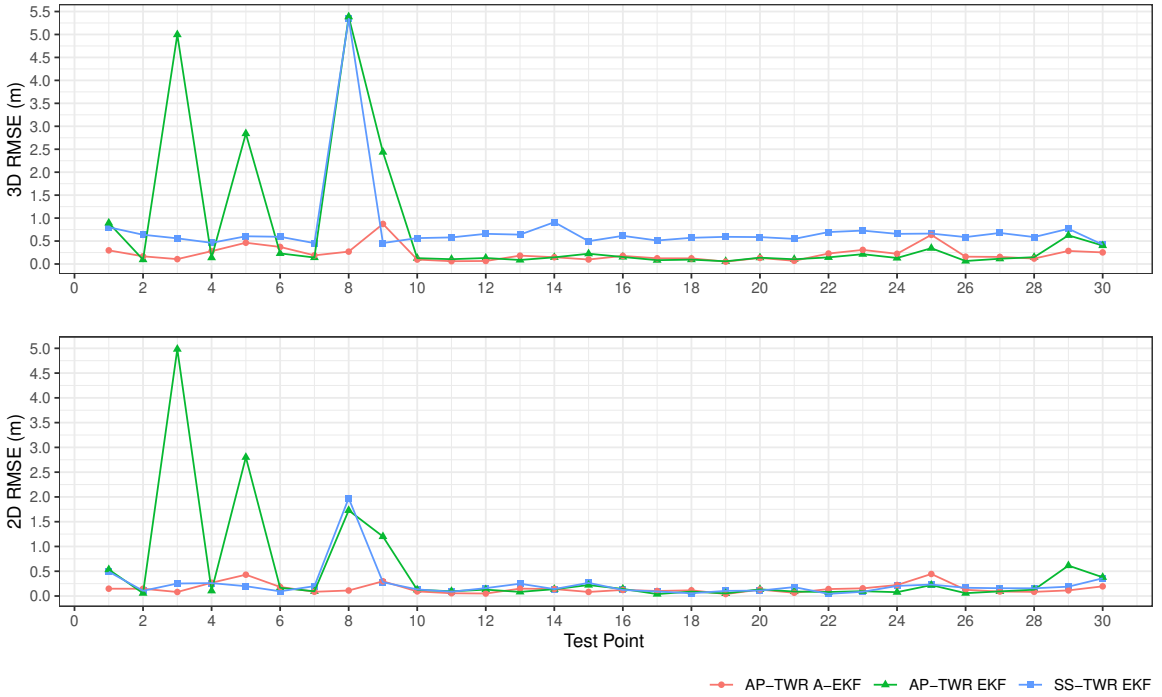
IEEE *Access*

Laadung *et al.*: Adaptive Extended Kalman Filter Position Estimation Based on Ultra-Wideband Active-Passive Ranging Protocol

test points of the baselines. The following analysis gives an overview of the behavior of A-EKF compared to other methods in the most significant test points.

At the high-error test points 1, 3, 5, 8, 9, and 29 of AP-TWR, the proposed A-EKF method reduces the RMSE respectively by 0.387, 4.902, 2.370, 1.617, 0.904, and 0.501 m, providing a large reduction in the absolute values of errors in every one of the high error test points. One minor drawback can be identified at test point 25, where the proposed method provides slightly lower performance than the baseline AP-TWR, with according RMSE of 0.445 m and 0.220 m. In terms of 2D RMSE, the proposed method performs better than AP-TWR in 18 of the 30 test points.

Comparing the proposed method to the SS-TWR in terms of 2D RMSE, it can be observed that the errors at TP_1 and TP_8 are reduced by 0.343 m and 1.863 m, correspondingly. Even though the proposed method provides slightly higher 2D errors at TP_5 and TP_{25}, the opposite is true for the 3D case where the A-EKF provides slightly better RMSE performance than SS-TWR. In conclusion, the proposed method provides a lower RMSE than SS-TWR at 17 of the 30 test points.

Although the test points show rather similar trends in the 3D RMSE, we see that in typical cases not involving the large error test points, the proposed method alongside the

AP-TWR provides consistently about 0.4 m lower RMSE.

All of the high error test points 1, 3, 5, 8, 9, and 29 of AP-TWR are again subsequently reduced by 0.597, 4.890, 2.378, 5.117, 1.565, and 0.340 m using the proposed method. Comparing the 3D results, it is evident that the proposed A-EKF method provides a reduction in RMSE at half of the test points when compared to AP-TWR, including the previously mentioned points where the error magnitude was reduced significantly.

Similarly, the high error points 8 and 14 of SS-TWR are also mitigated by the proposed method, which reduces 3D RMSE by 5.074 and 0.763 m, correspondingly. Moreover, the A-EKF outperformed the SS-TWR positioning in 29 out of the 30 test points, providing moderately higher RMSE at only TP_9.

On average, the tested methods achieved the following RMSE in 2D positioning: AP-TWR 0.492 m, SS-TWR 0.238 m, and A-EKF 0.149 m, meaning that the proposed method achieved almost 1.6 times better performance in 2D as the next best method, the SS-TWR. The 3D results showed the average RMSE of the methods to be AP-TWR 0.693 m, SS-TWR 0.765 m, and A-EKF 0.224 m, showing that the proposed method achieved over 3 times lower RMSE than the next best method i.e, AP-TWR.

IEEE Access

Laadung *et al.*: Adaptive Extended Kalman Filter Position Estimation Based on Ultra-Wideband Active-Passive Ranging Protocol
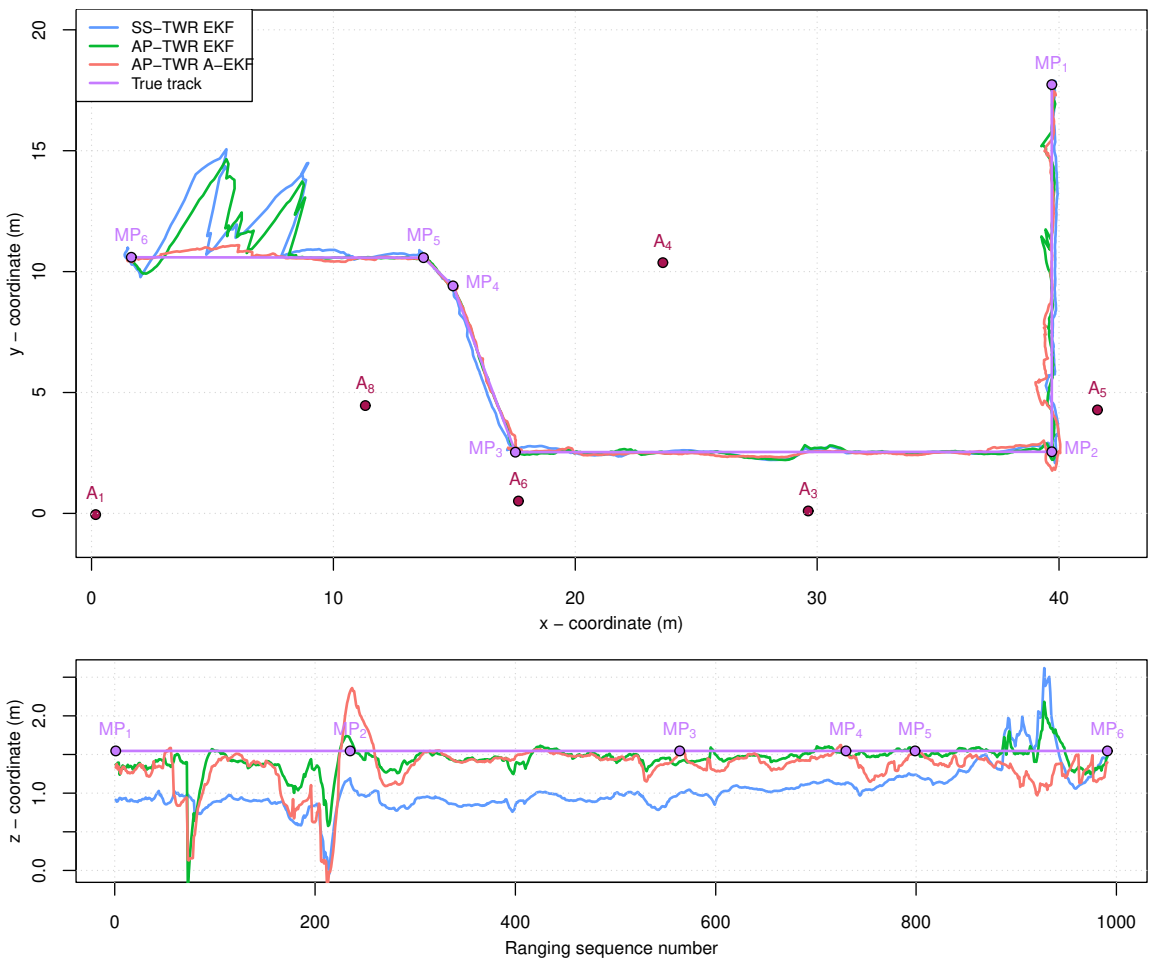
FIGURE 6. The movement paths of the second set of tests. The upper figure displays the tested methods' x and y coordinates, while the lower figure displays the z-coordinate across the ranging sequences. The critical points of the true movement path are marked with consecutive purple dots noted as MP on the respective figures. Note that on the z-coordinate plot, the movement path critical points are marked approximately in regards to the sequence number, as the shelf trolley needed to be stopped and its direction adjusted for the next segment of the movement.

B. MOVEMENT TESTS

The experiments with a moving tag were conducted to validate the results achieved by the stationary tests to show that the initialization of the methods does not affect the position estimates. Due to the inherent requirement of knowing the true coordinate of the tag at each time step, the calculation of objective error metrics becomes infeasible as the necessary devices to acquire an accurate time series reference track were unfortunately unavailable to the authors. As a consequence, the resulting analysis should be approached with caution as it solely presents the visual movement paths of the tested methods without calculating objective performance parameters in regards to the true movement track.

Fig. 6 presents the results of the movement tests, which were described in detail in Section IV. Noting that although

the x-y coordinate plot is zoomed in for clarity such that A_2 is not visible, the anchor still took part in the experiments. To facilitate the presentation of the 3D data, it was partitioned into two distinct graphs: a two-dimensional representation depicting the x-y plane of the factory floor, and a depiction of the z-coordinate variation corresponding to the ranging sequence number.

The previously surveyed critical movement points are marked with numbered purple dots (MP), connected by purple lines to indicate the true track of the movement. The approximate locations of arrival at the critical points are marked with corresponding purple dots in the z-coordinate graph. The locations on the z-coordinate figure are approximate because at each critical point, the shelf trolley was stopped to re-position it for the next section of the movement, so parts of

IEEE *Access*

Laadung *et al.*: Adaptive Extended Kalman Filter Position Estimation Based on Ultra-Wideband Active-Passive Ranging Protocol

the plots also correspond to brief stationary moments during the movement.

The movement traces in Fig. 6 support the results achieved in the stationary test, where the proposed A-EKF and the standard AP-TWR method consistently provide more accurate results in the z-axis, as was evident in the 3D RMSE graphs in Fig. 5.

In the first segment of the movement, all of the methods show slightly higher deviation from the true track, especially in the z-axis. This increased noise can be explained by the presence of the mezzanine floor on the right side, since in the first segment the tag is moved in parallel and almost under the mezzanine floor, obstructing the LoS paths to anchors 2, 5, and 7.

The next 3 movement segments show rather similar performance for all of the methods, keeping in mind that the SS-TWR method consistently shows about 0.5 m lower z-coordinate value compared to the true track, than other methods.

The final movement segment is impaired by the same pipe mandrels discussed in the previous section, as can be seen by the large deviations from the true track of the SS-TWR and AP-TWR methods. These fluctuations achieve a maximum of about 4.5 m in the x-y plane and about 1 m in the z-axis, whereas the proposed A-EKF positioning method deviates by a maximum of 0.5 m in both the x-y plane and the z-axis, reducing the maximum errors by about 9 times.

VI. CONCLUSION

This paper presented a comprehensive overview and analysis of the possible NLoS error cases that may be encountered with the usage of the UWB AP-TWR protocol. This analysis was the basis for the proposed A-EKF method, which was experimentally tested in an industrial environment and benchmarked against EKF position estimators based on active-only SS-TWR and standard AP-TWR range estimates. The proposed method can be used in real-time applications and does not require any additional information on the environment, signal properties, error models, statistics, or training data, or cause any additional time delays in the position estimation process.

Although in 2D the tested methods typically operated with the same performance, a part of the test points provided unfavorable propagation conditions for the UWB system, inducing large errors for standard AP-TWR (maximum about 5 m error) and SS-TWR (maximum about 2 m error), which the proposed A-EKF method mitigated, reducing errors with a maximal of less than 0.5 m. On average, the A-EKF provided almost 1.6 times lower RMSE that the next best i.e., the SS-TWR positioning method.

Similar trends were apparent in the 3D RMSE results as well, with the exception that the SS-TWR method provided consistently about 0.4 m inferior results than the other methods. The large errors of some test points are also present in the 3D results, with a maximum of about 5.4 m for both the SS-TWR and AP-TWR methods, while the A-EKF provided

a maximum error of only 0.9 m. Across all of the test points, the average RMSE of the proposed method was more than 3 times lower than the next method, AP-TWR.

The movement tests confirmed the validity of A-EKF stationary tests by showing that the largest errors of AP-TWR and SS-TWR, caused by the presence of various assets in the factory, are reduced ninefold. Both sets of experiments showed the robustness of the proposed A-EKF positioning method with its ability to drastically reduce large errors caused by the propagation conditions.

While the current study has demonstrated the effectiveness of the A-EKF method, further investigation is warranted to identify and determine the optimal parameters for this approach. In-depth analyses and experimentations should be conducted to explore the impact of different parameter configurations on the method's performance, accuracy, and robustness. This exploration will contribute to refining the A-EKF algorithm.

The current paper has presented an overview of AP-TWR NLoS error cases. However, a more comprehensive and detailed analysis is required to identify and characterize specific NLoS error scenarios. In-depth investigations should be conducted to explore the possibilities of developing strategies to detect and mitigate these specific NLoS cases effectively. This analysis should encompass a broader range of environmental conditions, and diverse deployment scenarios to enhance the understanding and mitigation of AP-TWR NLoS errors.

REFERENCES

[1] IEEE, "IEEE Standard for Information technology– Local and metropolitan area networks– Specific requirements– Part 15.4: Wireless Medium Access Control (MAC) and Physical Layer (PHY) Specifications for Low-Rate Wireless Personal Area Networks (WPANs): Amendment 1: Add Alternate PHYs," IEEE Std 802.15.4a-2007 (Amendment to IEEE Std 802.15.4-2006), pp. 1–210, 2007.

[2] J. Kunhoth, A. G. Karkar, S. Al-Maadeed, and A. Al-Ali, "Indoor positioning and wayfinding systems: a survey," Human-centric Computing and Information Sciences, vol. 10, no. 1, 2020. [Online]. Available: https://doi.org/10.1186/s13673-020-00222-0

[3] T. Savić, X. Vilajosana, and T. Watteyne, "Constrained Localization: A Survey," IEEE Access, vol. 10, pp. 49 297–49 321, 2022.

[4] M. Ridolfi, A. Kaya, R. Berkvens, M. Weyn, W. Joseph, and E. D. Poorter, "Self-Calibration and Collaborative Localization for UWB Positioning Systems: A Survey and Future Research Directions," ACM Computing Surveys, vol. 54, no. 4, may 2021. [Online]. Available: https://doi.org/10.1145/3448303

[5] N. Smaoui, O. Gnawali, and K. Kim, "Study and Mitigation of Platform Related UWB Ranging Errors," in 2020 International Conference on COMmunication Systems and NETworkS, COMSNETS 2020. IEEE, 2020, pp. 346–353.

[6] L. Mainetti, L. Patrono, and I. Sergi, "A Survey on Indoor Positioning Systems," in 2014 22nd International Conference on Software, Telecommunications and Computer Networks (SoftCOM). IEEE, 2014, pp. 111–120.

[7] I. Guvenc and C.-C. Chong, "A Survey on TOA Based Wireless Localization and NLOS Mitigation Techniques," IEEE Communications Surveys & Tutorials, vol. 11, no. 3, pp. 107–124, 2009.

[8] DW1000 User Manual V2.18. Decawave. Accessed December 21, 2022. [Online]. Available: https://www.decawave.com/dw1000/usermanual/

[9] V. Barral, C. J. Escudero, J. A. García-Naya, and R. Maneiro-Catoira, "NLOS Identification and Mitigation Using Low-Cost UWB Devices," Sensors (Switzerland), vol. 19, no. 16, 2019.

[10] S. Krishnan, R. Xenia Mendoza Santos, E. Ranier Yap, and M. Thu Zin, "Improving UWB Based Indoor Positioning in Industrial Environments Through Machine Learning," in 2018 15th International Conference on Control, Automation, Robotics and Vision, ICARCV 2018, vol. 138632, no. 65. IEEE, 2018, pp. 1484–1488.

[11] F. Che, Q. Z. Ahmed, F. A. Khan, and P. I. Lazaridis, "Feature-Based Generalized Gaussian Distribution Method for NLoS Detection in Ultra-Wideband (UWB) Indoor Positioning System," IEEE Sensors Journal, vol. 22, no. 19, pp. 18 726–18 739, 2022.

[12] M. Shalihan, R. Liu, and C. Yuen, "NLOS Ranging Mitigation with Neural Network Model for UWB Localization," in 2022 IEEE 18th International Conference on Automation Science and Engineering (CASE), 2022, pp. 1370–1376.

[13] J. Wu, Z. Zhang, S. Zhang, Z. Kuang, and L. Zhang, "UWB Positioning Algorithm Based on Fuzzy Inference and Adaptive Anti-NLOS Kalman Filtering," Applied Sciences, vol. 12, no. 12, 2022. [Online]. Available: https://www.mdpi.com/2076-3417/12/12/6183

[14] R. Zandian and U. Witkowski, "Differential NLOS Error Detection in UWB-based Localization Systems using Logistic Regression," in 2018 15th Workshop on Positioning, Navigation and Communications (WPNC), 2018, pp. 1–6.

[15] K. Gururaj, A. K. Rajendra, Y. Song, C. L. Law, and G. Cai, "Real-Time Identification of NLOS Range Measurements for Enhanced UWB Localization," in 2017 International Conference on Indoor Positioning and Indoor Navigation (IPIN), 2017, pp. 1–7.

[16] Z. Cui, T. Liu, S. Tian, R. Xu, and J. Cheng, "Non-Line-of-Sight Identification for UWB Positioning Using Capsule Networks," IEEE Communications Letters, vol. 24, no. 10, pp. 2187–2190, 2020.

[17] C. Liu, Y. Cao, C. Sun, W. Shen, X. Li, and L. Gao, "An Outlier-Aware Method for UWB Indoor Positioning in NLoS Situations," in 2022 IEEE 25th International Conference on Computer Supported Cooperative Work in Design (CSCWD), 2022, pp. 1504–1509.

[18] J. Wang, K. Yu, J. Bu, Y. Lin, and S. Han, "Multi-Classification of UWB Signal Propagation Channels Based on One-Dimensional Wavelet Packet Analysis and CNN," IEEE Transactions on Vehicular Technology, vol. 71, no. 8, pp. 8534–8547, 2022.

[19] S. Tomović, K. Bregar, T. Javornik, and I. Radusinović, "Transformer-based NLoS detection in UWB localization systems," in 2022 30th Telecommunications Forum (TELFOR), 2022, pp. 1–4.

[20] M. Si, Y. Wang, H. Siljak, C. Seow, and H. Yang, "A Lightweight CIR-Based CNN With MLP for NLOS/LOS Identification in a UWB Positioning System," IEEE Communications Letters, pp. 1–1, 2023.

[21] D.-H. Kim, A. Farhad, and J.-Y. Pyun, "UWB Positioning System Based on LSTM Classification With Mitigated NLOS Effects," IEEE Internet of Things Journal, vol. 10, no. 2, pp. 1822–1835, 2022.

[22] K. Yu, K. Wen, Y. Li, S. Zhang, and K. Zhang, "A Novel NLOS Mitigation Algorithm for UWB Localization in Harsh Indoor Environments," IEEE Transactions on Vehicular Technology, vol. 68, no. 1, pp. 686–699, 2019.

[23] Z. Zeng, R. Bai, L. Wang, and S. Liu, "NLOS identification and mitigation based on CIR with particle filter," in 2019 IEEE Wireless Communications and Networking Conference (WCNC), 2019, pp. 1–6.

[24] C. Chen, Z. Huang, J. Wang, L. Yuan, J. Bao, and Z. Chen, "Channel-Quality-Evaluation-Based Anchor Node Selection for UWB Indoor Positioning," Electronics, vol. 11, no. 3, 2022. [Online]. Available: https://www.mdpi.com/2079-9292/11/3/436

[25] C. Jiang, J. Shen, S. Chen, Y. Chen, D. Liu, and Y. Bo, "UWB NLOS/LOS Classification Using Deep Learning Method," IEEE Communications Letters, vol. 24, no. 10, pp. 2226–2230, 2020.

[26] P. C. Chen, "A Non-Line-of-Sight Error Mitigation Algorithm in Location Estimation," in IEEE Wireless Communications and Networking Conference, WCNC, vol. 1, 1999, pp. 316–320.

[27] L. Jiao, J. Xing, X. Zhang, J. Zhang, and C. Zhao, "LCC-Rwgh: A NLOS Error Mitigation Algorithm for Localization in Wireless Sensor Network," in 2007 IEEE International Conference on Control and Automation, ICCA, vol. 00, 2007, pp. 1354–1359.

[28] Y. T. Chan, W. Y. Tsui, H. C. So, and P. C. Ching, "Time-of-Arrival Based Localization Under NLOS Conditions," IEEE Transactions on Vehicular Technology, vol. 55, no. 1, pp. 17–24, 2006.

[29] B. J. Silva and G. P. Hancke, "Non-Line-of-Sight Identification Without Channel Statistics," in IECON Proceedings (Industrial Electronics Conference), 2020, pp. 4489–4493.

[30] Q.-T. Ngo, P. Roussel, B. Denby, and G. Dreyfus, "Correcting Non-Line-of-Sight Path Length Estimation for Ultra-Wideband Indoor Localization,"

[31] B. Silva and G. P. Hancke, "Ranging Error Mitigation for Through-the-Wall Non-Line-of-Sight Conditions," IEEE Transactions on Industrial Informatics, vol. 16, no. 11, pp. 6903–6911, 2020.

[32] J. Borras, P. Hatrack, and N. B. Mandayam, "Decision Theoretic Framework for NLOS Identification," in IEEE Vehicular Technology Conference, vol. 2, 1998, pp. 1583–1587.

[33] J. Schroeder, S. Galler, K. Kyamakya, and K. Jobmann, "NLOS detection algorithms for Ultra-Wideband localization," in 4th Workshop on Positioning, Navigation and Communication 2007, WPNC'07 - Workshop Proceedings, vol. 2007, 2007, pp. 159–166.

[34] A. Abolfathi Momtaz, F. Behnia, R. Amiri, and F. Marvasti, "NLOS Identification in Range-Based Source Localization: Statistical Approach," IEEE Sensors Journal, vol. 18, no. 9, pp. 3745–3751, 2018.

[35] T. Laadung, S. Ulp, M. M. Alam, and Y. L. Moullec, "Novel Active-Passive Two-Way Ranging Protocols for UWB Positioning Systems," IEEE Sensors Journal, vol. 22, no. 6, pp. 5223–5237, 2022.

[36] T. Laadung, S. Ulp, M. M. Alam, and Y. Le Moullec, "Performance Evaluation of UWB Active-Passive Two-Way Ranging Distance Estimation Matrix Weighting Methods," in 12th International Conference on Indoor Positioning and Indoor Navigation (IPIN 2022). CEUR-WS, sep 2022, pp. 1–5.

[37] S. Wu, Y. Ma, Q. Zhang, and N. Zhang, "NLOS Error Mitigation for UWB Ranging in Dense Multipath Environments," in 2007 IEEE Wireless Communications and Networking Conference, 2007, pp. 1565–1570.

[38] G. Shen, R. Zetik, O. Hirsch, and R. S. Thomä, "Range-Based Localization for UWB Sensor Networks in Realistic Environments," Eurasip Journal on Wireless Communications and Networking, vol. 2010, 2010.

[39] R. Zandian and U. Witkowski, "Non-line of Sight Error Mitigation in Bayesian Differential Localization Systems," in 2018 15th Workshop on Positioning, Navigation and Communications, WPNC 2018. IEEE, 2018, pp. 1–6.

[40] C. K. Toth, G. Jozkow, Z. Koppanyi, and D. Grejner-Brzezinska, "Positioning Slow-Moving Platforms by UWB Technology in GPS-Challenged Areas," Journal of Surveying Engineering, vol. 143, no. 4, p. 04017011, 2017. [Online]. Available: https://ascelibrary.org/doi/abs/10.1061/%28ASCE%29SU.1943-5428.0000231

[41] S. A. R. Zekavat and R. M. Buehrer, Eds., Handbook of Position Location: Theory, Practice, and Advances, 2nd ed. Wiley, 2019.

[42] C. L. Sang, M. Adams, M. Hesse, T. Hörmann, T. Korthals, and U. Rückert, "A Comparative Study of UWB-based True-Range Positioning Algorithms using Experimental Data," in 2019 16th Workshop on Positioning, Navigation and Communications (WPNC), 2019, pp. 1–6.

[43] Q. Li, K. Li, and W. Liang, "A zero-velocity update method based on neural network and Kalman filter for vehicle-mounted inertial navigation system," Measurement Science and Technology, vol. 34, no. 4, p. 045110, jan 2023. [Online]. Available: https://dx.doi.org/10.1088/1361-6501/acabde

[44] D. Feng, C. Wang, C. He, Y. Zhuang, and X.-G. Xia, "Kalman-Filter-Based Integration of IMU and UWB for High-Accuracy Indoor Positioning and Navigation," IEEE Internet of Things Journal, vol. 7, no. 4, pp. 3133–3146, apr 2020. [Online]. Available: https://ieeexplore.ieee.org/document/8954658/

[45] S. Akhlaghi, N. Zhou, and Z. Huang, "Adaptive Adjustment of Noise Covariance in Kalman Filter for Dynamic State Estimation," in 2017 IEEE Power & Energy Society General Meeting, 2017, pp. 1–5.

[46] Y.-W. Chen and K.-M. Tu, "Robust self-adaptive Kalman filter with application in target tracking," Measurement and Control, vol. 55, no. 9-10, pp. 935–944, 2022. [Online]. Available: https://doi.org/10.1177/00202940221083548

[47] Eliko Tehnoloogia Arenduskeskus OÜ, "Eliko UWB RTLS," Available at https://eliko.ee/uwb-rtls-ultra-wideband-real-time-location-system/ (11.04.2023).

[48] Leica Geosystems AG, "Leica DISTO S910 User Manual," Available at https://shop.leica-geosystems.com/sites/default/files/2019-04/leica-disto-s910-user-manual-805080-808183-806677-en.pdf (11.04.2023).

[49] Krah Pipes OÜ, Available at http://www.krah-pipes.ee/eng/ (11.04.2023).

[50] T. Laadung and S. Ulp, "UWB Active-Passive Two-Way Ranging Protocol Data Captured in an Industrial Environment," IEEE Dataport, 2023. [Online]. Available: https://dx.doi.org/10.21227/4f5b-gx15

IEEE *Access*

Laadung *et al.*: Adaptive Extended Kalman Filter Position Estimation Based on Ultra-Wideband Active-Passive Ranging Protocol

TAAVI LAADUNG was born in Tallinn, Estonia in 1990. He received the B.Sc. and M.Sc. degrees in telecommunication from the Tallinn University of Technology, Tallinn, Estonia in 2013 and 2016, respectively. He is currently pursuing the Ph.D. degree in information and communication technology at Tallinn University of Technology. From 2015 to 2016, he was a course Practical Work Supervisor at Tallinn University of Technology. From 2017 to 2019, he worked in the Estonian Defence Forces as a Communication Systems R&D Specialist. Since 2019, he has been working as a Researcher at Eliko Tehnoloogia Arenduskeskus OÜ in Tallinn, Estonia. His research interests include the improvement of algorithms and methods utilized in wireless indoor tracking, positioning, and object-locating systems.

SANDER ULP received the M.Sc. degree in telecommunication and the Ph.D. degree in information and communication technology from Tallinn University of Technology, in 2013 and 2019, respectively. In 2018 he started working as a researcher at Eliko Tehnoloogia Arenduskeskus OÜ. Since 2019 he is the CTO of the competence center which develops novel indoor positioning research and technologies. His research interests are in distributed estimation, learning and adaptation over networks, digital signal processing, localization technologies, and indoor positioning.

ALEKSEI FJODOROV was born in Tallinn, Estonia in 1995. He received the B.Sc. and M.Sc. degrees in telecommunication from the Tallinn University of Technology (TUT), Estonia in 2017 and 2021, respectively. Currently, he is pursuing the Ph.D. degree in telecommunication from Tallinn University of Technology. Since 2021, he has been working as a Researcher at Eliko Tehnoloogia Arenduskeskus OÜ, Tallinn. His current research interest includes sensor fusion-enabled indoor positioning and tracking, IoT, electronics and communication technologies.

MUHAMMAD MAHTAB ALAM (Senior Member, IEEE) received the M.Sc. degree in electrical engineering from Aalborg University, Denmark, in 2007, and the Ph.D. degree in signal processing and telecommunication from the INRIA Research Center, University of Rennes 1, France, in 2013. He joined the Swedish College of Engineering and Technology, Pakistan, in 2013, as an Assistant Professor. He did his postdoctoral research at the Qatar Mobility Innovation Center, Qatar, from 2014 to 2016. In 2016, he joined as the European Research Area Chair holder and an Associate Professor with the Thomas Johann Seebeck Department of Electronics, Tallinn University of Technology, where he was elected as a Professor, in 2018. In 2019, he become the head of the Communication Systems Research Group and led several National and International projects. His research interests include the fields of wireless communications and connectivity, NB-IoT 5G/B5G smart networks and services, and low-power wearable networks for SmartHealth.

YANNICK LE MOULLEC (Senior Member, IEEE) received the M.Sc. degree from Université de Rennes I, France, in 1999, and the Ph.D. and HDR (accreditation to supervise research) degrees from Université de Bretagne Sud, France, in 2003 and 2016, respectively. From 2003 to 2013, he successively held Postdoctoral Researcher, Assistant Professor, and Associate Professor positions with the Department of Electronic Systems, Aalborg University, Denmark. He then joined Thomas Johann Seebeck Department of Electronics, Tallinn University of Technology, Estonia: Senior Researcher (2013 to 2016) and professorship (since 2017). His research interests include embedded systems, reconfigurable systems, the IoT, and the application thereof. He has supervised or co-supervised more than 50 MSc students and 11 PhD students. He has been involved in more than 20 projects, including five as PI, co-PI, or co-main applicant; one such notable project was the H2020 COEL ERA-Chair project from 2015 to 2019. He is an IEEE Senior Member and a member of the IEEE Sustainable ICT Technical Community and the IEEE Circuits and Systems Society.

. . .

Appendix 5

This Appendix presents the derivation of the rating system for ToF estimation protocols presented in Section 2.2. The analyzed ToF estimation protocols are given in Fig. 16, where the packet exchange procedure of OWR, SS-TWR, SDS-TWR, AltDS-TWR, and ADS-TWR ToF estimation protocols are presented, based on the initiator of the ranging process. For the sake of brevity, the visual representation of the protocols depicts a single A, but in actuality, the total number of anchors, N, is 3. The dotted line is indicative of the additional data transfer packet, which is needed in some local/central positioning cases, as is noted in Tab. 2.

The overall rating system of Tab. 2 was devised such that the following classes were separately rated: the initiator of the ranging process, the number of time interval values needed to transmit, the inclusion of a robustness penalty, and the total number of packets needed to transmit. Each class was assigned a maximum number of points that can be achieved, which were uniformly distributed among the possible options in that class, such that the best gets the maximum points, while the worst gets zero. The sum of the scores achieved in individual classes gives the final score.

The ranging sequence initiator was assigned a maximum of 2 points, such that a tag-initiated ranging sequence gets 2 points, while the anchor-initiated ranging gets zero. The reasoning behind this choice is explained in Section 2.2.6, as the Qorvo DW1000 UWB transceiver consumes the most energy in the receive mode, contributing to the largest part of the energy consumption of a tag.

The total number of packets sent during a ranging sequence was also assigned a maximum of 2 points, as this dictates the number of transmissions, therefore the time spent in the next most energy-consuming state - transmit mode. Moreover, the air time occupancy of the protocol is also dependent on the number of transmissions. Therefore, transmitting only a total of 1 packet per ranging sequence results in a rating of 2, while transmitting $2N + 2$ packets gives a rating of zero.

The robustness penalty was given a maximum of 0.5 points, such that not having the penalty bolstered 0.5 points while having it resulted in 0. Similarly, the number of time interval values needed to transmit over the air resulted in a 0.5-point maximum, such that transmitting a single value over the air was awarded 0.5 points, while transmission of $2N$ values resulted in 0. The lower weight of this parameter was chosen, as [70] suggests that the payload size, although not the dominant factor, still contributes to the power consumption of a tag.
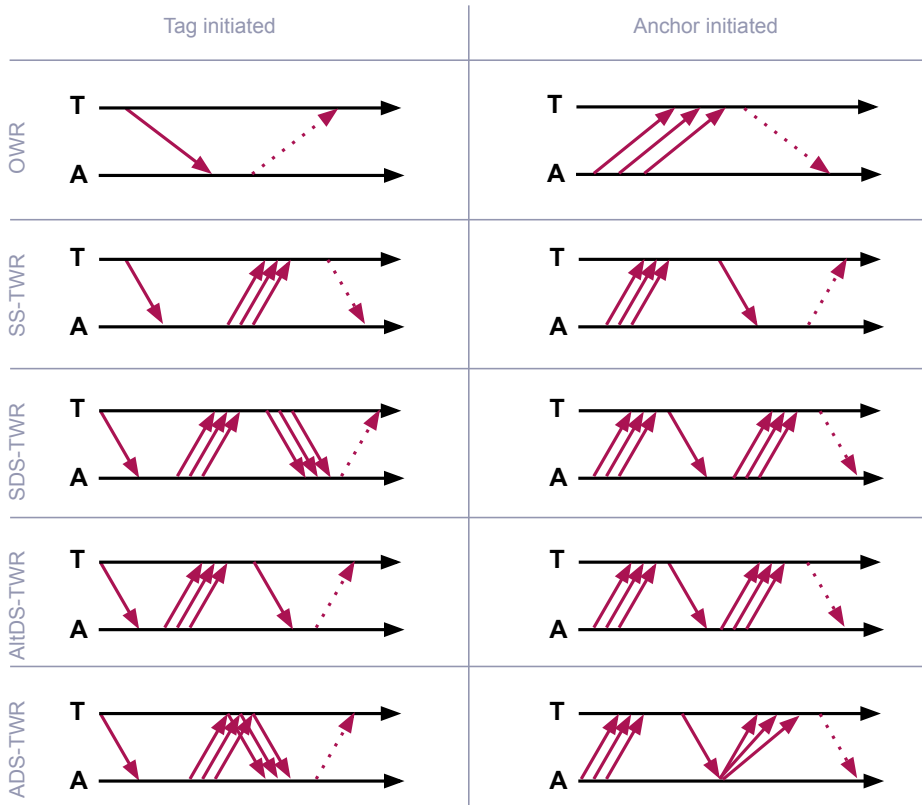
Figure 16: Visual representation of ToF estimation protocol packet exchange process, based on the initiator of the ranging sequence. The visuals depict three separate anchors as a single A.

Curriculum Vitae

1. Personal data

Name	Taavi Laadung
Date and place of birth	11 November 1990 Tallinn, Estonia
Nationality	Estonian

2. Contact information

Address	Tammiaugu tee 17,
	76916 Tiskre küla, Estonia
Phone	+372 56880747
E-mail	taavi.laadung@ttu.ee

3. Education

2019–…	Tallinn University of Technology, School of Information Technologies, Information and Communication Technology, PhD studies
2014–2016	Tallinn University of Technology, Department of Radio and Communication Engineering, Telecommunication, MSc *cum laude*
2010–2013	Tallinn University of Technology, Department of Radio and Communication Engineering, Telecommunication, BSc
2007–2010	Tallinn Technical Gymnasium, Secondary Education
2005–2007	Lasnamäe General Gymnasium, Comprehensive Education
1998–2005	Tallinn Tondiraba Secondary School, Basic Comprehensive Education

4. Language competence

Estonian	native
English	fluent
Russian	basic

5. Professional employment

2021–2022	Tallinn University of Technology , School of Information Technologies, Thomas Johann Seebeck Department of Electronics, Junior Researcher
2019– …	Eliko Competence Centre in Electronics-, Info- and Communication Technologies, Junior Researcher
2018–2019	Estonian Defence Forces, Cyber Command, Project manager
2017–2018	Estonian Defence Forces, Headquarters Support and Signal Battalion, Department of Strategic Communication, Specialist
2017	Headquarters of the Estonian Defence Forces, J6, Specialist
2015–2016	Tallinn University of Technology, Communication (IRT3930) practical work supervisor
2015–2016	Tallinn University of Technology, Lecturer, Popular science courses "Multimedia and Telecommunication"
2010	National Examination and Qualification Centre, Data entry operator

6. Voluntary work

2014–2015   Tallinn University of Technology, Student Satellite Programme,
              WP4 - Communication
2012–2013   AS Levira, Intern

7. Computer skills

- Operating systems: Windows, Linux

- Document preparation: Microsoft Office, LibreOffice, LaTeX

- Programming languages: C, Python

- Scientific packages: MATLAB, R

8. Honours and awards

- 2016, Vladimir Heinrichsen IT and telecommunication scholarship

9. Defended theses

- 2016, The Nonlinear Limitation on Achievable Transmission Distance in Fiber-optical Communication Systems, Tallinn University of Technology, MSc, supervisor Prof. Peter Avo Andrekson, co-supervisor MSc Egon Astra, Tallinn University of Technology, Department of Radio and Communication Engineering

- 2011, BSc Telecommunication, Tallinn University of Technology, Department of Radio and Communication Engineering

10. Field of research

- Indoor Positioning

11. Scientific work
Papers

1. T. Laadung, S. Ulp, M. M. Alam, and Y. Le Moullec, "Active-Passive Two-Way Ranging Using UWB," in *14th International Conference on Signal Processing and Communication Systems (ICSPCS)*, pp. 1–5, IEEE, dec 2020

2. T. Laadung, S. Ulp, M. M. Alam, and Y. Le Moullec, "Novel Active-Passive Two-Way Ranging Protocols for UWB Positioning Systems," *IEEE Sensors Journal*, vol. 22, no. 6, pp. 5223–5237, 2022

3. T. Laadung, S. Ulp, M. M. Alam, and Y. Le Moullec, "Performance Evaluation of UWB Active-Passive Two-Way Ranging Distance Estimation Matrix Weighting Methods," in *12th International Conference on Indoor Positioning and Indoor Navigation (IPIN 2022)*, pp. 1–5, CEUR-WS, sep 2022

4. T. Laadung, S. Ulp, A. Fjodorov, M. M. Alam, and Y. Le Moullec, "Adaptive Extended Kalman Filter Position Estimation Based on Ultra-Wideband Active-Passive Ranging Protocol," *Submitted to IEEE Access*, 2023

5. M. Tommingas, S. Ulp, M. M. Alam, I. Müürsepp, and T. Laadung, "Estimating UWB Positioning Integrity Based on Ranging Residuals," in *2023 24th International Conference on Applied Electromagnetics and Communications (ICECOM)*, pp. 1–6, Forthcoming, 2023

Conference presentations

1. T. Laadung, S. Ulp, M. M. Alam, Y. Le Moullec. *Active-Passive Two-Way Ranging Using UWB* , 2020 14th International Conference on Signal Processing and Communication Systems (ICSPCS): 14–16 December 2020, Adelaide, Australia (Virtual)

2. T. Laadung, S. Ulp, M. M. Alam, Y. Le Moullec. *Performance Evaluation of UWB Active-Passive Two-Way Ranging Distance Estimation Matrix Weighting Methods*, 2022 12th International Conference on Indoor Positioning and Indoor Navigation (IPIN): 5–7 September 2022, Beijing, China (Virtual)

Elulookirjeldus

1. Isikuandmed

Nimi	Taavi Laadung
Sünniaeg ja -koht	11.11.1990, Tallinn, Eesti
Kodakondsus	Eesti

2. Kontaktandmed

Aadress	Tammiaugu tee 17,
	76916 Tiskre küla, Estonia
Phone	+372 56880747
E-mail	taavi.laadung@ttu.ee

3. Haridus

2019–…	Tallinna Tehnikaülikool, Infotehnoloogia teaduskond,
	Info- ja kommunikatsioonitehnoloogia , Doktoriõpe
2014–2016	Tallinna Tehnikaülikool, Raadio- ja sidetehnika instituut,
	Telekommunikatsioon, MSc *cum laude*
2010–2013	Tallinna Tehnikaülikool, Raadio- ja sidetehnika instituut,
	Telekommunikatsioon, BSc
2007–2010	Tallinna Tehnikagümnaasium,
	Keskharidus
2005–2007	Lasnamäe Üldgümnaasium,
	Põhiharidus
1998–2005	Tallinn Tondiraba Keskkool,
	Põhiharidus

4. Keelteoskus

eesti keel	emakeel
inglise keel	kõrgtase
vene keel	algtase

5. Teenistuskäik

2021–2022	Tallinna Tehnikaülikool, Infotehnoloogia teaduskond,
	Thomas Johann Seebecki Elektroonikainstituut, Doktorant-nooremteadur
2019– …	Eliko Tehnoloogia Arenduskeskus OÜ,
	Nooremteadur
2018–2019	Eesti Kaitsevägi, Küberväejuhatus, Taktikalise side projektijuht
2017–2018	Eesti Kaitsevägi, Staabi- ja sidepataljon,
	Strateegilise side keskus, Spetsialist
2017	Eesti Kaitsevägi, Peastaap, J6 - Side- ja juhtimissüsteemide osakond, Spetsialist
2015–2016	Tallinna Tehnikaülikool, Side (IRT3930) laborijuhendaja
2015–2016	Tallinna Tehnikaülikool, Lektor, Populaarteaduslikud loengud
	"Multimeedia ja Telekommunikatsioon"
2010	Riiklik Eksami- ja Kvalifikatsioonikeskus, Andmesisestaja

6. Vabatahtlik töö

2014–2015   Tallinna Tehnikaülikool, Tudengisatelliidi programm,
              WP4 - Side
2012–2013   AS Levira, Praktikant

7. Computer skills

- Operatsioonisüsteemid: Windows, Linux

- Kontoritarkvara: Microsoft Office, libreOffice, LaTeX

- Programmeerimiskeeled: C, Python

- Teadustarkvara paketid: MATLAB, R

8. Autasud

- 2016, Vladimir Heinrichseni nimeline infotehnoloogia ja kommunikatsiooni stipendium

9. Kaitstud lõputööd

- 2016, Mittelineaarsustest tulenev piirang maksimaalsele edastuskaugusele fiiberoptilises sidesüsteemis, MSc, juhendaja Prof. Peter Avo Andrekson, kaasjuhendaja MSc. Egon Astra, Tallinna Tehnikaülikool, Raadio- ja sidetehnika instituut

- 2013, BSc Telekommunikatsioon, Tallinna Tehnikaülikool, Raadio- ja sidetehnika instituut

10. Teadustöö põhisuunad

- Sisepositsioneerimine

11. Teadustegevus
Teadusartiklite, konverentsiteeside ja konverentsiettekannete loetelu on toodud ingliskeelse elulookirjelduse juures.